UNIVERSITY OF NAIROBI

PHOTOCATALYTIC TREATMENT OF WASTEWATER FROM SELECTED TEA FACTORIES IN KENYA

BY

PATRICK KIMUTAI TUM

I80/93563/2013

A Thesis Submitted for Examination for the Degree of Doctor of Philosophy in Chemistry of the University of Nairobi.

2017

DECLARATION

"I declare that this thesis is my original work and has not been submitted elsewhere for examination, award of a degree or publication. Where other people's work, or my own work has been used, this has properly been acknowledged and referenced in accordance with the University of Nairobi's requirements".

Signature: _____ Date: _____

Patrick Kimutai TUM
DEPARTMENT OF CHEMISTRY
SCHOOL OF PHYSICAL SCIENCES
UNIVERSITY OF NAIROBI

"This thesis is submitted for examination with our approval as research supervisors".

1. Prof. David K. Kariuki
   Signature:_____ Date: _____
   Department of Chemistry
   University of Nairobi
   Nairobi, Kenya

2. Dr. Fredrick D.O. Oduor
   Signature:_____ Date:_____
   Department of Chemistry
   University of Nairobi
   Nairobi, Kenya.

3. Dr. John K. Wanyoko
   Signature:_____ Date:_____
   Kenya Agricultural & Livestock Research Organization (KALRO)
   Tea Research Institute (TRI)
   Kericho, Kenya

ABSTRACT

Wastewater from black tea (*Camellia sinensis)* processing factories is characterized by a persistent brown colour that conventional treatment works are unable to remove. In this work photocatalytic decolourization of persistent brick-red colour of black tea processing wastewater was investigated. Forty eight wastewater samples each of 500 cm^3 were collected from three black tea processing factories in the western Kenya highlands, and subjected to treatment by Titanium dioxide and Zinc oxide photocatalysts. Wastewater physico-chemical parameters were determined by analyzing Total Organic Carbon, Chemical Oxygen Demand, Turbidity, Total Suspended Solids and Total Dissolved Solids levels. Total Organic Carbon concentration was determined using the direct method, where 30% sodium persulfate, oxidizes dissolved organic carbon to carbon dioxide. The carbon present, is proportional to concentration of carbonaceous material present. Chemical Oxygen Demand was determined by closed reflux titrimetric method measuring chromates calorimetrically. Untreated wastewater samples were analysed for total metals of Mn, Al, Fe and Ni levels by Atomic Absorption Spectroscopy equipped with a deuterium background correction and air-acetylene burner. Total Al metal was analysed using a nitrous oxide-acetylene burner. The results obtained indicate concentrations levels Fe=1.46 mg/L; Mn=1.17 mg/L; Al=18.89 mg/L and Ni=0.32 mg/L. Sample concentration ranged between 0.26 – 18.89 mg/L. A GC-MS analysis of untreated samples indicated the presence of organic macromolecules that were identifiable and quantifiable. The number of molecules were as follows; (CBH= 9, KBH=14 and NBH= 12) respectively. An amount of 500 cm^3 of each wastewater sample was put in a photocatalytic reactor with a floor coated with a thin layer of ZnO to give a wastewater liquid height of approximately 2 cm. This was illuminated with Ultra violet lamps at 365 nm wavelength of intensity 3.0 mW/cm^2 for 180 mins, and solar light of intensity 1.4 mW/cm^2. Samples of 5 cm^3 were drawn every 15 minutes and analyzed using Ultra Violet/Visible spectrophotometer at λ = 410 nm. These experiments were repeated using TiO_2 coated floors. ZnO results indicate decolourization of 77% - 87% of the wastewater in 180 mins. Solar illumination produced higher efficiency of decolourization of 3% above Ultra violet lamp. On average decolourization of 61% solar illumination and 58% Ultra violet lamp was achieved in 60 minutes. Solar illumination intensity was 47% that of Ultra violet lamp.TiO_2 results indicate that decolourization of 70.4% - 78.5% of the wastewater was achieved in 180 mins. Solar illumination produced higher efficiency of 2.3% above Ultra violet lamp irradiation. Decolourization of 59.7% solar and 54.4 % Ultra violet lamp was achieved in

the first 60 minutes Solar radiation intensity used was 47% that of Ultra violet lamp for both photocatalytic systems. ZnO and TiO_2 photocatalysts were characterized by Laser Induced Breakdown Spectroscopy, X-ray Diffraction, Scanning Electron Microscope, Energy Dispersive X-Ray Spectroscopy, and surface area measurements. Laser Induced Breakdown Spectroscopy analysis revealed discrete atomic lines, indicating Ti and Zn spectral peaks at $\lambda = 400$ nm, X-Ray Diffraction/Scanning Electron Microscope analysis showed particle sizes of ZnO of 16.21 nm $\pm$ 2 nm and TiO_2 of 16.00 nm $\pm$ 2 nm and spherical in morphology, Energy Dispersive X-Ray Spectroscopy showed active catalyst element present 61.5%, Zn in ZnO and 61%, Ti in TiO_2 and specific surface area of 40.14 m^2/g ZnO and 31.76 m^2/g TiO_2. After 180 mins, Total Organic Carbon, Chemical Oxygen Demand, Turbidity, Total Suspended Solids and Total Dissolved Solids levels decreased by 74.8%, 58.5%, 45.1, 58.01% and 41.52% respectively but pH increased from acidity towards neutrality from 5.8 to 6.7. Treatment by Solar/Ultraviolet/ZnO system, indicated a 9.7% efficiency compared to Solar/Ultraviolet/TiO_2 system.

DEDICATION

This dissertation is dedicated to my parents who instilled in me the virtues of perseverance and commitment and relentlessly encouraged me to strive for excellence

ACKNOWLEDGEMENTS

Primarily I dedicate this dissertation to God almighty, without whose origin of wisdom and knowledge, my humanly endeavours would be futile.

Secondly I would like to express my greatest gratitude to my project supervisors Prof. David K. Kariuki, Dr. Fredrick D.O. Oduor and Dr. John K. Wanyoko for their invaluable advice and guidance during the entire duration of this project. It was an honour and privilege to have worked under such knowledgeable and resourceful supervisors, and without their input, this work would not have been made possible.

Thirdly, special thanks goes to the University of Witwatersrand through Dr. Dickson Andala of Multimedia University of Kenya for his guidance, support and assistance offered in the course of this project.

Fourthly, appreciation goes to all my mates in the laboratories where this work was achieved. I would further wish to thank, the Ministry of Environment and Forestry (Mines and Geology), Department of Chemistry - Technical University of Kenya, Departments of Physics, Biochemistry, Geology and Meteorology, University of Nairobi, for their support.

Lastly I would also like to express my sincere gratitude to my friends and family for their countless sacrifice, support and encouragement. This dissertation is dedicated to them. Above all, I am eternally grateful to the almighty God.

TABLE OF CONTENTS

LIST OF TABLES

LIST OF FIGURES

LIST OF APPENDICES

LIST OF ABBREVIATIONS / ACRONYMS AND SYMBOLS

ASTM	American Society for Testing and Materials
A	Absorbance
Abs	Absorbance of tea wastewater
A	Irradiated surface area
AOP	Advanced Oxidation Processes
APHA	American Public Health Association
BJH	Barrett Joiner Halenda
BET	Brunauer Emmett Teller
BOD	Biological Oxygen Demand
COD	Chemical Oxygen Demand
CW	Constructed Wetlands
c	Molar concentration ($mol.dm^{-3}$)
CTC	Cut Tear Curl
CFC	Chlorofluorocarbons
CFU	Continuous Fermentation Unit
DCM	Dichloromethane
d	Optical path (cm)
Eg	Band gap energy
E_{-cb}	Conduction band electron
EAP	Eastern Produce
EDTA	Ethylenediaminetetraacetic acid
EDS	Energy Diffractive X-Ray Spectroscopy
Ɛ	Molar extinction coefficient
Eg	Bandgap energy
EPK	Eastern Produce Kenya
FAS	Ferrous Ammonium Sulfate
FAO	Food Agriculture Organization
GOK	Government of Kenya
GC-MS	Gas Chromatography-Mass Spectrometry
h^+	vb valence band hole
hν	the symbol of a photon of a certain energy
HCFC	Hydrochlorofluorocarbons
HPLC	High Performance Liquid Chromatography

IC	Inorganic carbon
ICTP	Institute of Chemical Technology Prague
KTDA	Kenya Tea Devolvement Agency
LIBS	Laser Induced Breaking-Down Spectroscopy
LVEMP	Lake Victoria Environment Management Programme
NEMA	National Environment Management Authority
pzc	point of zero change
PET	Polyethylene Terephthalate
POP	Persistent Organic Pollutant
ppm	parts per million
PAH	Polyaromatic Hydrocarbons
RS	Raw sample
ROS	Relative Oxygen Species
SHE	Standard Hydrogen Electrode
SEM	Scanning Electron Microscope
SP	Stabilization Ponds
TF	Theaflavins
TR	Thearubigins
TOC	Total Organic Carbon
TSS	Total Suspended Solids
TDS	Total Dissolved Solids
T	Transmittance
t	Time (min)
TOC	Total Organic Carbon
TRI	Tea Research Institute
TUK	Technical University of Kenya
TBK	Tea Board of Kenya
TC	Total carbon
TS	Treated sample
TDK	Tea Directorate of Kenya
UV	Ultra violet
UON	University of Nairobi
UV	Ultra violet
UVA	Ultra Violet A (λ= 315 nm-400 nm)
UVB	Ultra Violet B (λ= 280 nm-315 nm)

UVR	Electromagnetic spectrum of UV radiation
VOC	Volatile Organic Carbon
XRD	X-ray Diffraction Analysis
λ	Wavelength (nm)

CHAPTER ONE

1 Introduction

1.1 Background

Tea (*Camellia sinensis)* grows in tropical and sub-tropical climates of the world and is enjoyed globally for its aromatic taste and non-alcoholic nature (Seenivasan *et al.,* 2008). As a drink, tea is the most popular beverage after water and is prepared by brewing hot water with processed cured tea leaves. A tea bush can remain productive for up to 100 years and produce between 3-5 kg of dry tea leaves annually.

A few tea bushes were first planted in Kenya around 1903 by the Caine brothers at Mabroukie-Limuru (Paul *et al.*, 1997). Large-scale tea growing spread to other regions of Kenya after 1930. The major tea growing areas in Kenya are mainly to the west and east of the Rift Valley (Owuor, 2011) . The tea growing areas have an ideal climate, fertile red volcanic soils and annual rainfall ranging between 1200 mm to 1400 mm.

Currently small-scale tea production in Kenya is managed by the Kenya Tea Development Agency (KTDA). By the year 2017, KTDA owned 66 tea processing factories, serving over 500,000 farmers, cultivating 150,000 ha of tea plantation. This represents over 60% of total tea production. The rest of the production is done by multinational tea companies (Mucheke, 2015). The bulk of tea processed in Kenya is majorly black tea, which is exclusively processed by the CTC (Cut, Tear and Curl) technique.

The KTDA manages 54 tea companies, owning 66 tea processing factories across Kenya, Eastern Produce (EAP) oversees 5 factories in Nandi and Kericho counties and James Finlay's (K) operates 4 factories in Kericho and Bomet counties. Tea production in Kenya reached 473 million kilograms in 2016 (TDK, 2016). The increase in demand for tea processing has consequently led to generation of large volumes of wastewater produced during processing and cleaning stages. The specific volumes of wastewater discharged from individual processing factories is dependent on the production capacity of each factory.

The major tea growing areas in Kenya are shown in Figure 1.1.

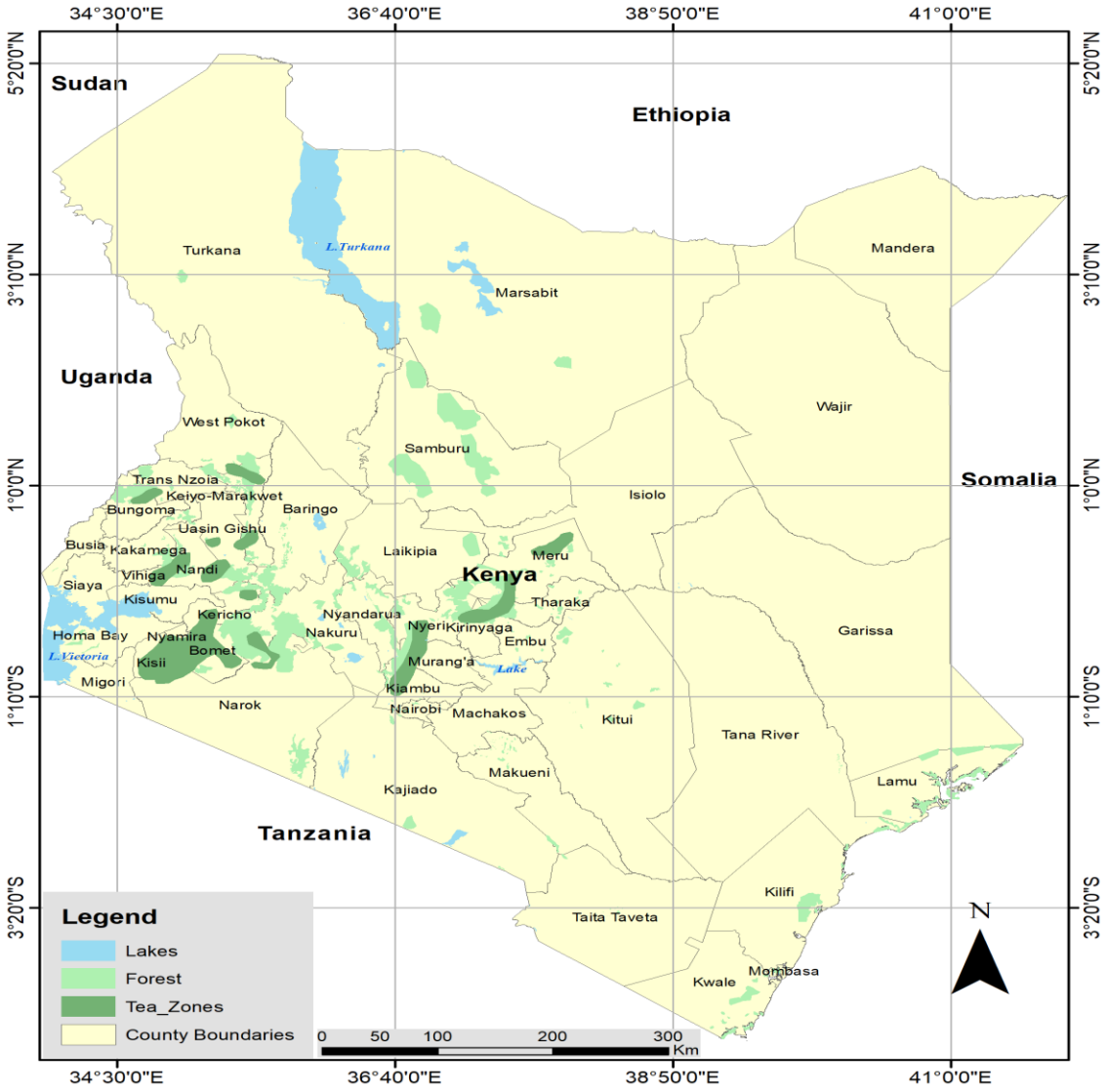

Figure 1.1 Tea growing areas of Kenya

Despite the huge volumes of wastewater produced, the majority of tea processing factories in Kenya lack effective wastewater treatment processes. Most factories rely almost entirely on constructed wetlands (CW), Stabilization Ponds (SPs) with vegetation systems and lagoons. The wastewater discharged from these factories is characterized by a persistent distinct brown colour, since the majority of products formed during tea processing are coloured (Roberts, 1958). The characteristic brown colour of wastewater renders it untenable for discharge into the environment. This study proposes the use of suitable select semi-conductor photocatalysts irradiated with Solar/UV light to remedy the challenge posed by the coloured wastewaters on the entire tea sector.

1.2 Tea processing wastewater

1.2.1 Characteristics of tea processing wastewater

Tea processing leads to the generation of large volumes of wastewater that is characterized by high organic matter, high suspended matter, heavy metals, odour, surfactants, and high oxygen demanding parameters. In addition, other wastewater components include: unprocessed tea leaves, detergents, waste grease and oil from machine parts (Tum *et al.*, 2016).

The greatest concern for the tea industry in Kenya, remains the persistent colour problem caused by large volumes of coloured wastewater discharged from their factories into the environment. The coloured wastewater results from the presence of organic macro-molecules, that are characterized by conjugated carbon-carbon bonds in their structures formed during tea processing (Graham, 1992; Maghanga *et al.*, 2009; Tum *et al*., 2016). Flavanols, which are colour pigments are responsible for the colouring of wastewater from tea processing factories. These flavanols that include theaflavins, are brick-red pigments characterized by conjugated aromatic rings (Haddis & Devi, 2008).

Discharge of untreated tea processing wastewater leads to contamination of the eco-system. This contamination leads to disruption of aquatic life by reducing the amount of sunlight penetrating into water bodies. Further contamination affects plants like algae and weeds that are consumed by fish and other aquatic animals thereby disrupting the food chain upwards (Onyatta *et al.,* 2016). Pollution also disrupts the oxygen cycle that sustains living organisms by disturbing the natural balance and affecting the environment in various ways.

1.2.2 Wastewater management- Tea processing wastewater

1.2.2.1 Wetlands

Wetlands are vegetative regeneration zones that allow rainfall to percolate into the ground allowing wastewater regeneration (Lin *et al.*, 2003). These wetlands are composed of vegetation that act as natural sponges (Chung *et al.*, 2008). They absorb particulate matter in wastewater thereby removing the characteristic brick-red colour. The retention ability of wetlands enables them to discharge and recharge surface and ground water respectively. According to (Lin *et al.*, 2003) wetlands cleanse wastewater by purifying it naturally, removing silts and sucking in toxins.

1.2.2.2 Lagoons

Tea processing factories use lagoons to treat their wastewater. These treatment system consists of one or several ponds built to hold wastewater for a certain duration of time. The construction of these ponds involves lining with material such as clay to prevent leaks to the ground water. The wastewater treatment is achieved by biological and chemical processes that occur naturally. The lagoons are designed to use aeration devices that increase oxygen in wastewater. Aeration improves wastewater treatment efficiency, to utilize less land area (Lawson, 2011)

1.2.2.3 Stabilization ponds (SPs)

These are man-made ponds in which tea processing wastewater is treated and discharged safely into river systems. Stabilization ponds are linked in a series that includes several types of ponds that include, (i) anaerobic ponds (ii) facultative ponds and (iii) aerobic ponds (Arthur, 1983). Aerobic and facultative ponds remove CODs while anaerobic ponds are designed to remove bacteria. Suspended solids are digested at the base of the ponds and aerobic ponds act as final stage treatment. The ponds are generally effective in treatment , however its disadvantage includes the long time it takes to treat wastewater and the large land mass required (Arthur, 1983).

1.2.2.4 Electro-coagulation (EC)

Involves the use of an electrochemical cell where contaminants in wastewater such as heavy metals, organics and inorganics are held together by electric charges. (Gilmore & Renk, 2014). An electric charge is applied on metallic plates inserted in the wastewater while a second charge is applied holding contaminating particles together. These are thereafter separated from the purified water. These particles coagulate forming a mass that is separated by filtration (Rajeshwar & Ibanez, 1995). Iron metal is preferred as the conducting material at both the anode and cathode (Mollah *et al.,* 2001). Electrocoagulation as a wastewater treatment technique has been investigated by several researchers including (Maghanga *et al.,* 2009).

1.3 Pollution of water resources

Water pollution results from natural and man-made activities. Large amounts of polluted wastewater in developing countries (80 - 90%) is discharged directly into surface water bodies with little or minimal treatment (Water, 2008). The pollution of these water resources has led to severe water stress and by the year 2025, it is predicted about two-thirds of the world's population would lack access to clean and safe water for domestic and industrial use (Clark, 2007).

Severe shortages in treated water, has caused humans and livestock to use water fetched from rivers and lakes that may not be safe for domestic use (Van der Bruggen & Braeken, 2006). In the past, wastes generated from industries, were dumped without treatment into rivers where they were subjected to dilution and self-purification (Karr & Chu, 2006). Large influxes of pollutants results in severe oxygen depletion negatively affecting the aquatic environment causing degradation (Zimmerman, 1993). These environmental problems include eutrophication which results from a decrease in sunlight penetration due to presence of pollutants, reducing the photosynthesis process of aquatic animals and visual pollution (Azad *et al*., 2014; Guillard *et al.*, 2003). The presence of high colour levels in wastewater affects its aesthetic qualities and reduces light penetration and affecting plant growth and habitat. Organic contaminants discharged in wastewater from various industries, are the major causes of degradation of water resources (Rajaram & Das, 2008).

The majority of rivers and streams in Kenya are heavily polluted. The sources of this pollution, includes domestic wastes and wastewater discharged from industries. Rivers situated near major towns and cities are worst affected as they are heavily contaminated with organic pollutants (Monteith *et al.,* 1995). Colour is a significant indicator of water quality, however the decolourization of industrial wastewater remains a great challenge requiring strict controls i.e. industries should consider new methods of wastewater decolourization and disposal (Monteith *et al.,* 1995). Coloured wastewater from tea processing factories adversely impact on animal and plant life in the environment (Monteith *et al.*, 1995).

1.4 National Environmental Legal Framework in Kenya

The Government of Kenya, through legislation requires all manufacturing industries to treat all wastewater before disposal. This is to regulate and protect surface water resources from adverse impacts. These regulations are enacted in the Water Quality Regulation act, 2006 and the Wetlands and River bank Regulations act, 2006.

These regulations prohibit the discharge of any substances into a flowing river, lake or wetland, if the substance would negatively affect Water quality. In addition, the (GOK Environmental Management and Coordination Act, 2009) prohibits the intentional discharge of noxious wastes into water resources.

Other laws that regulate wastewater disposal include; (GOK Water Bill, 2014); (GOK Strategic Assessment, Integrated Impact Assessment and Audit) Regulations, 2017 and GOK Occupational Safety and Health Act, 2007; Act No. 15 of 2007.

1.5 Problem Statement

Individual tea processing factories in Kenya require an average of 70 m^3 of fresh water daily during their cleaning and maintenance operations (EPK, 2010). This requirement is in contrast to the available fresh water reserves available in Kenya, which is water-scarce with 647 m^3 of freshwater available per capita. The wastewater that is formed after tea processing is largely released into the natural environment without effective treatment.

These wastewater is loaded with contaminants such as high organic matter, high suspended matter, heavy metals, odour, surfactants, and high oxygen demanding parameters that make the water unpalatable. Of great concern is the persistent problem of colour and other parameters that cannot and have never been removed through conventional wastewater treatment. Wastewater from Chebut, Kibwari and Nandi tea processing factories located in the Nandi hills catchment, in Nandi County, is discharged into tributaries for rivers Yala and Nyando that feed into Lake Victoria. Pollution load is highest on the Kenyan side of Lake Victoria due to these inflows. Communities living along the course of these tributaries and rivers have had to live with poor water quality as a result of this untreated wastewater from the factories. Women have to walk long distances in search of clean and safe water for domestic use. Water in these rivers leave deposits of sludge and slurry on vegetation and banks, thereby destroying the aquatic life in these waters. Fish stocks in river Nyando and Yala have been steadily declining over the years (Maghanga *et al*.,

2009). The destruction and loss of wetlands in the Nyando and Yala threatens to increase poverty and to undermine development. A decline in the health of the ecosystem due to pollution that has cut down fish stocks in the lake (Maghanga *et al.*, 2009). Industrial run-off, from the various factories in the catchment area has subsequently led to the invasion of water hyacinth in lake Victoria. Some tea procesing factories in Kenya have constructed wetlands (CW), where duckweed (*Lemna spp*) and other plants are grown and used to treat wastewater through phyto-remediation, Stabilization Ponds (SPs) and Lagoons. These methods have however largely been less effective leading to much of the wastewater being discharged into nearby rivers while still coloured.

1.6 Justification and significance of the study

The communities living along rivers that are contaminated by coloured wastewater from tea factories will benefit from clean water for their domestic use. In addition, the continued pollution of rivers flowing into Lake Victoria will be mitigated securing the livelihoods of close to 12 million people by maintaining and enhancing the beneficial services to secure livelihoods, food, water, health and security. The proposed utilization of solar light to treat wastewater will results in a cost-effective technique available to all tea processing factories in Kenya.

1.7 Main Objective

To develop a proto-type efficient treatment system for tea processing wastewater using photocatalysts.

1.7.1 Specific Objectives

The specific objectives were to:-

1) To determine the physical - chemical properties of tea processing wastewater.
2) To characterize Organic macro-molecules in tea effluent.
3) To determine metal species prevalent in tea processing wastewater: i.e. Fe, Al, Mn and Ni.
4) To characterize powder photocatalysts.
5) To develop a prototype batch photocatalytic reactor equipped with immobilized

photocatalysts on glass.

CHAPTER TWO

2 Literature review

2.1 Tea Varieties

Tea is enjoyed as a beverage mainly due to its taste, aroma and health benefits. In most parts of the world, tea is considered as a refreshing beverage proposed for consumption because of its therapeutic potential (Karakaya & El, 2006). It is also consumed for the same reasons as those of coffee (Zhu *et al.*, 2002). It is obtained from processing the leaves of *Camellia sinensis* plant (Li *et al.*, 2007).

According to the procedure that is followed during tea production, tea is categorized into green, black, oolong and white teas. Green tea is non-oxidized tea produced by drying and steaming the fresh leaves to inactivate the enzyme polyphenol oxidase that oxidizes polyphenols found in tea and cause the formation of brick-red colour. Among the four types of tea, black tea is the most processed. The production technique used for black tea ensures that it undergoes total oxidation that leads to the development of its distinct dark brown colour of its leaves (Li *et al.*, 2007). Oolong tea is mainly grown in China, and contains various polyphenols such as epigallocatechin, epigallocatechin gallate, epicatechin and polymerized polyphenol (Han *et al.*, 2007) and its production involves the partial oxidation of tea leaves and subsequent drying to preserve the natural flavors (Lin *et al.*, 2008); (Alcazar *et al.*, 2007). In addition, Oolong tea, undergoes partial fermentation that permits limited levels of enzymatic oxidation throughout preparation and has high anti-oxidative activities (Zhu *et al.*, 2002; Nakahara *et al.*, 1993; Han *et al.*, 1999; Ou *et al.*, 2002). Oolong tea is also broadly consumed in Asia as a result of its polyphenols that are of many biological and pharmaceutical benefits that include anticarcinogenic, antioxidative and hypolipidemic properties (Han *et al.*, 2007); (Kilmartin & Hsu, 2003).The organic structure of the Oolong tea polyphenols have been found to contain conjugated carbon-carbon double bonds (Han *et al.*, 2007).

White tea is produced by harvesting the tea leaves with their buds just before they fully open up when the buds are still covered in fine white hairs (Teixeira *et al.*, 2012). Further production techniques involve the steaming thoroughly of the leaves to activate the enzymes responsible for tea discolouration. The leaves are then subsequently dried in a dryer or the sun (Dufresne & Farnworth, 2001). The quality of tea processed is dependent

on various factors i.e. the geographical locations of the tea plantations, climatic conditions, soil profiles and tea processing technique.

2.2 Tea pigments

Tea consists of several pigments, which include theaflavins that are yellow-brown substances that contributes significantly to the astringency, briskness, brightness and colour of black tea. On average, theaflavins make up 0.3% to 1.8% on dry weight basis of the total black tea composition (Takino *et al.*, 1965). Thearubigins (TR) make up another important group of compounds that are formed during processing of black tea from catechins as well as by oxidative degradation of theaflavins (Lin *et al.*, 2005). They constitute 10% to 20% of dry weight and cause the colour and flavour of the tea (Roberts & Caserio, 1977).

2.2.1 Biochemical constituents of Tea

Tea plucking is either done physically by human tea pluckers or by specialized tea harvesters. It involves the plucking of crop shoots (apical bud and two terminal leaves). The nature of plucked tea leaves influences the biochemical characteristics which in turn influences the quality of the tea (Thomas *et al.*, 2006). Tea constitutes many biochemical components. These include, phenolic components, alkaloids, vitamins, enzymes, crude fiber, proteins, lipids and carbohydrates. Among the biochemical constituents, the phenolic compounds have been found to be prevalent (Ramaswamy, 1993).

Polyphenols found in tea, particularly theaflavins and thearubigins determine tea quality. The taste and flavour of the teas is due to the oxidative transformation of phenolic compounds. Enzymes like polyphenol oxidase and peroxidase act upon these phenolic molecules during fermentation in black tea processing (Ramaswamy, 1993). Tea is composed of 30% of polyphenols and catechins on the dry weight basis (Saravanan *et al.*, 2005). Catechins in the green leaf of tea is influenced by seasons and geographical considerations (Couladis *et al.*, 2003).

2.3 Tea processing in Kenya

Tea leaf processing in Kenya, involves Cutting, Tearing and Curling (CTC) technique. The technique mainly involves the reduction of leaf moisture content without any addition of water. The process of tea manufacture leads to the discharge of waste water generated from the process namely Cutting, Tearing and Curling (CTC) machine, Continuous Fermentation Unit (CFU) troughs and the driers (Wasewar *et al.*, 2009). In summary, black tea processing includes the following steps:-

(i) Withering – sun drying of tea leaves under the sun for up 18 hours, to reduce moisture content to 60%.

(ii) Rolling – this takes 1-3 hours, in which tea leaves are crushed to allow enzymatic oxidation of flavanols.

(iii) Fermentation – responsible for the distinct black tea flavour and colour. The fermentation process, is the most critical step and is dependent on oxygen availability, temperature, relative humidity, time and pH. The fermentation process produces dark-colored polymerization products of polyphenols.

(iv) Firing – tea leaves are passed through hot air dryers to prevent enzymatic fermentation

(v) Sorting – physical isolation of tea leaves into quality grades. Flavonoids contents and other polyphenols are affected by different types of processing (Chan *et al.*, 2009).

2.3.1 Coloured wastewater treatment techniques

Conventional wastewater treatment techniques such as flocculation and coagulation have proved ineffective in the treatment of coloured wastewater which have high organic load (Habib *et al.*, 2012). Various researchers in recent years have investigated alternative wastewater treatment methods. These techniques include advanced oxidation processes

(i) Advanced Oxidation Processes (Couladis *et al.*, 2003); H_2O_2/UV photocatalysis (Arslan & Balcioglu, 2001); Photo-Fenton (Lin & Chang, 2000).

(ii) Ozonation (Agustina *et al.*, 2005; Rice *et al*., 1996).

(iii) Sonolysis (Gogate & Pandit, 2004).

(iv) Gamma–radiolysis (Wojnarovits & Takacs, 2008).

(v) Electro-coagulation (Azarian *et al.*, 2007; Inan *et al.*, 2004).

(vi) Biological and combined anaerobic–photocatalytic treatment (Ndasi *et al.,* 2011; Chan *et al.,* 2009).

To remedy coloured industrial wastewater, various techniques have been proposed. However these methods have serious shortfalls (Chong *et al.,* 2010; Chan *et al.,* 2009). Traditional methods such as adsorption on waste materials, adsorption on activated carbons, precipitation, air stripping, flocculation, reverse osmosis and ultrafiltration have been successfully applied to remedy coloured wastewater. However these methods are merely phase transferring methods and require further treatment for disposal (Akpan & Hameed, 2009).

2.3.1.1 Phytoremediation

This techniques involves the use of select distinct plants for example duckweed to remedy coloured wastewater. The application of plants for coloured wastewater treatment has several advantages that remarkably efficient, cost-effective, driven by natural energy and requires minimal capital to set up. (Parra *et al.*, 2012). The floating plant, Lemna species has been identified as the most effective for use in photoremediation of wastewater. Favourable conditions for the duckweed to grow include, water temperature range of 17°C to 35°C (Iqbal, 1999). Another significant advantage of the duckweed is that they reproduce vegetatively, about 10 times in its lifecycle (Skillicorn *et al.*, 1993).

2.3.1.2 Physico-chemical techniques

These methods comprises precipitation, flocculation, coagulation, ion-exchange, adsorption, membrane separation, sedimentation, bleaching by ozone/chlorine, ion-exchange on synthetic adsorbent resins, reverse osmosis (Cooper, 1993). However physico-chemical methods remove or separate colour physically and require subsequent solid waste disposal that raises costs and is time consuming. Disadvantages of these methods include high sludge formation, handling and disposal problems, and expensive regeneration of adsorbent. (Frølund *et al.*, 1996).

2.3.1.3 Biological techniques

Involves mainly aerobic and anaerobic digestion, whereby colour removal is achieved by adsorption on activated sludge or by biological degradation of molecules. The

disadvantages includes slow process, the overall efficiency is dependent on performance of some external factors (pH and salts) and a large mass of land required for the treatment process (Bergamini *et al.*, 2009). Biological treatment of wastewater may be preferred over the physico-chemical methods, however they are time consuming and leads to the formation of large amounts of sludge. This poses a challenge of recycling or disposal (Bergamini *et al.*, 2009). Coloured wastewater discharged from industrial plants including from tea processing factories are highly resistant to biodegradation.

2.3.1.4 Electrochemical techniques

Involves dialysis or ion oxidation that combines oxidation of organic pollutants by electrolytic processes. A final process involves a physical-chemical precipitation of sludge and filtration. Disadvantages of this method includes formation of sludge and high electricity costs (Idota *et al.*, 1997).

2.3.1.5 Electromagnetic radiation

Utilizes light energy in the form of electromagnetic radiation and sensitivity of particles to this energy to achieve eventual mineralization of organic pollutants in wastewater. For wastewater treatment, the removal of colour from coloured wastewater is more important than removal of colourless contaminants present in the wastewater (Hussein & Abass, 2010).

2.3.1.6 Conventional methods

Traditional methods of wastewater treatment combines physical and biological processes to remove organic pollutants from solutions that include wastewater (Hammer, 1996). In conventional wastewater treatment methods, sedimentation is the first step. The settled and floated organic matter is removed. Biological treatment follows next. Then in the tertiary stage, specific chemicals are removed from the partially already purified water before final disinfection.

Depending upon the nature of the pollutant, tertiary treatment can include some of the chemical and physical processes, such as adsorption of nonpolar organic molecules onto activated carbon, removal of phosphate by its precipitation as the calcium salt, heavy metal removal by the addition of hydroxide or sulfide, desalination by reverse osmosis, electro dialysis or ion exchange. The conventional purification of drinking water follows similar

stages of purification as wastewater treatment, but the quality of drinking water must meet much more strict standards compared to wastewater treatment to avoid causing any health problems to water users (Doan *et al.*, 1999).

Aeration is commonly used as the first step in purification of drinking water to get rid of dissolved gases, such as H_2S, organosulphur compounds and other volatile organic compounds (VOCs) (Vinodgopal *et al.*, 1996). After aeration, settling and precipitation of colloidal particles achieved by adding Al^{3+} or Fe^{2+} salts, gelatinous hydroxides form at neutral and alkaline pH values that physically incorporate colloidal components (Doan *et al.*, 1999). To get rid of harmful bacteria and viruses from drinking water, disinfection is applied as a last step of purification. Various disinfection methods includes, chlorination, UVC radiation or Ozonation (De Lasa *et al.*, 2005).

2.3.1.7 Advanced Oxidation Processes (AOPs)

Advanced Oxidation Processes (AOPs) techniques are dependent on production of powerful oxidizing species that effectively treat wastewater (Parsons, 2004). The subsequent generation of hydroxyl radicals (•OH), which are powerful oxidation species leads to the quick non-selective reaction with the majority of electron-rich sites of organic pollutants (Doan *et al.*, 1999).

With UV light irradiation and appropriate photocatalyst, electron/hole pairs with free electrons are produced in the unfilled conduction band, leaving positively charged holes in the valence band. These electron/hole pairs start a chain of chemical reactions that mineralize organic contaminants into CO_2 and water. The process gradually degrades organic contaminants. This method prevents the formation of sludge and leads to no secondary pollution. Advanced Oxidation Processes (AOPs) have been used to treat and remove organic contaminants in wastewater (Oppenlander, 2003; De Lasa *et al.*, 2003) Suitable powder photocatalyst including TiO_2 and ZnO act as semi-conductor photocatalysts to degrade organic and inorganic pollutants into H_2O and CO_2 (Habib *et al.*, 2012; Mahmood *et al.*, 2003). This process involves the cleavage of the conjugated carbon–carbon double bonds found in polyphenols by (•OH) radicals that causes decolorization of coloured wastewater and mineralization to CO_2 and H_2O.

It has been established that TiO_2/ZnO powder photocatalysts, with UV irradiation mineralizes organic pollutants present in wastewaters into harmless products such as CO_2, and H_2O (Singh *et al.*, 2013). Photocatalytic reactions readily eliminate from wastewater all organic impurities. Its applications in slurry type suspensions is limited due to the

challenge caused by catalyst separation after photocatalytic treatment (Mehrvar *et al.*, 2001; Khezrianjoo & Revanasiddappa, 2012). The development of knowledge in semi-conductor electrochemistry has led to tremendous growth in the field of photocatalysis (Heller, 1981). The application of photocatalytic degradation to remove cyanide in wastewater has been investigated by Frank & Bard, 1977). The authors accurately predicted great developments in the field of environmental purification that led to extensive efforts to build up knowledge in the field of photocatalysis (Ollis & Ekabi- Al, 1993; Fox & Dulay, 1993; Akira Fujishima *et al.*, 1999; Akira Fujishima & Rao, 1997). (Mathews, 1988) conducted studies to investigate the viability of using TiO_2 and ZnO to degrade by photosensitized oxidation aromatic hydrocarbons containing phosphorus, Sulphur, nitrogen and halogen. The end products were CO_2, H_2O, $PO4^{3-}$ and SO_4^{2-}. Photocatalytic degradation experiments have been applied as a remedial technique to remove organic pollutants in wastewater (Gaya & Abdullah, 2008).

Photocatalysis as a novel wastewater treatment technique involves a light induced process that results in the oxidation of organic compounds by oxidation-reduction reactions activated by electron–hole pairs that form on the surface of powder catalysts (Chen *et al.*, 2011).

2.4 Photocatalytic degradation mechanism

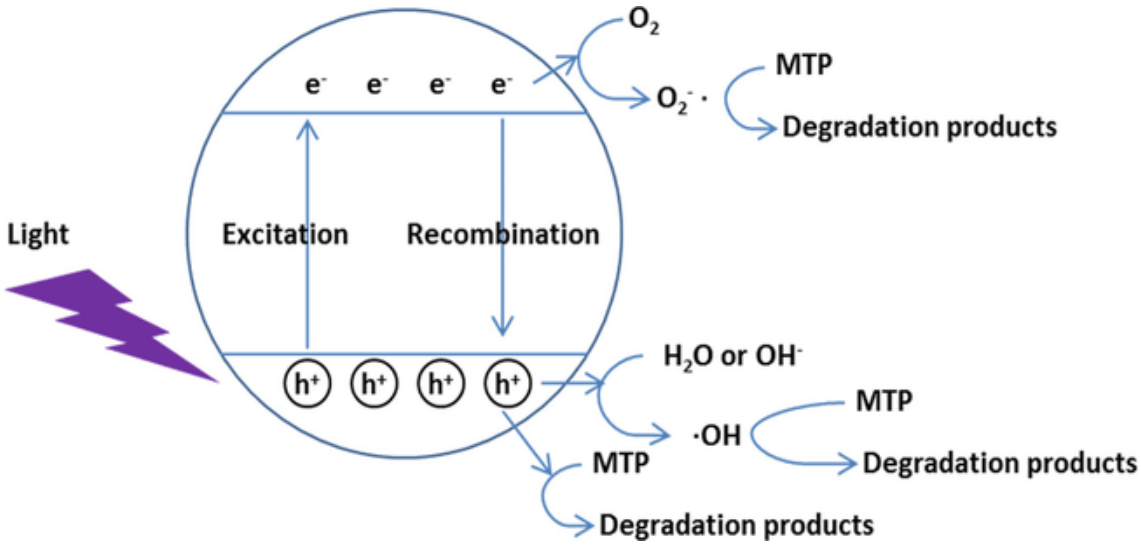

Figure 2.1: Description of photocatalytic degradation photocatalysis in solutions containing oxidative and reductive species

Source: (Rajeshwar & Ibanez, 1995).

The photogenerated holes formed after the excitation of electrons migrate from the valence band to conduction band. The holes possess extreme oxidizing potential and the photogenerated electrons are reduced to form superoxides from Dioxygens (Akira Fujishima *et al.*, 2000). (Akira Fujishima & Honda, 1972) promoted extensively the study of photocatalysis. They described the "Honda-Fujishima effect" where they explained the photochemical splitting of H_2O into H_2 and O_2 using titanium dioxide. Photocatalysis was described as cost effective, simple and promising method to achieve complete mineralization of organic molecules in waste water into CO_2 and H_2O. This new process of wastewater treatment was referred to as the Advanced Oxidation Process (AOPs) (Khataee *et al*., 2009).

2.4.1 Applications of Photocatalytic degradation

2.4.1.1 Destruction of organics

Photocatalytic degradation has been used to mineralize organic compounds in particular alcohols, carboxylic acids, chlorinated aromatics, phenolic derivatives into harmless end products e.g. CO_2 and water (Bhatkhande *et al.*, 2002; Pirkanniemi & Sillanpaa, 2002). Another application of photocatalytic degradation is the treatment of wastewater streams contaminated with oil (Grzechulska *et al.*, 2000).

2.4.1.2 Water disinfections

Heterogeneous photocatalytic reactions are applicable in reactions to eliminate bacteria and viruses that may include streptococcus natuss, Streptococcus mutans, Streptococcus cricetus, Escherichia coli, Saccharomyces cerevisisas, Lactobacillus acidophilus and Poliovirus 1 (Mills & Le Hunte, 1997). Microcystin toxins have been successfully photocatalytically degraded by immobilized TiO_2 catalyst (Shephard *et al.*, 2002). Cholera Vulgaris which has a thick cell wall, can be eliminated from wastewater streams by photo disinfection sensitized by TiO_2 (Shephard *et al.*, 2002). Several authors have reported TiO_2 as a microbiocide effective at photokilling Lactobacillus acidophilus, Saccharomyces cerevisiae and Escherichia coli. (Matsunaga *et al.*, 1985; Fujishima *et al.*, 1986) reported using TiO_2 to photokill tumor cells (Hela cells). (Sonawane *et al.*, 2004) concludes that Fe^{2+} doped TiO_2 films could decolourize 95% of methyl orange dye in solar light illumination for a duration of 3-4 hrs. Highly hydrophilic TiO_2 surfaces with excellent

anti-fogging and self-cleaning properties have been developed (Wang *et al.,* 1997). The examples below illustrate a few applications of photocatalysis.

Figure 2.2: TiO_2 coated tent material

Source: (Fujishima *et al.,* 2000)

In Figure 2.2 TiO_2 is used as a coat on building materials. The TiO_2 films possess self-cleaning qualities as a result of strong oxidizing properties.

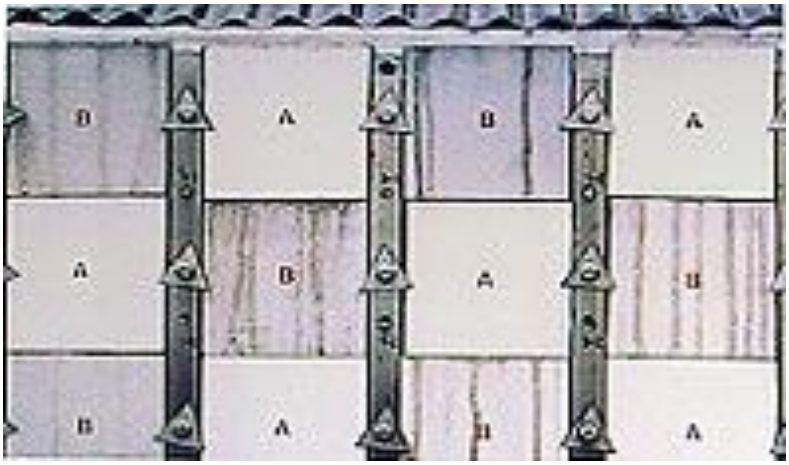

Figure 2.3: TiO_2 coated exterior tiles

Source: (Fujishima *et al.,* 2000)

In Figure 2.3 the sections labelled A and B represent;-

A. Tiles coated photocatalytic super hydrophilic layer
B. Ordinary painted wall tiles

Figure 2.4 TiO_2 coated mirror
Source: (Fujishima *et al*., 2000)

In Figure 2.4 with ordinary mirrors, when fog comes into contact with glass, droplets of water are formed fogging the glass. In glass coated with TiO_2, the water forms a continuous flat sheet preventing fogging.

2.4.1.3 Photocatalytic treatment of natural organic matter

The use of humic acid has been investigated by (Al-Rasheed & Cardin, 2003) as a model substance to decrease organic content using Advanced Oxidation Processes (AOPs). During the process no toxic byproducts or sludge were created. The findings indicate that after 1 hr. of UV light irradiation and 1g/L of TiO_2 , about 40% of Total Organic Carbon (TOC) and 75% of colour was eliminated at λ = 400 nm (Bekbölet & Özkösemen, 1996). In other work related to Humic Acid, 80% of commercial humic acid was eliminated by UV light illumination with TiO_2 (Minero *et al.*, 1999). An aqueous solution of TiO_2 illuminated by UV light showed high photocatalytic activity within the lowering of Humic Acid (HA) concentrations (approximately 50% elimination was achieved in 10 minutes (Eggins *et al.*, 1997). To raise the rates of photocatalytic degradation of organic substances including humic acid, photocatalytic degradation has been applied along with other physical methods sono-photocatalysis, Ozonation photocatalysis (Davydov *et al.*, 2001; Kerc *et al.*, 2003).

2.4.1.4 Seawater treatment

An investigation into sea water reveals that it could be decomposed under UV light irradiation by TiO_2 using an artificial light source (Ziolli & Jardim, 2002).

2.4.2 Principles of semi-conductor photocatalysis

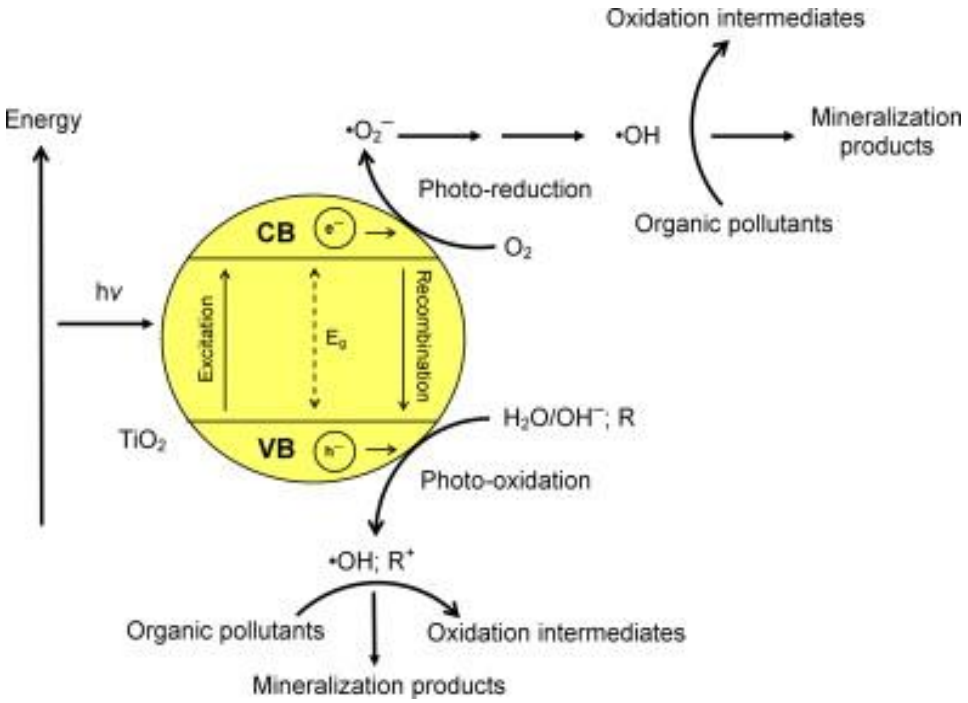

Figure 2.5: principles of heterogenous photocatalysis

Source: (Ajmal *et al.*, 2014)

An important feature of photocatalytic reactions is conduction and valence band are on different energy levels. All photochemical reactions are characterized by an activation energy related to the absorption of at least one photon by a molecule. The range of wavelengths generally used in photochemistry lies in UV/Vis spectrum λ = 200 nm to 700 nm (Turro *et al.*, 2009).

Semi-conductors are characterized by certain non-stoichiometry, unlike oxides such as MgO or Al_2O_3, which are insulators. These oxides have their valence bands filled with electrons and their conduction bands empty. Semi-conductors e.g. ZnO/TiO_2 have their valence and conduction bands on different energy levels (Demkov & Posadas, 2014).

The principle of photocatalytic degradation is dependent on UV light, in the form of a photon, with energy equal or greater than the band gap energy (E_g) falling on the surface of a catalyst causing the promotion of electrons from the valency band to conduction band.

This leads to the formation of electron/hole (e^-/h^+) pairs with free electrons in the empty conduction band leaving an electron vacancy/hole in the valence band. The formation of these holes allows adsorbed water to be oxidized to strong (•OH) radicals whose strong oxidative species (2.8 V vs. SHE) oxidize most organic compounds (Guan *et al.*, 2008). The organic intermediates formed are oxidized by O_2 or (•OH) radicals and mineralized to CO_2 and H_2O. Hydroxyl radicals (•OH) are strong oxidants that rapidly react most electron-rich sites of organic pollutants (Zimbron & Reardon, 2009).

2.4.2.1 Photocatalytic oxidation

Photocatalytic processes are initiated by the absorption of UV light (λ<400 nm) in a semi-conductor generating electrons and holes in the valency and conduction bands. The photogenerated holes that avoid recombination move to the semi-conductor surface and react with adsorbed (•OH) or H_2O forming trapped holes. Trapped holes are usually shown as surface-bound or adsorbed (•OH). Hydroxyl radicals generated at the surface of a semiconductors leaves the surface into the bulk solution to forming free (•OH). In oxygen rich environments, oxidative species, such as H_2O_2 are formed in their reduction sites (Konstantinou & Albanis, 2004).

2.4.2.2 Photosensitized oxidation

Photosensitized oxidation represents photocatalytic degradation reactions induced by visible light (λ>400 nm) irradiation. Organic pollutants absorb light (λ>400 nm and inject an electron on to the conduction band of the powder photocatalyst. Excited organic molecules convert to cationic radicals ($organic^+$) and the photocatalyst leads to the formation of oxidation species O_2^- , HO_2 or HO^- that drive the mineralization process (Konstantinou & Albanis, 2004).

2.4.3 Heterogenous photocatalytic degradation

Heterogeneous photocatalysis is a powerful technique for the total mineralization of almost all the organic pollutants (Mahmoodi *et al.*, 2006). In this mechanism a metal oxide is selected as a semi-conductor, a source of UV light identified to drive the photodegradation process. Not all metal oxides can act as a semi-conductor. Research has

shown that some metal oxides like ZnO, WO_3 and $SrTiO_3$ have also proven to be photoactive like TiO_2 (Ullah & Dutta, 2008).

2.4.4 Homogenous photocatalytic degradation (Photo-Fenton Reaction)

The Photo-Fenton process, an example of Advanced Oxidation Processes (AOPs), is a technique used to effectively treat wastewater (Lopez-Alvarez *et al.*, 2012; Lucas *et al.*, 2013). The Photo-Fenton oxidation process depends on the oxidation potentials of (•OH) radicals. The radicals are formed by the decomposition of H_2O_2 catalyzed by Fe^{2+} ion (Fenton reaction) and the photo-reduction of Fe^{3+} (Photo-Fenton reaction) (Lucas *et al.*, 2013). The Hydroxyl radicals (•OH) formed in aqueous mediums oxidize and degrade organic pollutants.

The Photo-Fenton reactions can be summarized as follows;

$$Fe^{2+} + H_2O_2 \rightarrow Fe^{3+} + (OH\bullet) + OH^- \quad (1)$$

$$Fe^{3+} + H_2O_2 \rightarrow Fe^{2+} + HOO\bullet + H^+ \quad (2)$$

(Wadley & Waite, 2004)

Reaction 1: (Fenton reaction) - Decomposition of H_2O_2 catalyzed by Fe^{2+} and leads to the oxidation of Fe^{2+} to Fe^{3+} producing (•OH) radicals in acidified aqueous mediums.

Reaction 2: (Photo-reduction) of Fe^{3+} by UV/Vis light generates (•OH) radicals that enables the photo-Fenton catalytic cycle process, where Fe is interchanged between the (+2) and (+3) oxidation states. (Wang, 2008).

2.5 Solar induced photocatalytic degradation

UV light irradiation is responsible for the excitation of electrons from valency to conduction band of a selected semi-conductor. The UV component in solar irradiation comprises only 5% of the incident solar radiation. This means only 5% is made available to TiO_2 and ZnO photocatalytic degradation of organic pollutants (Thiruvenkatachari *et al.*, 2008; Anpo & Takeuchi, 2003). Solar light mediated heterogenous photocatalytic degradation is promising process for environmental remediation. Practically its effectiveness is dependent on efficient photocatalysts (Ajmal *et al.*, 2014; Muruganandham *et al.*, 2014; Tachibana *et al.*, 2012; Bizani *et al.*, 2006; Kubacka *et al.*, 2011; Galian & Perez-Prieto, 2010). Zinc oxide (ZnO) as a potential semi-conductor under

solar light irradiation, demonstrates great efficiencies in the degradation of organic contaminants (Strunk *et al.,* 2009). Considering various photocatalysts, ZnO and TiO_2 remain the most practical because of high photosensitivity, nontoxicity and low cost. This is despite their utilization of a tiny fraction of solar radiation (3% – 5%) in the UV region as a result of their large bandgap energies (Palaez et al., 2012; Chong et al., 2010; Chen et al., 2011; Cho *et al.*, 2011).

2.5.1 Solar Ultra-violet radiation (UVR)

The composition of UV light radiation in solar light is about 5%. The UV component of solar irradiation from the sun at midday comprises 95% UVA and 5% UVB. In addition to direct solar rays, reflections of solar light from certain ground surfaces contributes in large proportions to the total amount of scattered UVR (Moseley, 1988).

Levels of Solar UV radiation is influenced by the following factors. (i) Time of the day. (ii) Season – variance in terrestrial UV irradiance is less significant near the equator (Diffey, 1991) (iii) Geographic latitude – yearly UVR exposure dose diminishes with increasing distance from the equator (Diffey, 1991) (iv) Altitude – it is estimated that each 300 metre increase in altitude increases sunburning of solar light by 4% (Diffey, 1991) (v) Clouds – cloud cover interferes with the amount of irradiation through reflection, refraction, absorption. Total cloud cover may prevent about 50% of UVR energy from reaching the surface of the Earth (Diffey, 1991).

2.5.2 Advantages of Solar induced photocatalytic degradation

The advantages include, cost-effective, no sludge formation like other methods such as adsorption, coagulation and flocculation. It's also environmentally friendly. It is extremely an energy self-sufficient process as it can work under solar radiation. Finally the method does not generate any other secondary pollutant like other methods as the final products are CO_2 and H_2O (Sharma & Bhattacharya, 2017). The selected catalyst possess no toxicity to human health, have wide applications especially to molecular structured complex contaminants and the energy at $\lambda < 365$ nm comprising at least 5% of solar light illuminating the surface of the earth (Tang *et al.*, 2014).

2.5.3 Limitations of Solar induced photocatalytic degradation

Lack of consistency and reliability in solar light availability caused by erratic weather patterns is a significant drawback in solar induced photocatalytic treatment (Moseley, 1988). Solar systems rely on the steady absorption of sunlight. Factors such as latitude and cloud cover affect the overall availability of solar radiation reaching the earth (Gokmen *et al.,* 2013).

2.6 Zinc oxide and Titanium dioxide photocatalysts - (Semi-conductors)

Among several semi-conductors, TiO_2 and ZnO have been extensively investigated as potentially efficient photocatalysts. In particular, ZnO is a potential alternative to TiO_2, considering band gap energy and greater photoactivity that has been reported for ZnO compared to TiO_2 (Cho *et al*., 2010; Hayashi *et al.*, 2007; Huang *et al.,* 2008). ZnO and TiO_2 photocatalysts have shown tremendous potential to eliminate toxic organic contaminants in wastewater streams (Akpan & Hameed, 2009).

Various factors such as the surface area and defects of metal semi-conductor oxides such as ZnO and TiO_2 are important factors that enhance photocatalysis (Mahmood & Dutta, 2012; Tipton & Slack, 2005). Zinc oxide has shown great potential in the field of nanotechnology, ZnO has a large band gap and excitation binding energy (Staszkiewicz, 2004; Dai *et al.,* 2003). The form of TiO_2 and ZnO nanoparticles catalysts immobilized on suitable substrates e.g. glass and stainless steel affects the efficiency of photocalytic systems (Ali & Hassan, 2008; Baruah & Dutta, 2009).

2.6.1 Theory of semi-conductors

Most of the photocatalytic degradation studies have been tested at wavelengths between 320 nm – 400 nm (Thiruvenkatachari *et al.*, 2008). These wavelengths are related to the band gap energies of TiO_2 and ZnO (Robel *et al.,* 2007). Therefore the light source that supplies optimum radiation can be selected i.e. UV light or solar light. In most typical photocatalytic reactors, UV light irradiation is supplied by fluorescent low-pressure and medium mercury lamps emitting low and high intensity UV light respectively (Thiruvenkatachari *et al.*, 2008). Various types of photocatalytic degradation systems have

been investigated for wastewater treatment. These include TiO_2, ZnO, ZrO_2, CdS, and WO_3 (Kim *et al.*, 2010; Mohabansi *et al.*, 2011).

Several metal oxides are known to have their band-gap energies in the UV region. Thus their band gap energies are $\geq$ 3.36 e.V. at λ = 390 nm (Thiruvenkatachari *et al.*, 2008). These catalysts support photocatalytic degradation processes under UV light illumination (Sung-Suh *et al.*, 2004).

2.7 Suspension photocatalysis

Suspension photocatalysis has several advantages and disadvantages. It ensures a larger surface area, improving higher efficiency, due to uniform photocatalyst distribution. Catalyst fouling is minimized because the catalyst is continuously removed. The greatest disadvantage is the requirement of a filter to separate the catalyst which increases the unit costs. The method is expensive after scaling-up because catalyst particle recovery is difficult and expensive (Angeles *et al.*, 2014).

2.8 Thin film photocatalysis

Thin film photocatalysis describes the immobilization of powder photocatalysts onto a suitable substrate or support. These substrates include (i) glass (ii) fibers (iii) stainless steel (iv) inorganic materials (v) sand (vi) activated carbons (ACs). The immobilized catalysts on suitable substrates allow for re-use for reactions taking place at room temperature and reduces the drawbacks of photolysis reactions because organic contaminants are oxidized to harmless compounds such as CO_2 and H_2O (Aramendia *et al.*, 2008; Malabo *et al.*, 2003).

Immobilized catalysts on thin films is a continuous process and not requiring a separation step after the reaction. Compared to suspension photocatalysis, it is less effective because the surface area available for reactions are lower compared to the suspension technique. A more suitable alternative is the immobilization of powder catalysts onto various particulate layers or catalytic supports without reducing photocatalytic activity (Staszkiewicz, 2004; Al-Rasheed, 2005; Mok, 2009).

2.8.1 Ideal Photocatalysts

Suitable photocatalytic materials should possess the following characteristics (i) active photocatalytic activity (ii) biochemical inertness, (iii) photocorrosion resistance (v) UV/Vis light absorption ability (vi) affordable (vi) non- toxic

Table 2.1 shows a list of various types of semi-conductors and their band-gap energies at 0 K.

Table 2.1: Bandgap energies for various semi-conductors at 0 K

Semi-conductors	Bandgap energy (eV)
TiO_2	3.32
ZnO	3.37
Diamond	5.4
CdS	2.42
ZnS	3.6
SnO_2	3.54
WO_3	2.76
Si	1.17
Ge	0.744
ZrO_2	3.87
Cu_2O	2.172

Source: (Thiruvenkatachari *et al.*, 2008)

2.8.1.1 Nano – photocatalysts

Due to surface area considerations, nano-scale powder photocatalysts show a greater photocatalytic activity than the normal scale powder photocatalysts. The nano-particles have larger surface area available for contact between reactants. Smaller particle sizes reduces the time needed for the carrier diffusing out of the photocatalyst pores to the photocatalysts surface (Mehrvar *et al.*, 2001).

2.8.1.2 Titanium dioxide photocatalyst

Significant amounts of research on TiO_2 as a suitable photocatalyst have been carried out over the last five decades (Akira Fujishima *et al.,* 2000). TiO_2 has been investigated as an ideal photocatalyst but is limited by certain characteristics such as poor absorption of visible light radiation and a fast recombination of photogenerated electron/hole pairs. Extensive research shows that TiO_2 is a highly efficient photocatalyst due to its high photoactivity and photochemical stability.

TiO_2 has found applications in photocatalytic treatment of wastewater, pesticide degradation and water splitting by TiO_2 to generate H_2 (Mor *et al.,* 2006; Thomson & Yates, 2006; Chen & Mao, 2007). The TiO_2 driven photocatalytic degradation of coloured wastewater maybe achieved through excitation of the coloured organic compounds onto semiconductor surfaces under a visible light mediation in a process referred to as photosensitized photocatalysis (Vinodgopal *et al.,* 1996). Some drawbacks for example, include a band gap of 3.32 e.V that corresponds to 388 nm and thus does not absorb visible light (Carp *et al.,* 2004). This means it only absorbs solar light in the UV region of solar light. Solar spectrum comprises about 40% of the visible region (400 nm to 700 nm) and characterized by rapid recombination rates of photogenerated electron–hole pairs which lowers degradation rates (Ajmal *et al.,* 2014). The equations below indicate the reactions that take place when TiO_2 acts as a semi-conductor.

$$TiO_2 + hv \rightarrow e^-_{CB} + h^+_{VB} \quad (3)$$

$$O_2 + e^-_{CB} \rightarrow O_2^{\cdot -} \quad (4)$$

$$H_2O + h^+_{VB} \rightarrow OH^- + H^+ \quad (5)$$

TiO_2 exists in several crystalline modifications, the significant ones being anatase and rutile. Anatase form is the most practical and can be applied in many photocatalytic applications, since it's biologically and chemically inert (Pal & Dutta, 2002; Souther & Alspaugh, 1957). TiO_2 has been applied to remove organic contaminants in wastewater (Sakthivel & Kisch, 2003; Akyol *et al.,* 2004; Inan *et al.,* 2004). Sakthivel demonstrated that TiO_2 is a superior photocatalyst compared to other semi-conductors e.g. WO_3, α-Fe_2O_3, SnO_2 and ZrO_2 under similar experimentation conditions (Ameta & Ameta, 2016). Another investigator, Augugliaro concluded that TiO_2 displays superior photochemical stability compared to ZnO. However, ZnO is photochemically more active compared to TiO_2 despite its lower surface to volume ratio (Augugliaro *et al.,* 1988).

2.8.1.3 Zinc oxide photocatalyst

Several researchers have indicated that ZnO photocatalyst demonstrates high photocatalytic efficiencies for the mineralization of organic contaminants (Strunk *et al.*, 2009; Gilmore & Renk, 2014; Ullah & Dutta, 2008; Huang *et al*., 2012).ZnO as a select photocatalyst has been studied to achieve complete mineralisation of organic pollutants in the environment (Kansal *et al.*, 2007; Gaya & Abdullah, 2008; Nirmala *et al.*, 2010). ZnO has been studied as an excellent photocatalytic material applied to remedy wastewater such as printing and dyeing wastes, dairy and food wastewater, drugs and pesticides wastewater, textile wastewater, papermaking wastewater e.t.c. (Rizzo, 2011).

The photocatalytic efficiency of ZnO is better than most photocatalysts (Georgekutty *et al.*, 2008). It has extensively been used to as a remedy for environmental pollution, ZnO as a semi-conductor photocatalyst has received attention from many researchers (Li *et al.*, 2007). Zinc oxide nanoparticles have been widely utilized for opt-electronics, antimicrobial activity because of its excellent properties in UV absorption and reflective properties. ZnO has further been used widely in semiconductors, cosmetics, sunscreens, plastic additives, and pigments among a wide range of other applications (Wu *et al*., 2010; Li *et al.*, 2013). As a photocatalyst the band gap energy of ZnO is similar to that of TiO_2. The band gap energy of ZnO is approximately (3.2 e.V) making it a suitable semi-conductor catalyst (Garcia and Semancik, 2007). In some applications ZnO has shown a greater tendency towards photodegradation and mineralisation of organic or inorganic pollutants compared to TiO_2 (Gouvea *et al.*, 2000; Hayashi *et al*., 2007; Huang *et al.*, 2008). If ZnO absorbs a photon of energy equal to or greater than its band gap width (3.2 e.V), an electron may be excited from the valency band to the conduction band leaving behind an electron vacancy or hole in the valency band.

$ZnO + UV \rightarrow$ electron (e^-) + positive hole (h^+) (formation of electron–hole pair) (6)

ZnO photocatalytic characteristics is dependent on its morphology, crystal size, density and structure, and crystallographic orientation (Garcia & Semancik, 2007; Wang, 2004).

Zinc oxide has been seen as an efficient semi-conductor catalyst used for water treatment , organic pollutant decontamination and various types of photolysis because it generates hydrogen peroxide (H_2O_2) more proficiently (Carraway *et al.*, 1994). Reactions with ZnO have shown high levels of mineralization and reaction rates as a result of more active sites (Akyol *et al.*, 2004). Zinc oxide photocatalyst is affordable and exhibits high photochemical sensitivity, utilizing solar energy (Yang *et al.*, 2004). Application of ZnO

nanoparticles as a potential photocatalyst material to decompose environmental contaminants have been widely investigated (Li *et al.,* 2008). It has been suggested that for better photocatalytic efficiency in various applications, ZnO should absorb UV radiation in addition to visible light (Li *et al.,* 2012). As a semi-conductor ZnO has been used to develop surface coatings for a variety of engineering applications because of its wide band gap energy, these applications include, synthesis of advanced ceramics, binding energy (60 e.V) and natural synthesis of nanocrystalline materials (Li *et al.,* 2007). Zinc oxide powder has been shown to be the most effective practical material for photocatalytic degradation reactions as a photocatalyst promotes the generation of Reactive Oxygen Species (ROS) under illumination with energy at or above its band gap energy 3.37 e.V (equivalent to 368 nm wavelength) (Ma *et al.,* 2011).

ZnO absorbs UV light radiation at wavelengths equal or less than 385 nm (Nirmala *et al.,* 2010). To enable ZnO absorb visible light, its band gap can be narrowed or divided into several band gaps (Wang *et al.,* 2013; Kim & Park, 2009). ZnO has been identified as a suitable replacement for TiO_2, since their photodegradation mechanisms have been proven to be similar (Gouvea *et al.,* 2000; Krishnakumar *et al.,* 2010). Zinc oxide absorbs a large amount of UV radiation at a corresponding wavelength of 425 nm (Behnajady *et al.,* 2006), this makes ZnO a better photocatalyst especially under the visible light excitation. Investigations show that ZnO is an effective photocatalyst in the treatment of some organic pollutants in aqueous systems (Gouvea *et al.,* 2000; Krishnakumar *et al.,* 2010). The cost of ZnO is affordable compared to TiO_2 especially for large-scale treatment systems (Daneshvar *et al.,* 2004). ZnO can replace TiO_2 as a catalyst, since their photocatalytic treatment mechanisms are identical (Krishnakumar *et al.,* 2010; Wu *et al.,* 2010; Pirkanniemi & Sillanpää, 2002). The reactions below explain the photocatalytic reaction taking place with ZnO as a photocatalyst.

$$ZnO + hv \rightarrow h^+ + e^- \quad (7)$$

$$H_2O \rightarrow H^+ + \bullet OH$$

$$H^+ + OH^- \rightarrow HO\bullet$$

$$H^+ + H_2O \rightarrow H^+ + \bullet OH$$

$$e^- + O_2 \rightarrow \bullet O_2$$

$$O_2^- + H^+ \rightarrow HO_2\bullet$$

$$2HO_2\bullet \rightarrow \bullet O_2 + H_2O_2$$

$$H_2O_2 + \bullet O_2^- \rightarrow \bullet OH + OH^- + O_2 \quad (8)$$

(Mehrvar *et al.,* 2001)

2.8.2 Influence of TiO_2 and ZnO Structural and morphological character on wastewater photocatalytic treatment

The photocatalytic activity of a particular photocatalyst is affected by its structural and morphological characterization. The parameters that relate a photocatalyst and its efficiency include: - (i) light absorbing properties (ii) rate of reduction and oxidation of the molecule by photogenerated holes (iii) rate of electron hole recombination.
The particle and crystal size of individual catalyst powders affect photocatalytic treatment efficiency. Surface area measurements are calculated by the Brunauer Emmett Teller (BET) method. X-ray Diffraction (XRD) determines catalyst particle size and another technique used to estimate crystal size is Scanning Electron Microscope (SEM) technique, from which crystal sizes can be estimated by observing the scanned images.

2.8.2.1 Structural and Morphological characterization – ZnO/TiO_2

2.8.2.1.1 Scanning Electron Microscope (SEM)/ Brunauer Emmett Teller (BET)

The number of photon striking the photocatalyst controls the rate of reaction which signifies that the reaction takes place only in the absorbed phase of the photocatalyst availability of active sites where oxidative reactions can take place (Wang, 2004). The amount of the surface-adsorbed water and hydroxyl groups is related to the crystallite form and surface area. A large surface positively influences certain photodegradation reactions, as a large amount of adsorbed molecules promotes the reaction rate. (Cernigoj *et al.*, 2007).

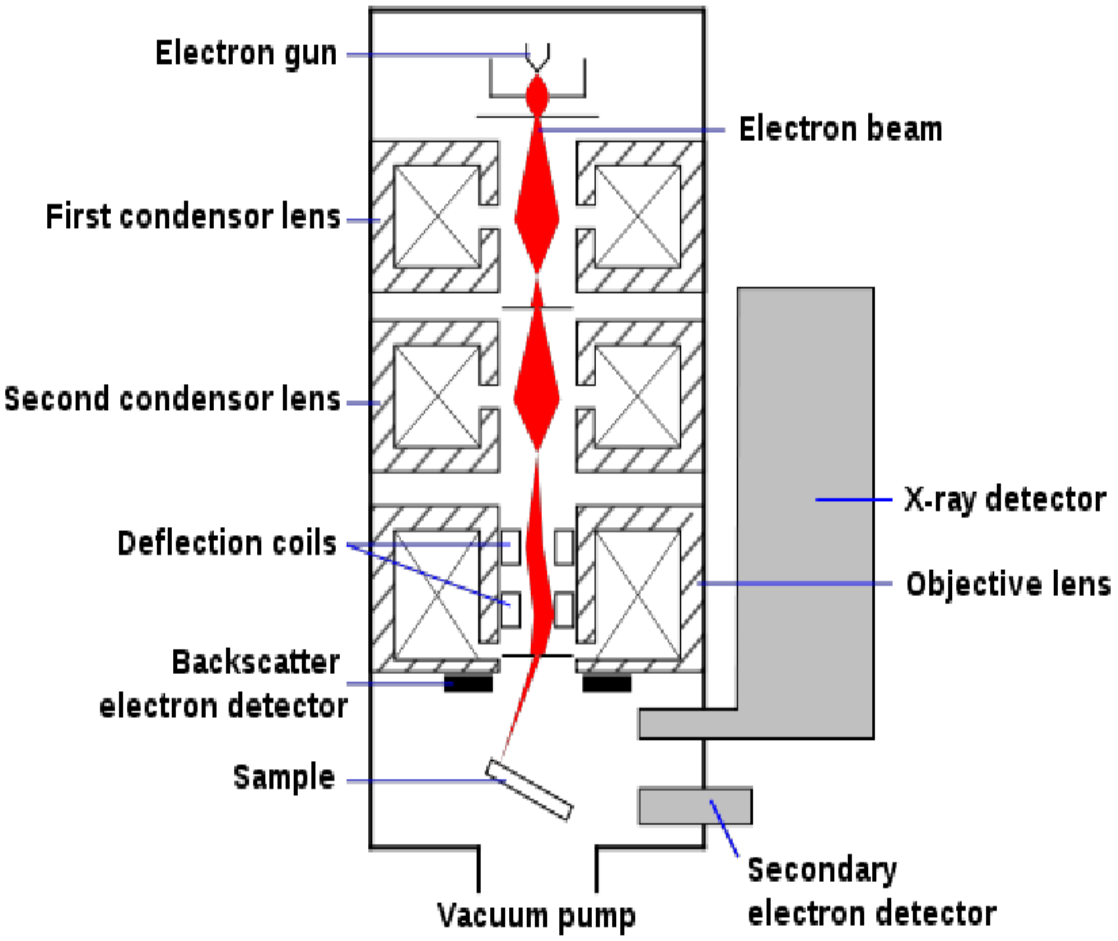

Figure 2.6 Scanning Electron Microscope apparatus

Source: (Cernigoj *et al.*, 2007)

2.8.2.1.2 X-Ray Diffraction (XRD)

Surface morphology such as particle size and agglomerate size, is an important factor to be considered in photocatalytic degradation process because there is a direct relationship between organic compounds and surface coverage of the photocatalyst (Yang, 2004). Particle size is an important parameter for photocatalytic efficiency, since the predominant way of electron/hole recombination may be different depending on the particle size (Cernigoj *et al.*, 2007). When the crystallite dimension of a semiconductor particle falls below a critical radius of approximately 10 nm, the charge carriers appear to behave quantum mechanically (Hoffmann *et al.*, 1995). A perfect balance between surface area and crystallinity must be found in order to obtain the highest photoactivity.

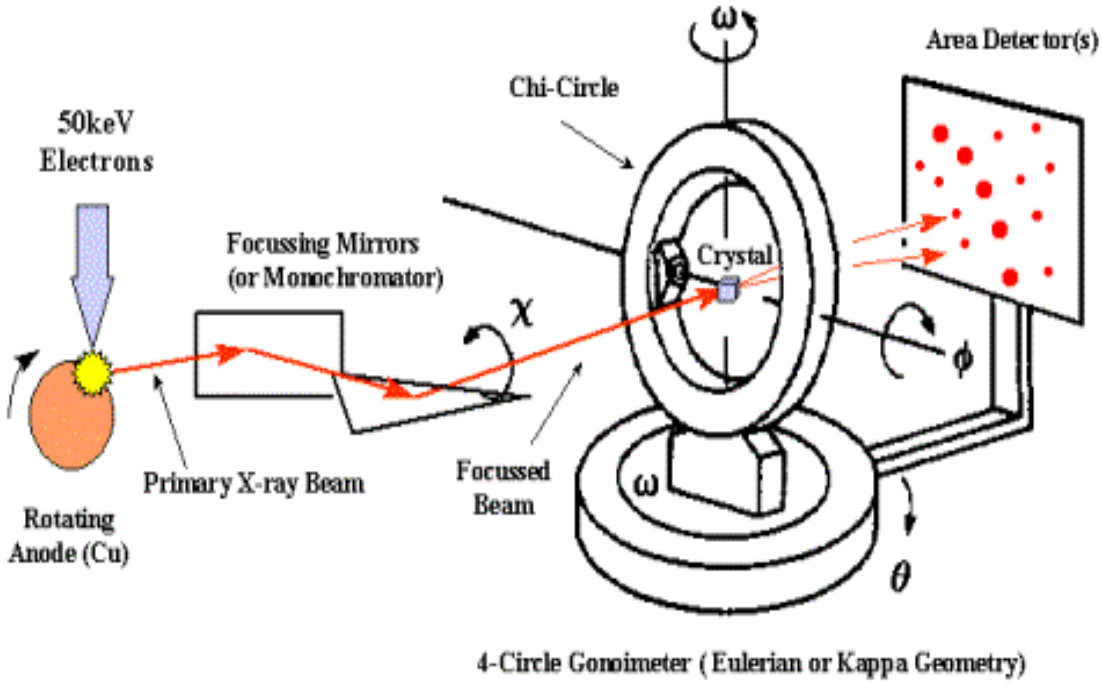

Figure 2.7 X-Ray Diffraction apparatus

Source: (Hoffmann *et al.*, 1995)

The crystal size of TiO_2 and ZnO powder is calculated using Scherrer's equation;

$$D = \frac{k\lambda}{\beta \cos\theta} \quad (9)$$

Where,

D Diameter of the grain,

K scherer constant (0.9) which depends on crystal shape, how width is determined, and the size distribution,

λ wavelength of X-rays in nanometers (λ= 0.15418 nm or 1.54Å),

β angle between the incident and diffracted beams in degrees (Full Width at Half Maximum, FWHM) in radians obtained by using the formula,

$\beta=2(\theta_2-\theta_1)$ (10)

θ Bragg's angle.

2.8.2.1.3 Energy Dispersive X-Ray Spectrometry (EDS)

Energy Dispersive X-Ray spectroscopy is a technique that analyses and characterizes samples to determine their elemental and chemical composition (Russ, 1984). This method relies on investigating the interactions between x-ray magnetic radiation and matter. It analyses the X-rays emitted by the matter after bombardment with charged particles. Each element has a distinct unique atomic structure (Russ, 1984). The number and energy of the X-rays emitted from the samples is measured by use of an Energy Dispersive Spectrometer. The energy of the X-rays is characteristic of the difference in energy between two energy levels of the element from which they are emitted. This allows the elemental compostion of the samples to be determined (Russ, 1984). The EDS experimental system comprises the following components.

i. X-Ray detector – detects and converts X-rays into electronic signals
ii. Pulse processor – measures the electronic signals to determine energy of each X-ray detected
iii. Multiple channel analyzer – displays and interprets X-ray data

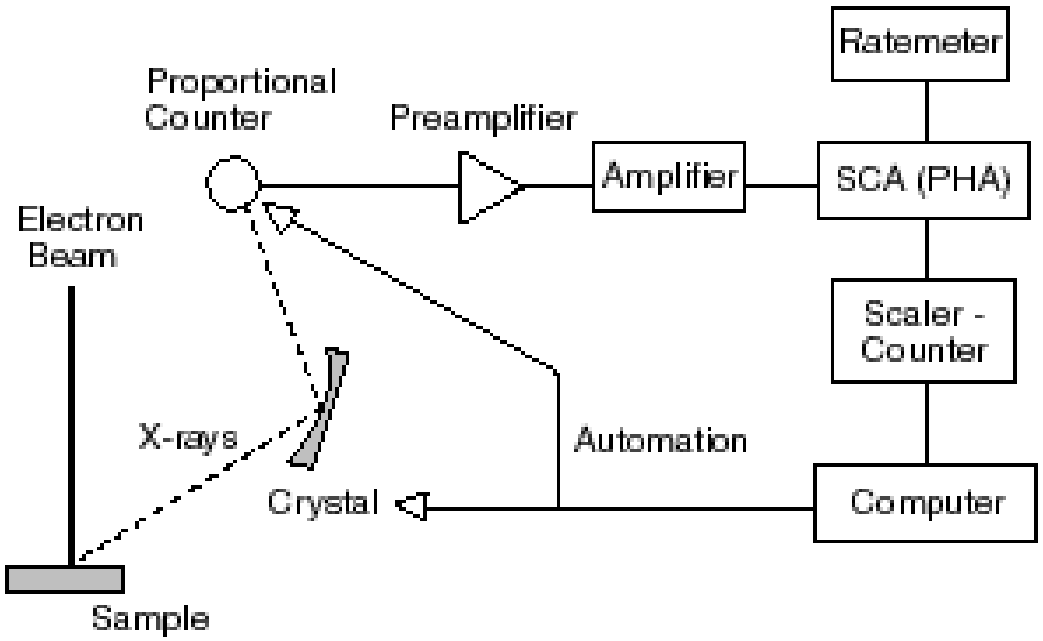

Figure 2.8 Energy Dispersive X-Ray Spectroscopy
Source: (Russ, 1984)

2.8.2.1.4 Laser Induced Break-down Spectroscopy (LIBS)

The LIBS system is used to analyse the elemental identification of chemical substances on the basis of atomic emission spectroscopy. The intense laser beam interacts with the samples and create a signal which is collected and transmitted to camera equipped with a delay generator.

The recorded emission spectrum represents the signature of various elements present in the samples (Gondal *et al.*, 2016). Ultra Violet and visible emission from the plasma can be resolved spectrally and recorded for quantitative and qualitative sample analysis.

It is important to optimize the experimental set-up, factors such as the delay time between excitation and data acquisition and laser influence on LIBS signal intensity. The wavelength of light provides information on the identity of elemental composition and the intensities indicate relative abundance (Gondal *et al.*, 2016).

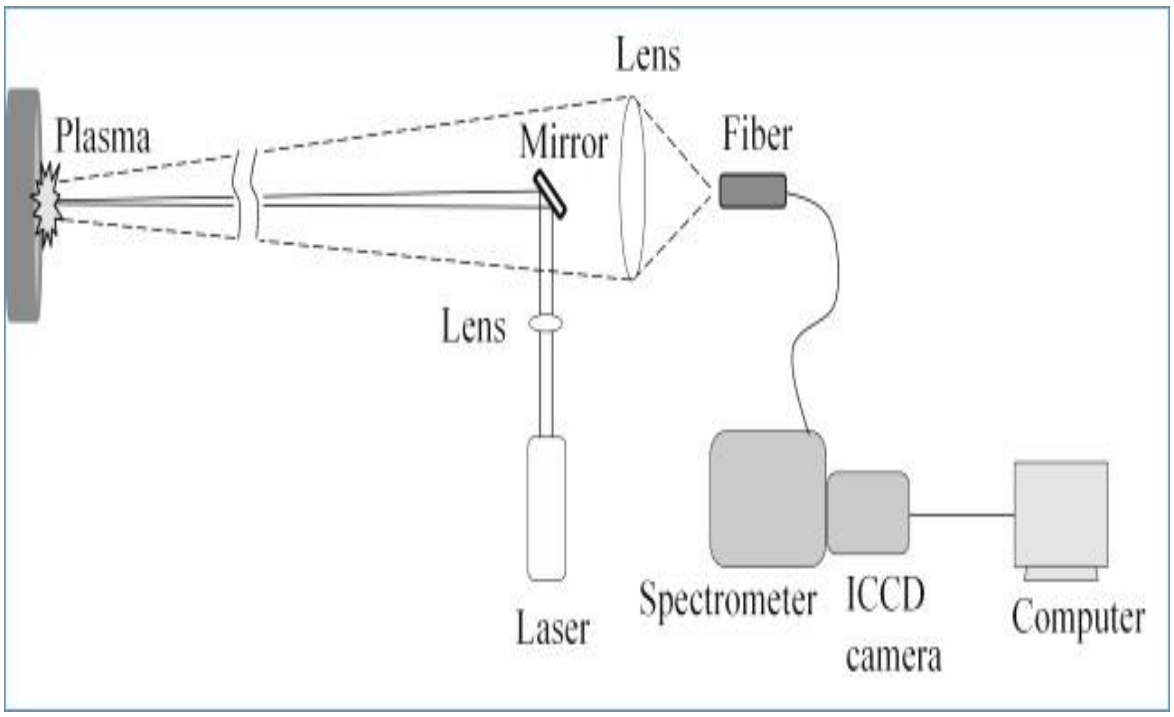

Figure 2.9 Laser Induced Breakdown Spectroscopy setup

Source: (Gondal *et al.*, 2016)

2.8.2.1.5 Ultra-violet / Visible spectrophotometry (UV/Vis)

The spectrophotometer measures the absorbance of a liquid sample in the UV (200 nm-400 nm) and Vis (400 nm-800 nm) regions of light spectrum. In coloured wastewater samples, treatment that leads to decolourization is measured as the decrease in colour intensity at a specific wavelength on the basis of the experimental measurements (Ajmal *et al.,* 2014. Colour as a water quality parameter is optimally monitored in the visible region. The Lambert-beer law gives the relationship between wastewater concentration and absorbance (Akyol *et al.,* 2004). To measure accurate changes in colour, accurate readings of light absorbance at different wavelengths in and near the visible part of the spectrum must be made.

$A = \varepsilon cd$

Where A is absorbance measured using spectrophotometer
c is concentration ($mol.dm^{-3}$)
ε is the molar extinction coefficient ($dm^3\ mol^{-1}\ cm^{-1}$)
d is the optical length (cm)

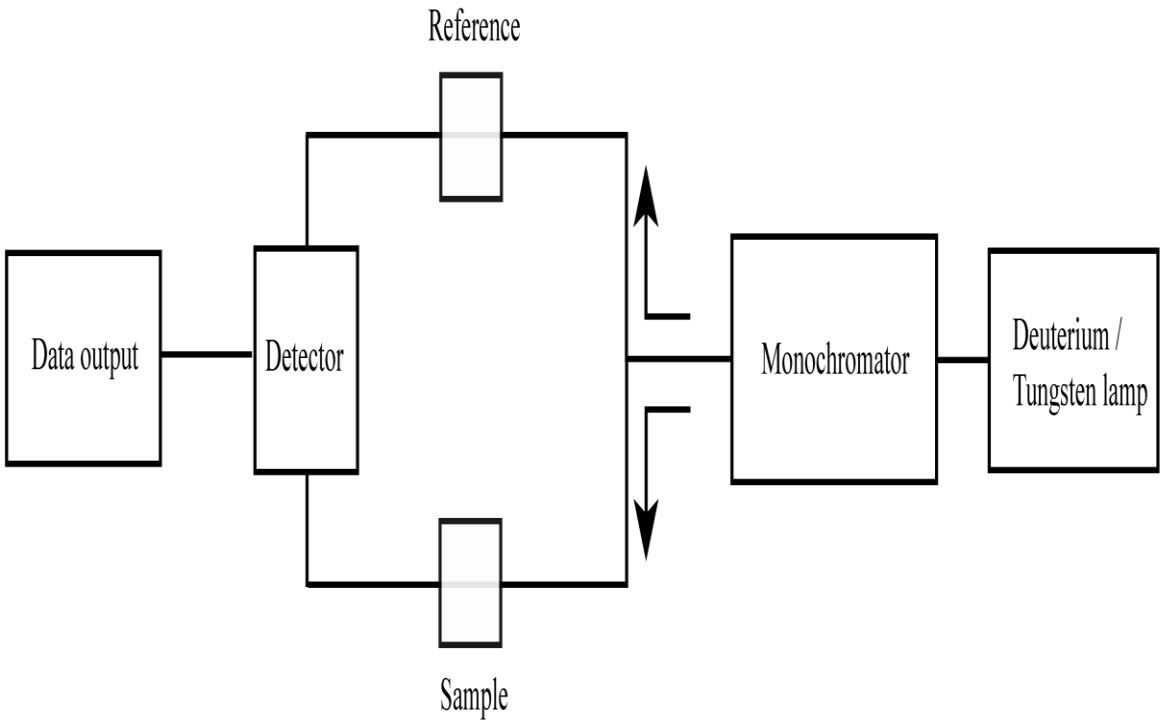

Figure 2.10 UV-Vis spectrophometry
Source: (Akyol *et al.*, 2004)

2.8.2.1.6 Atomic Absorption Spectroscopy (AAS)

Atomic Absorption Spectroscopy is an analytical method that quantifies/qualifies elements. The method supports procedures that determine the absorbance of radiation at a specific wavelength by vapour composed of ground state atoms. The concentrations of chemical elements present in a liquid sample based on energy absorbed from certain wavelengths of light (200 nm - 900 nm) measured in mg/l. An AAS instrument consists of a primary source that produces the spectrum of the element under detection, a monochromator and photon detector (Sharma and Bhattachrya, 2017). The persistent challenge caused by the brown colour of tea processing wastewater required the investigation of the levels of Al, Mn, Ni and Fe which are colour impactors and heavily present in tea infusions.

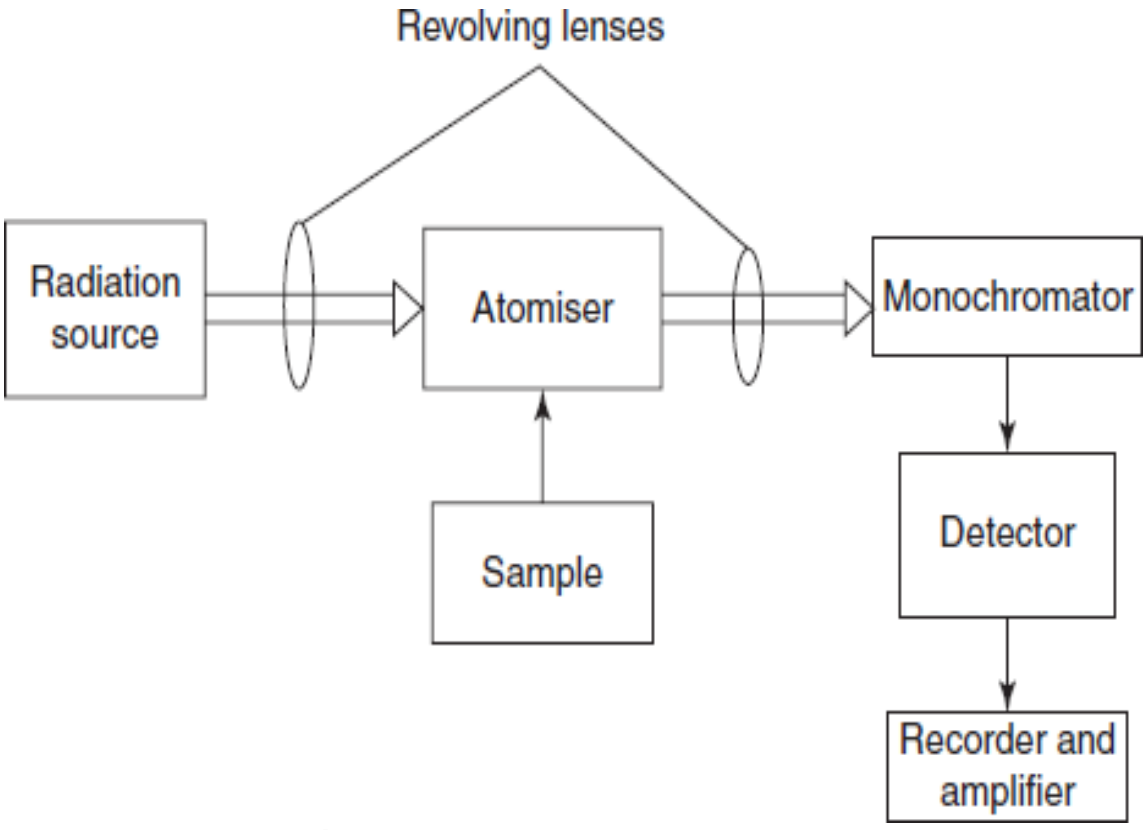

Figure 2.11 Atomic Absorption Spectroscopy

Source: (Sharma and Bhattachrya, 2017)

2.8.2.1.7 Gas Chromatography – Mass Spectroscopy (GC-MS)

GC-MS is an analytical technique that identifies unknown macromolecules present in a sample. The advantage of the GC-MS technique comes from the fact that not only are components of a mixture separated and detected quantitatively, but the detector provides information about the structure of each of the components identified. Compounds are identified by comparing the retention time to a standard and its mass spectrum. Unknown components are identified solely on its mass spectrum eliminating the need to run standards for retention time data. The column used in GC-MS is composed of a capillary column. Different columns may have bonded phases of different characteristics depending on the type of separation to be carried out (Lin *et al.*, 2013).

The formed components are ionized by electron impact. Various ions will have different amounts of internal energy. A parent ion has the same mass in atomic mass units as the neutral molecule. It reflects the highest mass peak in the spectrum. By using the same energy electrons to ionize the components, the mass spectra become highly reproducible. In this way, libraries of mass spectral data have been generated and an unknown compound can be identified by searching through and matching the mass spectra (Lin *et al.*, 2013).

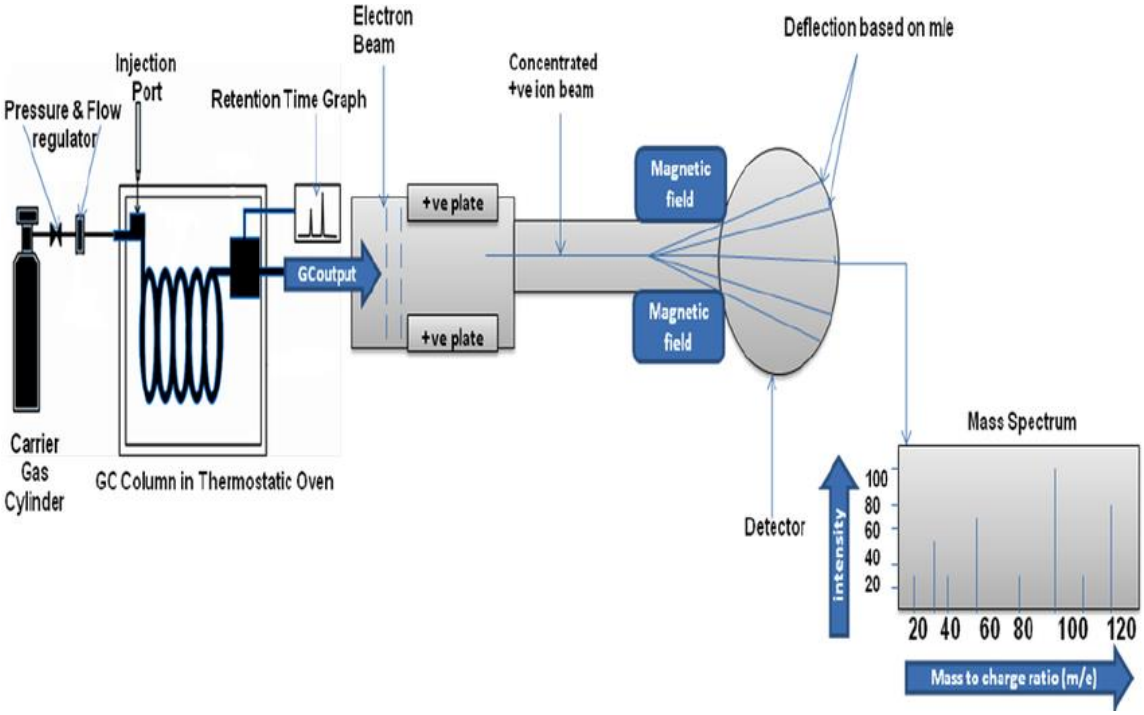

Figure 2.12 Gas Chromatography- Mass Spectrometry

Source: (Lin *et al.*, 2013).

CHAPTER THREE

3 Materials and methods

3.1 Sample collection

Five litres wastewater samples were collected every week, in the 3 factories for a duration of 8 months. The samples were collected in two 2.5 litre glass amber coloured bottles, placed in a cooler box at refrigeration 4°C. A total of 48 samples, 16 from each factory were collected.

3.1.1 Sampling sites

Three black tea processing factories found in Nandi County that include Chebut (CBH), Kibwari (KBH), and Nandi (NBH) were investigated were sampled for processing wastewater out of a total of 19 factories found in the whole county. The 19 factories process 600,000 Kgs green leaf daily. The altitudes and locational coordinates are indicated in Table 3.1 below.

Table 3.1 Location of sampling sites

Sampling sites	Altitude (metres)	Longitude	Latitude
CBH	1980	0°12´14´´N	35°6´18´´E
KBH	2114	0°5´32´´N	35°11´20´´E
NBH	2147	0°5´32´´N	35°11´20´´E

As shown in Table 3.1, the terrain in Nandi County is hilly and therefore suitable for black tea plantations.

3.1.2 Sampling period and atmospheric temperature

The average atmospheric temperature in Nandi County and the sampling duration recorded in Table 3.2 below.

Table 3.2 Sampling duration

Sampling sites	Sampling duration	Mean wastewater temperature
CBH	27/9/2015 – 29/11/2015	24.6°C
KBH	6/12/2015 – 28/2/2016	25.2°C
NBH	13/3/2016 – 29/5/2016	25.6°C

As shown in Table 3.2 the average atmospheric temperature in Nandi County during the entire duration of study was 25.1°C. Samples were collected over a duration of 8 months. The climatic conditions in Nandi County that lies in the Western Kenya highlands, are generally cool, humid and wet with an average annual rainfall of 2000 mm.

3.1.2.1 Map - Nandi County

Figure 3.1 shows an administrative map of Nandi County

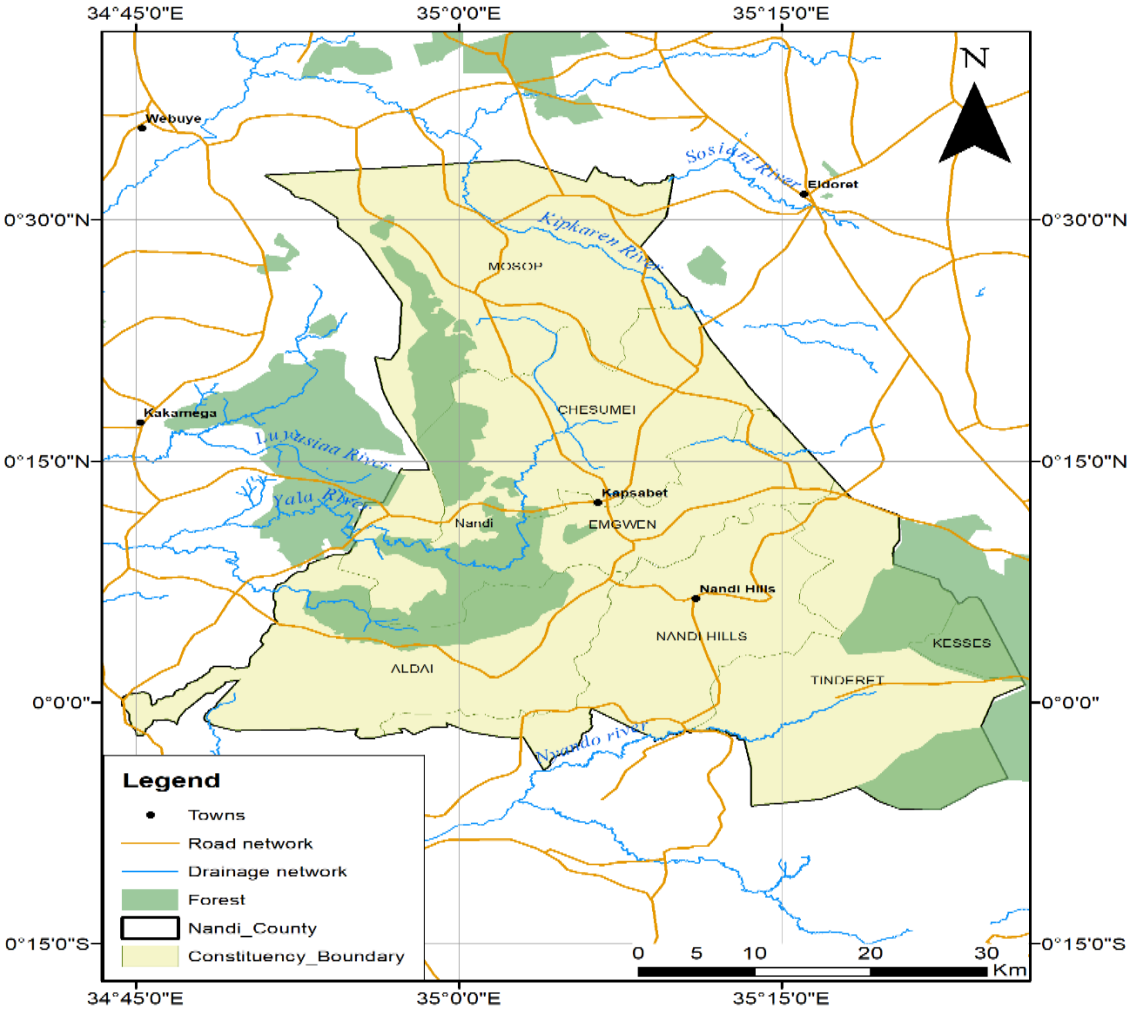

Figure 3.1: Map - Nandi County

Nandi County is one of the tea growing areas in the western Kenya highlands and also a major catchment area for rivers flowing into Lake Victoria. Chebut, Kibwari and Nandi tea processing factories are located around Nandi hills that forms a major catchment area for tributaries flowing into Yala and Nyando rivers. In 2017, production of green leaf stood at 71.4 Million Kgs, earning kshs. 21.4 billion.

3.1.2.2 Map - CBH factory

The location of the factory is shown in Figure 3.2 below.

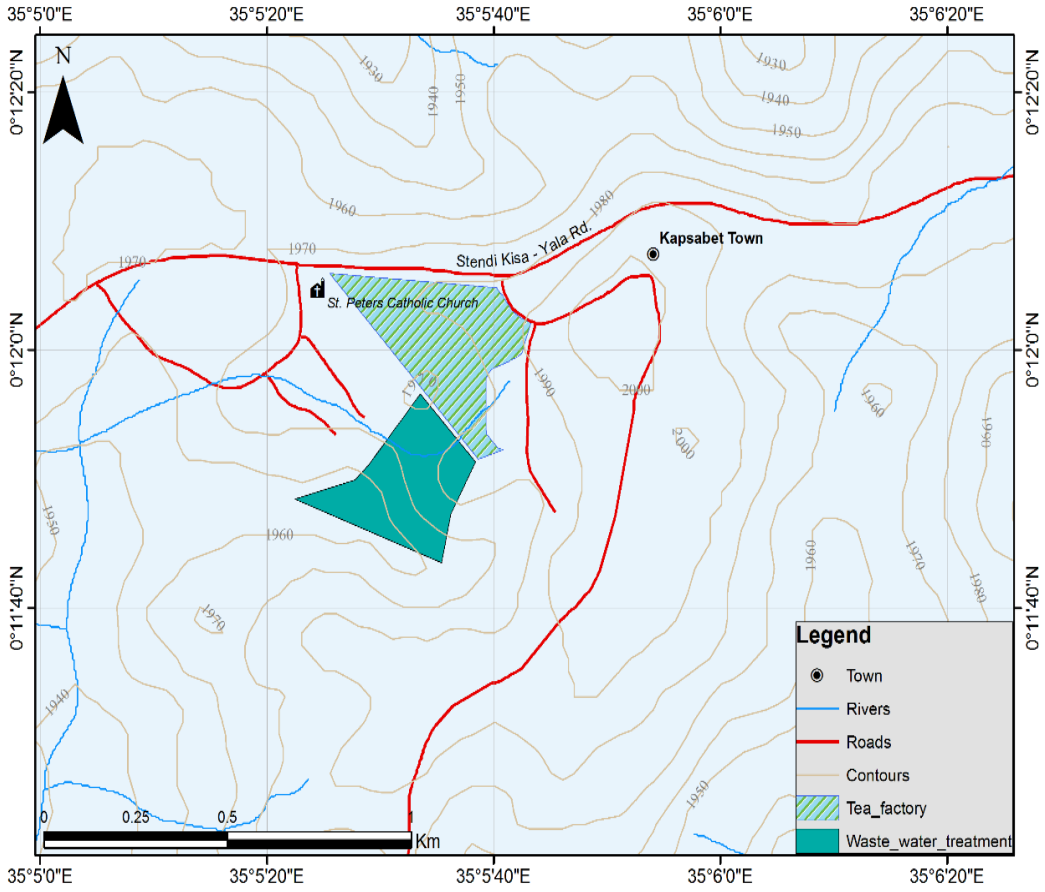

Figure 3.2 Map - CBH factory

CBH factory processes an average of 20 million Kgs annually through the CTC method. The large volumes of wastewater generated require effective treatment before eventual discharge into the environment.

3.1.2.3 Map - NBH factory

The location of the factory is shown in Figure 3.3 below.

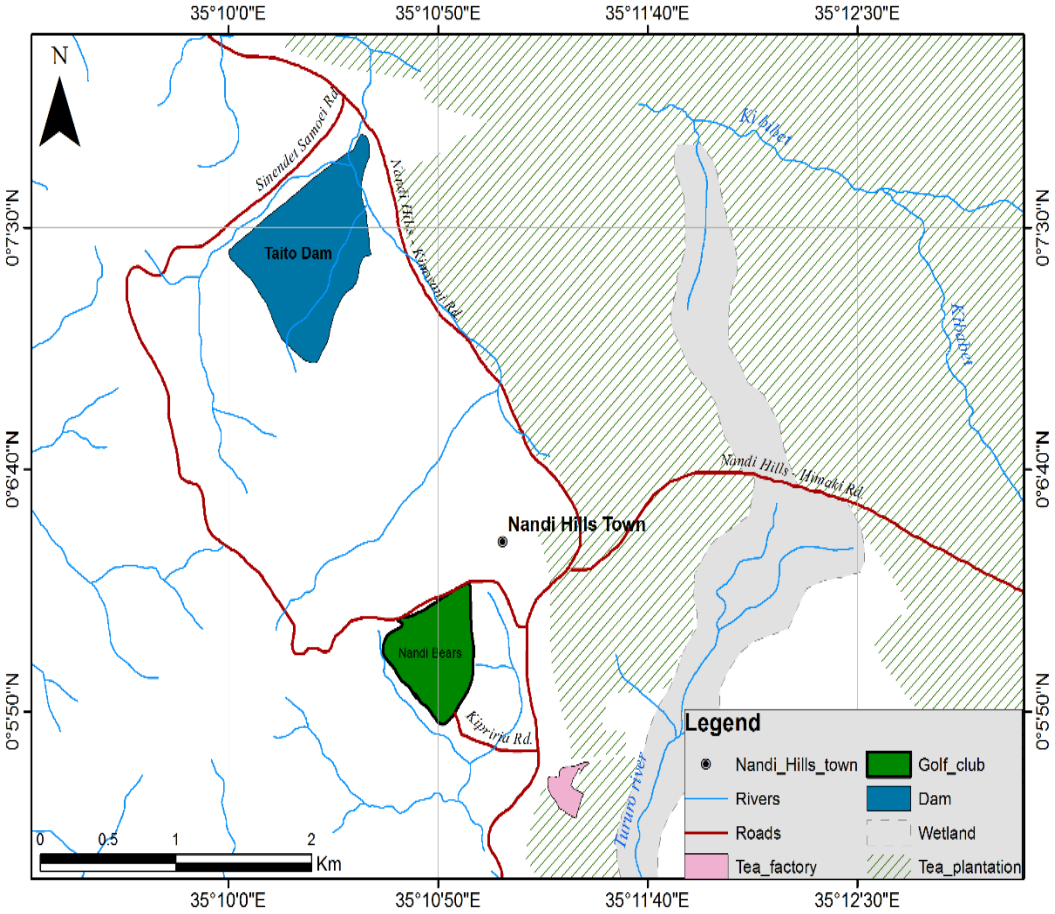

Figure 3.3 NBH factory

NBH factory processes 6 million Kgs of green leaf annually using the CTC technique. The subsequently generated wastewater is treated using a system of lagoons and stabilization ponds (SPs) found within the vicinity of the factory.

3.1.2.4 Map - KBH factory

Figure 3.4 below shows the location of KBH factory.

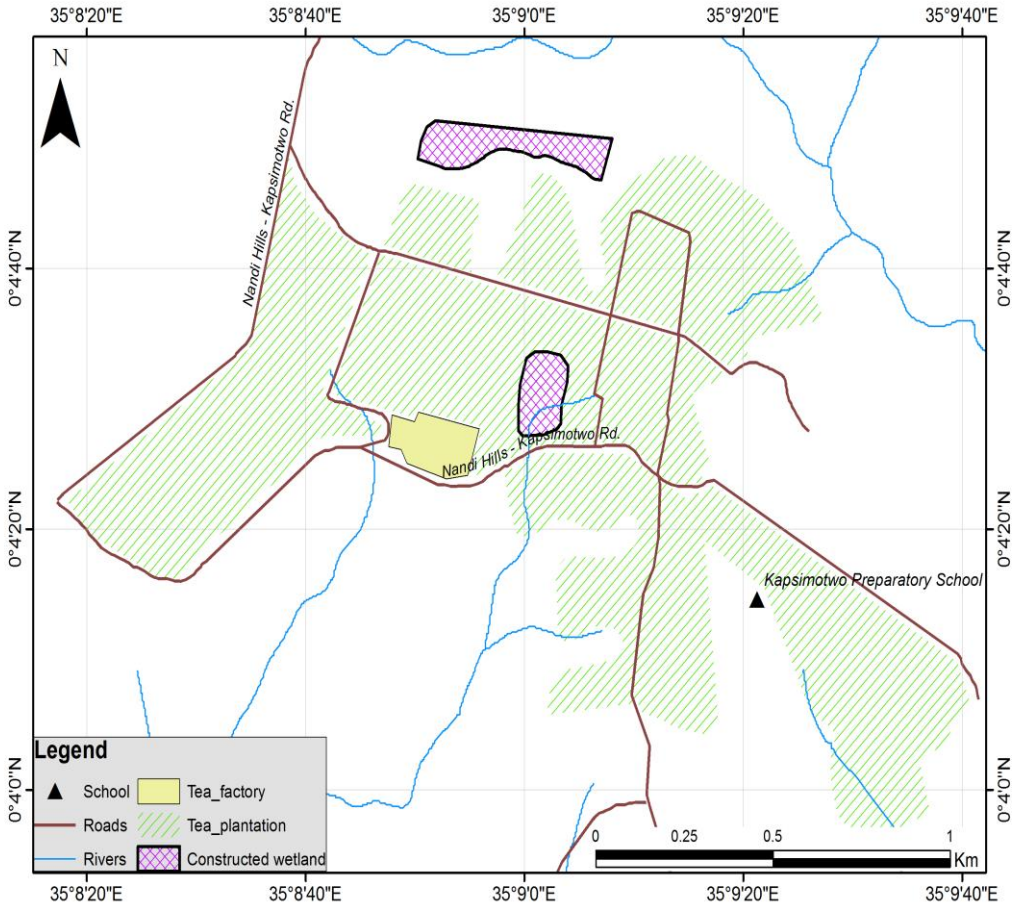

Figure 3.4 KBH factory

The factory is located near Nandi Hills town and has an annual processing capacity of 4 million Kgs using the CTC processing technique. The wastewater that forms after processing is diverted to a nearby constructed wetland (CW).

3.1.2.5 Rivers in Nandi County

Figure 3.5 shows the major rivers in Nandi County.

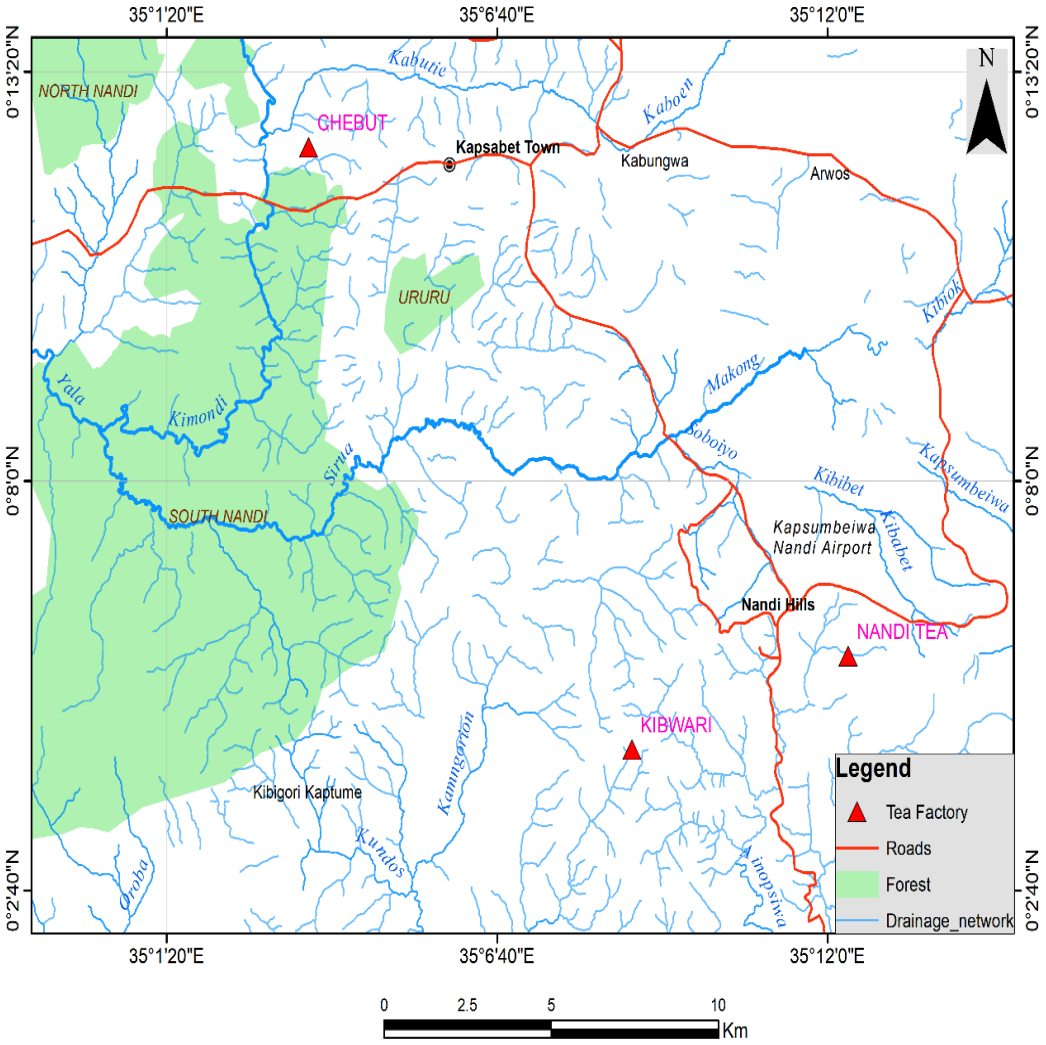

Figure 3.5: Major river systems in Nandi County

The rivers in Nandi County eventually flow into the Yala before eventually discharging into Lake Victoria. The rivers in Figure 3.5 flow from east to west.

3.2 Chemicals and Reagents

The chemicals and reagents used in the study are listed in Table 3.3 below.

Table 3.3 chemicals and reagents

Item No.	Chemical	Concentration	Manufacturer
1	Zinc oxide	500 g	ACME chemicals Ltd
2	Titanium dioxide	500 g	Degussa
3	Cellulose binder	2 g	ACME chemicals Ltd
4	Potassium dichromate	0.0042 M	Vishnu chemicals Ltd
5	Sulfuric acid	0.042 M	Sigma Ltd
6	Silver (II) sulfate	0.4 g	Okmar chemicals Ltd
7	Ferrous (II) Sulphate	0.695g	Vishnu chemicals Ltd
8	Mercuric sulphate	0.4 g	Vishnu chemicals Ltd
9	Sulphamic acid	100 ml	E.T Monks Ltd
10	Buffer solutions		Sigma-Aldrich Ltd
11	Ferrion indicator	2-3 drops	Sigma-Aldrich Ltd
12	Ferrous ammonium sulphate	0.25 M	Choice organochem Ltd
13	1,10-phenanthroline	1.485 g	Kobian Kenya Ltd
14	Cyclohexane	250 cm^3	E.T Monks Ltd
15	Ethyl acetate	300 cm^3	Kobian Kenya Ltd
16	Anhydrous sodium sulfate	60 g	Muby chemicals Ltd
17	Dichloromethane	500 cm^3	Sigma Ltd
18	Hexane	300 cm^3	Sigma Ltd
19	Acetone	200 cm^3	Kobian Kenya Ltd

The glass used to fabricate photoreactor was purchased from Eldoret Glazers. Reusable glassware such as (test tubes, conical flasks, measuring cylinders, beakers, volumetric, round bottomed flasks etc.), washed in hot soapy water before being rinsed in distilled water. They were then dried in an electric oven at 105°C for 1 hour and allowed to cool at room temperature before use.

3.3 Instruments

Table 3.4 below shows the list of equipment used in the study.

Table 3.4 equipment

Item No.	Equipment	Model
1	X- Ray Diffractometer	Philips X'pert MPD
2	UVP – radiometer Light intensity meter	UVA-365
3	UV/Vis spectrophotometer	Cecil 2041
4	Turbidity Meter La Motte	TC-3000
5	Atomic Absorption Spectrophotometer	AA 500
6	Gas Chromatography – Liquid Spectrometry	Agilent technologies 6890N
7	Laser Induced Breakdown Spectroscopy	Ocean Optics 2500
8	Scanning Electron Microscope	Tescan VEGA3
9	Energy Dispersive X-ray Spectroscopy	Oxford xMaxN
10	Pyranometer (Actinometer)	
11	Centrifuge	Mikro 200R Hettich
12	Oven	Fischer Scientific A-160
13	TOC-VE	Shimadzu
14	Pelletizer	NSP 001
15	Magnetic stirrer	LMS-1003
16	Artificial UV lamps – 15W Black light fluorescent lamps	Sylvania
17	Weight balance	Memmert UM 400
18	Calciner	classic Clare 4.0
19	Heating mantle	Labtech Ltd
20	Homogenizer	Model – UP 2005
21	Carbon analyzer	TCA-08
22	300-mm double surface condenser	Liebig, Friedrichs, West
23	Nephlometric turbid meter	2100P
24	pH meter	Japan Ltd

3.3.1 UV light source (UV lamps)

The first set of experiments required UV light irradiation from 2 UV lamps 15 W and 18 cm long fitted 10 cm above the wastewater solution in the reactor proto-type. The lamps emitted light of wavelengths between 320 nm - 400 nm. All the UV light induced photocatalytic degradation reactions took place at room temperature.

3.3.2 Solar light

A second set of experiments mediated by solar light was repeated following the procedure described in (section 3.3.1). The solar mediated photocatalytic treatment reactions were done between 11 am and 3 pm to maximize on the sunshine hours available.

3.3.3 Preparation of ZnO and TiO_2 surface layers

Several TiO_2 and ZnO surface layers of dimensions (18 cm × 13 cm) were prepared on clean and degreased borosilicate glass plates by immobilization from sediments of their aqueous suspensions c = (10 gL^{-1}) in a rounded-bottomed flask of volume 250 cm^3. An ultra-sonic homogenizer was used to break-down any agglomerates that may be present in the aqueous suspension making suspension uniform. A 10 cm^3 syringe of was used to immobilize 28.8 cm^3 of the prepared suspension onto the glass layers ensuring an optimum catalyst loading of 0.5 mg/cm^2. The surface layers were left to dry in ambient air for about 2 hours and further dried in an oven at a temperature t = 50 °C. In order to fixate the catalyst suspension on the glass layer, the surface layers were finally annealed at 300°C for 1 hour.

3.3.4 Preparation of ZnO and TiO_2 pellets

Small pellets comprising ZnO and TiO_2 powder catalysts were prepared using a pelletizer by measuring an amount of 0.5 g of the powder catalyst and 0.1 g of a cellulose binder. The mixture was then mixed uniformly before being pressed together to from the pellets.

3.3.5 Fabrication of photocatalytic reactors

3.3.5.1 Photocatalytic reactor fitted with UV lamps

A reactor proto-type of dimensions (20 cm×15 cm×10 cm) fitted with 2 UV lamps was fabricated from borosilicate glass as depicted in Fig. 3.6. The reactor was fitted with two 15 W UV lamps emitting UV light of irradiation flux intensity (I=3.0 mW/cm^2) and a magnetic stirrer. A volume of 500 cm^3 of filtered wastewater sample was put into the photoreactor to a height of approximately 2 cm. The base of the photoreactor was fitted with the surface layer containing ZnO or TiO_2 powder photocatalyst prepared in (Section 3.3.3) above. The UV lamps were fitted at a height of cca. 10 cm above the wastewater samples in the reactor. To monitor progress in photocatalytic treatment, 3 cm^3 of the samples were removed after every 15 minutes and its absorbance measured at $\lambda = 410$ nm by a UV/Vis spectrophotometer. The wastewater samples were treated for a duration of 180 mins.

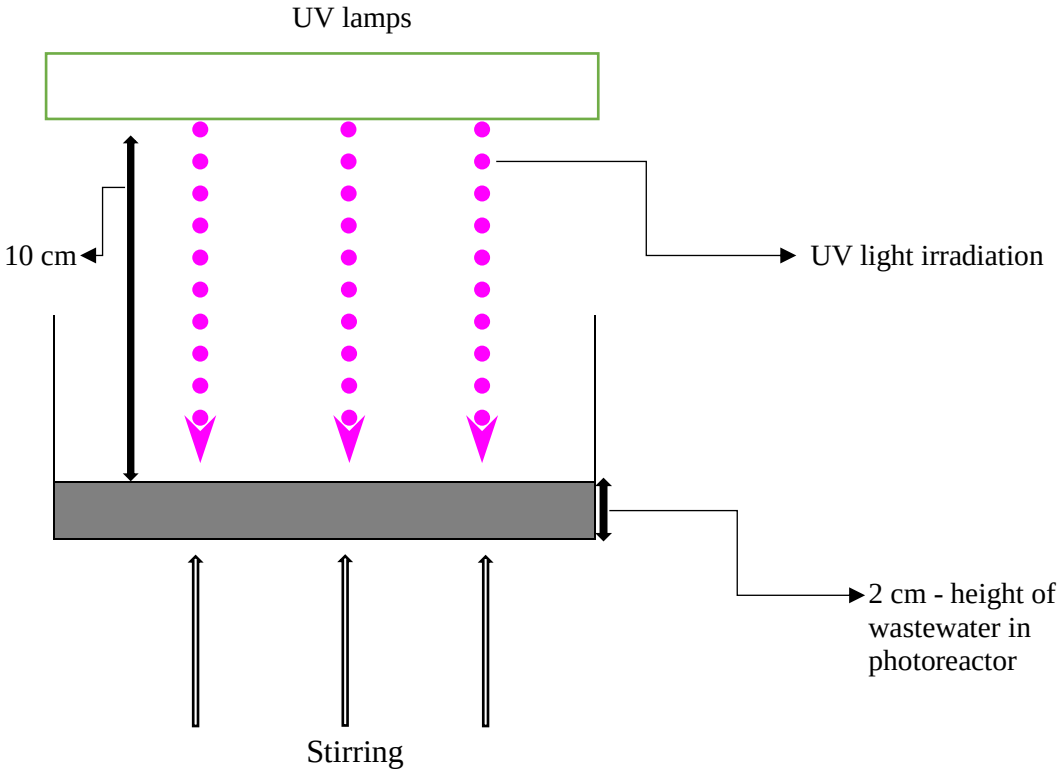

Figure 3.6: UV lamps induced photocatalytic reactor

3.3.5.2 Photocatalytic reactor irradiated by solar light

A second set of experiments similar to the reactions described in section (3.3.5.1) were repeated mediated by solar light as shown in Fig. 3.7. The average irradiation flux intensity was measured and determined to be 1.45 mW/cm^2. To monitor photocatalytic degradation of wastewater samples, 3 cm^3 were drawn every 15 minutes using a pipette and its absorbance determined by a UV/Vis spectrophotometer at $\lambda = 410$ nm. The photocatalytic treatment reactions were done for a maximum irradiation time of 180 minutes. The solar mediated treatment reactions were done between 11 am and 3 pm to maximize on the sunshine hours available.

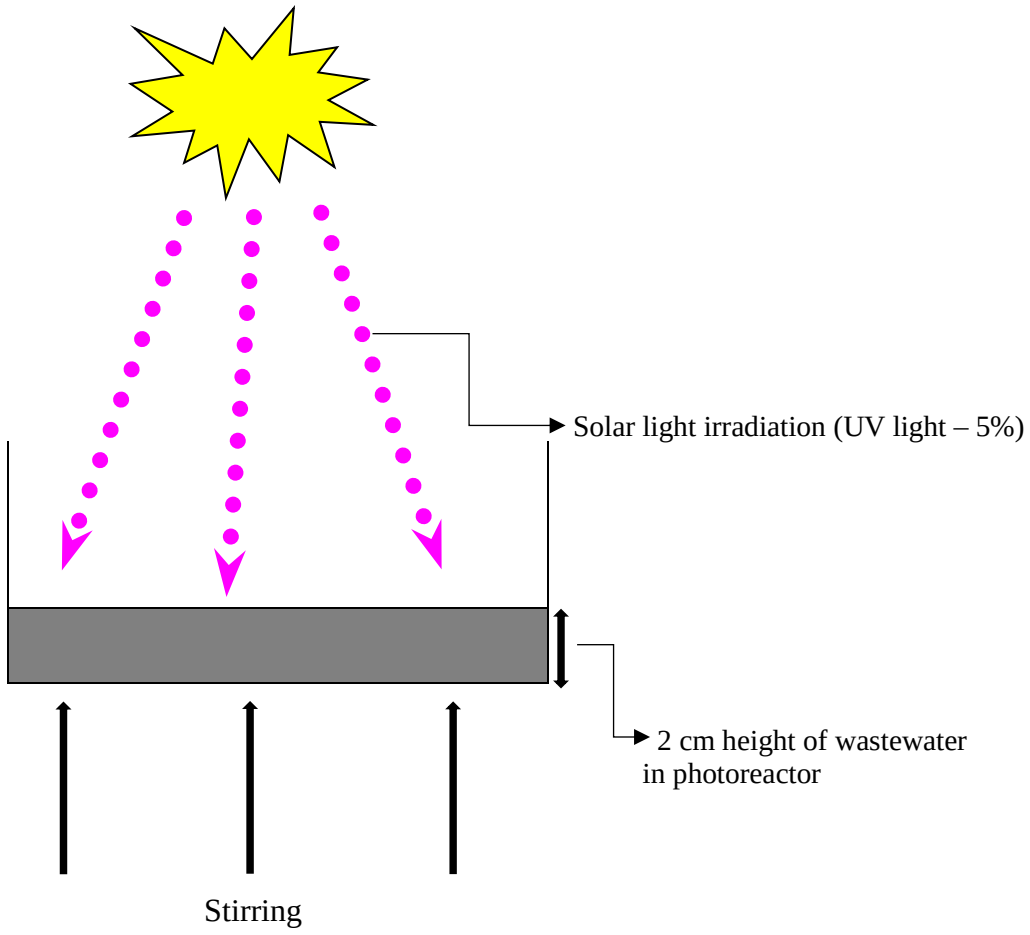

Figure 3.7: Photocatalytic reactor irradiated with solar light

3.3.6 Experimental design

A volume of 500 cm^3 of wastewater was sampled and filtered under gravity into 250 cm^3 Erlenmeyer flasks and placed into 500 cm^3 beakers. The filtered solution was then put into photocatalytic reactors described in sections whose base was coated with a layer of ZnO or TiO_2 catalyst powders as described in Sections (3.3.5.1) and section (3.3.5.2).
The wastewater sample in the photoreactor was at a height of cca 2 cm from bottom bed. The photoreactor was placed on top of a magnetic stirrer to ensure sample homogeneity during the photocatalytic degradation reactions. The photoreactor was illuminated using 2 UV lamps producing irradiation at wavelength λ =365 nm of intensity 3.0 mW/cm^2 for a maximum duration of 180 mins. A second set of experiments were repeated as above with solar light irradiation of intensity (I= 1.45 mW/cm^2). The degradation of colour intensity of the wastewater sample was measured using a UV/Vis spectrophotometer at λ= 410 nm. Samples of 5cm^3 were drawn every 15 minutes and absorbance measured for a duration of 180 minutes.

3.4 Methods

3.4.1 Measuring light intensity

3.4.1.1 UV lamps

The intensity (amount of UV energy on the wastewater per unit area expressed in (mW/cm^2) of the UV lamps was measured by a radiometer (UVA-365) to measure the maximum irradiation flux density. The radiometer was placed at a height (10 cm) similar to distance between the UV lamps and wastewater sample. The UV metre directly faced the UV lamps emitting radiation. The readings were taken as a grid i.e. from right, left and centre to determine the homogeneity of the result. The intensity is measured as energy output in mW/cm^2 in the range between 200 nm - 400 nm. The results show spectra irradiance i.e. intensity at each wavelength.

3.4.1.2 Solar light

A Pyranometer was used to measure solar irradiance on a planar surface. The solar light irradiance were recorded at a meteorological station in Nandi County.

3.5 Physico-Chemical characterization of Raw and Treated wastewater

Wastewater was analysed to determine their physico-chemical properties i.e. colour, pH, Turbidity, Total Organic Compounds, Chemical Oxygen Demand, Total Suspended Solids and Total Dissolved solids.

3.5.1 pH

The digital pH meter was switched on and allowed to stand for some time and then calibrated using appropriate standards supplied by the manufacturer.

- 30 cm^3 of the sample was poured into a beaker
- The probe was then thoroughly rinsed with distilled water and the pH mode switched on.
- The probe was then immersed into the sample
- Homogeneity between the probe and the sample was insured by stirring the sample using a stirring bar to establish equilibrium.
- The pH reading was read and recorded
- The electrode was then rinsed thoroughly with distilled water
- After use, the electrode was placed in the beaker containing distilled water

3.5.2 Turbidity

The operating mode of the turbid meter was selected at “auto” mode.

- Three clean matched sample cells were used.
- The turbid meter was switched on and calibrated according to the manufacturer supplied operating manual and supplied standards.
- A sample cell was rinsed and cleaned with distilled water and the wastewater sample.
- The wastewater samples were rapidly poured into the sample cell avoiding touching the cell walls.
- Any condensation that forms on the walls of the sample cell was wiped using a clean lenses tissue.

- The sample cells containing the samples were inserted into the cell holder and digital turbidity readings recorded.
- The procedure was repeated at least twice using fresh samples until sequential readings fall within ± 10 percent and recorded in Nephlometric Turbidity Units (N.T.U) units.

3.5.3 Total Organic Carbon – Direct method

The direct method involved wastewater samples being oxidized to carbon dioxide by persulfate digestion. The carbon dioxide that is formed then diffuses into a coloured pH indicator solution where converted to carbonic acid was. The resulting colour change is directly proportional to the concentration of carbon present in the samples. The procedure proceeded as follows.

- A volume of $10cm^3$ of the sample was added to a persulfate solution placed in a digestion tube. The persulfate and digestion reagent oxidised the carbon in the wastewater sample to carbon dioxide.
- An opened ampule of pH indicator reagent was inserted into the digestion tube.
- The tube was then securely sealed
- The assembled unit was digested at 105°C for a duration of 2 hours. The carbon dioxide formed diffuses into the inner ampule and forms carbonic acid. The acid converts the pH of the indicator and colour. The change in colour (indicator) is related to the initial amount of organic carbon present in the wastewater sample. The amount of carbon present in the wastewater sample is equal to the concentration of carbonaceous material in the wastewater.
- After cooling, the complete unit was placed into a suitable photometer for colour measurements.

3.5.4 Chemical Oxygen Demand (COD) (mg/L) – closed reflux titrimetric method

The dichromate technique was used to determine COD of the wastewater samples. The excess chromate was determined through back titration with ferrous ammonium sulphate using the ferrion indicator to detect the end point. The chemicals required to measure the COD of wastewater samples included;

1) 0.042 M Sulfuric acid

2) standard potassium dichromate solution (made by dissolving 12.3 g of $K_2Cr_2O_7$ primary standard grade, dried at 103 °C for 2 hours, in distilled water and diluted to 1 litre);
3) 0.0042 M dilute standard potassium dichromate solution (made by diluting 100 ml of the standard potassium dichromate solution to 1 litre);
4) 0.25 M of standard ferrous ammonium sulphate solution (made by dissolving 98 g of $Fe(NH_4)_2 (SO_4)_2 .6H_2O$ analytical grade crystals in distilled water added to 20 ml of H_2SO_4 and diluted to 1 litre)
5) 0.025 M dilute standard ferrous ammonium sulphate solution (made by diluting 100 ml of the standard ferrous ammonium sulphate solution to 1 litre), standardized against the 0.0042 M dilute standard potassium dichromate;
6) 0.4 g silver sulphate, reagent powder directly in powder form;
7) mercuric (II) sulphate, analytical grade crystals;
8) ferroin indicator solution 0.695 g of ferrous sulphate, $FeSO_4.7H_2O$ dissolved in H_2O to which 1.485 g of 1,10-phenanthroline monohydrate was added , swirling until the solution is dissolved and then diluted to 100 cm^3,
9) Sulphamic acid, analytical grade to eliminate interference of nitrites (APHA, 2005).

Procedure

20 cm^3 of the sample and 10 cm^3 of standard dichromate solution were transferred into a 250 cm^3 Erlenmeyer flask. 0.4 g of Mercuric (II) Sulphate and 30 cm^3 of the concentrated, sulphuric acid was carefully poured into the solution and thoroughly mixed until a uniform solution was appeared. The flask containing the solution was covered with a clean cover glass and allowed to stand for at least 30 minutes in a boiling water bath. The solution in the flask was topped up to 75 cm^3 with distilled water. 2-3 drops of ferrion indicator was added and solution titrated with ferrous ammonium sulphate. The solution changed from yellow-orange to blue-green. At end point, the solution turns reddish brown and the results tabulated. A reagent blank was also prepared using 20 cm^3 of distilled water (APHA, 2005).

3.5.5 Total Suspended Solids (TSS)

Total suspended solids (TSS) in the samples were determined by the following steps:-

- 3 dry filtration papers were weighed to measure their weights (mg)
- 3 samples each of volume 1 L were filtered into 1000 cm^3 flat-bottomed flasks.
- The 3 filter papers containing residue from filtration were dried in an oven at a temperature of 105°C
- The filter paper was removed from the oven and its weight measured every 60 minutes until there was little or no change in its weight.
- The TSS of the samples in (mg/L) was determined by the averages in the differences between the weight of dry filter papers and final weight of the oven dried filter papers.

3.5.6 Total Dissolved Solids (TDS)

100 cm^3 wastewater filtered in (3.4.6) above was used to determine Total Dissolved Solids (TDS). The procedure included:-

- The weights of 3 empty 50 cm^3 beakers (g) was determined
- 100 cm^3 of the wastewater is transferred into each of the 3 beakers
- The beakers are placed into an oven heated to a temperature of t = 105°C for a duration of 2 hours.
- After 2 hours the beakers are taken out of the oven and weighed
- The average differences in weights between the beakers before and after heating is the TDS of the samples in (mg/L).

3.6 Decolourization of wastewater

3.6.1 Colour measurement by UV/Vis spectrophotometer

Colour of the wastewater samples were analysed by measuring their absorbance using a UV/Vis Spectrophotometer. Quartz cuvettes were used in the analysis. A cuvette containing distilled water (blank) was placed in the sample compartment with the transparent sides facing the light source and the sample compartment lid was closed. The transparent sides of the cuvette were kept dry and clean.

- The auto zero button was pressed to set zero absorbance
- The distilled water was discarded and a cuvette containing the wastewater sample was placed in measuring position.
- The sample compartment lid was closed and the “start button” pressed to start colour measurement

- The absorbance units obtained were recorded and reported as colour units

3.6.2 Spectral analysis of wastewater

Decolourization of the wastewater was measured as a decrease in colour intensity using a UV-Vis spectrophotometer.

- A volume of 20 cm^3 of CBH, NBH and KBH samples were filtered into a 50 cm^3 beaker
- One quartz cuvette was cleaned and dried using distilled water and linen tissue to ensure the transparent side remained clear.
- UV-Vis spectrophotometer was switched on
- A cuvette (optical length 1 cm) containing distilled water (blank) was placed in the sample compartment with the transparent sides facing the light source and the sample compartment lid was closed.
- The auto zero button was pressed to set zero absorbance
- A full UV-Vis scan of CBH, KBH and NBH samples was done at wavelengths between 350 nm-520 nm.

3.6.3 Photocatalytic decolourization of wastewater

Changes in colour intensity with increase photocatalytic treatment time was measured by a UV-Vis spectrophotometer. Reduced absorbance values with increased solar-UV light irradiation light showed increased wastewater decolourization efficiency.

To determine changes in absorbance, mixing and irradiation of the wastewater is interrupted every 15 mins. Afterwich 3 cm^3 of the sample is removed from the reactor and put into a cuvette of optical length 1 cm and its absorbance measured at 410 nm. After absorbance measurements, the sample is placed back into the reactor and irradiation resumed. The photocatalytic treatment proceed for a reaction time of 180 mins. Confirmatory reactions time indicates minimal changes in absorbance beyond 3 hrs of treatment.

The decolourization efficiency for the samples was calculated as follows;

$$\text{Decolourization (\%)} = \frac{Co-C}{Co} \times 100 = \frac{Ao-A}{Ao} \times 100 \quad (11)$$

Where Co is the initial concentration

c variable concentration

Ao is the initial absorbance

A variable absorbance

In addition to colour intensity, the final Total Organic Carbon and Chemical Oxygen Demand parameters of the samples are useful to estimate progress in photocatalytic treatment.

3.6.4 UV-ZnO film decolourization system

A description of the photoreactor set-up is described in section (3.3.5.1) and equipped with two 15W UV lamps. In addition, a ZnO surface layer prepared as described in section (3.3.3) and fitted at the base of the photoreactor. 500 cm^3 of wastewater sample was put into the reactor and irradiated by UV lamps whose irradiation flux intensity (W/cm^2) was measured by a digital UVP meter. A stirrer was used to ensure uniform mixing in the photoreactor.

3.6.5 Solar-ZnO film decolourization system

The photoreactor set-up is described in section (3.3.5.2). The experimental conditions are similar to those described in section (3.5.4) apart from solar light that supplied irradiation for photocatalytic treatment. The solar irradiation flux density (mW/cm^2) was measured over a period of 6 months using a solar intensity meter during sunny days between 11am to 3pm.

3.6.6 UV/TiO_2 film – decolourization system

The photoreactor set-up for the reactions is described in section (3.3.5.1). A TiO_2 Surface layer is inserted at the base of the photoreactor fitted with two 15W UV lamps that irradiated 500 cm^3 of wastewater. The intensity of the UV lamps (W/cm^2) was measured using a digital UVP meter.

3.6.7 Solar /TiO_2 film – decolourization system

This experimental procedure was similar to section (3.6.5). TiO_2 was immobilized on a glass surface layer

3.7 Macro-molecules in tea processing wastewater

3.7.1 Gas Chromatography –Mass Spectrometry

1) A volume of 50 cm^3 of wastewater was mixed with anhydrous sodium sulphate (20 g) and transferred into an Erlenmeyer flask with a mixture of 100 cm^3 hexane, acetone (60:40, v/v) and dichloromethane.
2) The flask containing the solution, was put into an ultrasonic bath for 30 minutes. The extract was then filtered through another layer of anhydrous sodium sulphate.
3) The filtrate obtained after solvent evaporation was dissolved in 5 cm^3 solution mixture of cyclohexane: ethyl acetate (50:50, v/v) and filtered through the polytetrafluoroethylene (PTFE) filter with a pore size of 1 µm.
4) The step of PAHs isolation cleanup procedure was carried out by gel permeation chromatography (GPC) and column TSK Gel G1000HXL (300 mm x 7.8 mm, 5 µm).
5) Chromatographic separation was performed by isocratic method with mixture cyclohexane: ethyl acetate (50:50, v/v) used as mobile phase. Samples were eluted at a flow rate of mobile phase of 0.8 cm^3/min.
6) The purified extract of PAHs was subjected to concentration, then dissolved in toluene and analysed by GC-MS solution software was used for data processing, and Shimadzu GC-MS Metabolites spectral Database and NIST 2008 mass spectral library were used as the mass spectral libraries.

3.8 Chemical elements in tea processing wastewater

3.8.1 Atomic Absorption Spectroscopy

Wastewater samples were collected using new PET bottles and transported to the laboratory for analysis in a cooler box at temperatures below 4°C. The samples were stored under refrigeration in the laboratory. The following steps were followed to determine the chemical elements in wastewater:

The process of atomic absorption spectroscopy involves two steps;

a) Atomization of the wastewater
b) Absorption of radiation from a light source to free atoms

Preparation of standard solutions

Standard solutions of Aluminum (Al), Manganese (Mn), Nickel (Ni) and Iron (Fe) metal concentrations in water were prepared in water .The standards were prepared within the working range of the method and stored under refrigeration at 4°C.

For the procedure involving air-acetylene flame:

1) Installation of the hollow cathode lamp for the specific metal being analysed at roughly at the desired wavelength
2) The slit-width and lamp current is set and the instrument allowed to warm up until stability is achieved.
3) The wavelengths were adjusted until optimum energy is gained. The lamp was thereafter aligned according to manufacturer's instructions.
4) The air-acetylene burner was installed and the burner head position adjusted turn on air and adjust flow rates to give maximum sensitivity for the metal being measured. Acetylene was then turned and adjusted to ignite flame.
5) A standard solution of the desired metal was aspirated and adjusted. The aspiration rate of the nebulizer was also adjusted to ensure maximum sensitivity. A standard solution was aspirated near the middle of the linear working range and the burner adjusted vertically and horizontally to obtain maximum response. The instrument was then ready for use.
6) On completion the flame is extinguished by turning off the acetylene first and then followed by air.

For determination involving nitrous oxide acetylene, the process proceeds as in (1) to (3) above followed by:

4) The nitrous oxide-acetylene burner was installed and its burner head adjusted to position. The acetylene was turned on without igniting the flame and its flow rate adjusted to the specified value. The nitrous oxide was then turned on. After ignition the burner was allowed to come to thermal equilibrium before analysis is started.
5) A standard solution of the desired metal was aspirated and the aspiration rate of the nebulizer adjusted to achieve maximum sensitivity. A standard solution was aspirated near the middle of the linear working range and the burner adjusted vertically and horizontally to achieve maximum response.
6) The instrument was then ready for analysis

Further measurements involve:

1.) Filtration of the sample when necessary to avoid clogging the atomizer burner
2.) Each sample and standard was atomized, scale reading observed and recorded.
3.) The process in (2) above is repeated and an average of the two values recorded
4.) The concentrations (mg/L) of the chemical elements in the sample was obtained from a plot of scale readings of standards. A working curve from each set of samples was determined.

3.9 Surface morphology characterization of TiO_2 and ZnO

Particles of the catalyst powders were characterized to determine their particle size, surface area and chemical composition by Scanning Electron Microscope (SEM), X-Ray diffraction (XRD), Brunauer Emmett-Teller (BET) and Laser Induced Breakdown Spectroscopy (LIBS).

3.9.1 Laser Induced Breakdown Spectroscopy (LIBS)

The samples were prepared into pellet form by binding with cellulose as described in section (3.3.4). A compact ocean optics spectrometer controlled by a computer installed with Oolibs software was used.

1) The experimental set-up was switched on and the laser allowed to warm up for about 30 minutes.
2) The icon was clicked to start-up the spectrometer program.
3) On the main screen of the Oolibs program the integration time box was located. Then an appropriate integration time of 500 milliseconds was selected. The integration time is the time the detector spends collecting photons. Long integration times means more intense peaks.
4) The averaging box was set at 1 to enable the spectrometer to respond faster. However after the integration time was checked to be satisfactory, the averaging was increased to 7 in order to improve the quality of recorded spectra
5) The ZnO and TiO_2 were alternatively affixed onto sample discs using a double-sided tape
6) The sample disc was then placed back into the vacuum chamber and then closed
7) The start button was pressed on the Q-switch control section of the laser control panel

From the fourth harmonic of Nd: YAG laser, 500 mm spectrograph and gated ICCD camera with in-built delay generator.

8) Make the laser hit the samples and save the generated spectra in the computer
9) Optimize by varying the number of shots, ablations, incident laser energy, and gate time delay time.

3.9.2 Energy-Dispersive X-ray spectroscopy (EDS)

An oxford xMaxN EDS measuring instrument was used to determine the elemental composition of the samples.

1) The crystalline phase was determined using an Analytical Empyrean X-Ray Diffractometer (XRD), employing a scanning rate of 0.12 °C/min in a 2θ range from 20° to 70° with Cu Kα radiation (λ = 1.5418 Å).
2) The working distance was set at 14 mm and the acceleration voltage adjusted to 20 KV.
3) The detector was moved down to 45 mm by turning the knob located below the detector
4) The sample (ZnO/TiO_2) was focused
5) On the computer screen, the X-ray setup icon was clicked-on and enabled for a live time of about 200 seconds
6) The X-ray icon was activated and the cursor placed on the spectrum window and the total number of counts read per second and the dead time (DT) at the spectrum window noted.
7) The dead time (DT) was adjusted to between 25-30% by manipulating the spot size.
8) The current spectrum was erased and a new X-ray spectrum measured
    a. To identify the peaks, possible existing elements in the samples were checked with the periodic table to determine whether the peaks were matching
9) The spectrums were saved in the computer

3.9.3 Scanning Electron Microscope (SEM) – Crystal size

A Tescan VEGA3 Scanning Electron Microscope (SEM) equipped by a field emission source (FESEM) which was preferred over regular SEM with Lanthanum hexaboride, LaB6, filament as a high voltage source for morphological characterization due to its high resolution and brightness at low accelerating voltages.

1) Prior to SEM analysis, the samples were first mounted on an aluminum stub using a double sided carbon tape, and then coated with a thin layer (10 nm - 30 nm) of 60/40 gold-palladium alloy by means of vacuum sputtering coating using a Denton Desk 1 Sputter-Coater under a 70 mtorr vacuum.

Other conditions:

SEM HV	20.0 kV
View field	6.36 μm
SEM mag	30.0 kx

2) The two samples were inscribed for identification
3) The samples were dried at an oven 60°C for 3 hours
4) The samples were loaded into the SEM holder and the valves of the nitrogen gas tanks are opened and the vent button located at the display panel of the microscope table pressed. The sample holder were set at their mounting holes and tightened effectively.
5) When the vacuum reaches an optimum level the filaments light went on and the key switch put on and the monitor lit up.
6) The acceleration voltage was set at 20 KV, lowest magnification (30X) and TV mode scan selected.
7) The coarse focus was switched on and the focus knob adjusted to a safe working distance of 14 mm.
8) The focus was switched to slow scan mode and magnification increased. The samples stage was brought up slowly by pressing z-axis UP key. The variable button was opened up to open a small variable window on the screen. The image was focused within the small screen using outer focus ring and inner focus ring until indicator light reaches the middle.

9) The image was previewed and adjusted to contrast and the image set-up window closed. The image acquire icon was clicked to record the image formed and the image saved.

3.9.4 X-Ray Diffractometry (XRD) – Crystallite size

X-Ray diffraction (XRD) measurements were done:

- at ambient temperature at an angle 2θ set for the range 5° - 90° at a rate of 0.5°/min using a diffractometer fitted with Ni-filtered Cu Kα radiation (λ=1.5406Å).
- Finely ground crystalline powder were placed in the path of monochromatic x-ray beam, diffraction occurred from planes in those crystallites which happen to be oriented at the correct angle to fulfill the Bragg condition.

1) The enclosure doors were opened and the samples loaded
2) The slide doors were carefully and gently pressed together until they interlocked
3) On the computer the XRD commander was expanded and the following working parameters included
4) Scan parameters: start and end 2q limits 0 -130 - 2q
5) Step size 0.5 -0.1 – 2q
6) Step time (1 sec)
7) Start scan
8) When scan was completed the file was saved

Particle sizes are calculated by XRD using the Scherer's equation $l = k\lambda / \beta \cos \theta$.
Where λ is the wavelength of rays, k is a constant taken to be 0, 9 (assuming no crystal distortions in the lattice), β is the full width at half maximum of the radians corrected for the instrumental broadening and θ is the diffraction angle in degrees

3.9.5 Brunauer Emmett Teller (BET) – surface area analysis

The BET surface area was measured through a multipoint method utilizing adsorption data in the relative pressure (P/Po) in the range 0.005-0.3 using nitrogen (99.99%) physico-sorption at 200°C.

1) The system used liquid nitrogen in a 500 cm^3 Dewar flask placed on the stage of the instrument.
2) Sample housing and samples holder were cleaned using a damp wipe
3) Stubs were screwed into a specimen holder
4) ZnO and TiO_2 were first evacuated for 2 hours at 150°C to eliminate adsorbed water
5) The specimen chamber was evacuated and specimen holder set onto specimen stage
6) The HT icon was pressed after the samples were loaded and the ACB, AF and AS icons clicked to observe the images formed.
7) The image qualities were adjusted using the contrast, brightness, focus and stig X, stig Y buttons.
8) To observe at high magnification, the focus was set at low magnification first and then magnification was raised gradually
9) The resolution of the images formed were set at 80 seconds
10) SEM Data Display tab displayed selected SEM data on the image. The photo button was selected and the samples scanned and saved.
11) The SEM image list tab showed a list of the images taken

CHAPTER FOUR

4 Results and Discussion

4.1 Physico-Chemical Characterization - untreated wastewater

Table 4.1 below summarizes the physico-chemical characteristics of untreated tea processing wastewater from CBH, KBH and NBH tea factories.

Table 4.1 Physico-chemical characterization of tea processing wastewater

Sample	pH	Turbidity (NTU)	TOC [mg/l]	COD [mg/l]	TSS [mg/l]	TDS [mg/l]
CBH	6.1	62.3	210	547.34	312	1326.37
KBH	5.6	65.9	236	562.31	327	1368.52
NBH	5.9	64.0	213	553.06	319	1338.13

The physico-chemical characteristics of wastewater as outlined in Table 4.1 are summarized in Sections (4.1.1 – 4.1.6) below.

4.1.1 pH

Table 4.1 shows averaged pH for wastewater samples. The pH of untreated wastewater are recorded in Table 4.1 above. The pH values of aqueous systems is an important parameter for photocatalytic degradation reactions because it affects the adsorption pollutants that takes place on the surface of selected photocatalysts. The generation of •OH is dependent on the pH of wastewater. The pH values of CBH, KBH and NBH samples were measured at 6.1, 5.6 and 5.9 respectively. The untreated samples were slightly acidic, while CBH sample was noted to be less acidic in comparison to KBH and NBH samples. The pH influences the surface properties of selected photocatalysts. Greater photocatalytic treatment is normally observed at neutral pH. This is due to the point of zero change (pzc) of the photocatalysts. The pH values measured are a factor of climatic conditions, soil types and the compositional macro-molecules in the initial tea varieties. In strongly acidic wastewater systems, the • OH radicals generated are quickly discarded that there is little time to react with the pollutants

4.1.2 Turbidity

The turbidity of the wastewater samples were measured according to the procedure described in section (3.5.2) and the values recorded in Table 4.1 above. The values were found to be 62.3 N.T.U, 65.9 N.T.U and 64.0 N.T.U for CBH, KBH and NBH respectively. The results indicate greatest turbidity in KBH sample and least turbidity in CBH sample. These findings are consistent with Total Suspended Solids findings recorded in Section (4.1.5) and Total Dissolved Solids in Section (4.1.6) Turbidity as a water quality parameter is influenced by TSS and TDS. Higher TSS and TDS values increase the turbidity of wastewater solutions. KBH sample showed high Turbidity, TSS and TDS values compared to samples form CBH or NBH.

4.1.3 Total Organic Compounds (TOC)

The Total Organic Carbon (TOC) level for the wastewater samples were analysed according to the procedure in section (3.5.3). According to Table 4.1, the TOC of CBH, KBH and NBH was analysed to be 210 mg/L, 236 mg/L and 213 mg/L respectively. The greatest levels of TOC were observed in KBH and the least levels in CBH sample. This results show that the greatest contamination was present in KBH sample and the least in CBH.

4.1.4 Chemical Oxygen Demand (COD)

The COD for the wastewater samples was determined according to the procedure in section (3.5.4). The findings in Table 4.1 indicate that, CBH, KBH and NBH samples showed COD values of 547 mg/L, 562.31 mg/L and 553.06 mg/L. The greatest levels of COD were observed in KBH sample and the least in CBH. There exists a direct correlation between COD and TOC of wastewater systems. From the values indicated in Table 4.1, Section (4.1.4) and (4.1.5) KBH sample showed the greatest TOC and COD values and CBH sample the least. The volatility of the organic components present in the wastewater influenced the relationship between TOC and COD of the wastewater. In Section (4.4.1), GC-MS analysis of wastewater showed the macro-molecules present in wastewater as follows; CBH = 9, KBH= 14 and NBH= 12 respectively. These values show that is KBH sample the oxygen demand is highest due to the total number of compounds identified. Sample CBH had least number of compounds identified.

4.1.5 Total Suspended Solids (TSS)

The values of the Total Suspended Solids are presented in Table 4.1 and measured at 312, 327 and 319 mg/l for CBH, KBH and NBH. These values were determined as per the procedure described in section (3.5.5). Sample KBH had the highest amounts of suspended matter and sample CBH had the least. The levels of suspended matter present in the wastewater affected its turbidity. The values correlate with the Turbidity values as shown in section (4.1.2).

4.1.6 Total Dissolved Solids (TDS)

The TDS for the samples were determined as per the procedure in section (3.5.6) and the values obtained for the 3 sample recorded as CBH=1326.37 mg/L, KBH= 1368.52 mg/L and NBH= 1338.13 mg/L. The levels of dissolved solids influenced the turbidity of the samples as discussed in section (4.1.2). The results show that the KBH sample had the greatest amounts of dissolved solids that also elevated its turbidity and sample CBH the least dissolved solids and turbidity.

4.2 Analysis of macro-molecules in tea processing wastewater

4.2.1 Gas Chromatography –Mass Spectrometry (GC-MS)

Table 4.2 Macro-molecules in tea processing wastewater

Compound	Retention Times (mins)	Molecular formula	Molecular weight (g/mol)
(2-Butanone, 4-(2, 6, 6-trimethyl-1-yl)-	9.054	$C_{13}H_{22}O$	194
1-{2-[3-(2-Acetyloxiran-2-yl)-1, 1-dimethylpropyl] cycloprop-2-enyl} ethanone	9.280	$C_{14}H_{20}O_3$	236
Tetradecanoic acid	10.023	$C_{14}H_{28}0_2$	228
Acetic acid	10.286	$C_{14}H_{22}O_3$	238
3, 7, 11, 15-Tetramethyl-2-hexadecen-1-ol	10.872	$C_{20}H_{40}O$	296
Caffeine	11.677	$C_8H_{10}N_40_2$	194
n-Hexadecanoic acid	13.604	$C_{16}H_{32}O_2$	256
Phytol	17.138	$C_{20}H_{40}O$	296
9, 12, 15-Octadecatrienoic acid	19.164	$C_{18}H_{30}O_2$	278
Octadecanoic acid	19.470	$C_{18}H_{36}O_2$	284
Ethyl iso-allocholate	21.320	$C_{26}H_{44}O_5$	436
1, 2-Benzenedicarboylic acid	24.030	$C_{24}H_{38}O_4$	390
2, 6, 10, 14, 18, 22-Tetracosahexane, 2, 6, 10, 15, 23-hexamethyl-	27.595	$C_{30}H_50$	410
7-(1,3-Dimethylbuta-1,3-dienyl)-1,6,6-trimethyl-3,8-dioxatricyclo[5,1,0,0(2,4)]octane	9.057	$C_{15}H_{22}0_2$	234
Acetic acid	10.307	$C_{14}H_{22}O_3$	238
Caffeine	11.705	$C_8H_{10}N_4O_2$	194
n-Hexadecanoic acid	13.991	$C_{16}H_{32}O_2$	256
Phytol	17.284	$C_{20}H_{40}O$	296
9, 12, 15-octadecatrienoic acid	19.432	$C_{18}H_{30}O_2$	278

octadecanoic acid	19.750	$C_{18}H_{36}O_2$	284
1, 2-Benzenedicarboxylix acid, diisooctyl ester	24.138	$C_{24}H_{38}O_4$	390
Oleic acid, eicosyl ester	26.703	$C_{38}H_{74}O_2$	562
1-Heptatriacotanol	9.038	$C_{37}H_{76}O$	536
Ppropiollic acid	10.237	$C_{13}H_{20}O_3$	224
Caffeine	11.262	$C_8H_{10}N_4O_2$	194
Phthalic acid	12.829	$C_{26}H_{42}O_4$	418
Phytol	17.089	$C_{20}H_{40}O$	296
9, 12, 15-octadecatrienoic acid	18.976	$C_{18}H_{30}O_2$	278
Octadecanoic acid	19.364	$C_{18}H_{36}O_2$	284
α-Amyrin	20.891	$C_{30}H_{50}O$	426
ϒ-Tocopherol	21.456	$C_{28}H_{48}O_4$	416
1, 2-Benzenedicarboxylic acid	24.028	$C_{24}H_{38}O_4$	390
Vitamin E	25.933	$C_{29}H_{50}O_2$	430
2, 2, 4-Trimethyl-heptadeca-3, 7, 11, 15-tetraenyl)-cyclohexanol	26.587	$C_{30}H_{52}O$	428
Hexadecanoic acid	13.442	$C_{16}H_{32}O_2$	256

Table 4.2 presents molecules found in tea processing wastewater from CBH, KBH and NBH factories. The macro-molecules present included carboxylic acids, alcohols, caffeine among others. The presence of this molecules in the wastewater was responsible for its acidity and characteristic brown colour as described in (section 1.7) indicating that some of the identified compounds were chromophores. In addition the retention times for the identified compounds ranged from (9.038 – 27.595 minutes). The molecular weights of the compounds ranged from 194 – 562 g/mol. The findings suggest that the molecules identified were large.

4.3 Total chemical elements in tea processing wastewater

Figure 4.1 below indicates the total chemical Fe, Mn, Ni & Al elements in wastewater

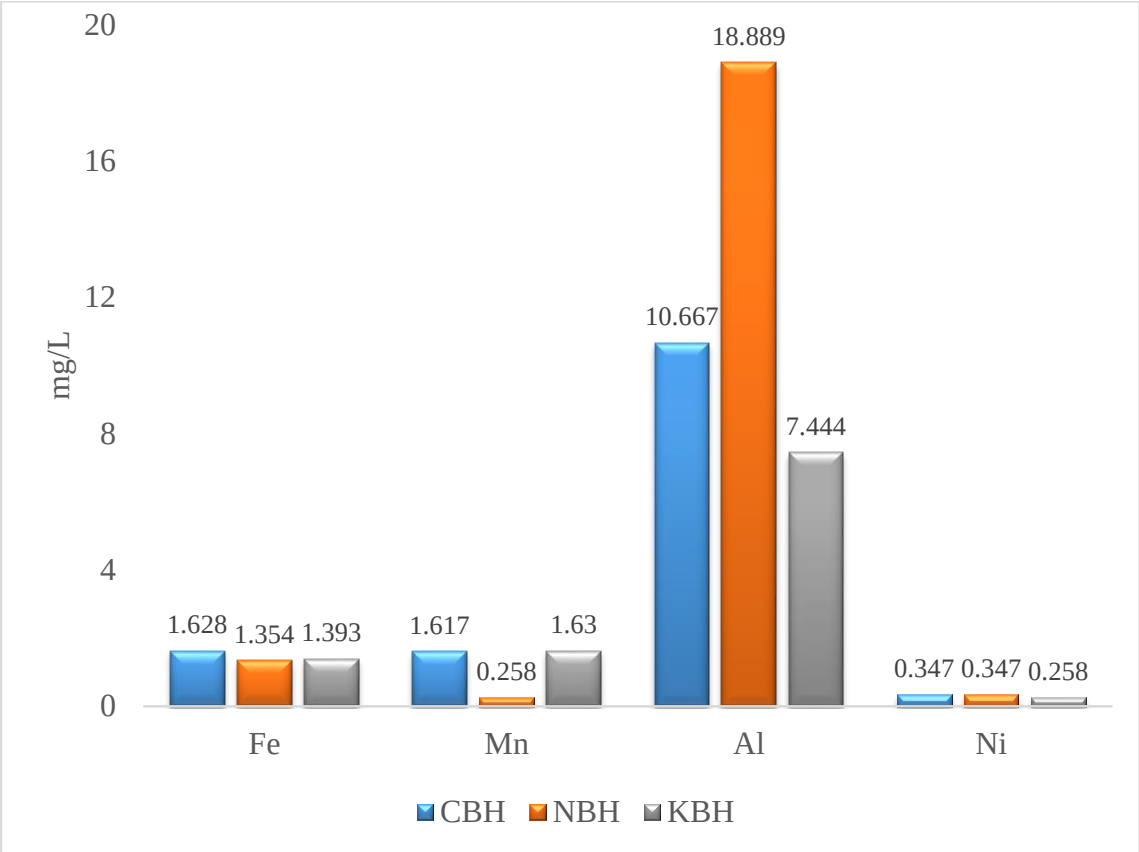

Figure 4.1 Total chemical elements – CBH, KBH and NBH

4.3.1 Total Chemical element – Ni

From the data presented in Figure 4.1, Ni is the least prevalent chemical element in the wastewater compared to Fe, Mn & Al. The Ni present in KBH was 0.258 mg/l. In CBH and NBH the amount of Ni present was 0.347 mg/l.

4.3.2 Total Chemical element – Al

Aluminum element was shown to be the most prevalent in all the 3 samples namely CBH, KBH and NBH. In NBH sample the Al present was determined to be 18.889 mg/l. In CBH the Al levels was measured as 10.667 mg/l and in KBH 7.444 mg/l.

4.3.3 Total Chemical element – Mn

The total Mn chemical element was measured as follows; KBH=1.63 mg/L, NBH= 0.258 mg/L and CBH= 1.617 mg/L. The greatest levels of Mn were measured in KBH and least in NBH.

4.3.4 Total Chemical element – Fe

The greatest levels of Fe element was observed in CBH = 1.628 mg/L. NBH = 1.393 mg/L showed lowest levels. The levels in KBH was 1.393 mg/L.

4.4 Photocatalytic treatment of tea processing wastewater

4.4.1 Spectral analysis of untreated CBH, KBH and NBH wastewater

Figure 4.2 below shows a UV/Vis spectral analysis of wastewater at wavelengths between (350 nm – 500 nm).

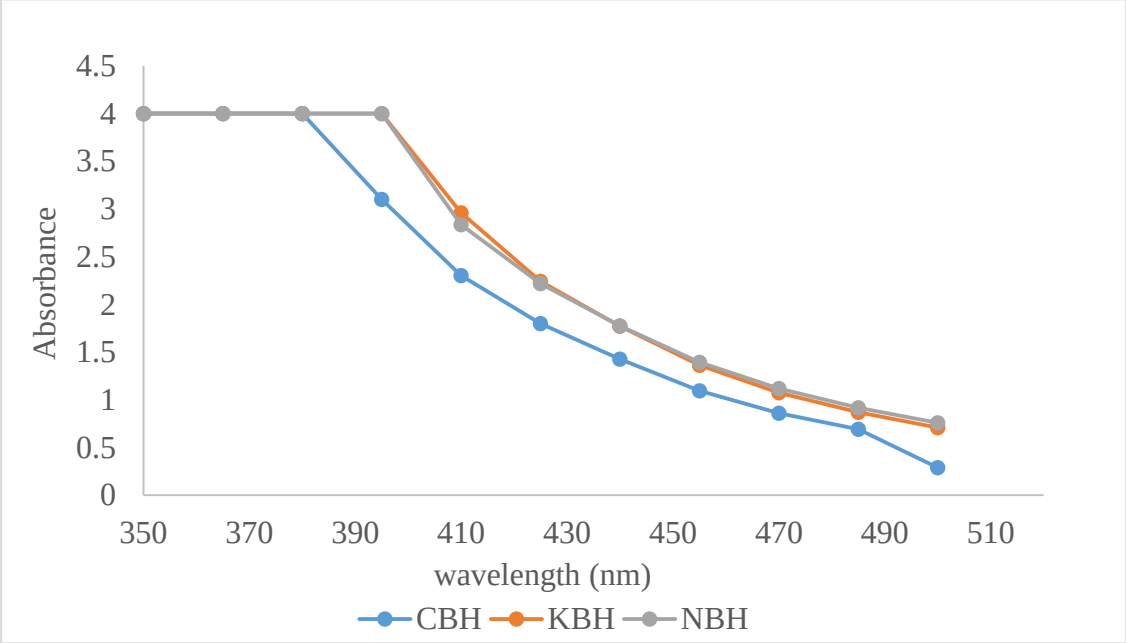

Figure. 4.2 Absorption spectra CBH, KBH and NBH

Several investigators observed a similar UV/Vis spectral profile of tea processing wastewater. The spectral profile reveals that the wastewater samples absorb light actively in the visible region of light spectrum λ = (400 nm – 800 nm). From the spectra in Figure 4.2 we observe that CBH sample showed significantly lower absorbance compared to

KBH and CBH samples which showed almost similar absorbance levels. For Enviromental and aesthetic concerns, the decolourization of the tea processing wastewater was more necessary than the removal of other colourless organic compunds. Semi-conductors photocatalysts i.e. ZnO or TiO_2 generally absorb different colour light depending on band-gap energy. The absorbance was measured at 410 nm to monitor the changes in the characteristic brown colour of the wastewater. The wavelength lies in the visible region of the electromagnetic spectrum.

4.4.2 Optimization of ideal reaction time

Figure 4.3 below shows the optimization of reaction conditions to determine optimum UV/ZnO irradiation reaction time.

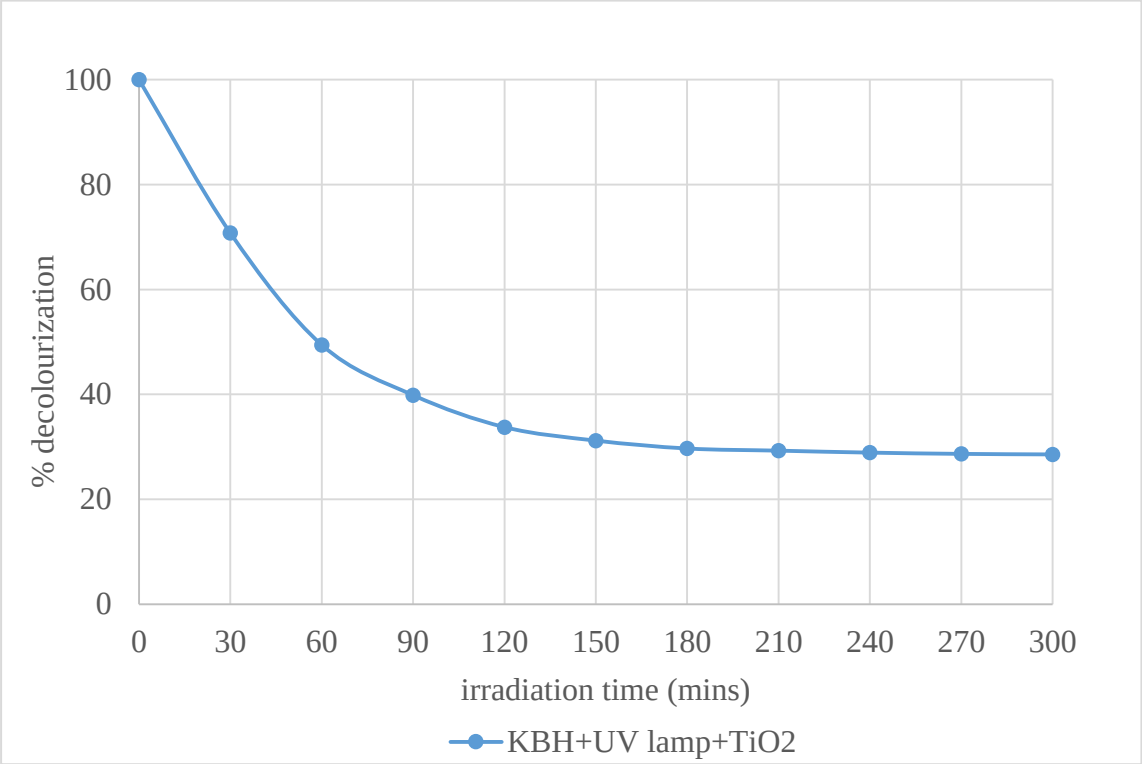

Figure 4.3 optimization of reaction time – UV/TiO_2 treatment of KBH sample

To determine the optimum reaction time required to treat wastewater, an experiment was done for 5 hours using KBH sample and a UV/TiO_2 treatment system. It was observed that after 3 hours of treatment, there was very little change in sample decolourization. In all the subsequent treatment experiments, the reaction time was set as 180 minutes for all UV/Solar light mediated reactions.

4.4.3 Photocatalytic treatment - UV /ZnO

Figure 4.4 below represents the results of photocatalytic treatment of CBH, KBH and NBH samples by UV light /ZnO treatment system.

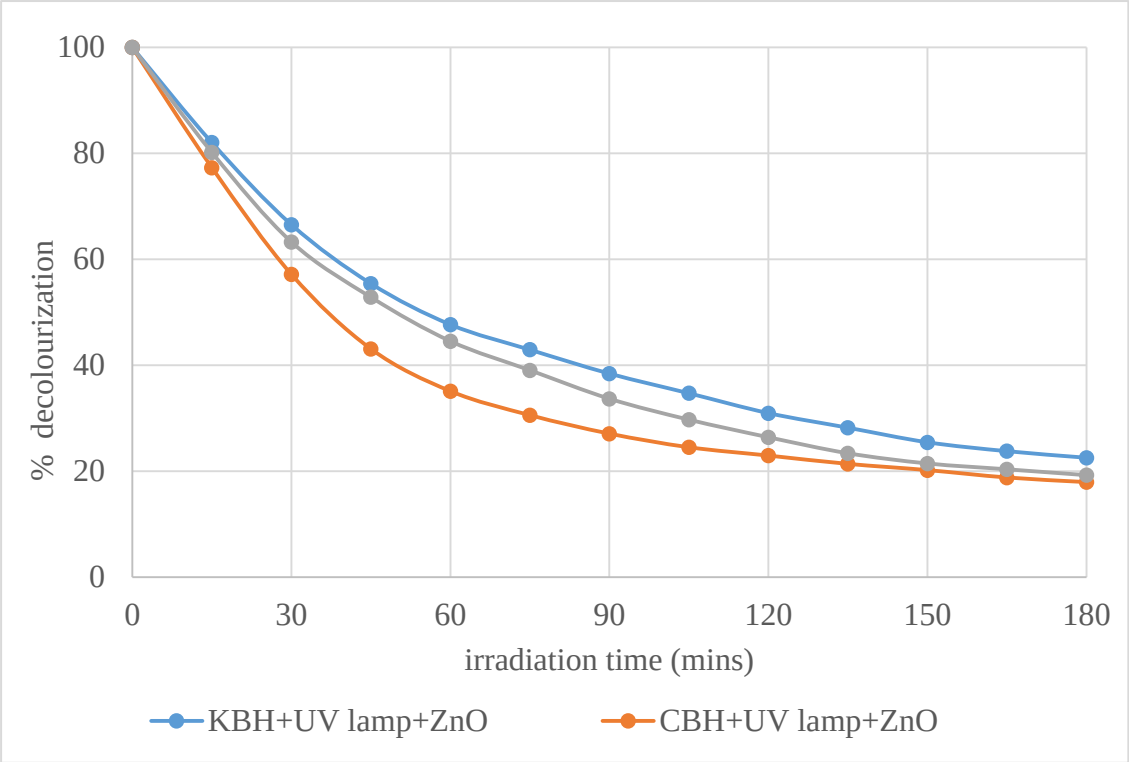

Figure 4.4: UV/ZnO photocatalytic treatment of KBH, CBH and NBH wastewater

The findings indicate that the treatment of the wastewater using ZnO/UV light system proved very effective. The results indicate that after 1 hour of treatment 64.9% of CBH, 55.5% of NBH and 52.4% of KBH colour had been degraded. After 3 hours of treatment an average of 80% of the persistent colour had been degraded from all the 3 samples. This results suggest that the coexistence of a suitable semi-conductor and light exposure is necessary for photocatalytic degradation of tea processing wastewater.

4.4.4 Photocatalytic treatment - solar /ZnO

The results in Figure 4.5 show the results obtained after KBH, CBH and NBH wastewater samples were treated using solar/ ZnO treatment system.

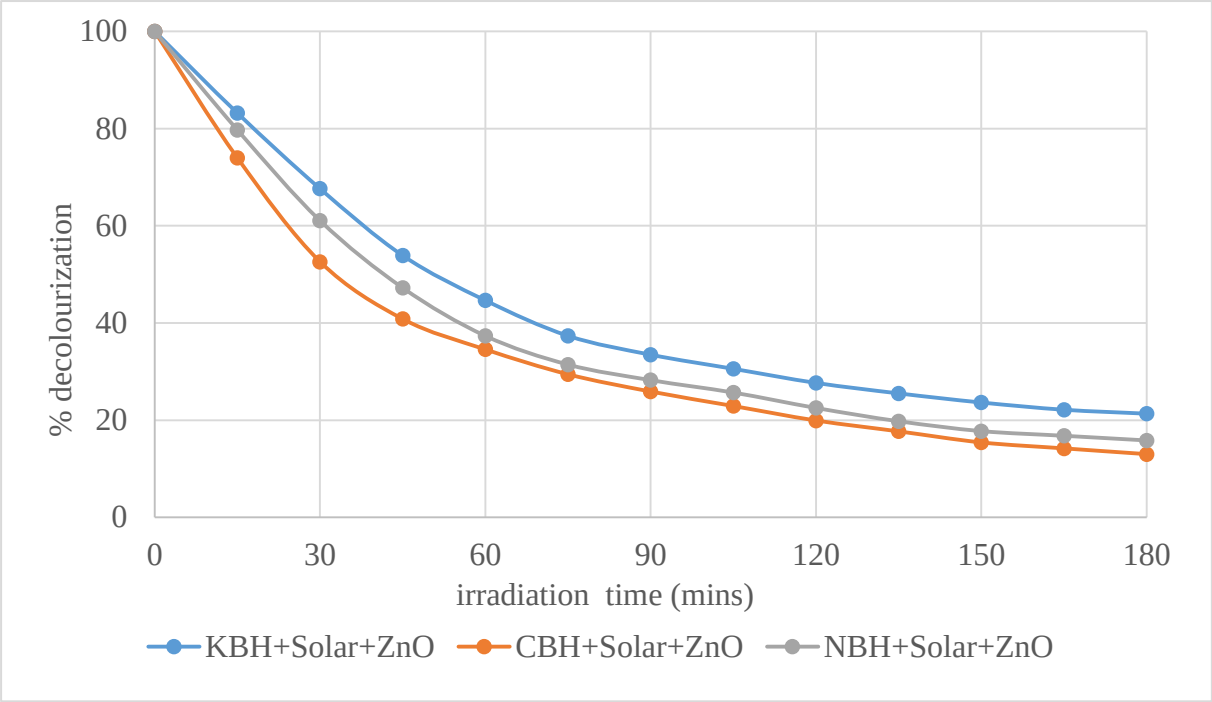

Figure 4.5: Solar/ZnO photocatalytic treatment of KBH, CBH and NBH wastewater

The findings indicate that after 1 hour. 65.5% of CBH, 62.7% of NBH and 55.4% of KBH colour had been removed. After 3 hrs. 87% of CBH, 84.2% of NBH and 78.7% of KBH colour had been degraded. From fig.4.5 the efficiency of colour removal was higher in CBH and least in KBH. ZnO absorbed visible light in addition to UV light results also indicate that solar light provided a viable source of energy to decolourize tea processing wastewater in the presence of ZnO.

4.4.5 Comparison of photocatalytic treatment efficiency between ZnO/ UV radiation/Solar

The findings shown in Figure 4.6, 4.7 and 4.8 relates Solar/ZnO and UV/ZnO wastewater treatment system to determine the effect of UV/Solar light source on photocatalytic treatment.

4.4.5.1 Comparison of UV/solar/ ZnO treatment system - KBH

Fig.4.6 below represents results obtained between Solar/ZnO and UV/ZnO treatment system of KBH wastewater.

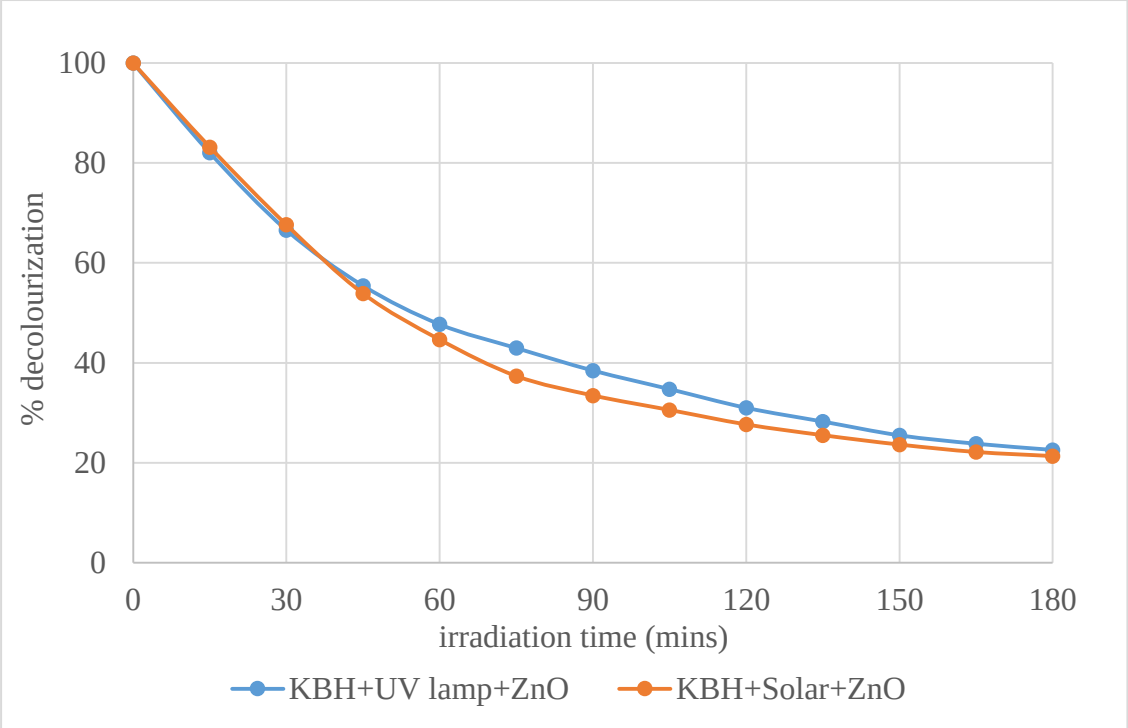

Figure 4.6: Solar/ZnO and UV/ZnO photocatalytic treatment system of KBH wastewater

After 1 hour of photocatalytic treatment 55.4% of solar/ZnO and 52.4% of UV/ZnO decolourization was achieved. After 3 hours of treatment 78.7% of solar/ZnO and 77.5% of UV/ZnO decolourization was achieved. The results were achieved despite the irradiation flux intensity for solar light (I=1.49 mW/cm^2) and UV lamp (I=3.0 mW/cm^2). These results were observed despite the UV irradiation from solar light being almost 50% lower than UV light. ZnO was determined as an effective photocatalyst that absorbed solar

light irradiation in addition to UV light. Solar light irradiation is a reliable and cost-effective because of its abundance.

4.4.5.2 Comparison of UV/solar/ ZnO treatment system – CBH

Figure 4.7 below represents findings obtained between Solar/ZnO and UV/ZnO treatment system of CBH wastewater.

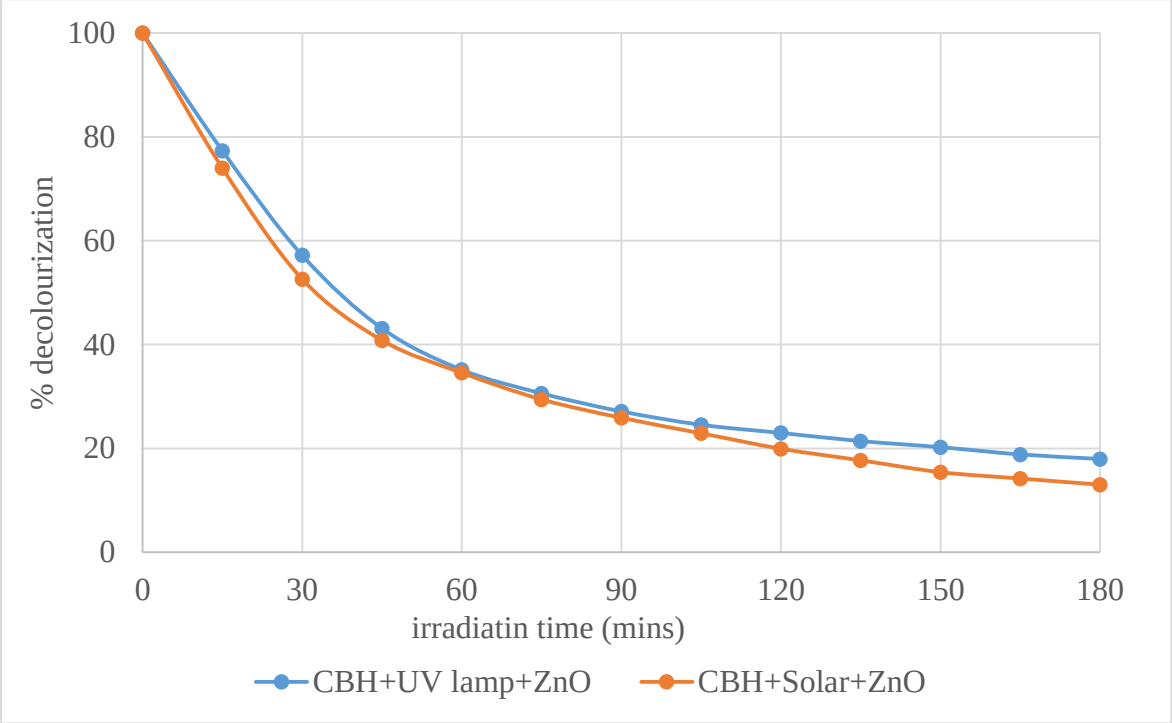

Figure 4.7: Solar/ZnO and UV/ZnO photocatalytic treatment system of CBH wastewater

After 1 hour of photocatalytic treatment 65.5% of solar/ZnO and UV/ZnO decolourization was achieved. After 3 hours of treatment 78.7% of solar/ZnO and 77.5% of UV/ZnO decolourization was achieved. The results were achieved despite the irradiation flux intensity for solar light being (I=1.49 mW/cm^2) and UV lamp (I= 3.0 mW/cm^2). These results were observed despite the UV irradiation from solar light being almost 50% lower than UV light. ZnO absorbed a wider range of light spectrum irradiation and is more applicable for solar mediated photocatalytic treatment. ZnO showed high electron mobility.

4.4.5.3 Comparison of UV/solar/ ZnO treatment system - NBH

Figure 4.8 below shows the results obtained between Solar/ZnO and UV/ZnO treatment system of NBH wastewater.

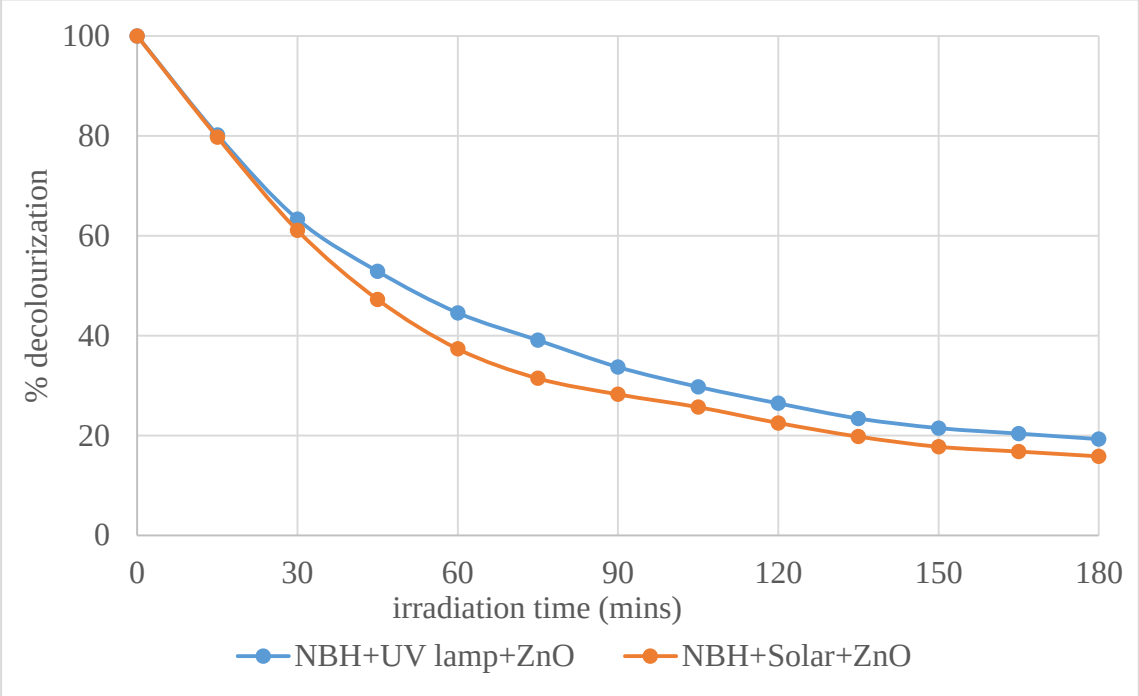

Figure 4.8: Solar/ZnO and UV/ZnO photocatalytic treatment system of NBH wastewater

After 1 hour of photocatalytic treatment 62.7% of solar/ZnO and 55.6% of UV/ZnO decolourization was achieved. After 3 hours of treatment 84.2% of solar/ZnO and 81.0% of UV/ZnO decolourization was achieved. The results were achieved despite the irradiation flux intensity for solar light being (I=1.49 mW/cm^2) and UV lamp (I= 3.0 mW/cm^2). These results were observed despite the UV irradiation from solar light being almost 50% lower than UV light. ZnO was determined as an effective photocatalyst that absorbed solar light irradiation in addition to UV light. Solar light irradiation is a reliable and cost-effective because of its abundance. Solar light also provided a good source of energy to degrade tea processing wastewater in the presence of ZnO.

4.4.6 Photocatalytic treatment - UV /TiO_2

Figure 4.9 below represents the results of photocatalytic treatment of CBH, KBH and NBH samples by UV light /TiO_2 treatment system.

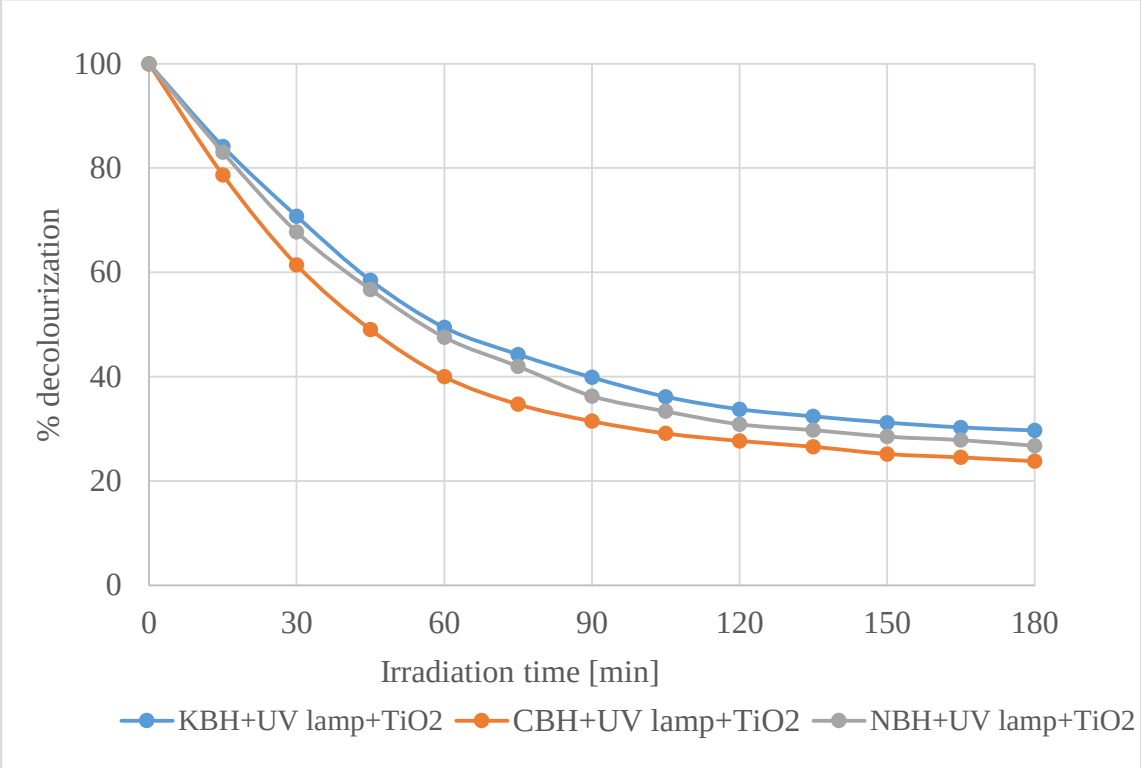

Figure 4.9: UV/TiO2 photocatalytic treatment of KBH, CBH and NBH wastewater

The findings indicate that the treatment of the wastewater using ZnO/ artificial UV light system proved very effective. The results indicate that after 1 hour of treatment 60.03% of CBH, 52.4% of NBH and 50.6% of KBH colour had been degraded. After 3 hours of treatment an average of 73.3% of the persistent colour had been degraded from all the 3 samples. This results suggest that the coexistence of a suitable semi-conductor and light exposure is necessary for photocatalytic degradation of tea processing wastewater. The investigations indicate that the coexistence of TiO_2 photocatalyst and light exposure is necessary for the decolourization of tea processing wastewater

4.4.7 Photocatalytic treatment - Solar/TiO_2

Figure 4.10 below represents the results of photocatalytic treatment of CBH, KBH and NBH samples by solar /TiO_2 treatment system.

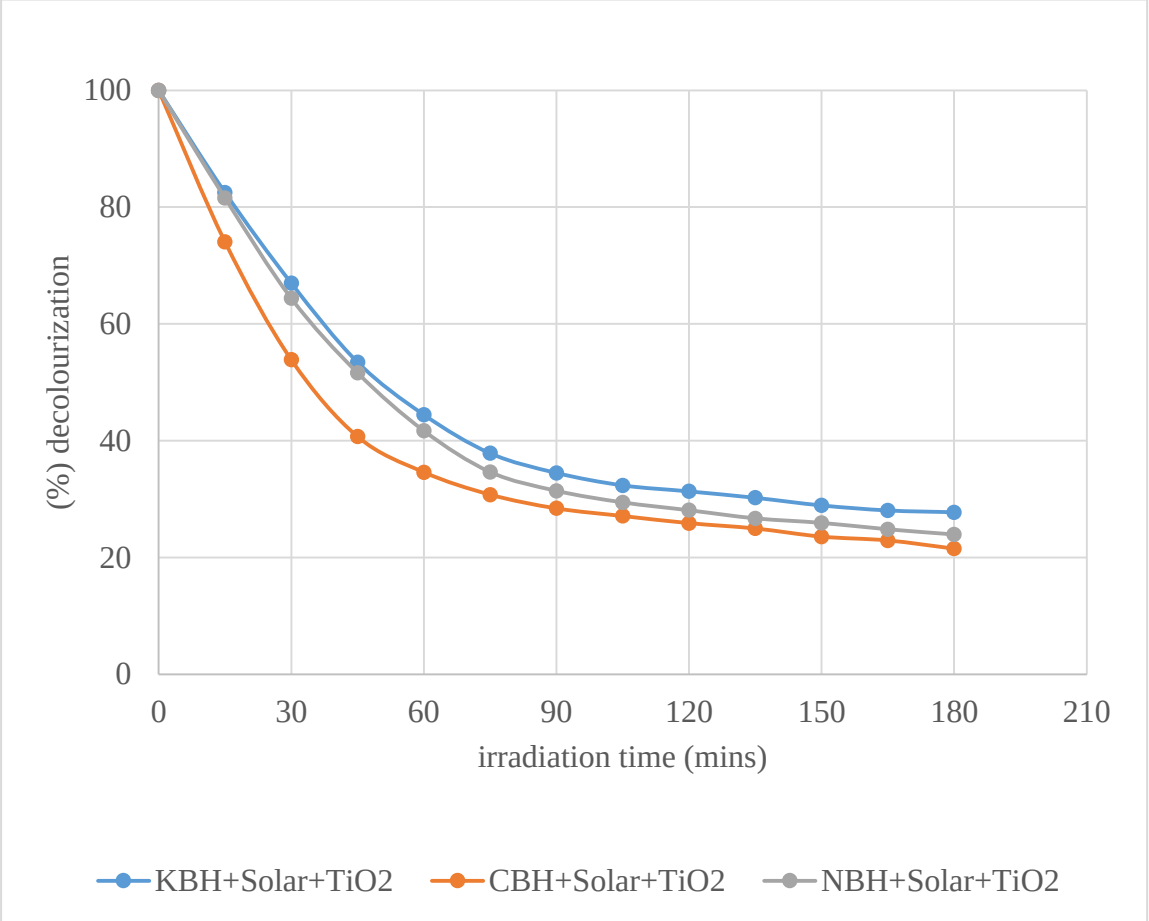

Figure 4.10: Solar/TiO_2 photocatalytic treatment of KBH, CBH and NBH wastewater

The findings indicate that after 1 hour. 65.4% of CBH, 58.3% of NBH and 55.6% of KBH colour had been removed. From fig.4.3 the efficiency of colour removal was higher in CBH and least in KBH. After 3 hours of treatment, an average of 75.6% of decolourization was achieved. The results indicate that solar light provided a viable source of energy to decolourize tea processing wastewater mediated by TiO_2. The findings indicate that solar irradiation could be used as a substitute cost effective light source because of its abundance.

4.4.8 Comparisons - photocatalytic treatment system (UV-Solar /TiO_2)

The results shown in Figure 4.11, 4.12 and 4.13 relates the Solar/TiO_2 and UV/TiO_2 wastewater treatment systems to determine the effect of UV/Solar light source on photocatalytic treatment.

4.4.8.1 Comparison - UV/solar/ TiO_2 treatment system - KBH

Figure 4.11 below represents results obtained between Solar/TiO2 and UV/TiO2 treatment system of KBH wastewater.

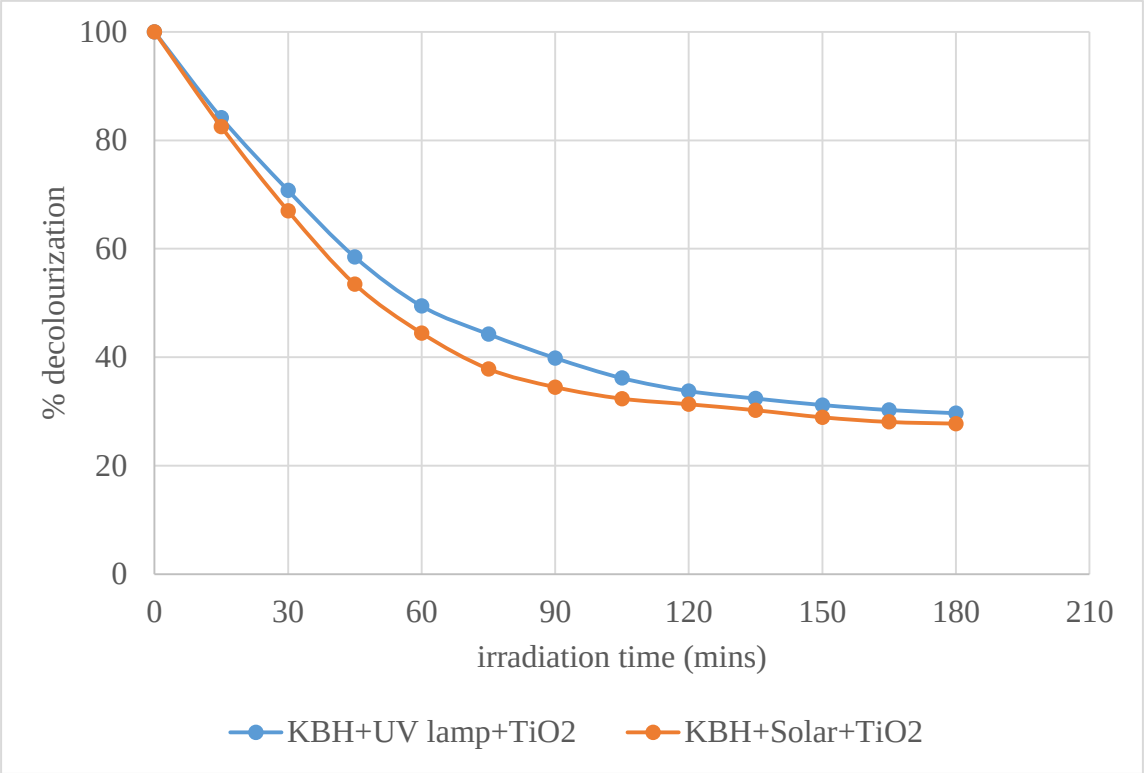

Figure 4.11: Solar/TiO_2 and UV/TiO_2 photocatalytic treatment system of KBH wastewater

After 1 hour of photocatalytic treatment 55.6% of solar/ZnO and 50.6% of UV/ZnO decolourization was achieved. After 3 hours of treatment 78.7% of solar/ZnO and 77.5% of UV/ZnO decolourization was achieved. The results were achieved despite the irradiation flux intensity for solar light being I=1.49 mW/cm^2 and UV lamp= 3.0 mW/cm^2. These results were observed despite the UV irradiation from solar light being almost 50% lower than UV light. Solar light irradiation is a reliable and cost-effective because of its abundance.

4.4.8.2 Comparison of UV/solar/ TiO_2 treatment system - CBH

Figure 4.12 below represents findings obtained between Solar/TiO_2 and UV/TiO_2 treatment system of CBH wastewater.

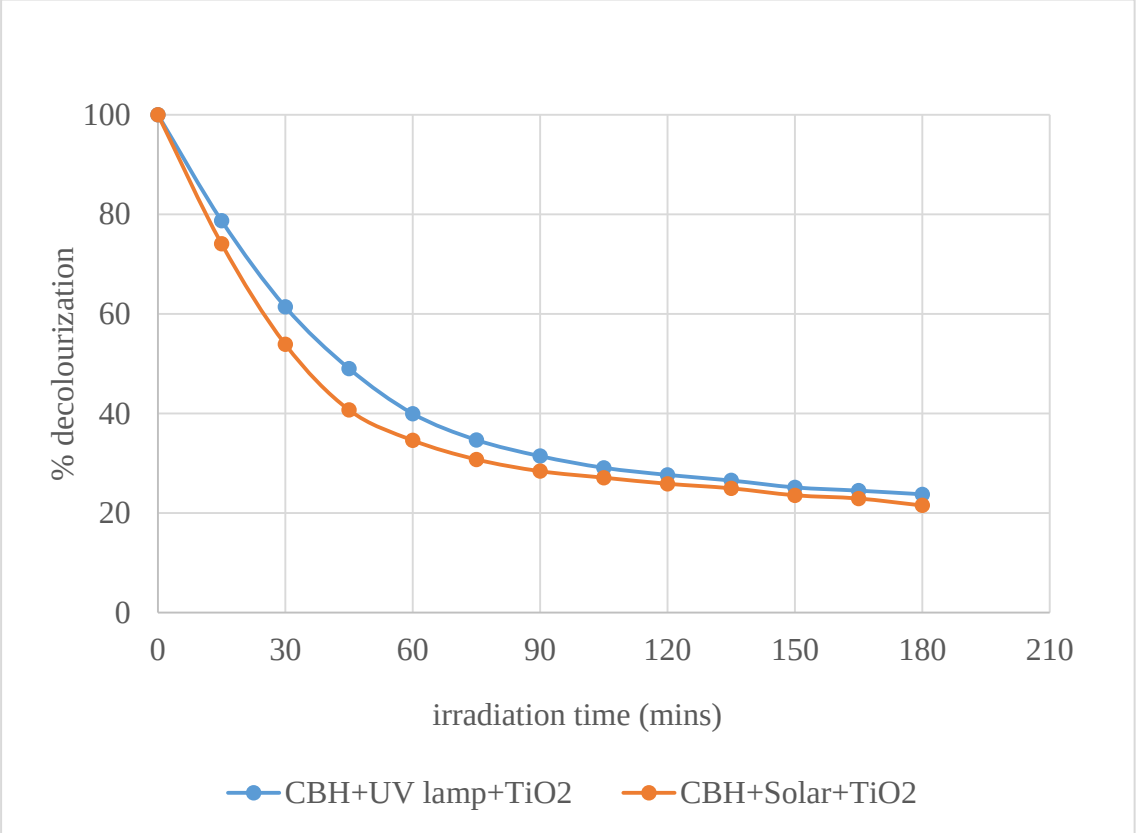

Figure 4.12: Solar/TiO_2 and UV/TiO_2 photocatalytic treatment system of CBH wastewater

The findings show that after 1 hour of photocatalytic treatment, 65.4% decolourization was achieved for solar/TiO_2 and 60.1% for UV/TiO_2 treatment systems. After 3 hours of treatment 78.7% of solar/TiO_2 and 77.5% of UV/TiO_2 decolourization was achieved. The results were achieved despite the irradiation flux intensity for solar light being I=1.49 mW/cm^2 and UV lamp= 3.0 mW/cm^2. These results were observed despite the UV irradiation from solar light being almost 50% lower than UV light.

4.4.8.3 Comparison of UV/solar/ TiO_2 treatment system - NBH

Figure 4.13 below shows the results obtained between Solar/TiO_2 and UV/TiO_2 treatment system of NBH wastewater.

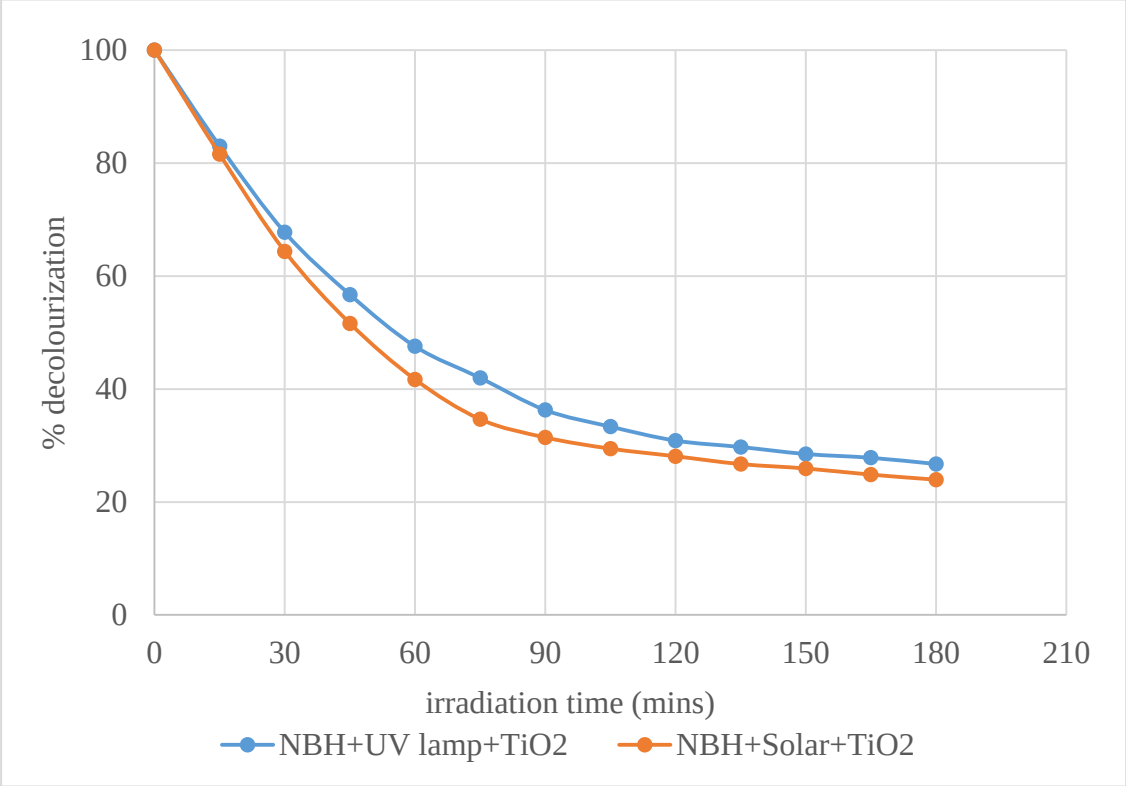

Figure 4.13: Solar/TiO_2 and UV/TiO_2 photocatalytic treatment system of NBH wastewater

After 1 hour of photocatalytic treatment 58.3% of solar/ZnO and 52.5% of UV/ZnO decolourization was achieved. After 3 hours of treatment 84.2% of solar/ZnO and 81.0% of UV/ZnO decolourization was achieved. The results were achieved despite the irradiation flux intensity for solar light being I=1.49 mW/cm^2 and UV lamp= 3.0 mW/cm^2. These results were observed despite the UV irradiation from solar light being almost 50% lower than UV light. Solar light irradiation is a reliable and cost-effective because of its abundance and provided a good source of energy to degrade tea processing wastewater in the presence of TiO_2.

4.5 Physico-chemical characterization - Treated wastewater

The physico-chemical characteristics of treated wastewater are indicated in Table 4.3 below.

Table 4.3 Physico-chemical characterization – treated wastewater

Sample	pH	Turbidity (NTU)	TOC [mg/l]	COD [mg/l]	TSS [mg/l]	TDS [mg/l]
CBH	6.8	34.8±0.37	48.8±0.71	224.27±0.78	129±0.13	785.4±0.6
KBH	6.6	35.6±0.44	63.7±0.16	239.29±0.23	132±0.39	801.6±0.2
NBH	6.7	35.2±0.24	51.3±0.39	226.96±0.57	130±0.08	788.7±0.09

The physico-chemical characterization of treated wastewater is discussed in sections (4.5.1 - 4.5.6) below.

4.5.1 pH

Table 4.3 above shows that photocatalytic treatment of wastewater led to a shift in pH from acidity to neutrality. Table 4.1 showed the pH of untreated wastewater samples which was measured as; (CBH=6.1, KBH=5.6 and NBH=5.9). After 180 minutes of treatment, the readings were as follows; (CBH=6.8, KBH=6.6, NBH=6.7).

This corresponds to the following (%) change; (CBH=10.29%, KBH=15.15% and NBH= 11.94% respectively. The average shift in pH for the 3 samples was measured at 12.46%. The greatest shift was measured in KBH sample at 15.15%.

4.5.2 Turbidity

Table 4.3 shows that photocatalytic treatment resulted in significant turbidity reduction for the 3 samples. Table 4.1 shows the turbidity of untreated wastewater measured as; (CBH=62.3 NTU, KBH=65.9 NTU and NBH= 64.0 NTU).

Photocatalytic treatment resulted in significant reductions in turbidity levels which were measured as; (CBH=34.8 NTU, KBH=35.6 NTU, NBH=35.2 NTU). This shift corresponded to the following shift (%); (CBH=44.14%, KBH=45.97% and NBH= 45.0%. The average shift for the 3 samples was determined at 45.03%. The greatest shift was measured in KBH sample at 45.97%.

4.5.3 Total Organic Compounds (TOC)

In Table 4.3 above shows that photocatalytic treatment resulted in the TOC of the 3 samples reducing significantly. The TOC of untreated wastewater was shown in Table 4.1 as follows; (CBH=210 mg/L, KBH=236 mg/L and NBH= 213 mg/L).

The TOC readings for treated wastewater samples were shown as; (CBH=48.78 mg/L, KBH=63.7 mg/L, NBH=51.26 mg/L). This corresponded to the following shift as follows; (CBH=76.77%, KBH= 73.1% and NBH= 75.93% shift in TOC respectively. The average TOC shift for the 3 samples was 75.27%. The greatest shift was measured in CBH sample at 76.77%.

4.5.4 Chemical Oxygen Demand (COD)

From Table 4.3 the results show that photocatalytic treatment lowered COD significantly. Table 4.1 showed COD measurements of untreated wastewater as follows; (CBH=547.34 mg/L, KBH= 562.31 mg/L and NBH= 553.06 mg/L).

The change in COD after photocatalytic treatment in Table 4.3 was measured as follows; (CBH= 224.27 mg/L, KBH= 239.29 mg/L, NBH=226.96 mg/L). This represented; (CBH= 59.02%, KBH= 57.45% and NBH= 58.96% respectively. The average COD shift for the 3 samples was measured at 58.48% and the greatest shift was measured in sample CBH at 59.02%.

4.5.5 Total Suspended Solids (TSS)

Table 4.3 shows that photocatalytic treatment lowered TSS for the 3 samples. Table 4.1 showed the TSS for untreated wastewater as follows; (CBH=312 mg/L, KBH= 327 mg/L and NBH= 319 mg/L).

The shift in TSS after photocatalytic treatment was represented in Table 4.3 as follows; (CBH= 129.09 mg/L, KBH= 132.28 mg/L, NBH=130.54 mg/L). This shift was determined as; (CBH= 58.63%, KBH= 59.54% and NBH= 59.07 %). The average shift for the 3 samples was measured at 59.08%. The greatest shift was measured in sample CBH at 59.54%.

4.5.6 Total Dissolved Solids (TDS)

From Table 4.3 the results show that photocatalytic treatment lowered TSS of the 3 samples. Table 4.1 showed TSS measurements for untreated wastewater as follows; (CBH=1326.37 mg/L, KBH= 1368.52 mg/L and NBH= 1338.13 mg/L).

Changes in TSS for the 3 samples after photocatalytic treatment was has been reported in Table 4.3 as follows; (CBH= 785.36, KBH= 801.56, NBH= 788.69). This change represented the following shift; (CBH= 40.79%, KBH= 41.43% and NBH= 41.1 %). The average shift for the 3 samples was measured at 40.12% and the greatest shift measured in sample KBH at 41.43%.

4.6 Characterization of TiO_2 and ZnO - Surface morphology

4.6.1 Laser Induced Breakdown Spectroscopy (LIBS)

4.6.1.1 TiO_2

The elemental composition of TiO_2 using LIBS at pulse energy (100 MJ) is shown in Figure 4.14 below.

Figure 4.14. LIBS spectra for TiO_2

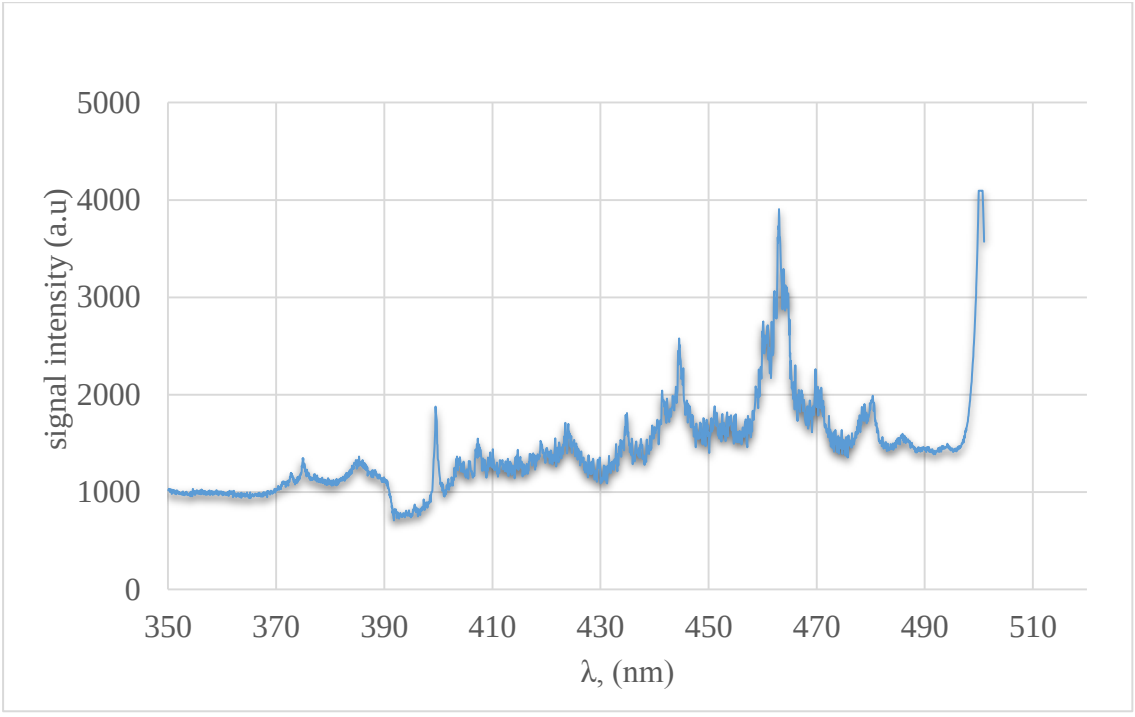

Figure 4.14: Libs spectrum - TiO_2

Fig. 4.14 indicates the LIBS spectra for TiO_2 (99.5% - purity; 100MJ - pulse energy). The LIBS spectrum depicted was recorded in the 350 nm -500 nm wavelength spectral range. Pronounced peaks were recorded indicating the following elements; (Ti=375 nm, 400 nm, 463 nm); (O= 407 nm, 444 nm, 465 nm, 469 nm); (Fe= 480 nm). Detection at this wavelengths signaled their elemental signature. This wavelength is within the active UV/Vis light range of 200 nm - 800 nm. Spectra measured at various pulse energies (70 MJ, 80 MJ and 90 MJ) are recorded in the appendix section.

4.6.1.2 ZnO

The LIBS spectra shown in Figure 4.15 analyses ZnO to determine its elemental composition at pulse energy - (100 MJ).

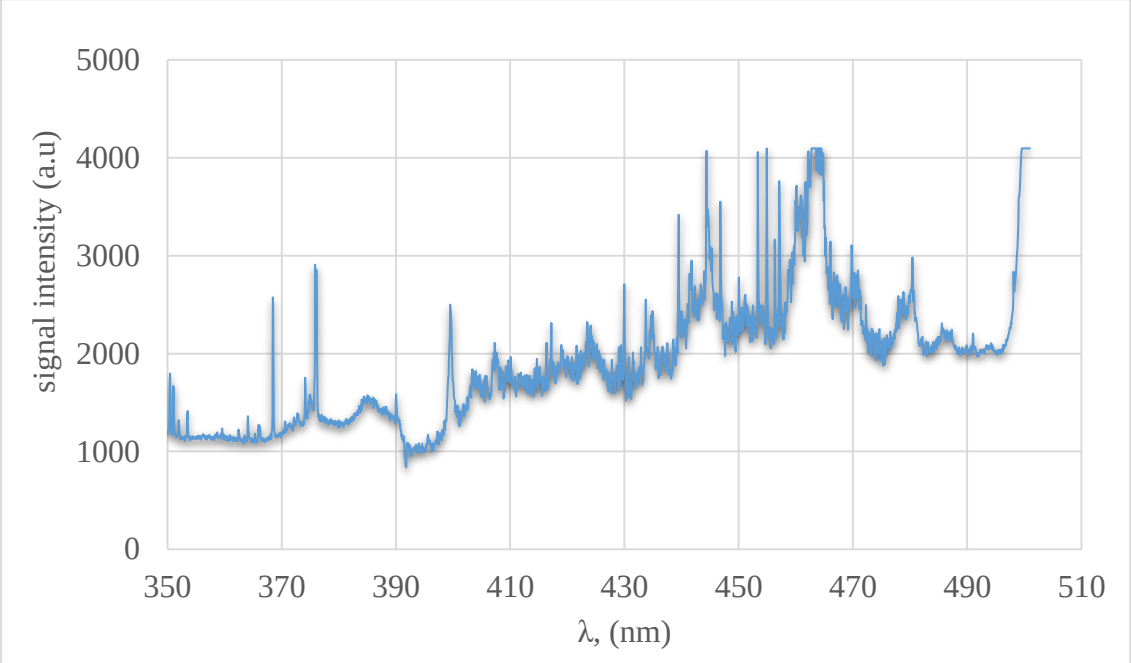

Figure 4.15: LIBS spectrum - ZnO

Fig. 4.15 indicates the libs spectra for TiO_2 (99.5% purity). The LIBS spectrum depicted was recorded in the 350 nm–500 nm wavelength spectral range. Pronounced peaks were recorded indicating the following elements ;(Zn= 370 nm, 375 nm, 400 nm, 440 nm, 444 nm and 454 nm) ;(O= 353 nm, 417 nm); (Na= 446 nm); (Ca= 407 nm, 434 nm); (Si= 460, 470 nm). Detection at this wavelengths signaled their elemental signature. This wavelength is within the active UV/Vis light range of 200 nm - 800 nm. Spectra measured at various pulse energies (70 MJ, 80 MJ and 90 MJ) are recorded in the appendix section

4.6.2 Energy Dispersive X-ray Spectroscopy (EDS)

4.6.2.1 ZnO

Analysis of ZnO by EDS to determine its elemental composition (wt. %) is represented in Figure 4.16 below.

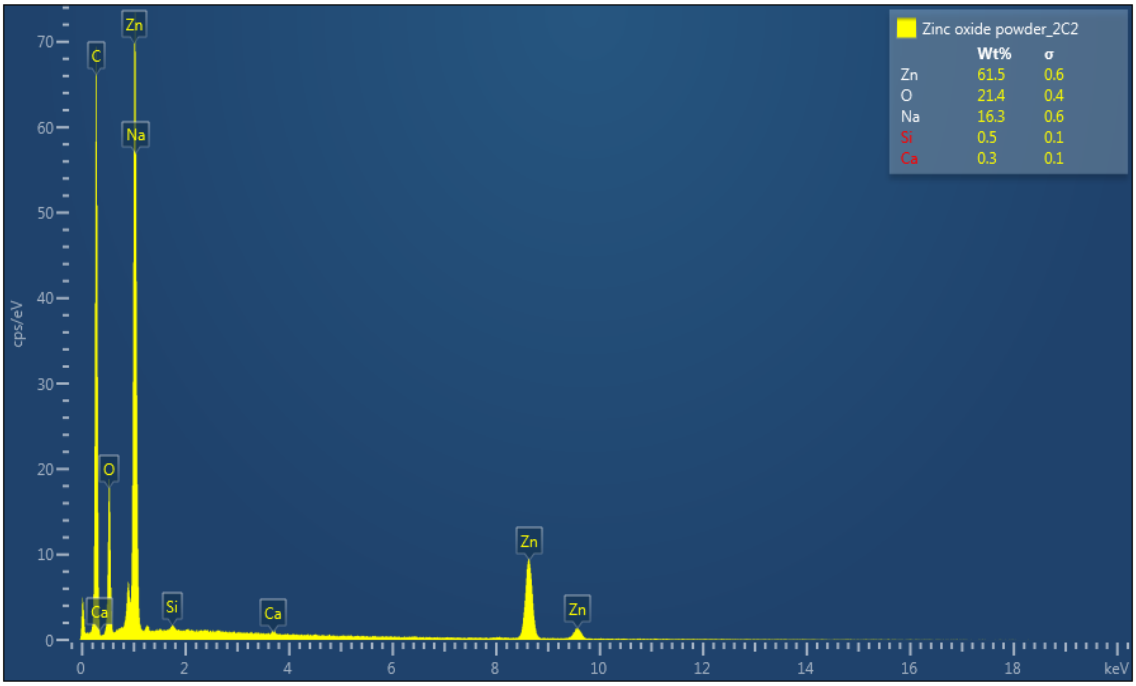

Figure 4.16 EDS spectrum - ZnO

The EDS spectrum indicates the presence of five peaks which were identified as zinc, oxygen, sodium, silicon and calcium. The most prevalent element was Zn- 61.5 wt.% , O -21.4 wt.%, Na – 16.3 wt.%, Si – 0.5 wt.% and Ca – 0.3 wt.%.

In Table 4.4 below, the elemental composition of ZnO is indicated.

Table 4.4 EDS compositional analysis - ZnO

Elements	Experimental results (Atomic wt. %)
ZnO	61.5
O	21.4
Na	16.3
Si	0.5
Ca	0.3

4.6.2.2 (TiO_2)

Analysis of ZnO by EDS to determine its elemental composition (wt. %) is represented in Figure 4.17 below.

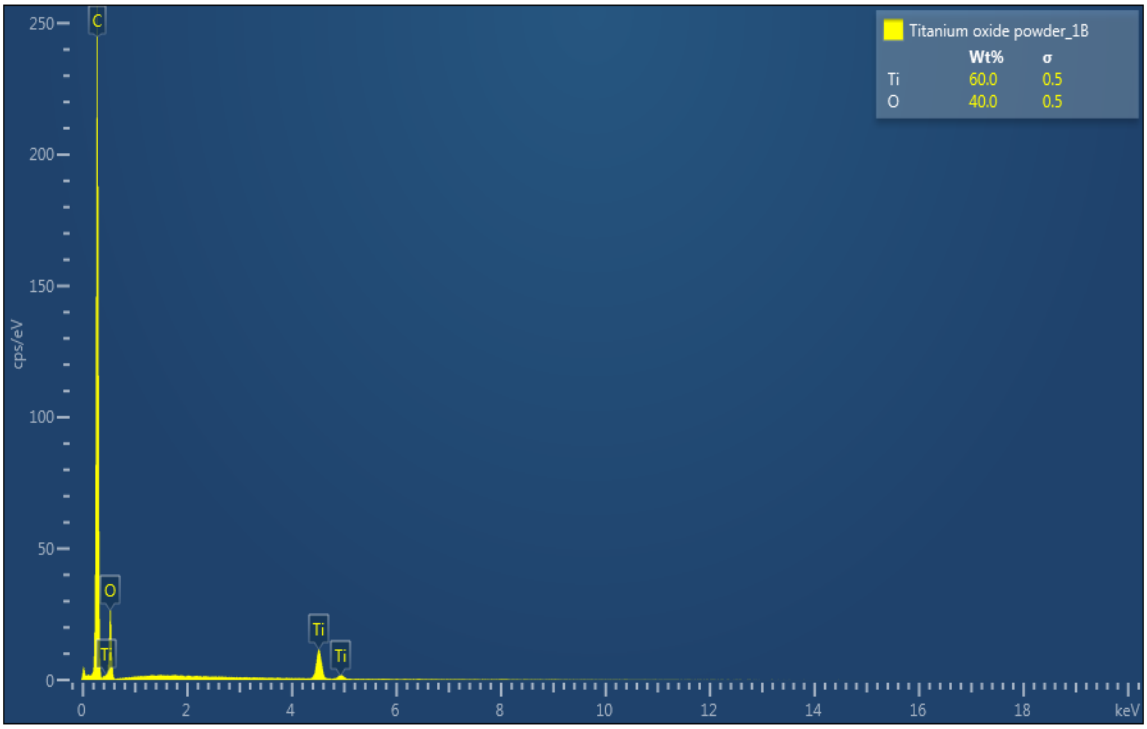

Figure 4.17 EDS spectrum - TiO_2

EDS spectrum indicates two peaks which were identified as Ti – 60 wt. % and O – 40 wt. %.

In Table 4.5 below, the elemental composition of TiO_2 is shown

Table 4.5 EDS compositional analysis - TiO_2

Elements	Experimental results (Atomic wt. %)
Ti	60.0
O	40.0

4.6.3 Scanning Electron Microscope (SEM)

4.6.3.1 TiO_2

Figure 4.18, 4.19, 4.20, 4.21, 4.22, 4.23, 4.24 and 4.25 show SEM images of TiO_2 powders used in this study. The images represent TiO_2 surface morphology and particle size. The catalyst particle size and morphology affects its photocatalytic efficiency. A crystalline structure promotes photocatalytic activity. The amount of the surface-adsorbed water and hydroxyl groups is related to the crystallite form and surface area. Particle size is an important parameter for photocatalytic efficiency, since the predominant way of electron/hole recombination may be different depending on the particle size

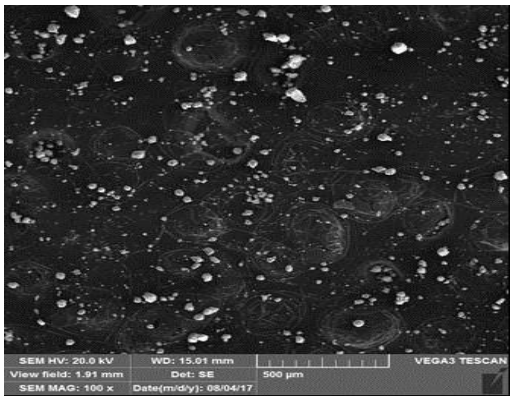

Figure 4.18: TiO_2_ (500µm- WD 15.01 mm)

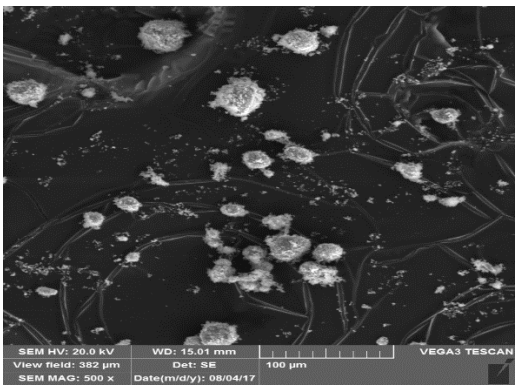

Figure 4.19: TiO_2_100µm (WD 15.01 mm)

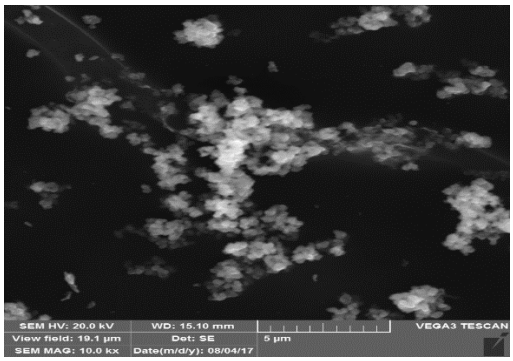

Figure 4.20:TiO_2 _ (5 µm –WD 15.10 mm)

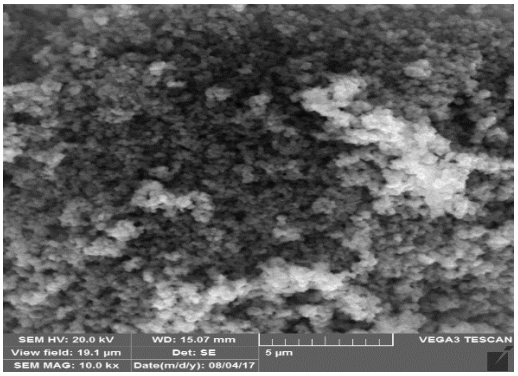

Figure 4.21:TiO_2_ (5µm- WD 15.07 mm)

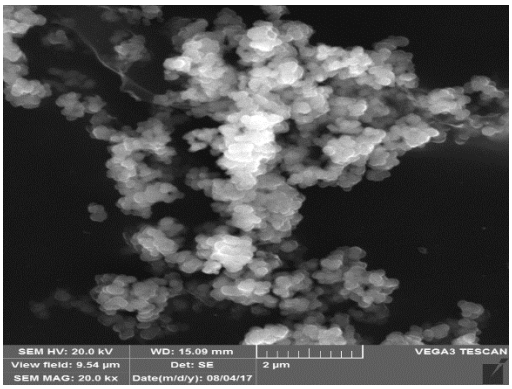

Figure 4.22: TiO_2(2 µm WD 15.09 mm)

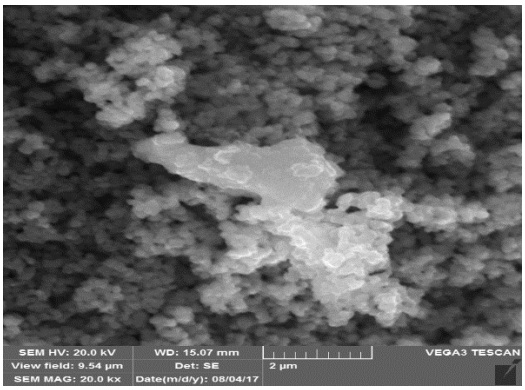

Figure 4.23: TiO_2_ (2µm WD 15.07mm)

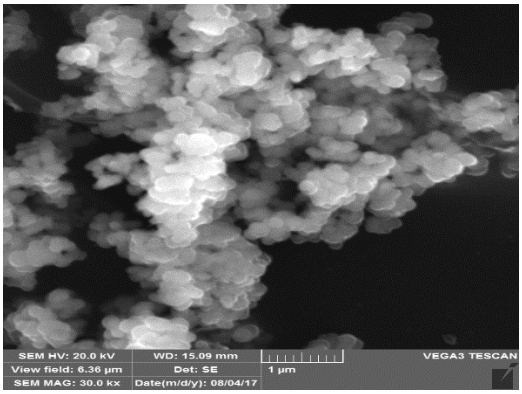

Figure 4.24: TiO_2 (1 µm – WD 15.09 mm)

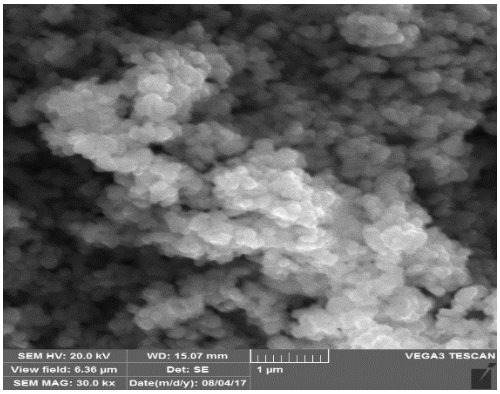

Figure 4.25: TiO_2 (1 µm – WD 15.07 mm)

The SEM images show that individual particle sizes to be approximately 16 nm and spherical in shape. This particle size observed is similar to the figure calculated from X-Ray Diffraction measurements in section 4.6.4.1.

The significance of particle size is significant because smaller sizes promote the recombination of photogenerated electrons and holes in the powder catalysts, leading to poor photocatalytic activity. This is observed because smaller particle size reduces the time needed for the carrier gas diffusing out of the photocatalyst pores to the photocatalysts surface.

4.6.3.2 ZnO

Figure 4.26, 4.27, 4.28, 4.29, 4.30, 4.31, 4.32 and 4.33 show SEM images of ZnO powder as used in the study. The images were characterized to determine particle size and morphology which affects its photocatalytic efficiency. A large surface area can be determining factor in certain photodegradation reactions, as a large amount of adsorbed molecules promotes the reaction rate.

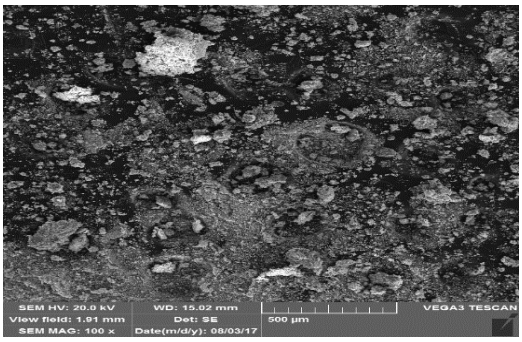

Figure 4.26: ZnO _ (500 µm-WD 15.02 mm)

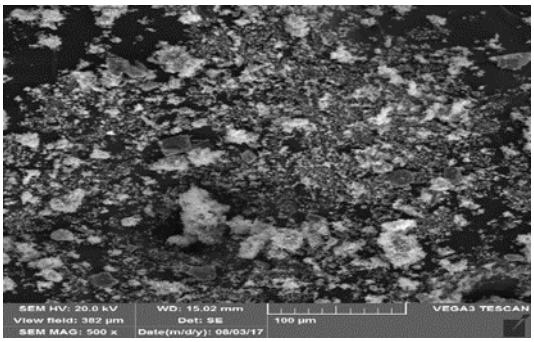

Figure 4.27: ZnO _ (2 µm – WD-15.02 mm)

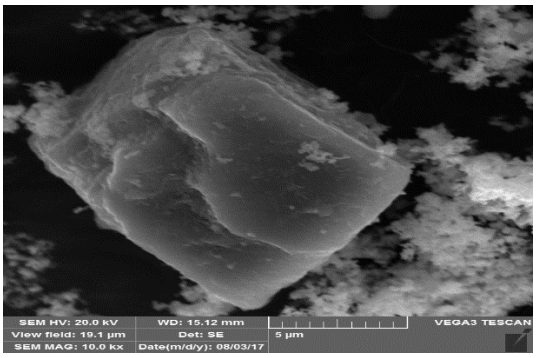

Figure 4.28: ZnO _ (5 µm- WD-15.12 mm)

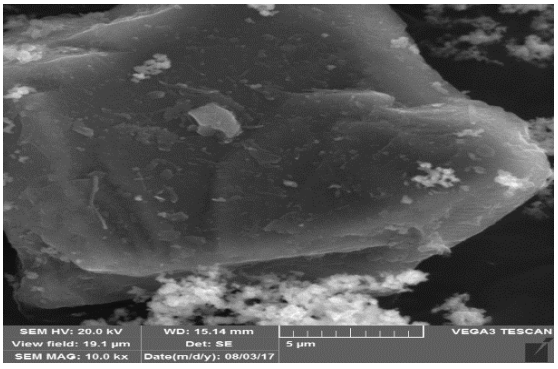

Figure 4.29: ZnO _ (5 µm- WD-15.14 mm)

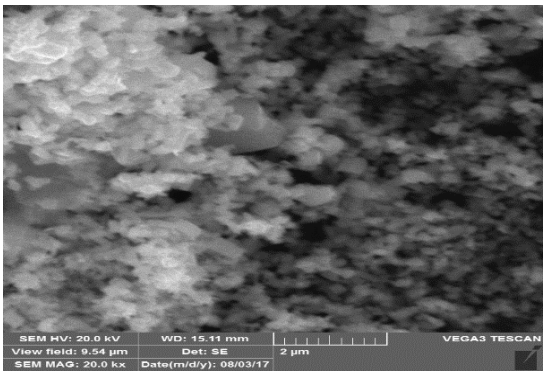

Figure 4.30: ZnO _ (2 µm- WD-15.11 mm)

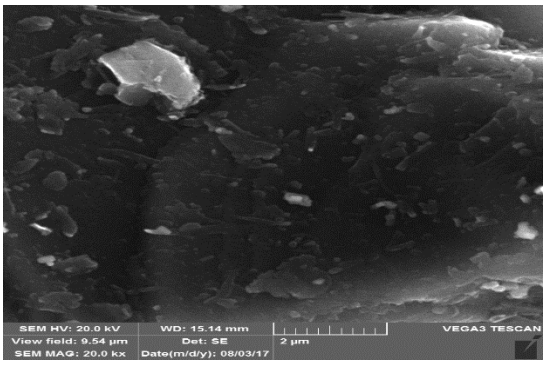

Figure 4.31: ZnO _ (2 µm- WD-15.14 mm)

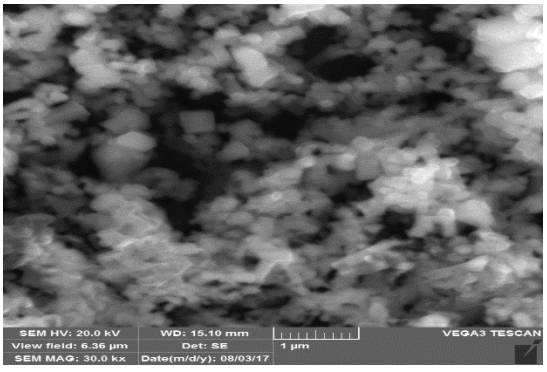

Figure 4.32: ZnO _ (1 µm- WD-15.10 mm)

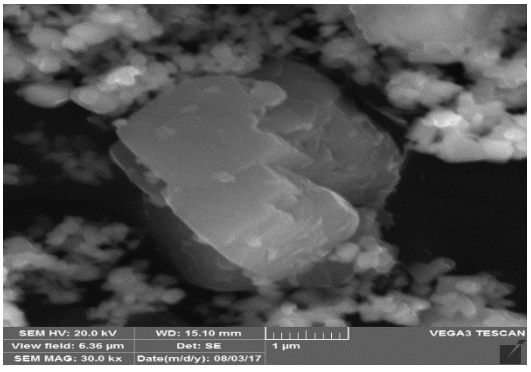

Figure 4.33: ZnO _ (1 µm- WD-15.10 mm)

From the SEM images, the particle size were estimated to be approximately 16 nm and hexagonal shape. This value is very close to the figure calculated from X-Ray Diffraction measurements in section 4.6.4.2.

The SEM images show that ZnO has an open porous structure that improves photocatalytic activity by providing adsorption sites for organic molecules on catalyst surface during photocatalytic treatment.

4.6.4 X-Ray Diffractometry (XRD)

4.6.4.1 TiO_2

Figure 4.34 shows an XRD analysis of TiO_2 to determine its crystallinity and particle size

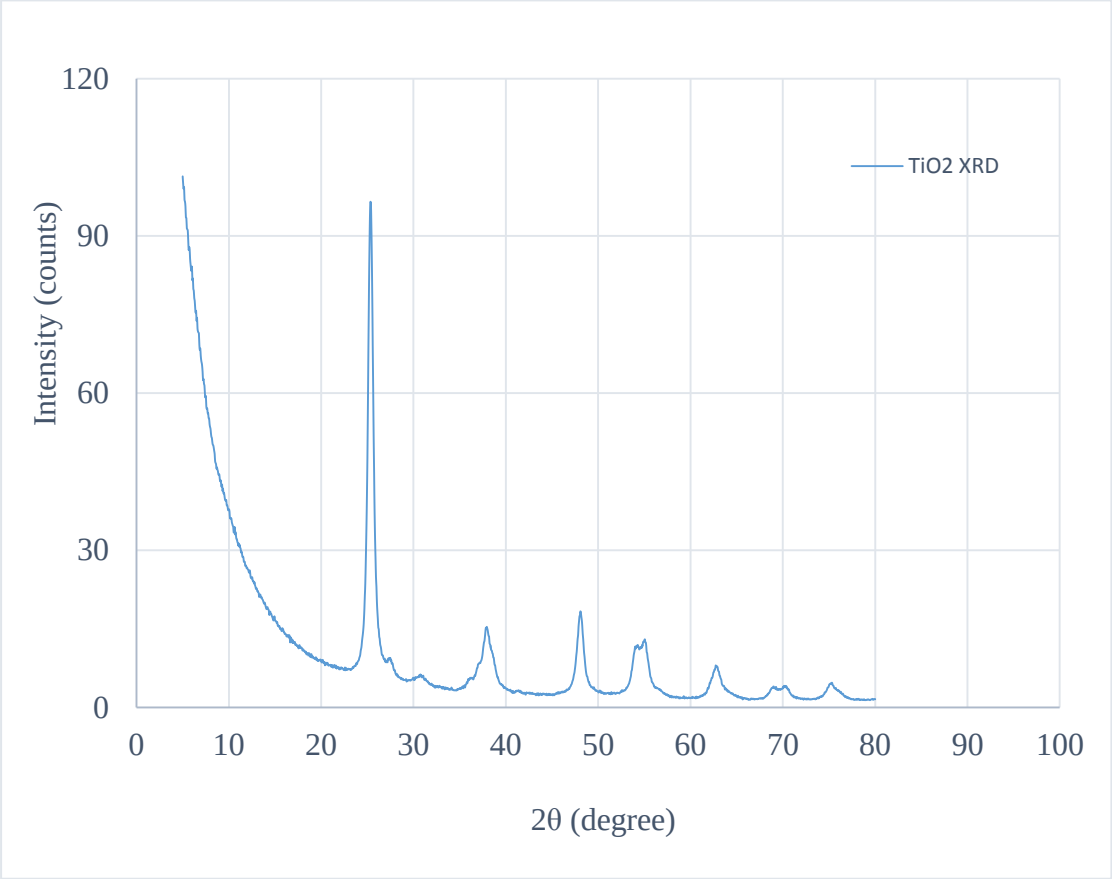

Figure 4.34: X-ray Diffraction patterns - TiO_2

The average crystallite size of TiO_2 was obtained from the most intense diffraction peak of anatase TiO_2 at 25.28°. The crystallite size was calculated at 16 nm.

Figure 4.34 shows a series of diffraction peaks at 2θ=25.28° (101), 37.69° (104, 112), 47.88° (200), 55.20° (105, 211), 62.28° (204, 211), 69.32° (116) and 74.54° (215)

From the XRD spectra in Figure 4.34 the crystal structure of TiO_2 has been revealed as amorphous. This provides more of active sites with high specific surface photoactivity.

Small variations in particle diameters often leads to great modifications in the surface/bulk ratio, thus modifying the significance of volume and surface electron-hole recombination.

4.6.4.2 ZnO

Figure 4.35 shows an XRD analysis of ZnO to determine its crystallinity and particle size

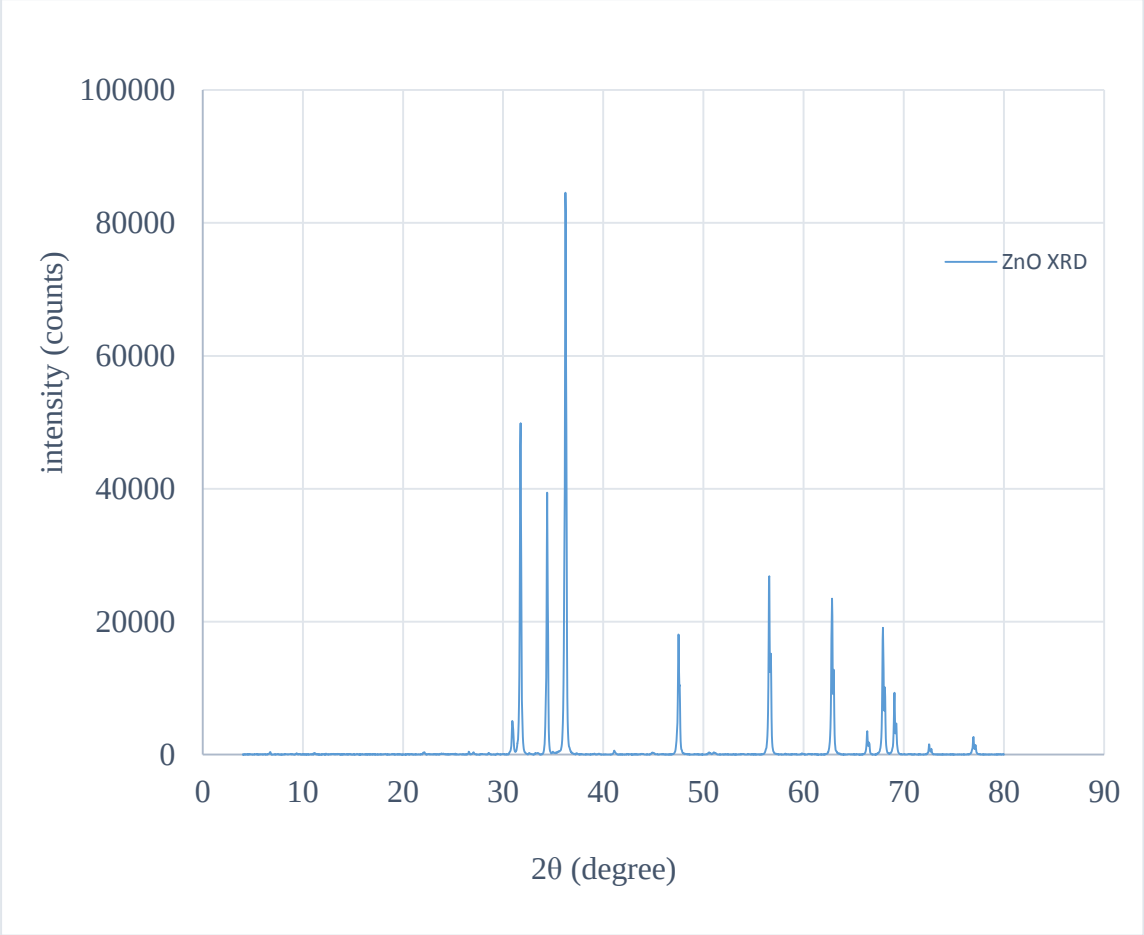

Figure 4.35: X-ray Diffraction patterns - ZnO

The average crystallite size of ZnO was obtained from the most intense diffraction peak of ZnO at 36.20° (84539).

The crystallite size was calculated at 16.21 nm. Fig.4.35 shows a series of diffraction peaks at 2Θ= 31.74° (46467), 34.38° (39405), 36.20° (84539), 47.52° (17962), 56.54°(26625), 62.8° (23470) , 67.93° (19051) and 69.06° (9272).

The sharp and intense peaks seen in Fig. 4.35 indicate high crystallinity in ZnO which affected its electronic and photocatalytic properties. It can absorb wider range of spectrum of radiation. When the crystallite dimension of a semiconductor particle falls below a

critical radius of approximately 10 nm, the charge carriers appear to behave quantum mechanically. It is well known that in the nanometer-size range, physical and chemical properties of particles including semiconductors are modified compared with bulk.
Increased crystallinity leads to better catalyst photocatalytic activity.

4.6.5 Brunauer Emmett Teller (BET) – surface area analysis

In Table 4.6 below, the surface area measurements for ZnO and TiO_2 are indicated.

Table 4.6: surface area measurements - ZnO and TiO_2

Powder photocatalyst	Surface area Uncalcined (m^2/g)
TiO_2	31.76
ZnO	40.14

The results from Table 4.6 indicates that the surface area for TiO_2 and ZnO was 31.76 m^2/g and 40.14 m^2/g. The results in this work show that treatment by Solar/Ultraviolet/ZnO system, indicated a 9.7% greater efficiency compared to Solar/Ultraviolet/TiO_2 system. This results indicate that ZnO is a better catalyst because of its morphology and increased surface area. The combination of surface area and particle size are important determining factors in photocatalytic treatment reactions because large surface areas lead to effective contact with organic pollutant molecules and this promotes higher reaction rates because more active sites are available for reactions to take place.
Despite smaller crystals having larger inner surface areas, smaller catalyst particles can also promote the recombination of photogenerated electrons and holes, which in turn leads to poor photoactivity. A balance between surface area and particle size must be found in order to find the optimum photocatalytic activity.

CHAPTER FIVE

5 Conclusions and Recommendations

5.1 Conclusions

Nandi is one of the tea growing Counties in Kenya, in addition to being a catchment area for rivers flowing into Lake Victoria. Wastewater from 3 black tea processing factories that include Chebut (CBH), Kibwari (KBH), and Nandi (NBH) were investigated, out of a total of 19 factories located in Nandi County. The annual processing capacities of black tea in the 3 factories was found to be CBH= 20 million kgs, KBH= 4 million kgs and NBH= 6 million kgs. This corresponds to CBH=11.142 m^3, KBH= 3.342 m^3 and NBH=2.228 m^3 respectively of wastewater. This data indicates production per annum, on average 1 kg of tea subsequently generates 0.557 litres of wastewater.

A total of 16 wastewater samples were collected from each individual factory, making a total of 48 samples over a period of 6 months. The samples were characterized by their physico-chemical parameters, macro-molecules and heavy metals. The results show that, CBH (pH= 6.1, Turbidity= 62.3 N.T.U, Total Organic Carbon= 201 mgL^{-1}, Chemical Oxygen Demand= 547.34 mgL^{-1}, Total Suspended Solids =312 mgL^{-1}; Total Dissolved Solids= 1326.37 mgL^{-1}, Total metals; Fe=1.63 mgL^{-1}, Mn=1.62 mgL^{-1}, Al=10.67 mgL^{-1} and Ni=0.35 mgL^{-1}). KBH (pH= 5.6, Turbidity= 65.9 N.T.U, Total Organic Carbon= 236 mgL^{-1}, Chemical Oxygen Demand= 562.31 mgL^{-1}, Total Suspended Solids =327 mgL^{-1}; Total Dissolved Solids= 1368.52 mgL^{-1}), Metals Fe=1.39 mgL^{-1}, Mn=1.63 mgL^{-1}, Al= 7.44 mgL^{-1} and Ni=0.26 mgL^{-1}). NBH (pH=5.9 Turbidity= 64.0 N.T.U, Total Organic Carbon= 213.0 mgL^{-1}, Chemical Oxygen Demand= 553.06 mgL^{-1}, Total Suspended Solids =319 mgL^{-1}; Total Dissolved Solids= 1338.13 mgL^{-1}) Fe= 1.35 mgL^{-1}, Mn=0.26 mgL^{-1}, Al=18.89 mgL^{-1} and Ni= 0.35 mg/L^{-1}.

The wastewater samples were spectrophotometrically analysed to determine the wavelength of absorption for the 3 samples, CBH, KBH and NBH. The absorption wavelength was determined at λ= 410 nm.

Two powders used in photocatalytic treatment and colour removal; TiO_2 and ZnO were characterized by Laser Induced Breaking down spectroscopy (LIBS), Brunauer Emmett

Teller (BET), Scanning Electron Microscope (SEM), Energy Dispersive X-Ray Spectroscopy (EDS), Laser Induced Breaking Down Spectroscopy (LIBS) and X-Ray Diffraction (XRD). The obtained values were; (TiO_2 = Laser Induced Breakdown Spectroscopy, indicating Ti spectral peak at λ = 400 nm, Brunauer Emmett Teller surface area of TiO_2 -31.76 m^2/g, X-Ray Diffraction and Scanning Electron Microscope showed particle sizes of TiO_2 (16 nm $\pm$ 2 nm) and Spherical morphology, Energy Dispersive X-ray Spectroscopy indicated the degree of Titanium (Ti) in TiO_2 as 60%. (ZnO=Laser Induced Breakdown Spectroscopy indicating Zn spectral peaks at λ = 400 nm. Brunauer Emmett Teller surface area of ZnO 40.14 m^2/g, X-Ray Diffraction and Scanning Electron Microscope analysis showed particle sizes of ZnO = (16.21 nm $\pm$ 2 nm) and hexagonal morphological shape. Energy Dispersive X-ray Spectroscopy indicated the degree of zinc (Zn) in ZnO as 61.5%.

A prototype batch photocatalytic reactor of dimensions (20 cm×15 cm×10 cm) constructed from borosilicate glass was placed onto a magnetic stirrer and illuminated with either UV lamps (I=3.0 mW/cm^2) or solar light (I= 1.49 mW/cm^2).

Physico-chemical parameters of treated wastewater indicated; (CBH pH= 6.8, Turbidity= 34.8 N.T.U, Total Organic Carbon= 48.78 mg/l, Chemical Oxygen Demand= 224.27 mg/l, Total Suspended Solids = 129.09 mg/l; Total Dissolved Solids= 785.36mg/l); (KBH - pH= 6.6, Turbidity= 35.6 N.T.U, Total Organic Carbon= 63.7 mg/l, Chemical Oxygen Demand= 239.29 mg/l, Total Suspended Solids = 132.28 mg/l; Total Dissolved Solids= 801.56 mg/l); (NBH - pH= 6.7, Turbidity= 35.2 N.T.U, Total Organic Carbon= 51.26 mg/l, Chemical Oxygen Demand= 226.96 mg/l, Total Suspended Solids = 130.54 mg/l; Total Dissolved Solids= 788.69 mg/l).

The photocatalytic treatment was found to minimize, Total Organic Carbon, Chemical Oxygen Demand, Turbidity, Total Suspended Solids and Total Dissolved Solids by 74.8 %, 58.5 %, 45.1 %, 59.07 % and 41.53 % respectively, and shifted pH from acidity to neutrality by 12.5 % from 5.6 to 6.8 after 180 minutes. A GC-MS analysis of untreated wastewater samples indicated the presence of organic macromolecules that were identifiable and quantifiable. The number of molecules were as follows; (CBH= 9, KBH=14 and NBH= 12) respectively.

Photocatalytic treatment led to the following results; (TiO_2 /UV lamps - CBH = 76.22%, KBH = 70.32%and NBH= 73.27%); ZnO/UV lamp - CBH= 82.05%, KBH= 77.5% and NBH= 80.73%); (TiO_2/solar - CBH= 78.47%, KBH=72.25% and NBH=76.05%); (ZnO/solar - CBH= 87.0%, KBH= 78.67% and NBH= 84.18%).

A UV/TiO_2 treatment system achieved an efficiency of 73.27% colour removal in 180 min compared to a solar/TiO_2 treatment system where, 75.59% of colour was eliminated. In addition a ZnO/UV lamp system achieved 80.09% colour removal efficiency in 180 min compared to 83.2% colour removal in a ZnO /solar light system.

The solar/TiO_2 treatment system, proved efficient compared to UV/TiO_2 by 2.3% and the solar/ZnO treatment system, proved more efficient compared to UV/ZnO treatment system by 3%, despite the solar radiation intensity(I=1.49 mW/cm^2) applied, being less than half that of UV lamp(I= 3.0 mW/cm^2). From the results solar light provided an efficient supply of UV photons to drive the photocatalytic treatment reactions.

The UV/ZnO treatment system, was found to be more efficient, compared to UV/TiO_2 by 6.8% and ZnO/solar light treatment system, more efficient compared to solar/TiO_2 by 7.6 %. ZnO is therefore a more effective photocatalyst compared to TiO_2. The experimental results indicate that for the effective treatment and colour removal of tea processing wastewater, a Solar/ZnO photocatalyst prototype would be effective.

5.2 Recommendations

- A large scale continuous flow photocatalytic reactor based on ZnO/solar light system be piloted for large scale wastewater treatment.
- The role of visible light in solar mediated photocatalytic treatment be investigated in relation to the 5% UV light present.
- Focus for the development of more reliable photocatalysts which can absorb visible and solar radiation or both.

REFERENCES

APHA (2005) Standard Methods for the Examination of Water and Wastewater, 21st edn. American Public Health Association, Washington, DC

Agustina, T. E., Ang, H., & Vareek, V. (2005). A review of synergistic effect of photocatalysis and ozonation on wastewater treatment. *Journal of Photochemistry and Photobiology C: Photochemistry Reviews, **6***(4), 264-273.

Ajmal, A., Majeed, I., Malik, R. N., Idriss, H., & Nadeem, M. A. (2014). Principles and mechanisms of photocatalytic dye degradation on TiO_2 based photocatalysts: A comparative overview. *Rsc Advances, **4***(70), 37003-37026.

Akpan, U., & Hameed, B. (2009). Parameters affecting the photocatalytic degradation of dyes using TiO_2-based photocatalysts: A review. *Journal of hazardous materials, **170***(2), 520-529.

Akyol, A., Yatmaz, H., & Bayramoglu, M. (2004). Photocatalytic decolorization of remazol red rr in aqueous ZnO suspensions. *Applied Catalysis B: Environmental, **54***(1), 19-24.

Al-Rasheed, R., & Cardin, D. J. (2003). Photocatalytic degradation of humic acid in saline waters. Part 1. Artificial seawater: Influence of TiO_2, temperature, pH, and air-flow. *Chemosphere, **51***(9), 925-933.

Al-Rasheed, R. A. (2005). *Water treatment by heterogeneous photocatalysis an overview*. Paper presented at the 4th SWCC acquired Experience Symposium held in Jeddah. Alcazar, A., Ballesteros, O., Jurado, J., Pablos, F., Martin, M., Vilches, J., & Navalon, A. (2007). Differentiation of green, white, black, Oolong, and pu-erh teas according to their free amino acids content. *Journal of agricultural and food chemistry, **55***(15), 5960-5965.

Ali, R., & Hassan, S. H. (2008). Degradation studies on paraquat and malathion using TiO_2/ZnO based photocatalyst. *The Malaysian Journal of Analytical Sciences, **12***(1), 77-87.

Ameta, R., & Ameta, S. C. (2016). *Photocatalysis: Principles and applications*: CRC Press.

Angeles, M., Leyva, C., Ancheyta, J., & Ramírez, S. (2014). A review of experimental procedures for heavy oil hydrocracking with dispersed catalyst. *Catalysis today*, ***220,*** 274-294.

Anpo, M., & Takeuchi, M. (2003). The design and development of highly reactive titanium oxide photocatalysts operating under visible light irradiation. *Journal of catalysis*, ***216***(1), 505-516.

Aramendía, M., Borau, V., Colmenares, J., Marinas, A., Marinas, J., Navío, J., & Urbano, F. (2008). Modification of the photocatalytic activity of Pd/TiO_2 and Zn/TiO_2 systems through different oxidative and reductive calcination treatments. *Applied Catalysis B: Environmental*, ***80***(1), 88-97.

Arslan, I., & Balcioglu, I. A. (2001). Advanced oxidation of raw and biotreated textile industry wastewater with O_3, H_2O_2/UV-C and their sequential application. *Journal of Chemical Technology and Biotechnology*, ***76***(1), 53-60.

Arthur, J. (1983). *Notes in the design and operation of waste stabilization ponds in warm climates of developing countries*: The World Bank.

Augugliaro, V., Palmisano, L., Sclafani, A., Minero, C., & Pelizzetti, E. (1988). Photocatalytic degradation of phenol in aqueous titanium dioxide dispersions. *Toxicological & Environmental Chemistry*, ***16***(2), 89-109.

Azad, S., Estim, A., & Rathi, A. (2014). Effects of cage culture on dissolved inorganic nutrient and surface sediment composition in sulaman bay lagoon, sabah, malaysia. *Journal of Environmental Science, Computer Science and Engineering Technology*, ***3,*** 818-827.

Azarian, G., Mesdaghinia, A., Vaezi, F., Nabizadeh, R., & Nematollahi, D. (2007). Algae removal by electro-coagulation process, application for treatment of the effluent

from an industrial wastewater treatment plant. *Iranian Journal of Public Health, **36***(4), 57-64.

Baruah, S., & Dutta, J. (2009). Hydrothermal growth of ZnO nanostructures. *Science and Technology of Advanced Materials, **10***(1), 013001.

Behnajady, M., Modirshahla, N., & Hamzavi, R. (2006). Kinetic study on photocatalytic degradation of CI Acid Yellow 23 by ZnO photocatalyst. *Journal of hazardous materials, **133***(1), 226-232.

Bekbölet, M., & Özkösemen, G. (1996). A preliminary investigation on the photocatalytic degradation of a model humic acid. *Water Science and Technology, **33***(6), 189-194.

Bergamini, R. B., Azevedo, E. B., & De Araújo, L. R. R. (2009). Heterogeneous photocatalytic degradation of reactive dyes in aqueous TiO_2 suspensions: Decolorization kinetics. *Chemical Engineering Journal, **149***(1), 215-220.

Bhatkhande, D. S., Pangarkar, V. G., & Beenackers, A. A. (2002). Photocatalytic degradation for environmental applications–a review. *Journal of Chemical Technology and Biotechnology, **77***(1), 102-116.

Bizani, E., Fytianos, K., Poulios, I., & Tsiridis, V. (2006). Photocatalytic decolorization and degradation of dye solutions and wastewaters in the presence of titanium dioxide. *Journal of hazardous materials, **136*****(**1), 85-94.

Carp, O., Huisman, C. L., & Reller, A. (2004). Photoinduced reactivity of titanium dioxide. *Progress in solid state chemistry, **32***(1), 33-177.

Carraway, E. R., Hoffman, A. J., & Hoffmann, M. R. (1994). Photocatalytic oxidation of organic acids on quantum-sized semiconductor colloids. *Environmental science & technology, **28***(5), 786-793.

Cernigoj, U. (2007) Photodegradation of organic pollutants in aqueous solutions catalyzed

by immobilized titanium dioxide: Novel towards higher efficiency, dissertation nova Gorica.

Chan, Y. J., Chong, M. F., Law, C. L., & Hassell, D. (2009). A review on anaerobic–aerobic treatment of industrial and municipal wastewater. *Chemical Engineering Journal, **155(**1), 1-18.

Chen, X., Liu, L., Peter, Y. Y., & Mao, S. S. (2011). Increasing solar absorption for photocatalysis with black hydrogenated titanium dioxide nanocrystals. *Science*, ***331***(6018), 746-750.

Chen, X., & Mao, S. S. (2007). Titanium dioxide nanomaterials: Synthesis, properties, modifications, and applications. *Chem. Rev*, ***107***(7), 2891-2959.

Cho, S., Jang, J.-W., Lee, J. S., & Lee, K.-H. (2010). Carbon-doped ZnO nanostructures synthesized using vitamin C for visible light photocatalysis. *CrystEngComm*, ***12***(11), 3929-3935.

Chong, M. N., Jin, B., Chow, C. W., & Saint, C. (2010). Recent developments in photocatalytic water treatment technology: A review. *Water research, **44***(10), 2997-3027.

Chung, A., Wu, Y., Tam, N. Y., & Wong, M. (2008). Nitrogen and phosphate mass balance in a sub-surface flow constructed wetland for treating municipal wastewater. *Ecological Engineering, **32***(1), 81-89.

Clark, G. (2007). Evolution of the global sustainable consumption and production policy and the united nations environment programme's (UNEP) supporting activities. *Journal of cleaner production*, ***15***(6), 492-498.

Cooper, P. (1993). Removing colour from dyehouse waste waters—a critical review of technology available. *Coloration Technology*, ***109***(3), 97-100.

Couladis, M., Tzakou, O., Verykokidou, E., & Harvala, C. (2003). Screening of some greek aromatic plants for antioxidant activity. *Phytotherapy research*, ***17***(2), 194-195.

Dai, Y., Zhang, Y., & Wang, Z. L. (2003). The octa-twin tetraleg ZnO nanostructures. *Solid State Communications*, ***126***(11), 629-633.

Daneshvar, N., Salari, D., & Khataee, A. (2004). Photocatalytic degradation of azo dye acid red 14 in water on ZnO as an alternative catalyst to TiO_2. *Journal of Photochemistry and Photobiology A: Chemistry*, ***162***(2), 317-322.

Davydov, L., Reddy, E. P., France, P., & Smirniotis, P. G. (2001). Sonophotocatalytic destruction of organic contaminants in aqueous systems on TiO_2 powders. *Applied Catalysis B: Environmental*, ***32(***1), 95-105.

De Lasa, H. I., Serrano, B., & Salaices, M. (2005). *Photocatalytic reaction engineering*: Springer.

Demkov, A. A., & Posadas, A. B. (2014). *Integration of functional oxides with semiconductors*: Springer Science & Business Media.

Diffey, B. (1991). Solar ultraviolet radiation effects on biological systems. *Physics in medicine and biology*, ***36***(3), 299.

Doan, L., Baird, H., Doan, Q., & Ali, S. (1999). *Performance of the sagd process in the presence of a water sand-a preliminary investigation.* Paper presented at the Annual Technical Meeting.

Dufresne, C. J., & Farnworth, E. R. (2001). A review of latest research findings on the health promotion properties of tea. *The Journal of nutritional biochemistry*, ***12***(7), 404-421.

Eggins, B. R., Palmer, F. L., & Byrne, J. A. (1997). Photocatalytic treatment of humic substances in drinking water. *Water research*, ***31***(5), 1223-1226.

Eastern Produce Kenya Limited Annual Report; 2010.

Fox, M. A., & Dulay, M. T. (1993). Heterogeneous photocatalysis. *Chemical reviews*, ***93***(1), 341-357.

Frank, S. N., & Bard, A. J. (1977). Heterogeneous photocatalytic oxidation of cyanide ion in aqueous solutions at titanium dioxide powder. *Journal of the American Chemical Society*, ***99***(1), 303-304.

Frølund, B., Palmgren, R., Keiding, K., & Nielsen, P. H. (1996). Extraction of extracellular polymers from activated sludge using a cation exchange resin. *Water research*, ***30***(8), 1749-1758.

Fujishima, A., Hashimoto, K., & Watanabe, T. (1999). *TiO_2 photocatalysis: Fundamentals and applications*: BKC Incorporated.

Fujishima, A., & Honda, K. (1972). Electrochemical photolysis of water at a semiconductor electrode. *nature*, ***238***(5358), 37-38.

Fujishima, A., Ohtsuki, J., Yamashita, T., & Hayakawa, S. (1986). Behavior of tumor cells on photoexcited semiconductor surface. *Photomed. Photobiol*, ***8***, 45-46.

Fujishima, A., & Rao, T. N. (1997). Recent advances in heterogeneous TiO_2 photocatalysis. *Journal of Chemical Sciences*, ***109***(6), 471-486.

Fujishima, A., Rao, T. N., & Tryk, D. A. (2000). Titanium dioxide photocatalysis. *Journal of Photochemistry and Photobiology C: Photochemistry Reviews*, ***1***(1), 1-21.

Galian, R., & Perez-Prieto, J. (2010). Catalytic processes activated by light. *Energy & Environmental Science*, ***3***(10), 1488-1498.

Garcia, S. P., & Semancik, S. (2007). Controlling the morphology of zinc oxide nanorods crystallized from aqueous solutions: The effect of crystal growth modifiers on aspect ratio. *Chemistry of materials*, ***19***(16), 4016-4022.

Gaya, U. I., & Abdullah, A. H. (2008). Heterogeneous photocatalytic degradation of organic contaminants over titanium dioxide: A review of fundamentals, progress and problems. *Journal of Photochemistry and Photobiology C: Photochemistry Reviews*, ***9***(1), 1-12.

Georgekutty, R., Seery, M. K., & Pillai, S. C. (2008). A highly efficient Ag-ZnO hotocatalyst: Synthesis, properties, and mechanism.

Gilmore, F. W., & Renk, R. R. (2014). Method and apparatus for producing high volumes of clean water by electro coagulation: Google Patents.

Gondal, M.A., Umair Baig, M., Dastageer, A and Mohsin, S. Determination of elemental composition of coffee using UV-pulsed laser induced breakdown spectroscopy. Proceedings of The Fifth Saudi International Meeting on Frontiers of Physics (SIMFP 2016) AIP Conf. Proc. 1742, 030007-1–030007-5.

Gogate, P. R., & Pandit, A. B. (2004). Sonophotocatalytic reactors for wastewater treatment: A critical review. *AIChE Journal*, ***50*** (5), 1051-1079.

GOK (2009): "Environmental Management and Coordination Act." Government printers.

GOK (2007): "Occupational Safety and Health act no. 15 of 2007." Government printers.

GOK (2017): "Strategic Assessment, Integrated Impact Assessment and Audit Regulations." Government printers

GOK (2014): "Water act no. 27." Government printers

GOK (2006): "Water resources management (water) rules." Government printers

GOK (2006): "Wetlands and River bank Regulations." Government printers.

Gokmen, T., Gunawan, O.T., Todorov, K.M and Mitzi, B. (2013) Band tailing and efficiency limitation in kesterite solar cells. *Applied Physics Letters*, **103**(10), 10-35.

Gouvea, C. A., Wypych, F., Moraes, S. G., Duran, N., Nagata, N., & Peralta-Zamora, P. (2000). Semiconductor-assisted photocatalytic degradation of reactive dyes in aqueous solution. *Chemosphere*, ***40***(4), 433-440.

Graham, H. N. (1992). Green tea composition, consumption, and polyphenol chemistry. *Preventive medicine*, ***21***(3), 334-350.

Grzechulska, J., Hamerski, M., & Morawski, A. W. (2000). Photocatalytic decomposition of oil in water. *Water research*, ***34***(5), 1638-1644.

Guan, H., Zhu, L., Zhou, H., & Tang, H. (2008). Rapid probing of photocatalytic activity on titania-based self-cleaning materials using 7-hydroxycoumarin fluorescent probe. *Analytica chimica acta*, ***608***(1), 73-78.

Guillard, C., Lachheb, H., Houas, A., Ksibi, M., Elaloui, E., & Herrmann, J.-M. (2003). Influence of chemical structure of dyes, of ph and of inorganic salts on their photocatalytic degradation by TiO_2 comparison of the efficiency of powder and supported TiO_2. *Journal of Photochemistry and Photobiology A: Chemistry*, ***158***(1), 27-36.

Habib, M. A., Ismail, I. M. I., Mahmood, A. J., & Ullah, M. R. (2012). Photocatalytic decolorization of brilliant golden yellow in TiO_2 and ZnO suspensions. *Journal of Saudi Chemical Society*, ***16***(4), 423-429.

Haddis, A., & Devi, R. (2008). Effect of effluent generated from coffee processing plant on the water bodies and human health in its vicinity. *Journal of hazardous materials*, ***152***(1), 259-262.

Hammer, M. (1996). Hammer jr. *Water and Wastewater technology*, *5*.

Han, L., Takaku, T., Li, J., Kimura, Y., & Okuda, H. (1999). Anti-obesity action of oolong tea. *International Journal Of Obesity & Related Metabolic Disorders*, ***23***(1) 29 - 42

Han, S.-P., Gan, W.-E., & Su, Q.-D. (2007). On-line sample digestion using an electromagnetic heating column for the determination of zinc and manganese in tea leaf by flame atomic absorption spectrometry. *Talanta, **72***(4), 1481-1486.

Hayashi, H., Nakajima, Y., & Ohta, K. (2007). Novel degradation method of organic compounds in human surroundings using iron oxide. *Rep. Technol. Res. Institute Osaka Pref, **21***, 79-83.

Heller, A. (1981). Conversion of sunlight into electrical power and photoassisted electrolysis of water in photoelectrochemical cells. *Accounts of Chemical Research, **14***(5), 154-162.

Hoffmann, M.R., Martin, S. T., Choi, W and Bahnemann, D.W. (1995) Environmental applications of semiconductor photocatalysis. Chem. Rev. 95, 69-96.

Huang, J., Xu, X., Gu, C., Wang, W., Geng, B., Sun, Y., & Liu, J. (2012). Effective VOCs gas sensor based on porous SnO_2 microcubes prepared via spontaneous phase segregation. *Sensors and Actuators B: Chemical, **173,*** 599-606.

Huang, Y.-H., Huang, Y.-F., Chang, P.-S., & Chen, C.-Y. (2008). Comparative study of oxidation of dye-reactive black b by different advanced oxidation processes: Fenton, electro-fenton and photo-fenton. *Journal of hazardous materials, **154***(1), 655-662.

Hussein, F. H., & Abass, T. A. (2010). Photocatalytic treatment of textile industrial wastewater. *International Journal of Chemical Sciences, **8***(3).

Idota, Y., Kubota, T., Matsufuji, A., Maekawa, Y., & Miyasaka, T. (1997). Tin-based amorphous oxide: A high-capacity lithium-ion-storage material. *Science, **276***(5317), 1395-1397.

Inan, H., Dimoglo, A., Şimşek, H., & Karpuzcu, M. (2004). Olive oil mill wastewater treatment by means of electro-coagulation. *Separation and purification technology, **36***(1), 23-31.

Iqbal, S. (1999). Duckweed aquaculture. *Potentials, possibilities and limitations for combined wastewater treatment and animal feed production in developing countries. San-DEC Report*(6/99).

Kansal, S., Singh, M., & Sud, D. (2007). Studies on photodegradation of two commercial dyes in aqueous phase using different photocatalysts. *Journal of hazardous materials*, ***141***(3), 581-590.

Karakaya, S., & El, S. N. (2006). Total phenols and antioxidant activities of some herbal teas and in vitro bioavailability of black tea polyphenols.

Karr, J. R., & Chu, E. (2006). Seven foundations of biological monitoring and assessment. *Biologia Ambientale*, ***20***(2), 7-18.

Kerc, A., Bekbolet, M., & Saatci, A. M. (2003). Effect of partial oxidation by ozonation on the photocatalytic degradation of humic acids. *International Journal of Photoenergy*, ***5***(2), 75-80.

Khataee, A., Vatanpour, V., & Ghadim, A. A. (2009). Decolorization of ci acid blue 9 solution by UV/nano-TiO_2, fenton, fenton-like, electro-fenton and electrocoagulation processes: A comparative study. *Journal of hazardous materials*, ***161***(2), 1225-1233.

Khezrianjoo, S., & Revanasiddappa, H. (2012). Langmuir-hinshelwood kinetic expression for the photocatalytic degradation of metanil yellow aqueous solutions by ZnO catalyst. *Chemical Sciences Journal*.

Kilmartin, P. A., & Hsu, C. F. (2003). Characterisation of polyphenols in green, oolong, and black teas, and in coffee, using cyclic voltammetry. *Food Chemistry*, ***82***(4), 501-512.

Kim, J., Lee, C. W., & Choi, W. (2010). Platinized WO_3 as an environmental photocatalyst that generates oh radicals under visible light. *Environmental science & technology*, ***44***(17), 6849-6854.

Kim, S.-J., & Park, D.-W. (2009). Preparation of ZnO nanopowders by thermal plasma and characterization of photo-catalytic property. *Applied Surface Science, **255***(10), 5363-5367.

Konstantinou, I. K., & Albanis, T. A. (2004). TiO_2 assisted photocatalytic degradation of azo dyes in aqueous solution: Kinetic and mechanistic investigations: A review. *Applied Catalysis B: Environmental, **49***(1), 1-14.

Krishnakumar, B., Selvam, K., Velmurugan, R., & Swaminathan, M. (2010). Influence of operational parameters on photodegradation of acid black 1 with ZnO. *Desalination and Water Treatment, **24***(1-3), 132-139.

Kubacka, A., Ferrer, M., Fernández-García, M., Serrano, C., Cerrada, M. L., & Fernández-García, M. (2011). Tailoring polymer–TiO_2 film properties by presence of metal (Ag, Cu, Zn) species: Optimization of antimicrobial properties. *Applied Catalysis B: Environmental, **104***(3), 346-352.

Lawson, E. (2011). Physico-chemical parameters and heavy metal contents of water from the mangrove swamps of lagos lagoon, lagos, nigeria. *Advances in Biological Research, **5***(1), 8-21.

Li, B., Liu, T., Wang, Y., & Wang, Z. (2012). ZnO/graphene-oxide nanocomposite with remarkably enhanced visible-light-driven photocatalytic performance. *Journal of colloid and interface science, **377***(1), 114-121.

Li, J., Shen, D., Zhang, J., Zhao, D., Li, B., Lu, Y., Liu, Y., & Fan, X. (2007). The effect of Mn^{2+} doping on strcuture and photoluminescence of ZnO nanofilms synthesized by sol–gel method. *Journal of luminescence, **122***, 352-354.

Li, M., Lin, D., & Zhu, L. (2013). Effects of water chemistry on the dissolution of ZnO nanoparticles and their toxicity to escherichia coli. *Environmental pollution, **173***, 97-102.

Li, Q., Mahendra, S., Lyon, D. Y., Brunet, L., Liga, M. V., Li, D., & Alvarez, P. J. (2008). Antimicrobial nanomaterials for water disinfection and microbial control: Potential applications and implications. *Water research, **42***(18), 4591-4602.

Li, Y.-H., Gu, W., & Ye, S. (2007). Expression and location of caffeine synthase in tea plants. *Russian Journal of Plant Physiology, **54***(5), 698-701.

Lin, A. Y.-C., Debroux, J.-F., Cunningham, J. A., & Reinhard, M. (2003). Comparison of rhodamine wt and bromide in the determination of hydraulic characteristics of constructed wetlands. *Ecological Engineering, **20***(1), 75-88.

Lin, J.Z., Pan Pan, Z.X., Hairong, L., & Yaoping, X.C (2013. Discrimination of oolong tea (Camellia sinensis) varieties based on feature extraction and selection from aromatic profiles analysed by HS-SPME/GC–MS. *Food chemistry*,**141**(1),259-265.

Lin, D., Tu, Y., & Zhu, L. (2005). Concentrations and health risk of polycyclic aromatic hydrocarbons in tea. *Food and Chemical Toxicology, **43***(1), 41-48.

Lin, L.-Z., Chen, P., & Harnly, J. M. (2008). New phenolic components and chromatographic profiles of green and fermented teas. *Journal of agricultural and food chemistry, **56*(**(**17), 8130-8140.

Lin, S. H., & Chang, C. C. (2000). Treatment of landfill leachate by combined electro-fenton oxidation and sequencing batch reactor method. *Water research, **34***(17), 4243-4249.

Lopez-Alvarez, B., Torres-Palma, R. A., Ferraro, F., & Peñuela, G. (2012). Solar photo-fenton treatment of carbofuran: Analysis of mineralization, toxicity, and organic by-products. *Journal of Environmental Science and Health, Part A, **47***(13), 2141-2150.

Lucas, M. S., Beltrán-Heredia, J., Sanchez-Martin, J., Garcia, J., & Peres, J. A. (2013). Treatment of high strength olive mill wastewater by fenton's reagent and aerobic

biological process. *Journal of Environmental Science and Health, Part A,* ***48***(8), 954-962.

Ma, X., Weng, H., & Zhang, J. (2011). Regional characteristics and trend of heavy metals and nutrients of sewage sludge in china. *China Environmental Science,* ***31***(8), 1306-1313.

Maghanga, J. K., Segor, F. K., Etiégni, L., & Lusweti, J. (2009). Electrocoagulation method for colour removal in tea effluent: A case study of chemomi tea factory in rift valley, kenya. *Bulletin of the Chemical Society of Ethiopia,* ***23***(3).

Mahmood, A. J., Jabbar, M., & Akhtar, S. (2003). Influence of light on the degradation of a dye in homogeneous and heterogeneous media. *J. Bangladesh Chem. Soc,* ***16***, 57-70.

Mahmood, M. A., & Dutta, J. (2012). Microwave assisted hydrothermal synthesis of zinc hydroxystannate films on glass substrates. *Journal of sol-gel science and technology,* ***62***(3), 495-504.

Mahmoodi, N. M., Arami, M., Limaee, N. Y., Gharanjig, K., & Ardejani, F. D. (2006). Decolorization and mineralization of textile dyes at solution bulk by heterogeneous nanophotocatalysis using immobilized nanoparticles of titanium dioxide. *Colloids and Surfaces A: Physicochemical and Engineering Aspects,* ***290***(1), 125-131.

Malato, S., Blanco, J., Campos, A., Cáceres, J., Guillard, C., Herrmann, J., & Fernandez-Alba, A. (2003). Effect of operating parameters on the testing of new industrial titania catalysts at solar pilot plant scale. *Applied Catalysis B: Environmental*, ***42***(4), 349-357.

Mathews, R. (1988). Kinetics of photocatalytic oxidation of organic solutes over titanium dioxide catalysis. *Journal of catalysis,* ***111,*** 264-272.

Matsunaga, T., Tomoda, R., Nakajima, T., & Wake, H. (1985). Photoelectrochemical sterilization of microbial cells by semiconductor powders. *FEMS Microbiology letters,* ***29***(1-2), 211-214.

Mehrvar, M., Anderson, W. A., & Moo-Young, M. (2001). Photocatalytic degradation of aqueous organic solvents in the presence of hydroxyl radical scavengers. *International Journal of Photoenergy*, ***3***(4), 187-191.

Mills, A., & Le Hunte, S. (1997). An overview of semiconductor photocatalysis. *Journal of Photochemistry and Photobiology A: Chemistry*, ***108***(1), 1-35.

Minero, C., Pelizzetti, E., Sega, M., Friberg, S., & Sjö blom, J. (1999). The role of humic substances in the photocatalytic degradation of water contaminants. *Journal of dispersion science and technology*, ***20***(1-2), 643-661.

Mohabansi, N., Patil, V., & Yenkie, N. (2011). A comparative study on photo degradation of methylene blue dye effluent by advanced oxidation process by using TiO_2/ZnO photo catalyst. *Rasayan Journal of Chemistry*, ***4***(4), 814-819.

Mok, N. (2009). *Photocatalytic degradation of oily wastewater: Effect of catalyst concentration load, irradiation time and temperature.* UMP.

Mollah, M. Y. A., Schennach, R., Parga, J. R., & Cocke, D. L. (2001). Electrocoagulation (ec)—science and applications. *Journal of hazardous materials*, ***84***(1), 29-41.

Monteith, H., Parker, W., Bell, J., & Melcer, H. (1995). Modeling the fate of pesticides in municipal wastewater treatment. *Water environment research*, ***67***(6), 964-970.

Mor, G. K., Varghese, O. K., Paulose, M., Shankar, K., & Grimes, C. A. (2006). A review on highly ordered, vertically oriented TiO_2 nanotube arrays: Fabrication, material properties, and solar energy applications. *Solar Energy Materials and Solar Cells*, ***90***(14), 2011-2075.

Moseley, H. (1988). *Non-ionising radiation: Microwaves, ultraviolet and laser radiation*: Hilger.

Mucheke , C. M. (2015). Capacity utilization, quality of tea and returns to KTDA factories in kenya.

Muruganandham, M., Suri, R., Jafari, S., Sillanpää, M., Lee, G.-J., Wu, J., & Swaminathan, M. (2014). Recent developments in homogeneous advanced oxidation processes for water and wastewater treatment. *International Journal of Photoenergy*.

Nakahara, K., Kawabata, S., Ono, H., Ogura, K., Tanaka, T., Ooshima, T., & Hamada, S. (1993). Inhibitory effect of oolong tea polyphenols on glycosyltransferases of mutans streptococci. *Applied and Environmental Microbiology, **59***(4), 968-973.

Ndasi, N. P., Augustin, M., & Bosco, T. J. (2011). Biodecolourisation of textile dyes by local microbial consortia isolated from dye polluted soils in Ngaoundere (Cameroon). *International Journal of Environmental Sciences, **1***(7), 1403.

Nirmala, M., Nair, M. G., Rekha, K., Anukaliani, A., Samdarshi, S., & Nair, R. G. (2010). Photocatalytic activity of ZnO nanopowders synthesized by dc thermal plasma. *Afr. J. Basic Appl. Sci, **2***(5-6), 161-166.

Ollis, D. F., & Al-Ekabi, H. (1993). *Photocatalytic purification and treatment of water and air: Proceedings of the 1st international conference on TiO_2 photocatalytic purification and treatment of water and air, london, ontario, canada, 8-13 november, 1992*: Elsevier Science Ltd.

Onyatta, J.O., Tum, P.K., Kithure, J.G.N and Oduor, F.D.O.(2016) Photocatalytic Degradation of Acid Orange II dye on selected Titanium dioxide catalysts. International Journal of Advanced Research **4**(10), 1149-1155.

Oppenländer, T. (2003). *Photochemical purification of water and air: Advanced oxidation processes (aops)-principles, reaction mechanisms, reactor concepts*: John Wiley & Sons.

Ou, B., Hampsch-Woodill, M., Flanagan, J., Deemer, E. K., Prior, R. L., & Huang, D. (2002). Novel fluorometric assay for hydroxyl radical prevention capacity using fluorescein as the probe. *Journal of agricultural and food chemistry, **50***(10), 2772-2777.

Owuor, P. (2011). Tea in kenya: Production and country profile. *Two and a bud, **58***(10-18).

Pal, S. B. S. K., & Dutta, J. (2002). Nanostructured zinc oxide for water treatment. *Nanoscience and Nanotechnology-Asia*.

Parra, L.-M. M., Torres, G., Arenas, A. D., Sánchez, E., & Rodríguez, K. (2012). Phytoremediation of low levels of heavy metals using duckweed (lemna minor) *Abiotic stress responses in plants* (pp. 451-463): Springer.

Parsons, S. (2004). *Advanced oxidation processes for water and wastewater treatment*: IWA publishing.

Paul, S., Wachira, F., Powell, W., & Waugh, R. (1997). Diversity and genetic differentiation among populations of indian and kenyan tea (camellia sinensis (l.) o. Kuntze) revealed by aflp markers. *Theoretical and Applied Genetics, **94***(2), 255-263.

Pelaez, M., Nolan, N. T., Pillai, S. C., Seery, M. K., Falaras, P., Kontos, A. G., Dunlop, P. S., Hamilton, J. W., Byrne, J. A., & O'shea, K. (2012). A review on the visible light active titanium dioxide photocatalysts for environmental applications. *Applied Catalysis B: Environmental, **125***, 331-349.

Pirkanniemi, K., & Sillanpää, M. (2002). Heterogeneous water phase catalysis as an environmental application: A review. *Chemosphere, **48***(10), 1047-1060.

Rajaram, T., & Das, A. (2008). Water pollution by industrial effluents in india: Discharge scenarios and case for participatory ecosystem specific local regulation. *Futures, **40***(1), 56-69.

Rajeshwar, K., & Ibanez, J. (1995). Electrochemical aspects of photocatalysis: Application to detoxification and disinfection scenarios. *J. Chem. Educ, **72***(11), 1044.

Ramaswamy, S. R. (1993). Recovery of caffeine from tea trimmings and vegetable wastes: Google Patents.

Rice, R. G. (1996). Applications of ozone for industrial wastewater treatment—a review. *Ozone: science & engineering*, ***18***(6), 477-515.

Rizzo, L. (2011). Bioassays as a tool for evaluating advanced oxidation processes in water and wastewater treatment. *Water research*, ***45***(15), 4311-4340.

Robel, I., Kuno, M., & Kamat, P. V. (2007). Size-dependent electron injection from excited cdse quantum dots into TiO_2 nanoparticles. *Journal of the American Chemical Society*, ***129***(14), 4136-4137.

Roberts, E. (1958). The chemistry of tea manufacture. *Journal of the Science of Food and Agriculture*, ***9***(7), 381-390.

Roberts, J. D., & Caserio, M. C. (1977). *Basic principles of organic chemistry*: WA Benjamin, Inc.

Russ, J. C. (1984) Fundamentals of Energy Dispersive X-ray Analysis, Butterworths. London.

Sakthivel, S., & Kisch, H. (2003). Daylight photocatalysis by carbon-modified titanium dioxide. *Angewandte Chemie International Edition*, ***42***(40), 4908-4911.

Saravanan, M., John, K. M., Kumar, R. R., Pius, P., & Sasikumar, R. (2005). Genetic diversity of upasi tea clones (camellia sinensis (l.) O. Kuntze) on the basis of total catechins and their fractions. *Phytochemistry*, ***66***(5), 561-565.

Seenivasan, S., Manikandan, N., Muraleedharan, N. N., & Selvasundaram, R. (2008). Heavy metal content of black teas from south india. *Food control*, ***19***(8), 746-749.

Sharma, S., & Bhattacharya, A. (2017). Drinking water contamination and treatment techniques. *Applied Water Science*, ***7***(3), 1043-1067.

Shephard, G. S., Stockenström, S., de Villiers, D., Engelbrecht, W. J., & Wessels, G. F. (2002). Degradation of microcystin toxins in a falling film photocatalytic reactor with immobilized titanium dioxide catalyst. *Water research, **36***(1), 140-146.

Singh, P., Mondal, K., & Sharma, A. (2013). Reusable electrospun mesoporous ZnO nanofiber mats for photocatalytic degradation of polycyclic aromatic hydrocarbon dyes in wastewater. *Journal of colloid and interface science, **394***, 208-215.

Skillicorn, P., Spira, W., & Journey, W. (1993). *Duckweed aquaculture: A new aquatic farming system for developing countries*: World Bank.

Sonawane, R., Kale, B., & Dongare, M. (2004). Preparation and photo-catalytic activity of Fe/TiO_2 thin films prepared by sol–gel dip coating. *Materials Chemistry and Physics, **85***(1), 52-57.

Souther, R., & Alspaugh, T. (1957). Textile wastes: Recovery and treatment. *Sewage and Industrial Wastes, **29***(8), 918-935.

Staszkiewicz, N. (2004). Synthesis and characteristics of ZnO nanowires. *NNIN REU Research Accomplishments*, 132-133.

Strunk, J., Kähler, K., Xia, X., & Muhler, M. (2009). The surface chemistry of ZnO nanoparticles applied as heterogeneous catalysts in methanol synthesis. *Surface Science, **603***(10), 1776-1783.

Sung-Suh, H. M., Choi, J. R., Hah, H. J., Koo, S. M., & Bae, Y. C. (2004). Comparison of Ag deposition effects on the photocatalytic activity of nanoparticulate TiO_2 under visible and UV light irradiation. *Journal of Photochemistry and Photobiology A: Chemistry, **163***(1), 37-44.

Tachibana, Y., Vayssieres, L., & Durrant, J. R. (2012). Artificial photosynthesis for solar water-splitting. *Nature Photonics, **6***(8), 511-518.

Takino, Y., Ferretti, A., Flanagan, V., Gianturco, M., & Vogel, M. (1965). The structure of theaflavin, a polyphenol of black tea. *Tetrahedron Letters, **6***(45), 4019-4025.

Tang, H., Hessel, C. M., Wang, J., Yang, N., Yu, R., Zhao, H., & Wang, D. (2014). Two-dimensional carbon leading to new photoconversion processes. *Chemical Society Reviews, **43***(13), 4281-4299.

Tea Directorate of Kenya Annual Report: 2016

Technical Report, Eastern Produce Kenya Limited Annual Report; 2010

Teixeira, L. G., Lages, P. C., Jascolka, T. L., Aguilar, E. C., Soares, F. L. P., Pereira, S. S., Beltrão, N. R. M., Matoso, R. D. O., Nascimento, A. M. D, & Castilho, R. O. D. (2012). White tea (camellia sinensis) extract reduces oxidative stress and triacylglycerols in obese mice. *Food Science and Technology (Campinas), **32***(4), 733-741.

Thiruvenkatachari, R., Vigneswaran, S., & Moon, I. S. (2008). A review on UV/TiO_2 photocatalytic oxidation process (journal review). *Korean Journal of Chemical Engineering, **25***(1), 64-72.

Thomas, J., Vijayan, D., Joshi, S. D., Lopez, S. J., & Kumar, R. R. (2006). Genetic integrity of somaclonal variants in tea (camellia sinensis (l.) O kuntze) as revealed by inter simple sequence repeats. *Journal of biotechnology, **123***(2), 149-154.

Thompson, T. L., & Yates, J. T. (2006). Surface science studies of the photoactivation of TiO_2 new photochemical processes. *Chemical reviews, **106***(10), 4428-4453.

Tipton, G. A., & Slack, H. M. (2005). Cells and electrodes for electrocoagulation treatment of wastewater: Google Patents.

Tum, P.K., Kariuki, D.K., Oduor, F.D.O & Wanyoko, J.K.(2016) Zinc oxide photocatalytic decolourization of black tea(Camellia sinensis) wastewater from processing factories in Kenya.*International Journal of Advanced Research* **4**(11), 2206-2212.

Turro, N. J., Ramamurthy, V., & Scaiano, J. C. (2009). *Principles of molecular photochemistry: An introduction*: University science books.

Ullah, R., & Dutta, J. (2008). Photocatalytic degradation of organic dyes with manganese-doped ZnO nanoparticles. *Journal of hazardous materials*, ***156***(1), 194-200.

Van der Bruggen, B., & Braeken, L. (2006). The challenge of zero discharge: From water balance to regeneration. *Desalination*, ***188***(1-3), 177-183.

Vinodgopal, K., Wynkoop, D. E., & Kamat, P. V. (1996). Environmental photochemistry on semiconductor surfaces: Photosensitized degradation of a textile azo dye, acid orange 7, on TiO_2 particles using visible light. *Environmental science & technology*, ***30***(5), 1660-1666.

Wadley, S., & Waite, T. (2004). Fenton processes. *Advanced Oxidation Processes for Water and Wastewater Treatment*, 111-136.

Wang, R., Hashimoto, K., Fujishima, A., Chikuni, M., Kojima, E., Kitamura, A., Shimohigoshi, M., & Watanabe, T. (1997). Light-induced amphiphilic surfaces. *nature*, ***388***, 431-432.

Wang, S. (2008). A comparative study of fenton and fenton-like reaction kinetics in decolourisation of wastewater. *Dyes and Pigments*, ***76***(3), 714-720.

Wang, Y., Wang, Q., Zhan, X., Wang, F., Safdar, M., & He, J. (2013). Visible light driven type II heterostructures and their enhanced photocatalysis properties: A review. *Nanoscale*, ***5***(18), 8326-8339.

Wang, Z. L. (2004). Zinc oxide nanostructures: Growth, properties and applications. *Journal of Physics: Condensed Matter*, ***16***(25), R829.

Wasewar, K. L., Atif, M., Prasad, B., & Mishra, I. (2009). Batch adsorption of zinc on tea factory waste. *Desalination*, ***244***(1-3), 66-71.

Water, U. (2008). Transboundary waters: Sharing benefits, sharing responsibilities. *Thematic Paper*, 20.

Wojnarovits, L., & Takacs, E. (2008). Irradiation treatment of azo dye containing wastewater: An overview. *Radiation physics and chemistry*, ***77***(3), 225-244.

Wu, B., Wang, Y., Lee, Y.-H., Horst, A., Wang, Z., Chen, D.-R., Sureshkumar, R., & Tang, Y. J. (2010). Comparative eco-toxicities of nano-ZnO particles under aquatic and aerosol exposure modes. *Environmental science & technology*, ***44***(4), 1484-1489.

Yang, J. L., An, S. J., Park, W. I., Yi, G. C., & Choi, W. (2004). Photocatalysis using ZnO thin films and nanoneedles grown by metal–organic chemical vapour deposition. *Advanced materials*, ***16***(18), 1661-1664.

Zhu, Q. Y., Hackman, R. M., Ensunsa, J. L., Holt, R. R., & Keen, C. L. (2002). Antioxidative activities of Oolong tea. *Journal of agricultural and food chemistry*, ***50***(23), 6929-6934.

Zimbron, J. A., & Reardon, K. F. (2009). Fenton's oxidation of pentachlorophenol. *Water research*, ***43***(7), 1831-1840.

Zimmerman, M. C. (1993). The use of the biotic index as an indication of water quality. *Tested studies for laboratory teaching*, ***5***, 85-98.

Ziolli, R. L., & Jardim, W. F. (2002). Photocatalytic decomposition of seawater-soluble crude-oil fractions using high surface area colloid nanoparticles of . *Journal of Photochemistry and Photobiology A: Chemistry*, ***147***(3), 205-212.

APPENDICES

Appendix I

GC-MS analysis – KBH Sample

Appendix 1 Chromatogram – KBH sample

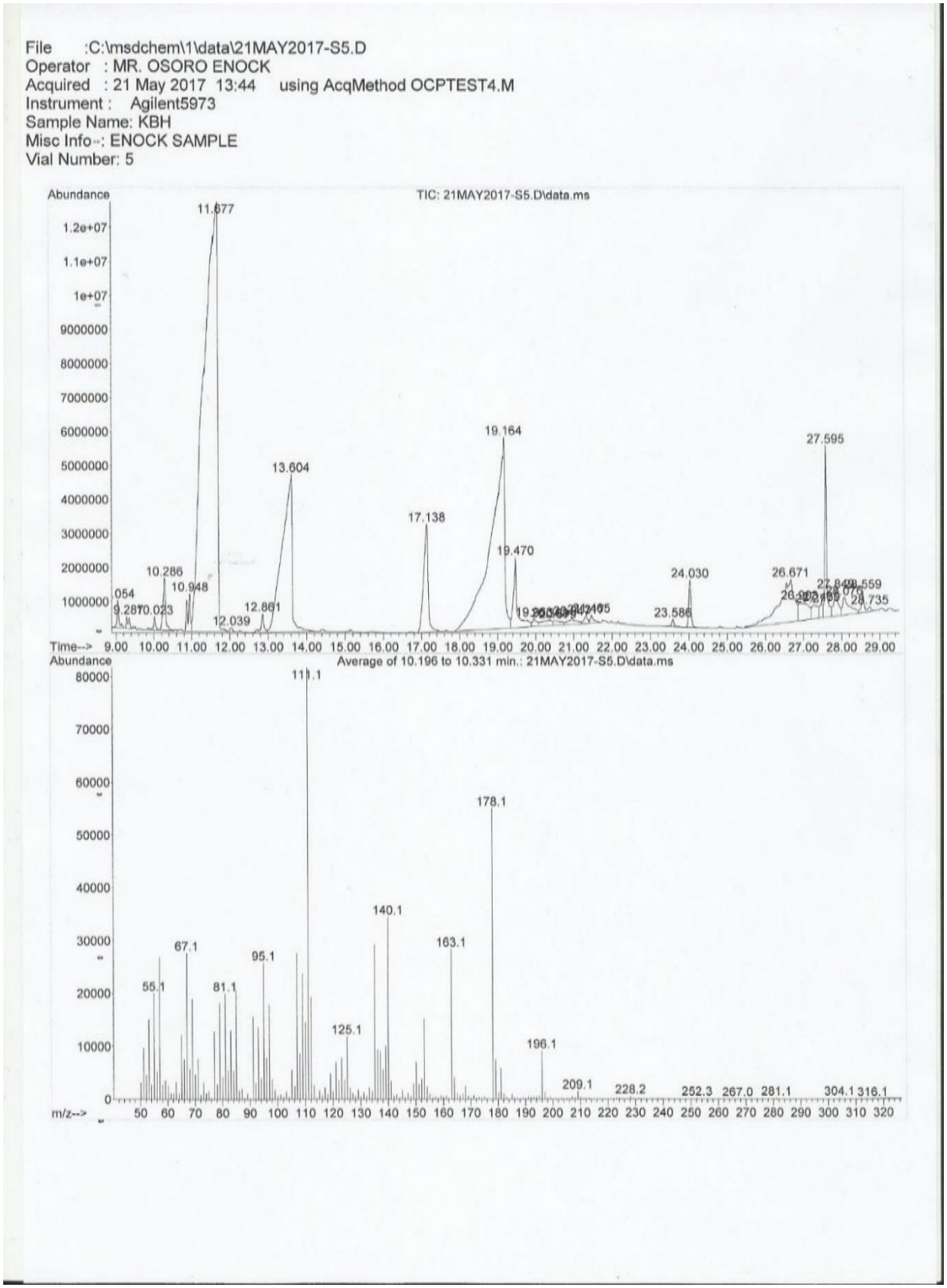

Appendix 2 (2-Butanone, 4-(2, 6, 6-trimethyl-1-yl)-

Hit 1 : 2-Butanone, 4-(2,6,6-trimethyl-1-cyclohexen-1-yl)-
$C_{13}H_{22}O$; MF: 761; RMF: 787; Prob 10.5%; CAS: 17283-81-7; Lib: replib; ID: 2932.

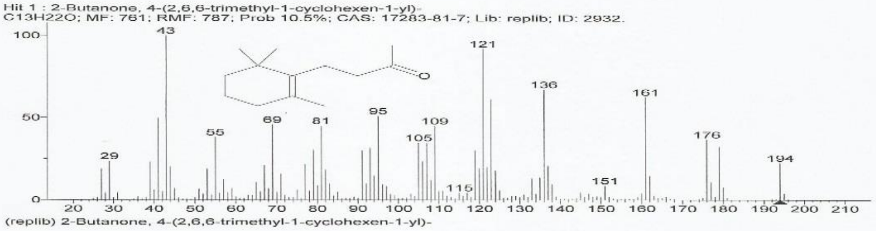

(replib) 2-Butanone, 4-(2,6,6-trimethyl-1-cyclohexen-1-yl)-

Name: 2-Butanone, 4-(2,6,6-trimethyl-1-cyclohexen-1-yl)-
Formula: $C_{13}H_{22}O$
MW: 194 CAS#: 17283-81-7 NIST#: 194690 ID#: 2932 DB: replib
Other DBs: TSCA, EINECS
Contributor: Chemical Concepts
10 largest peaks:
43 999 | 121 919 | 136 672 | 161 625 | 123 612 | 95 509 | 41 496 | 69 457 | 81 450 | 109 449 |

Unknown; InLib=-625

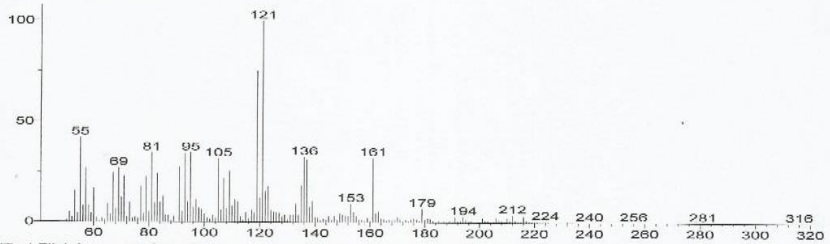

(Text File) Average of 9.022 to 9.076 min.: 21MAY2017-S5.D\data.ms

Name: Average of 9.022 to 9.076 min.: 21MAY2017-S5.D\data.ms
MW: N/A ID#: 1627 DB: Text File
Comment: KBH
10 largest peaks:
121 999 | 119 751 | 55 420 | 95 346 | 81 345 | 93 337 | 136 325 | 161 320 | 105 316 | 137 312 |

Appendix 3 1-{2-[3-(2-Acetyloxiran-2-yl)-1, 1-dimethylpropyl] cycloprop-2-enyl} ethanone

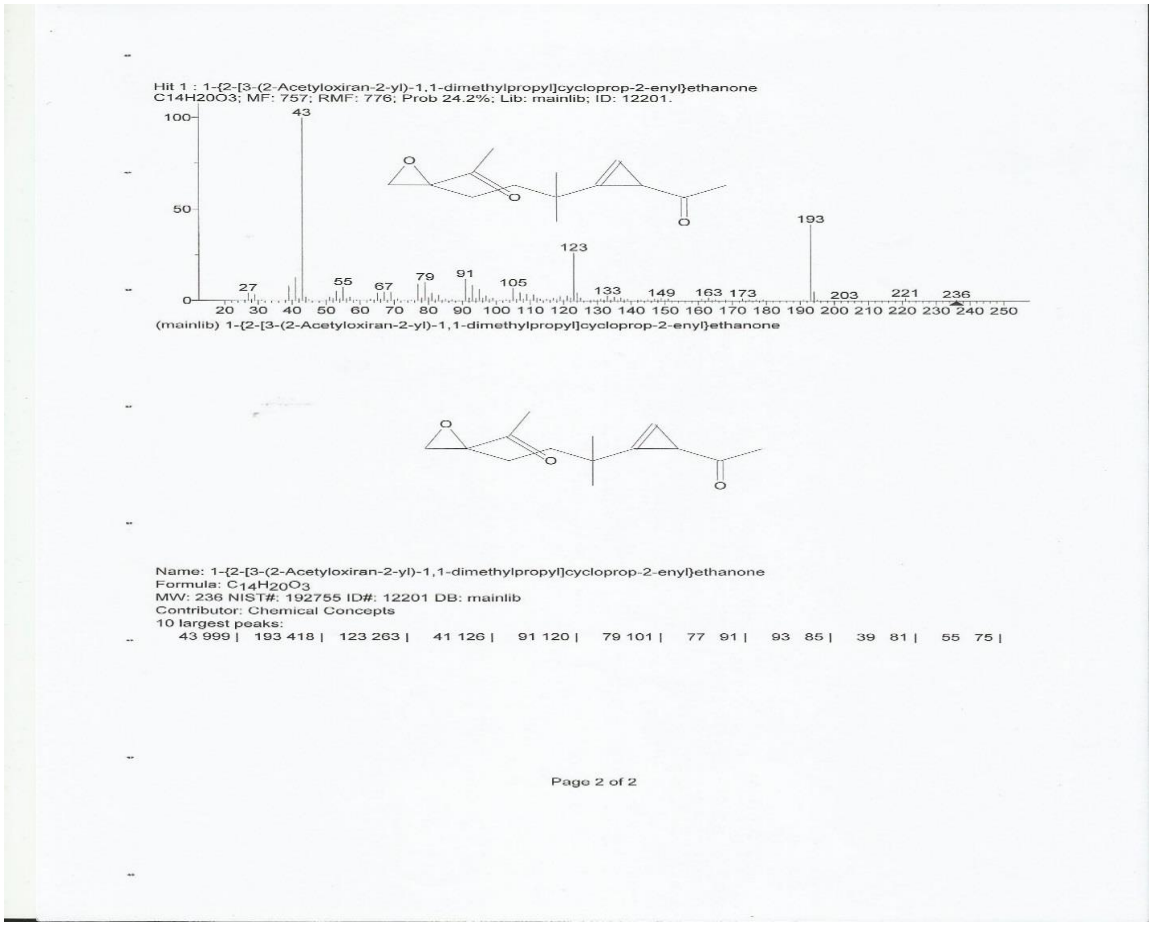

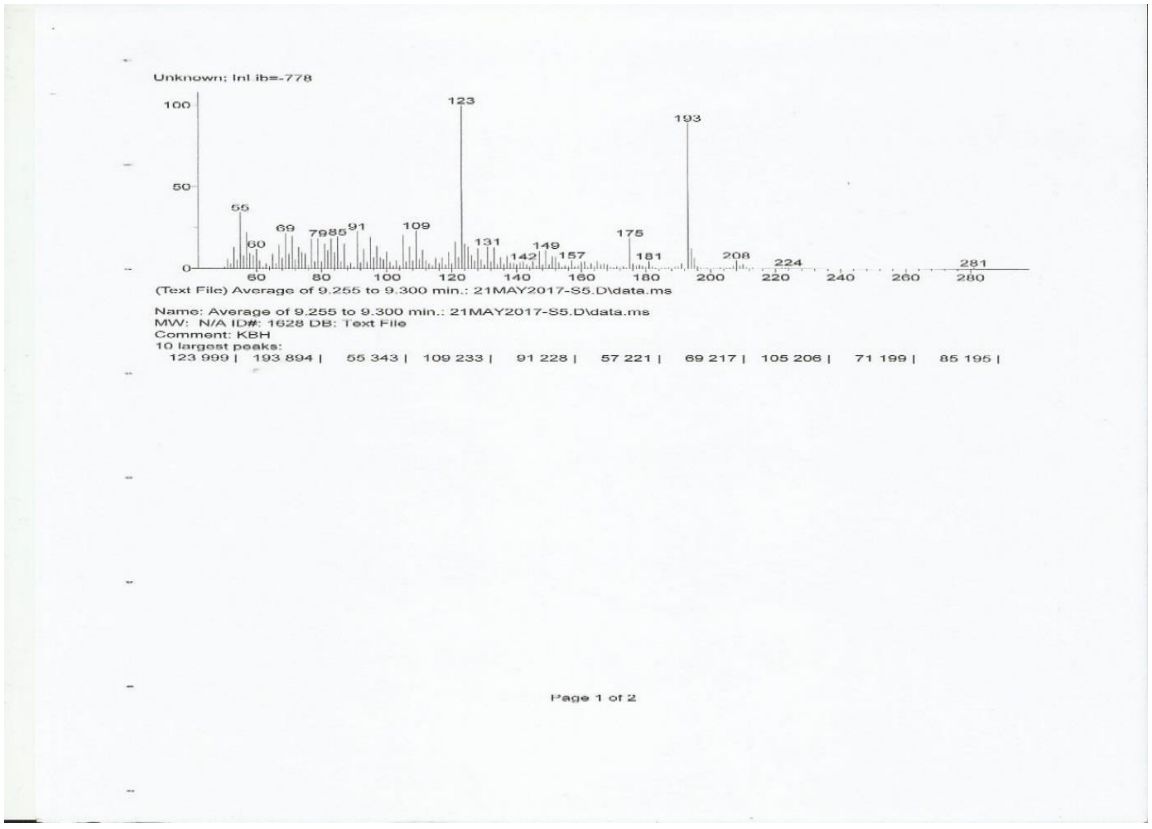

Appendix 4 Tetradecanoic acid

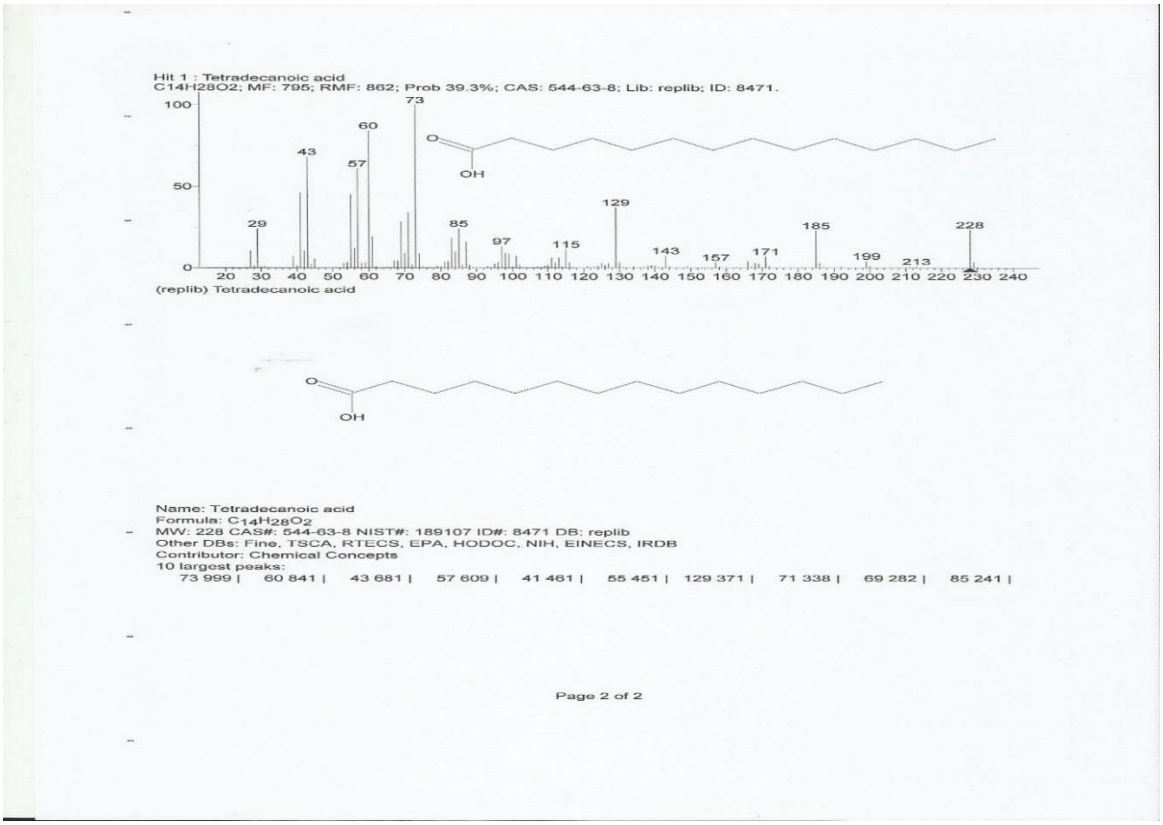

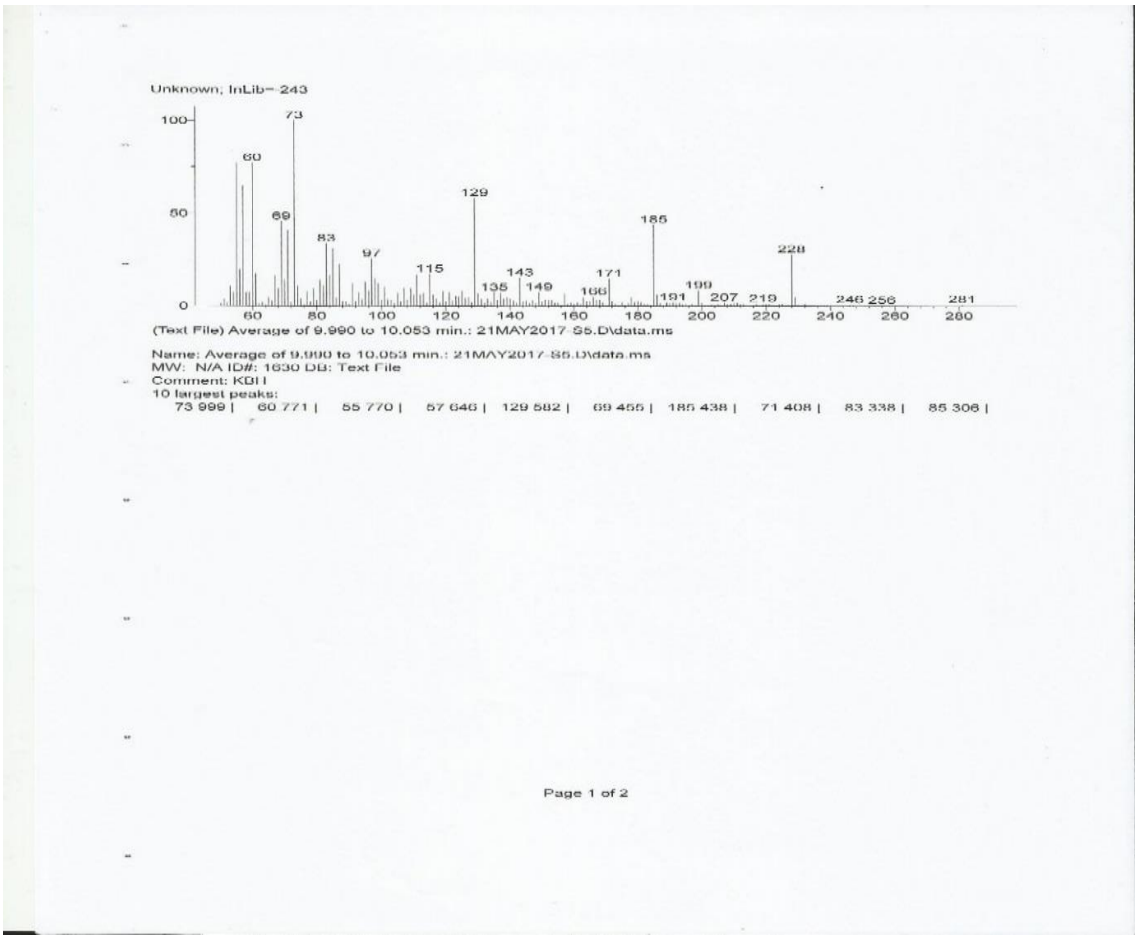

Appendix 5 Acetic acid

Hit 1 : Acetic acid, 2-(2,2,6-trimethyl-7-oxa-bicyclo[4.1.0]hept-1-yl)-propenyl ester
C14H22O3; MF: 710; RMF: 714; Prob 15.9%; CAS: 90165-14-3; Lib: mainlib; ID: 10244.

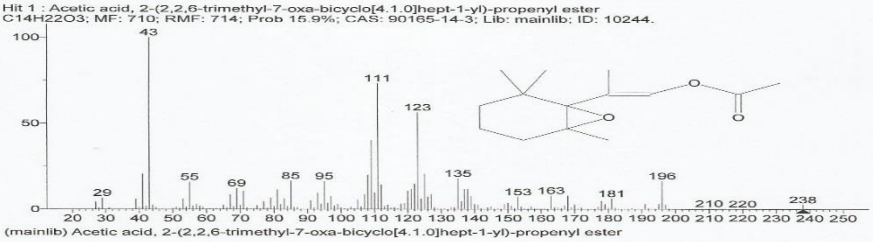

(mainlib) Acetic acid, 2-(2,2,6-trimethyl-7-oxa-bicyclo[4.1.0]hept-1-yl)-propenyl ester

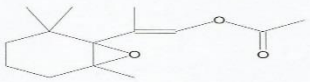

Name: Acetic acid, 2-(2,2,6-trimethyl-7-oxa-bicyclo[4.1.0]hept-1-yl)-propenyl ester
Formula: $C_{14}H_{22}O_3$
MW: 238 CAS#: 90165-14-3 NIST#: 194903 ID#: 10244 DB: mainlib
Other DBs: None
Contributor: Chemical Concepts
10 largest peaks:
43 999 | 111 731 | 123 563 | 109 400 | 41 206 | 125 206 | 108 199 | 135 179 | 85 166 | 95 164 |

Unknown; InLib=-984

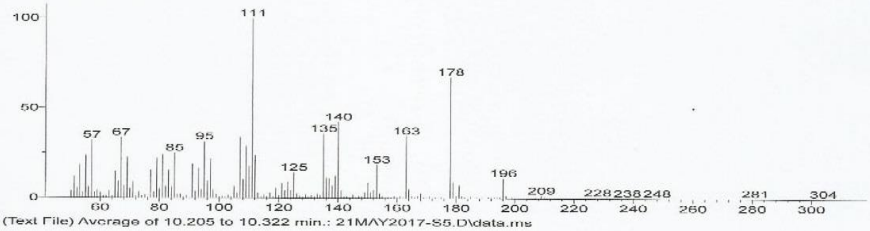

(Text File) Average of 10.205 to 10.322 min.: 21MAY2017-S5.D\data.ms

Name: Average of 10.205 to 10.322 min.: 21MAY2017-S5.D\data.ms
MW: N/A ID#: 1631 DB: Text File
Comment: KBH
10 largest peaks:
111 999 | 178 675 | 140 423 | 135 358 | 163 345 | 107 336 | 67 335 | 57 321 | 95 313 | 109 288 |

Appendix 6 3, 7, 11, 15-Tetramethyl-2-hexadecen-1-ol

Hit 1 : 3,7,11,15-Tetramethyl-2-hexadecen-1-ol
C20H40O; MF: 856; RMF: 942; Prob 29.0%; CAS: 102608-53-7; Lib: mainlib; ID: 43206.

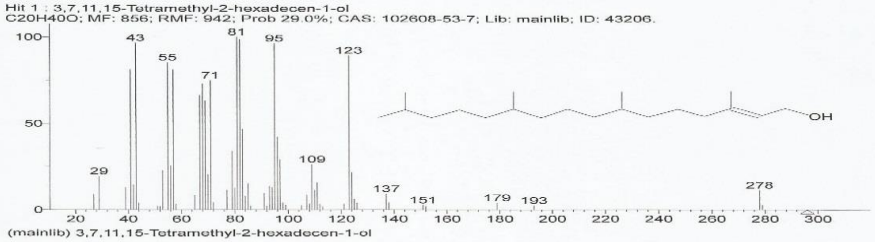

(mainlib) 3,7,11,15-Tetramethyl-2-hexadecen-1-ol

Name: 3,7,11,15-Tetramethyl-2-hexadecen-1-ol
Formula: $C_{20}H_{40}O$
MW: 296 CAS#: 102608-53-7 NIST#: 114703 ID#: 43206 DB: mainlib
Other DBs: IRDB
Contributor: NIST Mass Spectrometry Data Center, 1990.
10 largest peaks:
81 999 | 82 986 | 43 965 | 95 962 | 123 892 | 55 852 | 41 811 | 57 811 | 71 748 | 68 728 |

Page 2 of 2

Unknown; InLib=-181

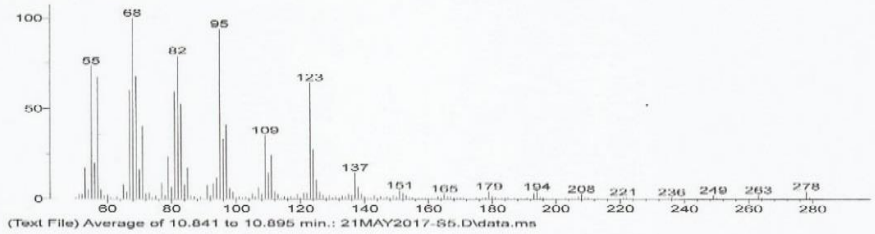

(Text File) Average of 10.841 to 10.895 min.: 21MAY2017-S5.D\data.ms

Name: Average of 10.841 to 10.895 min.: 21MAY2017-S5.D\data.ms
MW: N/A ID#: 1032 DB: Text File
Comment: KBH
10 largest peaks:
68 999 | 95 938 | 82 790 | 55 733 | 69 678 | 57 672 | 123 644 | 67 599 | 81 593 | 83 526 |

Page 1 of 2

Appendix 7 Caffeine

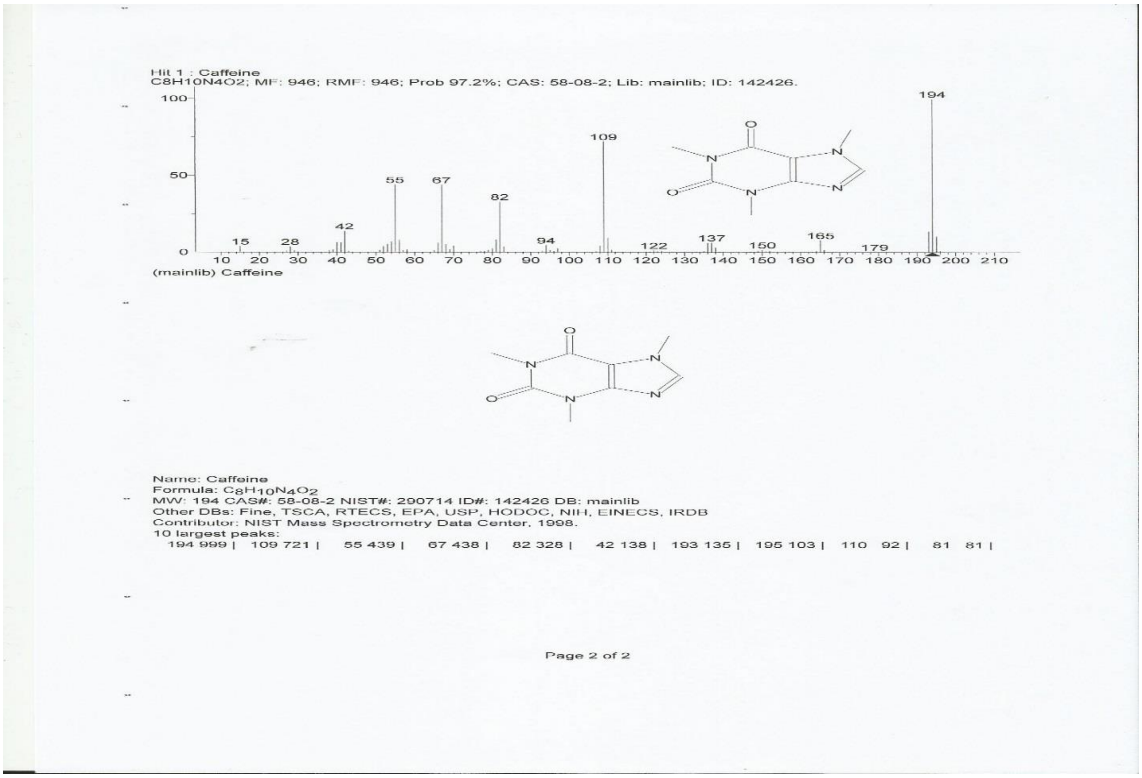

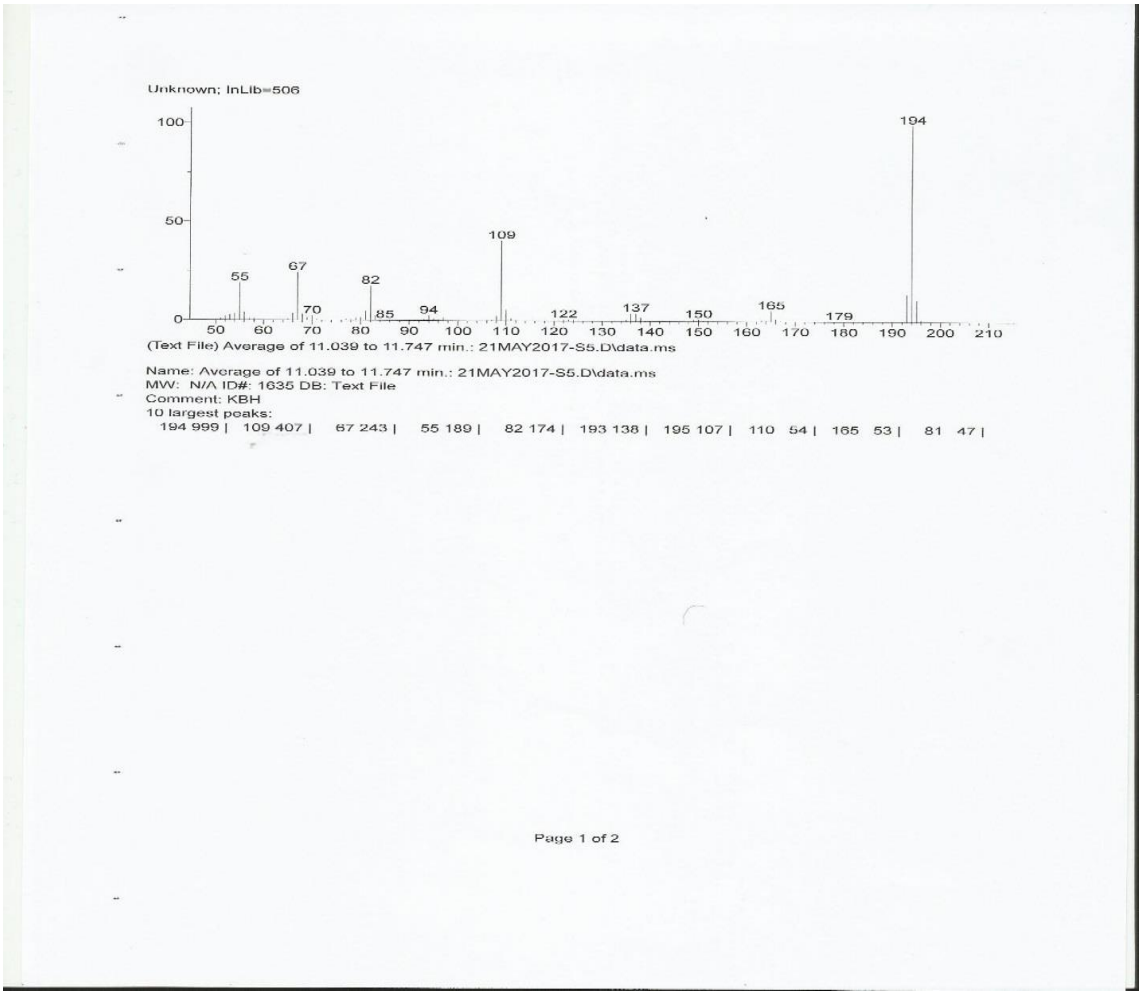

Appendix 8 (n-Hexadecanoic acid)

Hit 1 : n-Hexadecanoic acid
C16H32O2; MF: 919; RMF: 926; Prob 82.1%; CAS: 57-10-3; Lib: replib; ID: 6723.

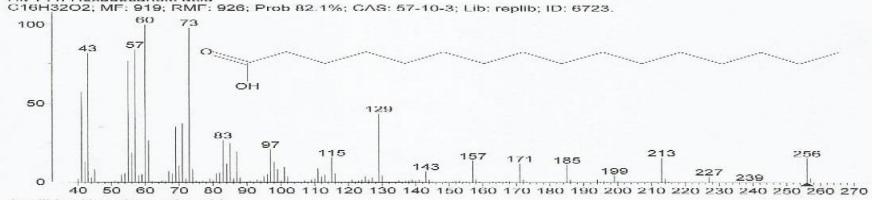

(replib) n-Hexadecanoic acid

Name: n-Hexadecanoic acid
Formula: $C_{16}H_{32}O_2$
MW: 256 CAS#: 57-10-3 NIST#: 335494 ID#: 6723 DB: replib
Other DBs: Fine, TSCA, RTECS, EPA, HODOC, NIH, EINECS, IRDB
Contributor: Drug Lab
10 largest peaks:
60 999 | 73 980 | 57 840 | 43 817 | 55 767 | 41 574 | 129 436 | 71 373 | 69 351 | 83 267 |

Unknown; InLib=178

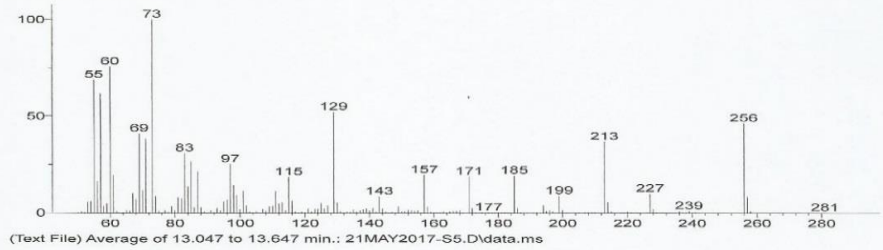

(Text File) Average of 13.047 to 13.647 min.: 21MAY2017-S5.D\data.ms

Name: Average of 13.047 to 13.647 min.: 21MAY2017-S5.D\data.ms
MW: N/A ID#: 1636 DB: Text File
Comment: KBH
10 largest peaks:
73 999 | 60 755 | 55 686 | 57 615 | 129 522 | 256 464 | 69 409 | 71 382 | 213 369 | 83 307 |

Appendix 9 Phytol

Hit 1 : Phytol
C20H40O; MF: 918; RMF: 945; Prob 79.7%; CAS: 150-86-7; Lib: replib; ID: 8051.

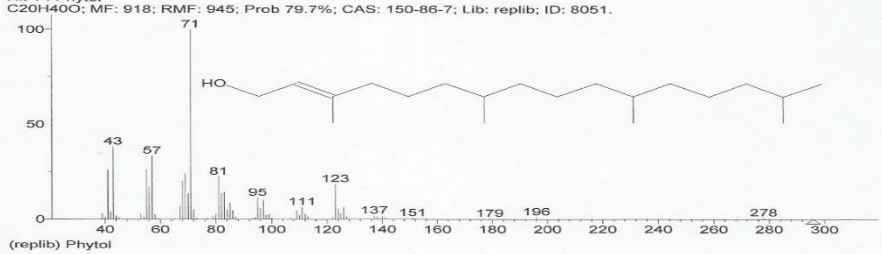

(replib) Phytol

Name: Phytol
Formula: $C_{20}H_{40}O$
MW: 296 CAS#: 150-86-7 NIST#: 108727 ID#: 8051 DB: replib
Other DBs: Fine, TSCA, RTECS, HODOC, EINECS
Contributor: Philip Morris R&D
10 largest peaks:
71 999 | 43 381 | 57 334 | 41 260 | 55 259 | 69 239 | 81 223 | 68 199 | 123 184 | 56 169 |

Unknown; InLib=216

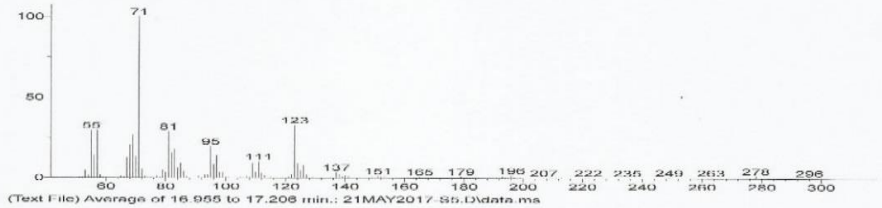

(Text File) Average of 16.955 to 17.206 min.: 21MAY2017-55.D\data.ms

Name: Average of 16.955 to 17.206 min.: 21MAY2017-55.D\data.ms
MW: N/A ID#: 1637 DB: Text File
Comment: KBH
10 largest peaks:
71 999 | 123 329 | 55 296 | 57 295 | 81 287 | 69 267 | 68 205 | 95 194 | 83 179 | 82 157 |

Appendix 10 9, 12, 15-Octadecatrienoic acid

Hit 1 : 9,12,15-Octadecatrienoic acid, (Z,Z,Z)-
C18H30O2; MF: 868; RMF: 881; Prob 26.7%; CAS: 463-40-1; Lib: mainlib; ID: 41695.

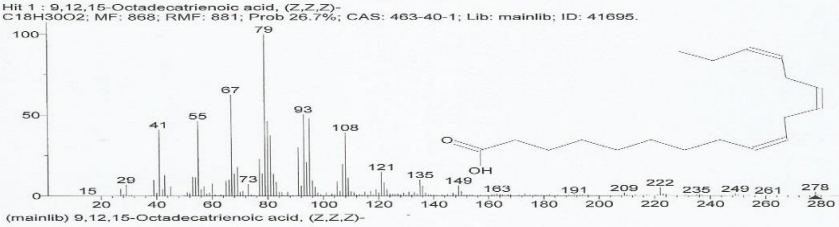

(mainlib) 9,12,15-Octadecatrienoic acid, (Z,Z,Z)-

Name: 9,12,15-Octadecatrienoic acid, (Z,Z,Z)-
Formula: $C_{18}H_{30}O_2$
MW: 278 CAS#: 463-40-1 NIST#: 333201 ID#: 41695 DB: mainlib
Other DBs: Fine, TSCA, HODOC, NIH, EINECS
Contributor: NIST Mass Spectrometry Data Center
10 largest peaks:
79 999 | 67 624 | 93 503 | 95 478 | 55 463 | 80 460 | 41 408 | 108 391 | 81 373 | 91 299 |

Page 2 of 2

Unknown; InLib=-135

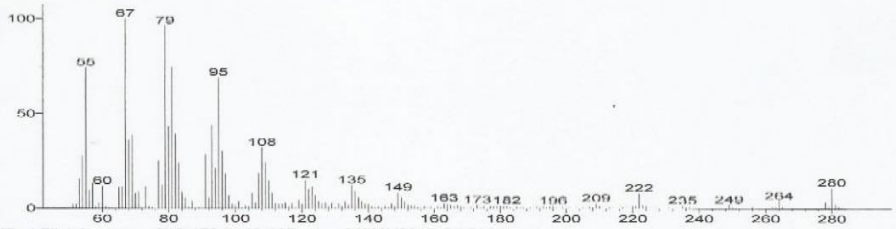

(Text File) Average of 18.470 to 19.187 min.: 21MAY2017-S5.D\data.ms

Name: Average of 18.470 to 19.187 min.: 21MAY2017-S5.D\data.ms
MW: N/A ID#: 1638 DB: Text File
Comment: KBH
10 largest peaks:
67 999 | 79 963 | 81 746 | 55 742 | 95 689 | 93 436 | 80 433 | 82 392 | 69 388 | 68 359 |

Page 1 of 2

Appendix 11 Octadecanoic acid

Hit 1 : Octadecanoic acid
C18H36O2; MF: 841; RMF: 857; Prob 62.3%; CAS: 57-11-4; Lib: mainlib; ID: 8481.

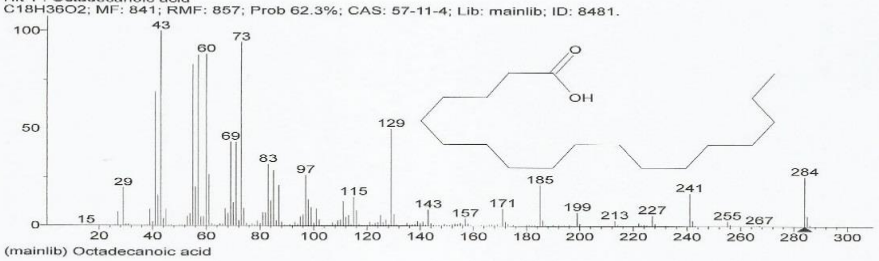

(mainlib) Octadecanoic acid

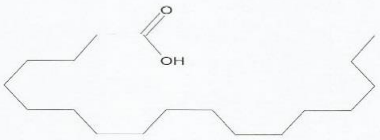

Name: Octadecanoic acid
Formula: $C_{18}H_{36}O_2$
MW: 284 CAS#: 57-11-4 NIST#: 290961 ID#: 8481 DB: mainlib
Other DBs: Fine, TSCA, RTECS, EPA, HODOC, NIH, EINECS, IRDB
Contributor: NIST Mass Spectrometry Data Center, 1998.
10 largest peaks:
43 999 | 73 942 | 60 881 | 57 875 | 55 827 | 41 688 | 129 500 | 69 432 | 71 429 | 83 317 |

Page 2 of 2

Unknown, InLib=-181

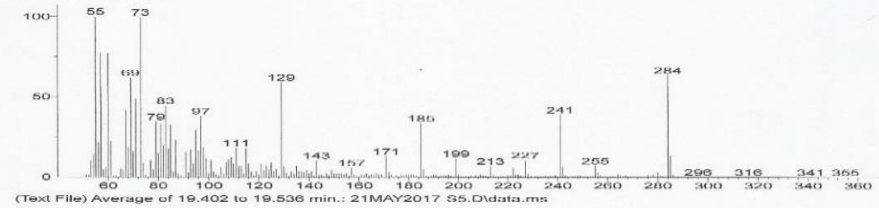

(Text File) Average of 19.402 to 19.536 min.: 21MAY2017 S5.D\data.ms

Name: Average of 19.402 to 19.536 min.: 21MAY2017-S5.D\data.ms
MW: N/A ID#: 1639 DB: Text File
Comment: KDII
10 largest peaks:
55 999 | 73 995 | 57 772 | 60 768 | 284 635 | 69 617 | 129 589 | 71 485 | 83 444 | 67 416 |

Page 1 of 2

Appendix 12 Ethyl iso-allocholate

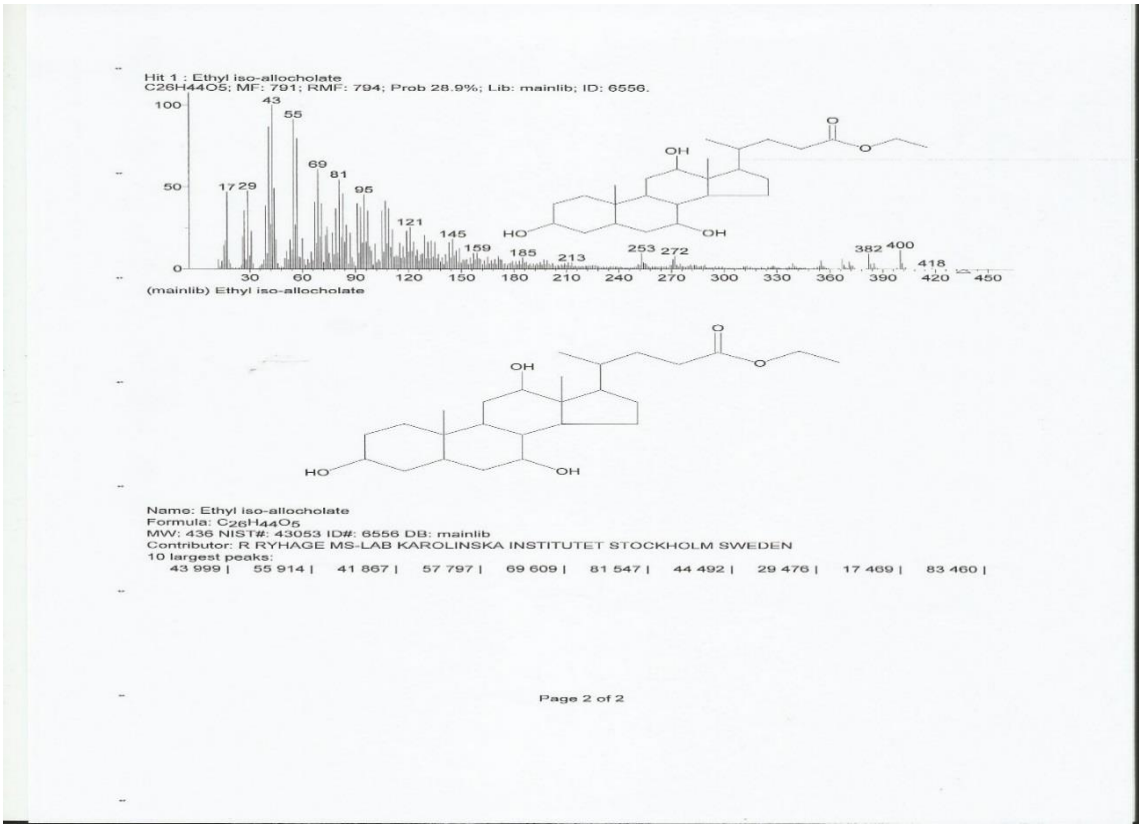

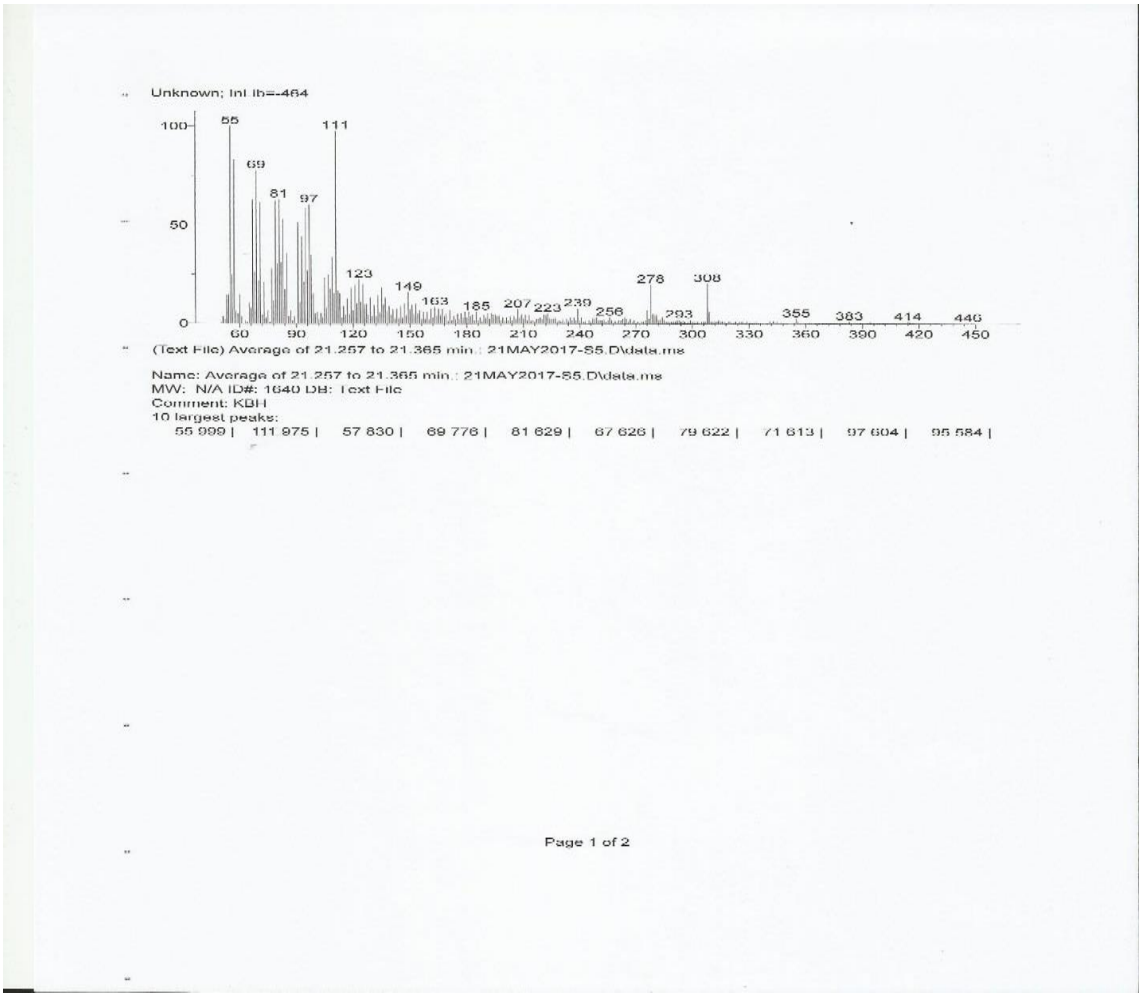

Appendix 13 1, 2-Benzenedicarboylic acid

Hit 1 : 1,2-Benzenedicarboxylic acid, diisooctyl ester
C24H38O4; MF: 873; RMF: 953; Prob 38.1%; CAS: 27554-26-3; Lib: replib; ID: 20061.

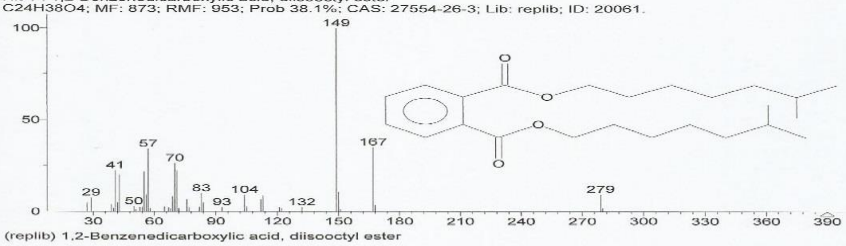

(replib) 1,2-Benzenedicarboxylic acid, diisooctyl ester

Name: 1,2-Benzenedicarboxylic acid, diisooctyl ester
Formula: $C_{24}H_{38}O_4$
MW: 390 CAS#: 27554-26-3 NIST#: 113206 ID#: 20061 DB: replib
Other DBs: Fine, TSCA, RTECS, EINECS, IRDB
Contributor: NIST Mass Spectrometry Data Center, 1990.
10 largest peaks:
149 999 | 167 350 | 57 341 | 70 264 | 41 225 | 71 224 | 55 218 | 43 200 | 150 107 | 83 100 |

Page 2 of 2

Unknown; InLib=-197

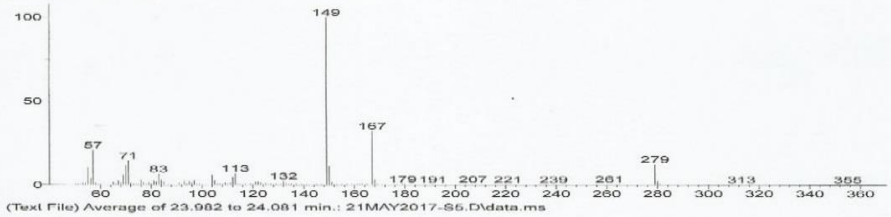

(Text File) Average of 23.982 to 24.081 min.: 21MAY2017-S5.D\data.ms

Name: Average of 23.982 to 24.081 min.: 21MAY2017-S5.D\data.ms
MW: N/A ID#: 1642 DB: Text File
Comment: KBH
10 largest peaks:
149 999 | 167 320 | 57 207 | 71 144 | 279 122 | 70 115 | 150 112 | 55 104 | 113 69 | 83 66 |

Page 1 of 2

Appendix 14 2, 6, 10, 14, 18, 22-Tetracosahexane, 2, 6, 10, 15, 23-hexamethyl-

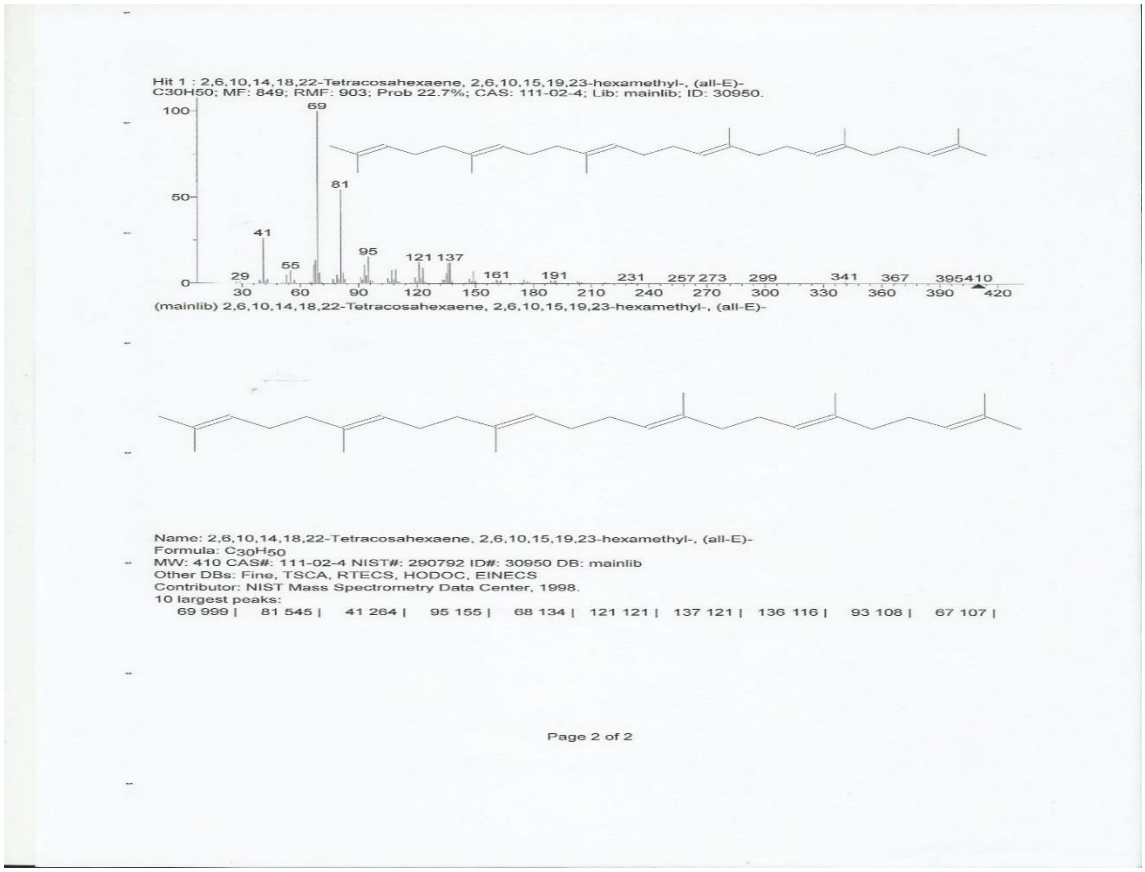

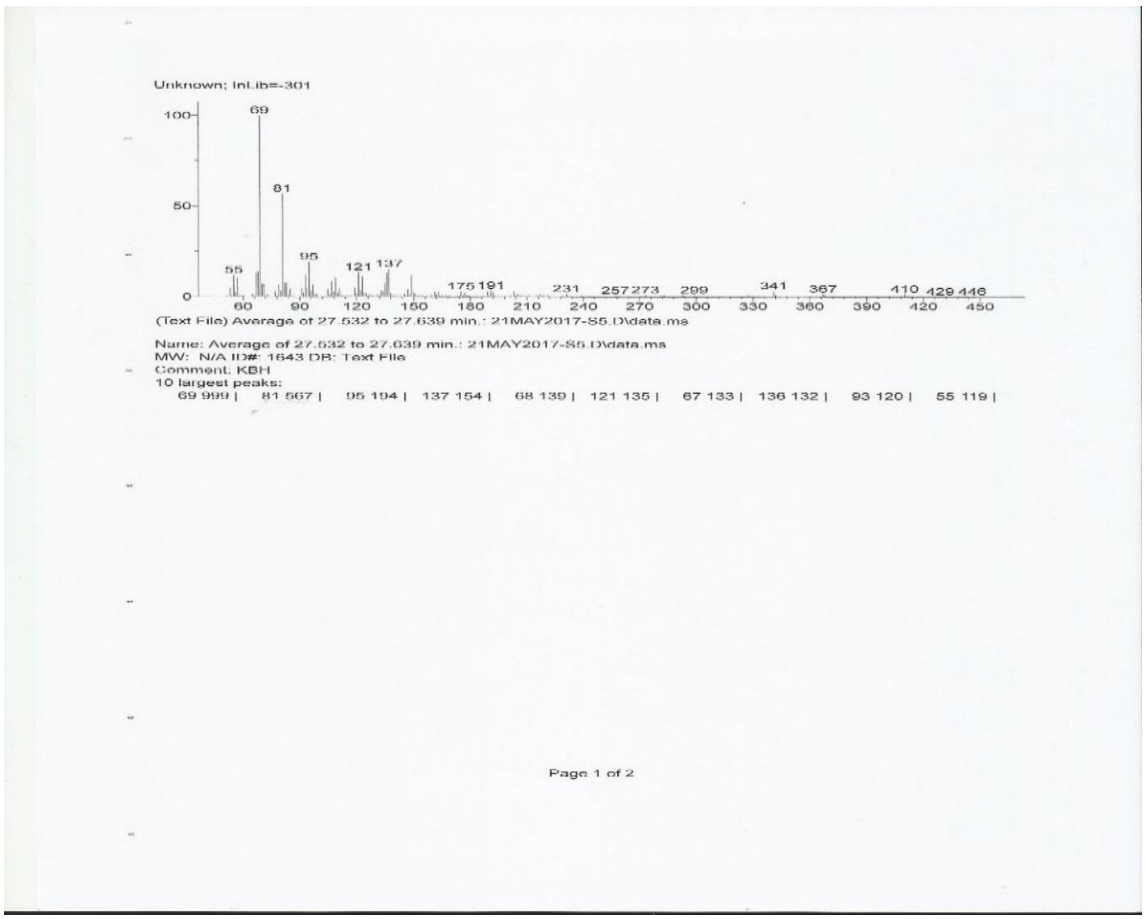

Appendix II

GC-MS analysis – CBH sample

Appendix 15 Chromatogram – CBH sample

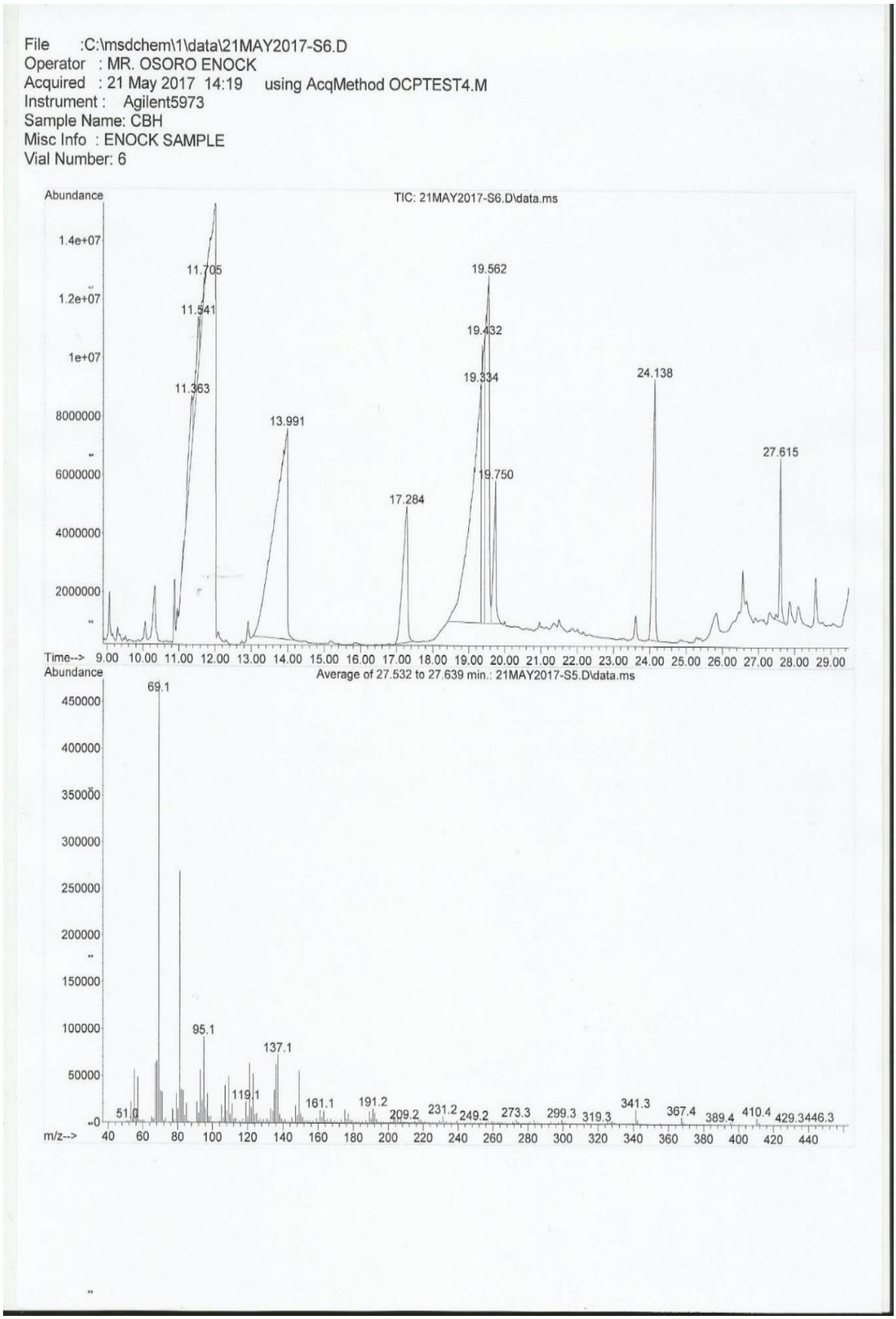

Appendix 16　7-(1,3-Dimethylbuta-1,3-dienyl)-1,6,6-trimethyl-3,8-dioxatricyclo[5,1,0,0(2,4)]octane

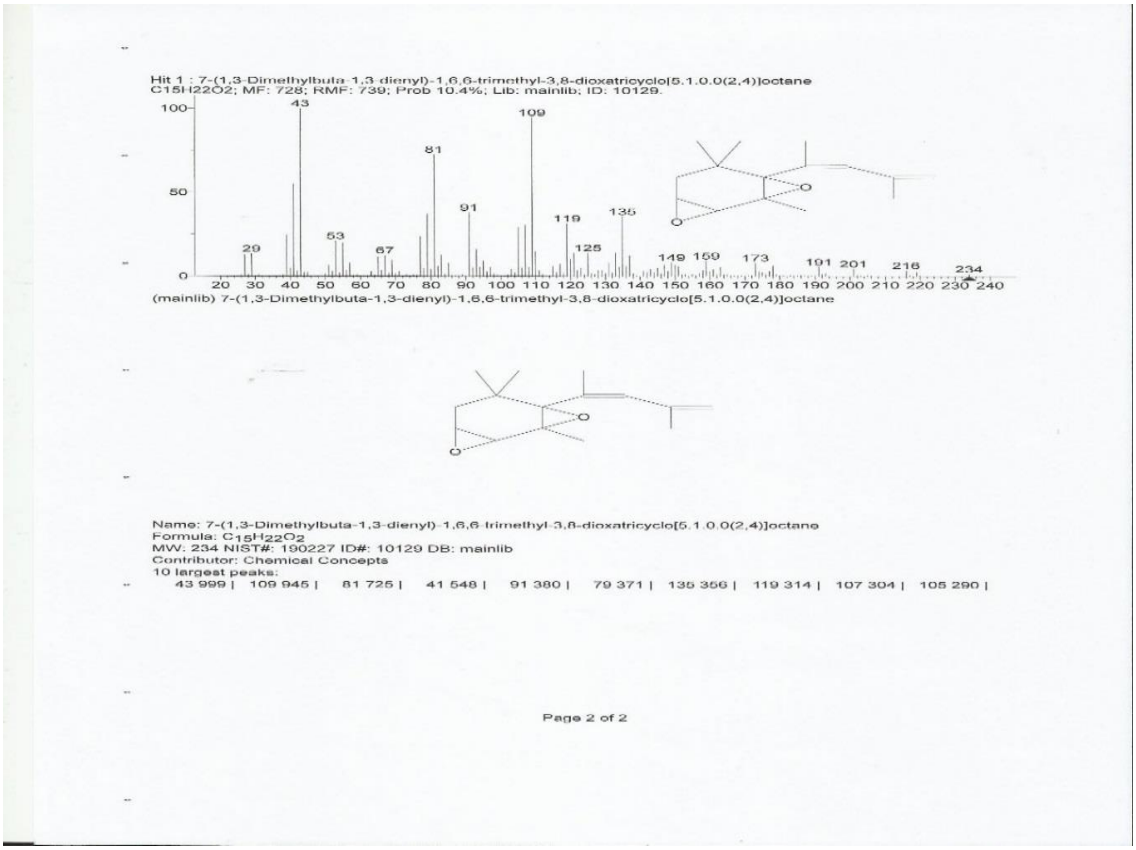

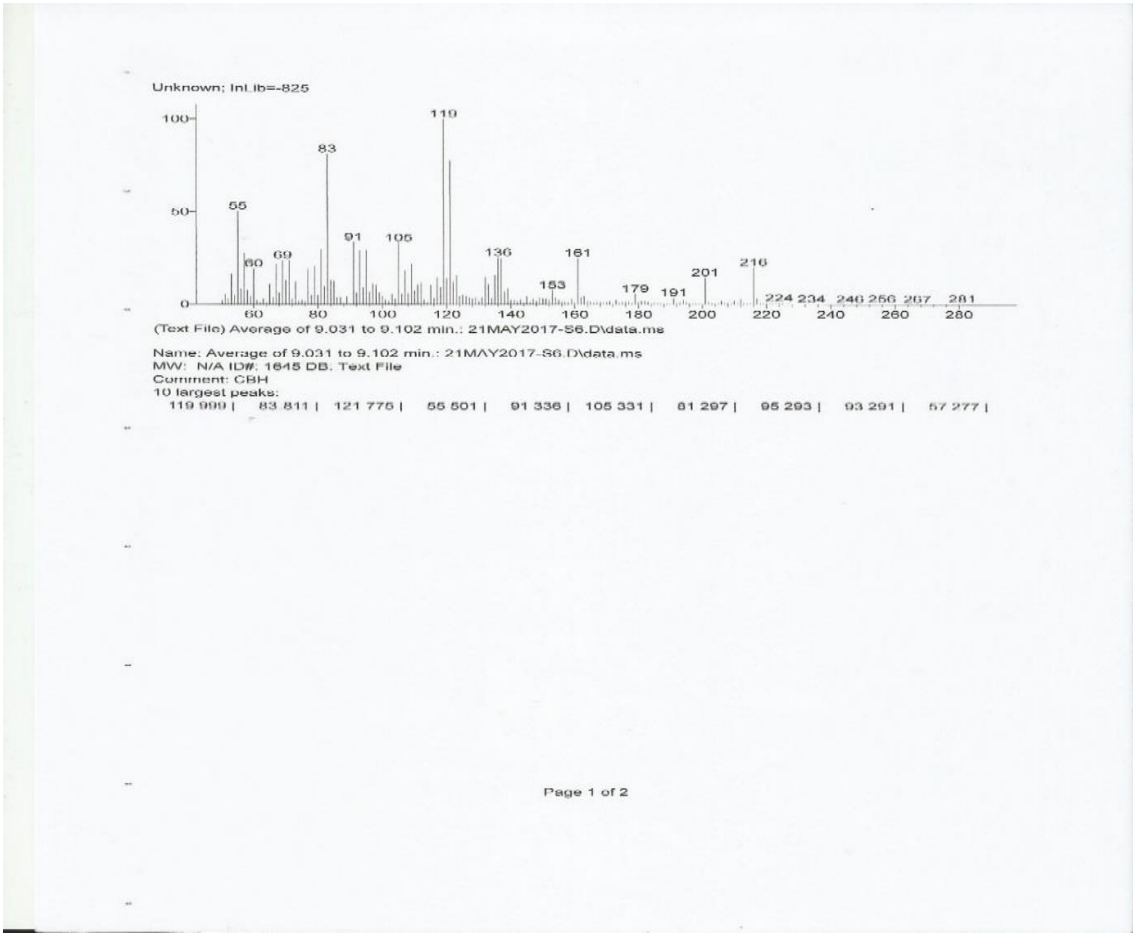

Appendix 17 Acetic acid

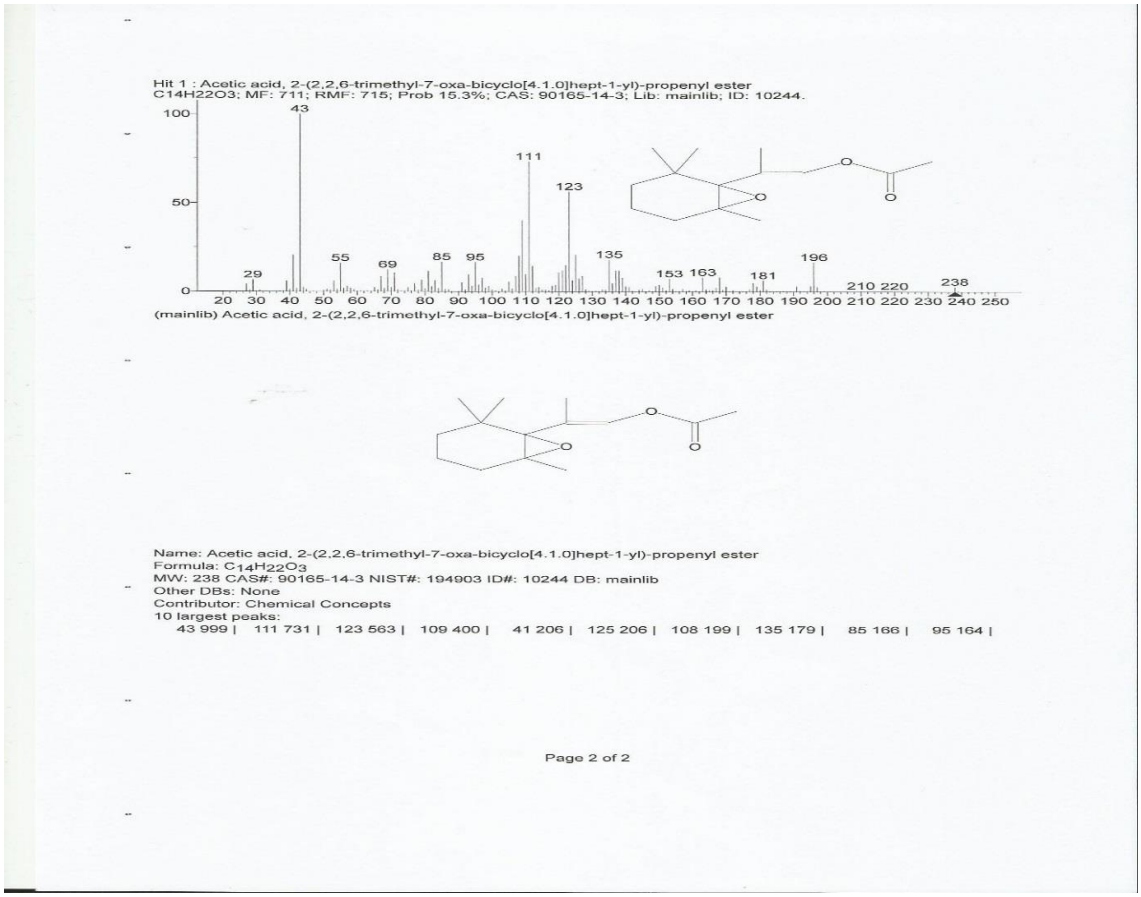

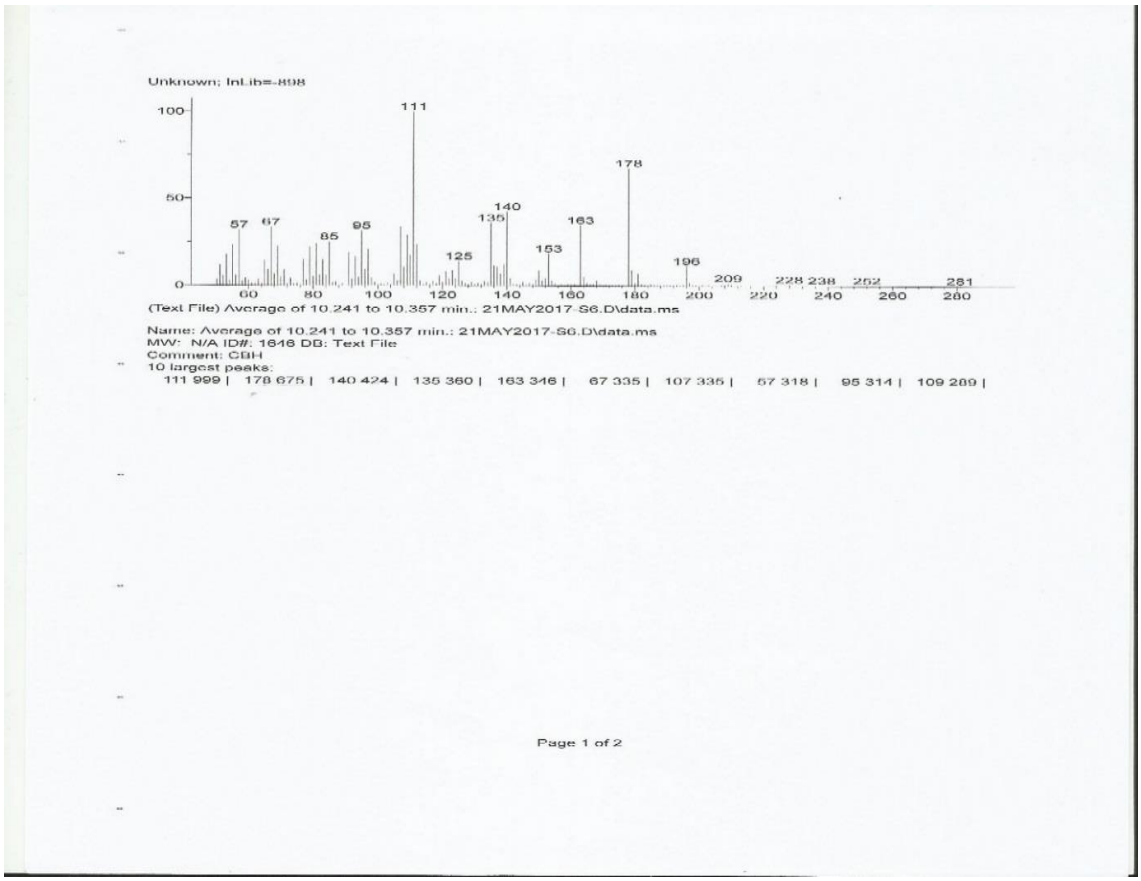

Appendix 18 Caffeine

Hit 1 : Caffeine
C8H10N4O2; MF: 935; RMF: 935; Prob 96.7%; CAS: 58-08-2; Lib: mainlib; ID: 142426.

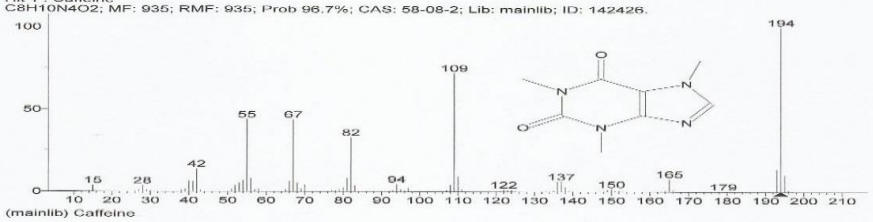

(mainlib) Caffeine

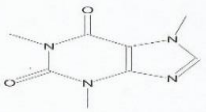

Name: Caffeine
Formula: $C_8H_{10}N_4O_2$
MW: 194 CAS#: 58-08-2 NIST#: 290714 ID#: 142426 DB: mainlib
Other DBs: Fine, TSCA, RTECS, EPA, USP, HODOC, NIH, EINECS, IRDB
Contributor: NIST Mass Spectrometry Data Center, 1998.
10 largest peaks:
194 999 | 109 721 | 55 439 | 67 438 | 82 328 | 42 138 | 193 135 | 195 103 | 110 92 | 81 81 |

Unknown; InLib=490

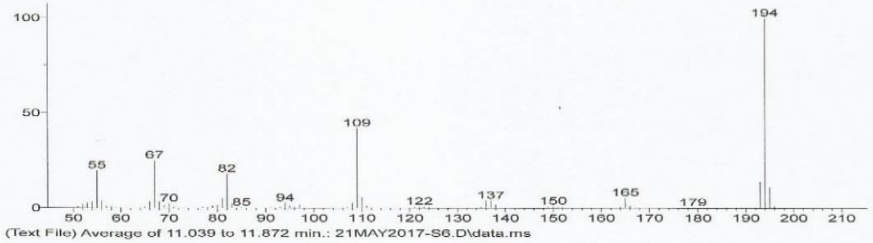

(Text File) Average of 11.039 to 11.872 min.: 21MAY2017-S6.D\data.ms

Name: Average of 11.039 to 11.872 min.: 21MAY2017-S6.D\data.ms
MW: N/A ID#: 1647 DB: Text File
Comment: CBH
10 largest peaks:
194 999 | 109 418 | 67 250 | 55 197 | 82 179 | 193 139 | 195 108 | 110 55 | 165 53 | 81 51 |

Appendix 19 n-Hexadecanoic acid

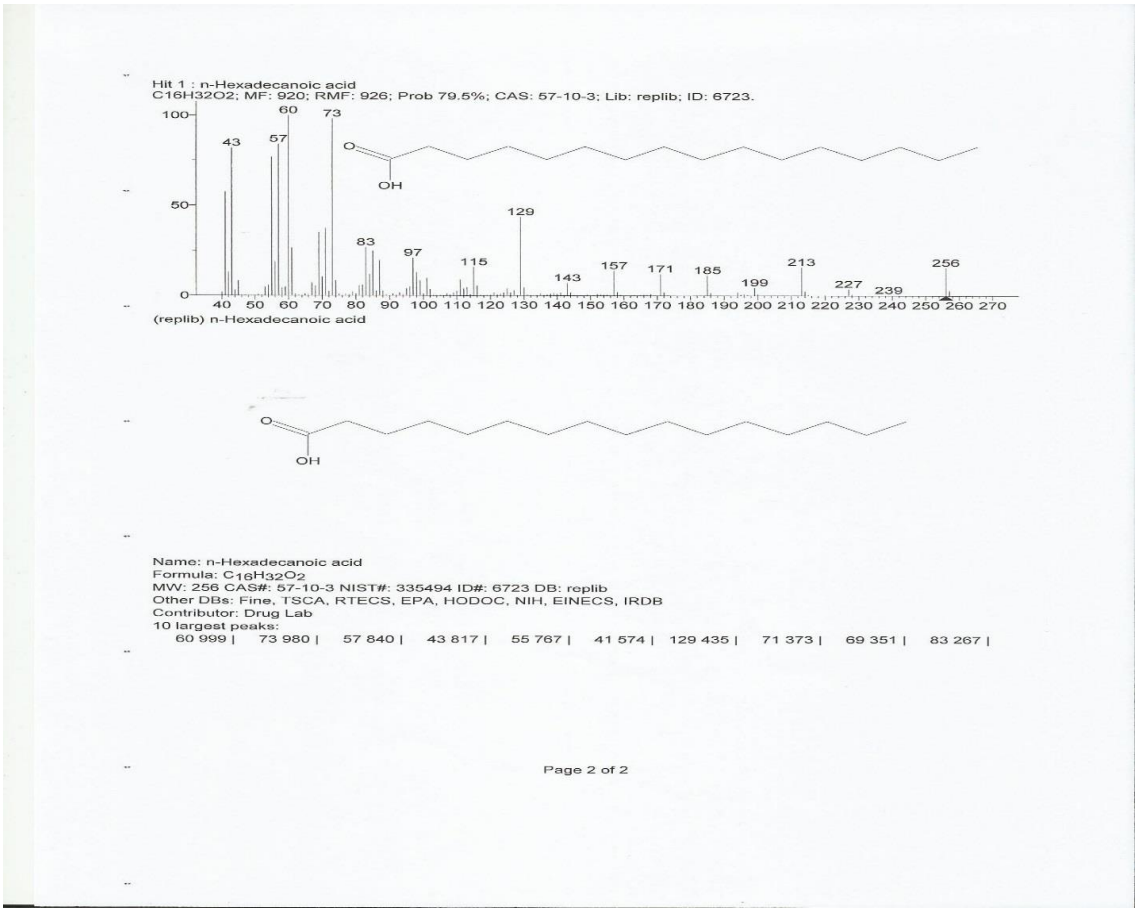

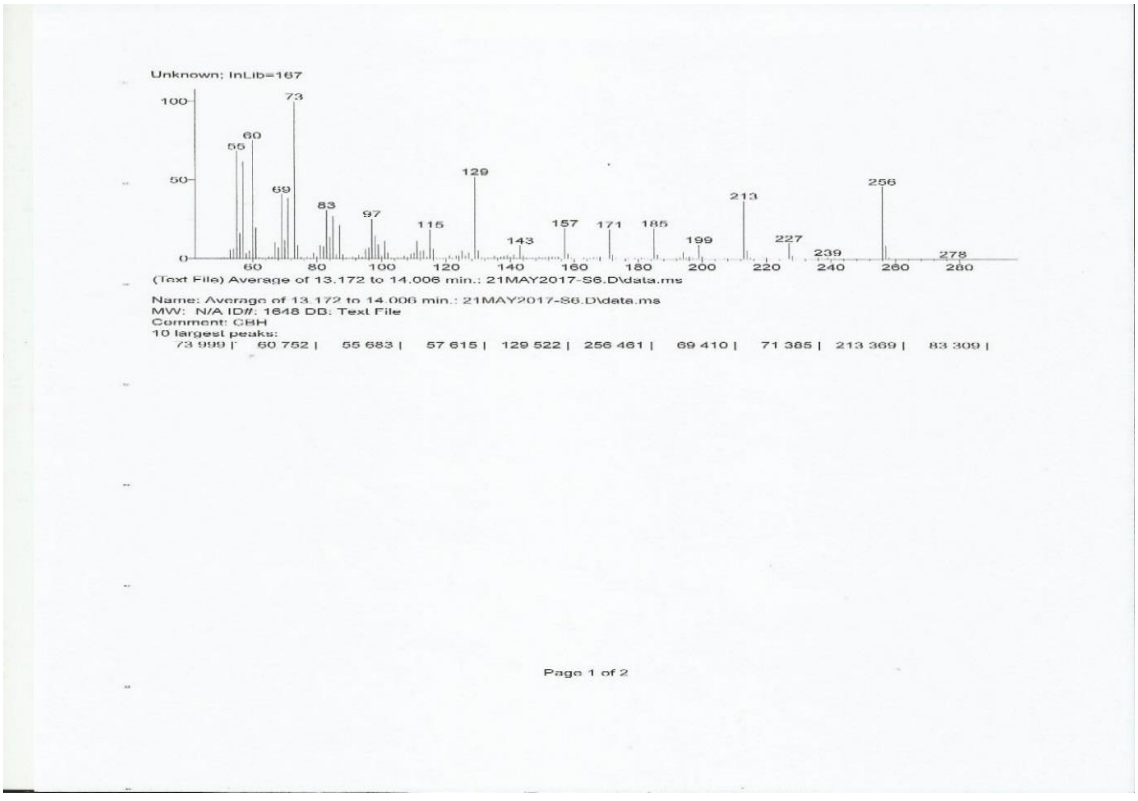

Appendix 20 Phytol

Hit 1 : Phytol
C20H40O; MF: 914; RMF: 946; Prob 74.1%; CAS: 150-86-7; Lib: replib; ID: 8051.

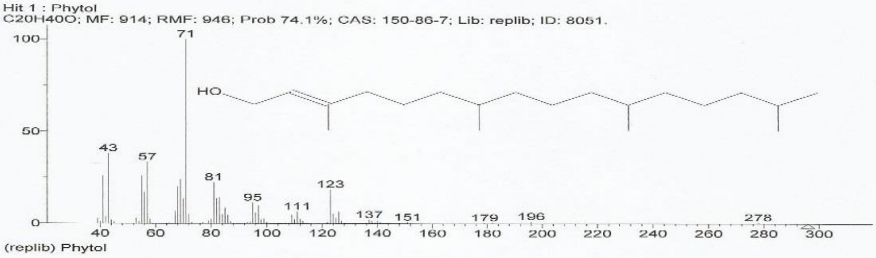

(replib) Phytol

Name: Phytol
Formula: $C_{20}H_{40}O$
MW: 296 CAS#: 150-86-7 NIST#: 108727 ID#: 8051 DB: replib
Other DBs: Fine, TSCA, RTECS, HODOC, EINECS
Contributor: Philip Morris R&D
10 largest peaks:
71 999 | 43 381 | 57 334 | 41 260 | 55 259 | 69 239 | 81 223 | 68 199 | 123 184 | 56 169 |

Unknown; InLib=242

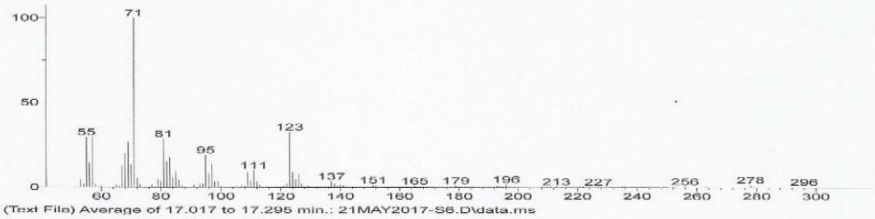

(Text File) Average of 17.017 to 17.295 min.: 21MAY2017-S6.D\data.ms

Name: Average of 17.017 to 17.295 min.: 21MAY2017-S6.D\data.ms
MW: N/A ID#: 1649 DB: Text File
Comment: CBH
10 largest peaks:
71 999 | 123 325 | 55 294 | 57 292 | 81 284 | 69 264 | 68 198 | 95 188 | 83 176 | 82 151 |

Appendix 21 9, 12, 15-octadecatrienoic acid

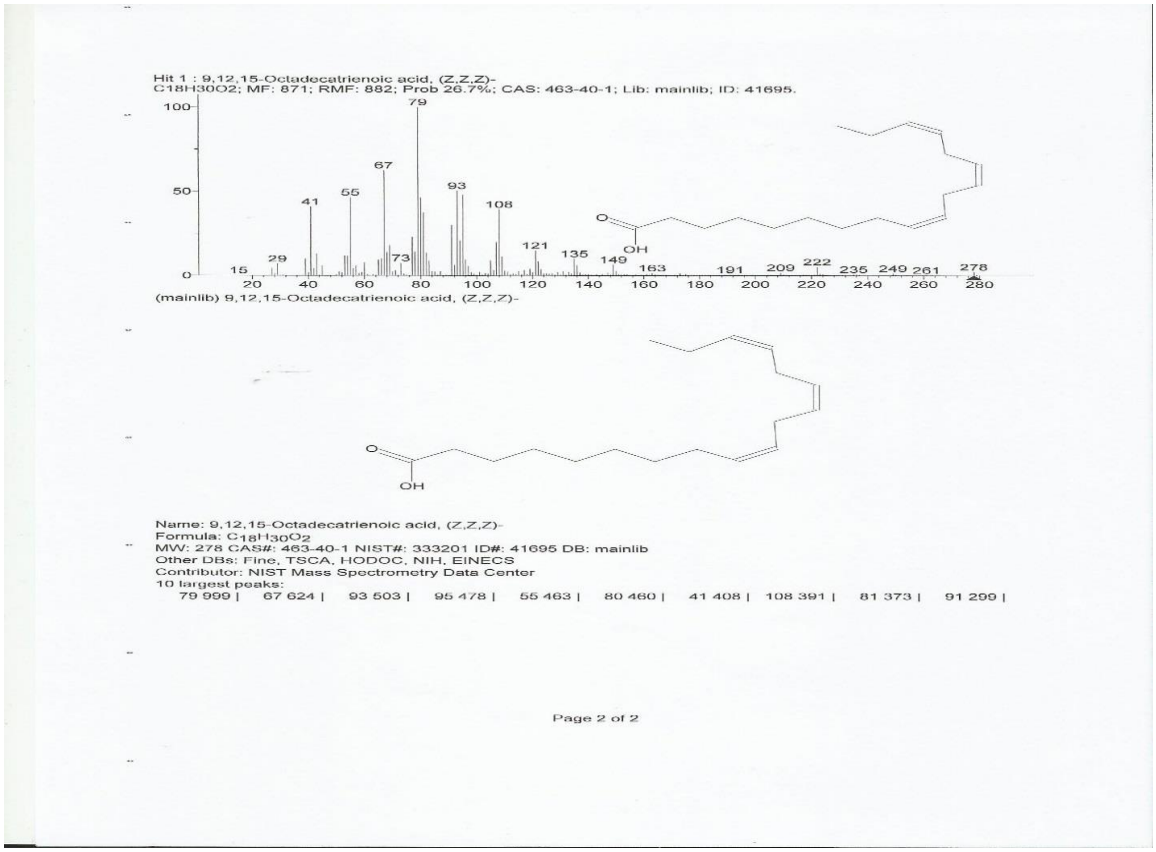

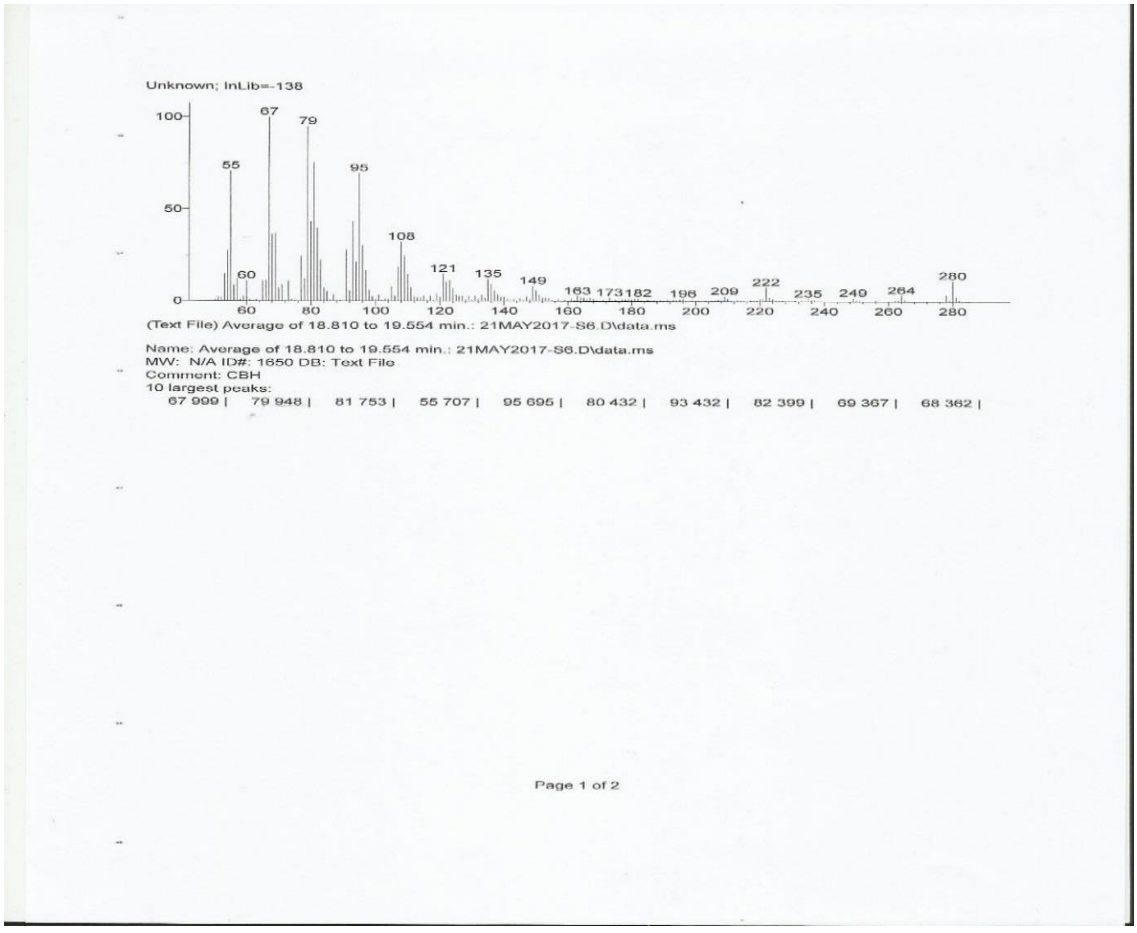

Appendix 22 octadecanoic acid

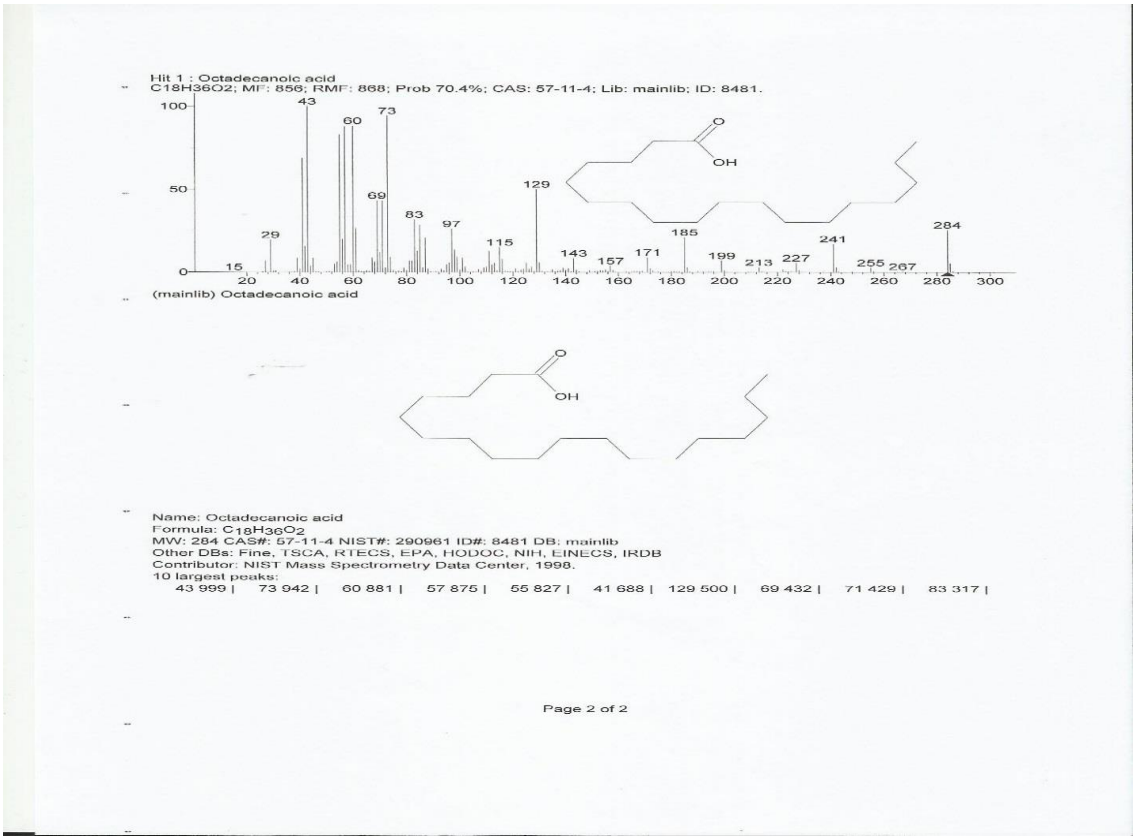

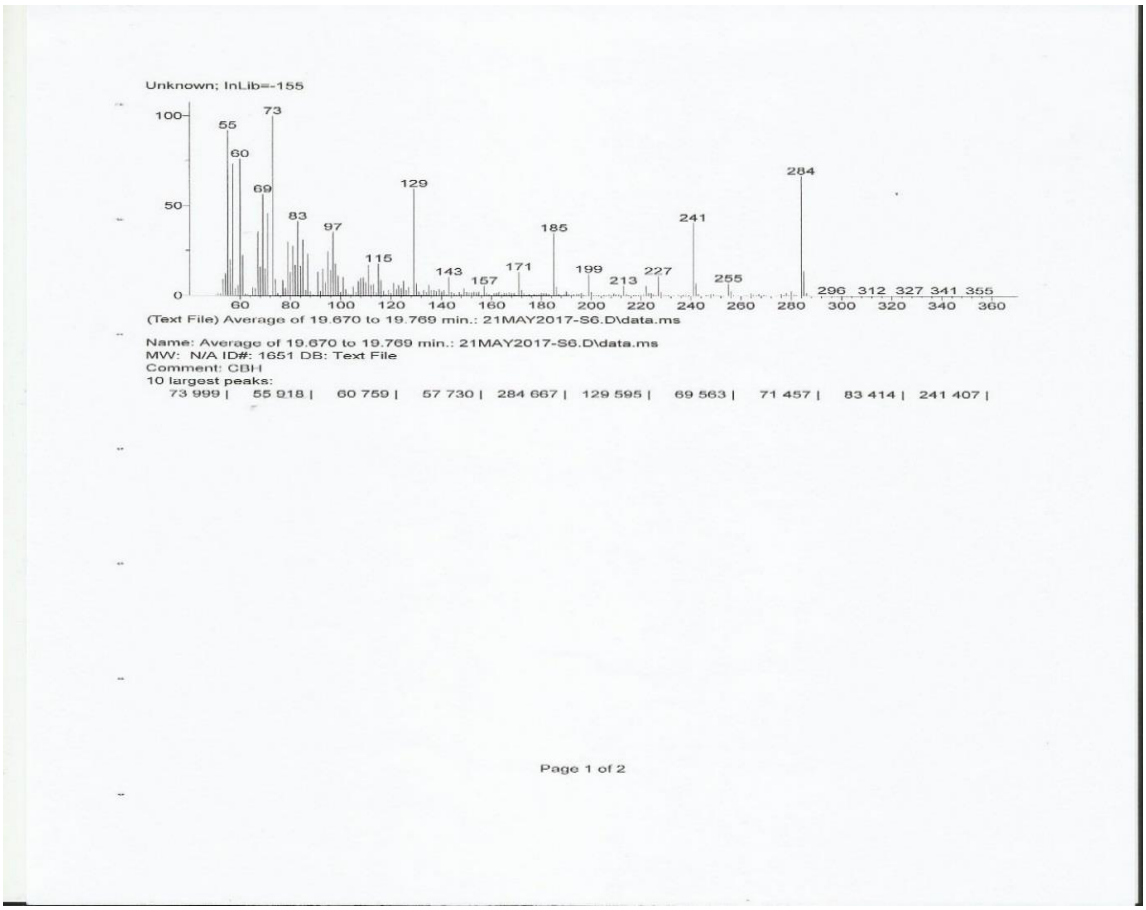

Appendix 23 1, 2-Benzenedicarboxylix acid, diisooctyl ester

Hit 1 : 1,2-Benzenedicarboxylic acid, diisooctyl ester
C24H38O4; MF: 925; RMF: 954; Prob 44.3%; CAS: 27554-26-3; Lib: replib; ID: 20061.

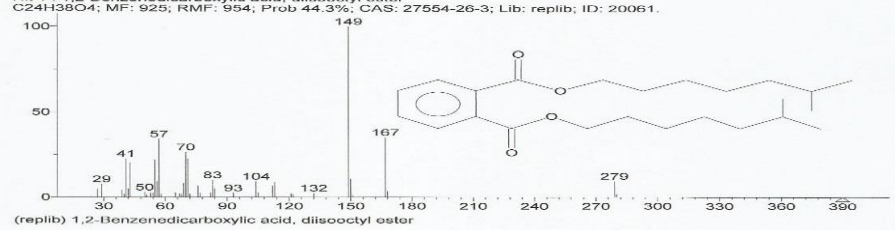

(replib) 1,2-Benzenedicarboxylic acid, diisooctyl ester

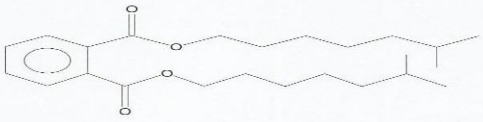

Name: 1,2-Benzenedicarboxylic acid, diisooctyl ester
Formula: $C_{24}H_{38}O_4$
MW: 390 CAS#: 27554-26-3 NIST#: 113206 ID#: 20061 DB: replib
Other DBs: Fine, TSCA, RTECS, EINECS, IRDB
Contributor: NIST Mass Spectrometry Data Center, 1990.
10 largest peaks:
149 999 | 167 350 | 57 341 | 70 264 | 41 225 | 71 224 | 55 218 | 43 200 | 150 107 | 83 100 |

Unknown; InLib=133

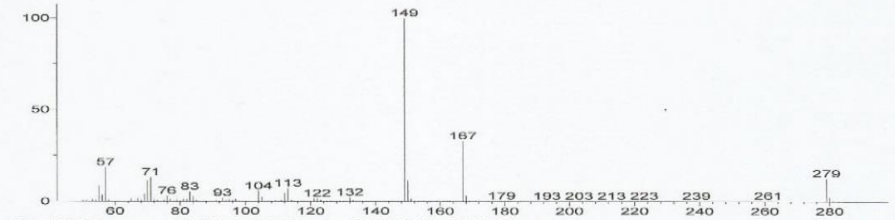

(Text File) Average of 23.991 to 24.224 min.: 21MAY2017-S6.D\data.ms

Name: Average of 23.991 to 24.224 min.: 21MAY2017-S6.D\data.ms
MW: N/A ID#: 1652 DB: Text File
Comment: CBH
10 largest peaks:
149 999 | 167 328 | 57 184 | 71 131 | 279 125 | 150 114 | 70 113 | 55 84 | 113 72 | 104 56 |

Appendix 24 Oleic acid, eicosyl ester

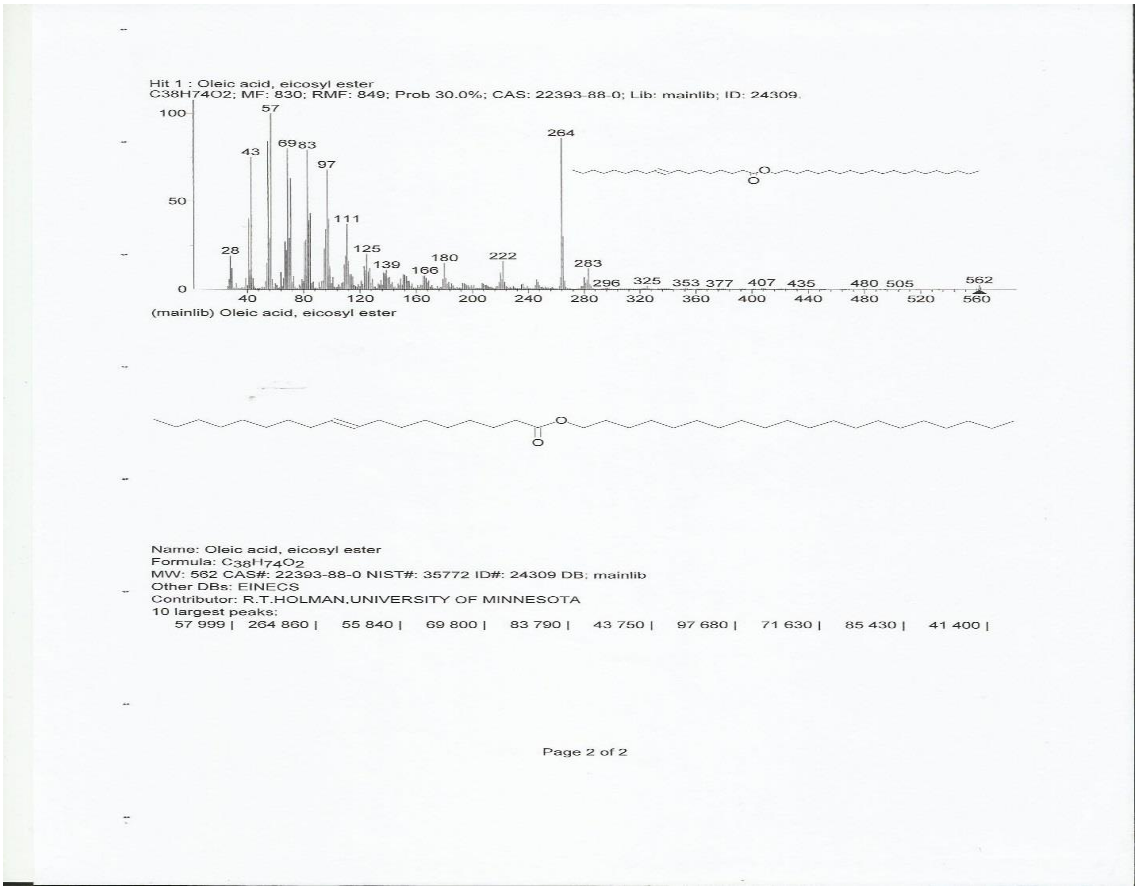

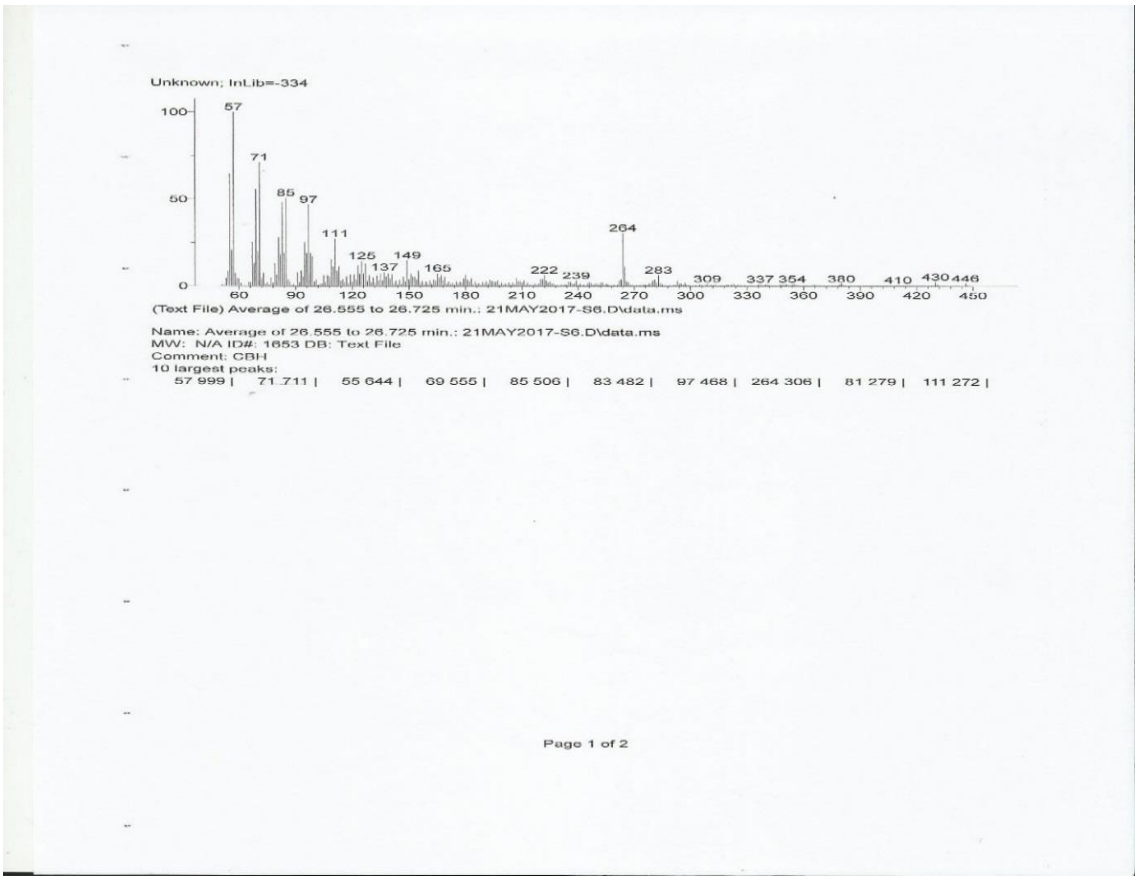

Appendix III

GC-MS analysis – NBH sample

Appendix 25 Chromatogram – sample NBH

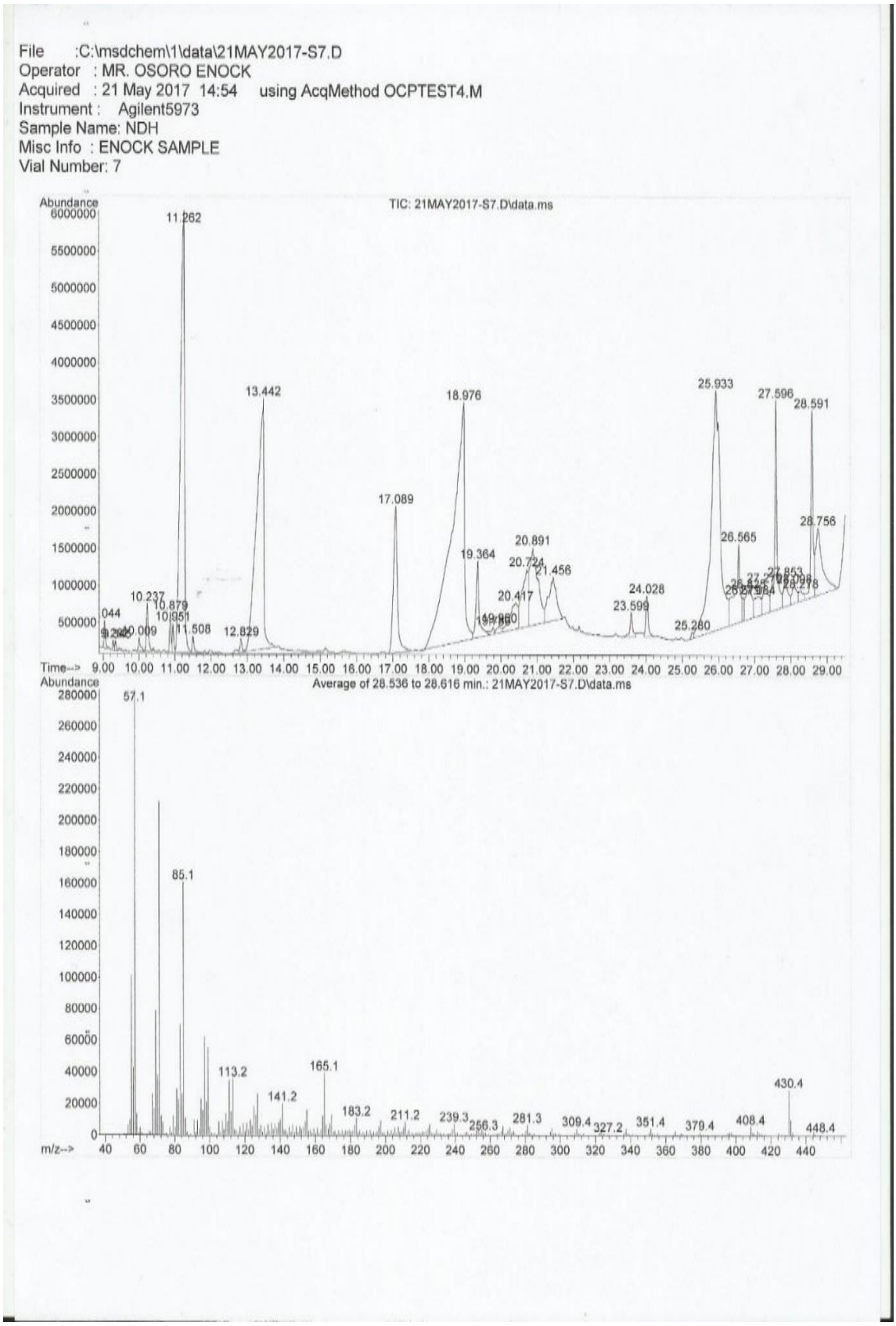

Appendix 26 1-Heptatriacotanol

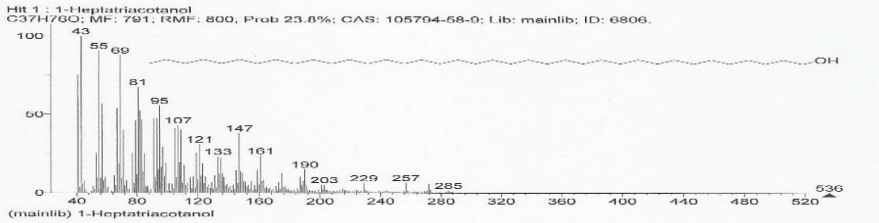

Name: 1-Heptatriacotanol
Formula: C37H76O
MW: 536 CAS#: 105794-58-9 NIST#: 127968 ID#: 6806 DB: mainlib
Other DBs: None
Contributor: LAC, NIDDK, NIH, Bethesda, MD 20892
10 largest peaks:
43 999 | 55 907 | 69 878 | 41 750 | 81 675 | 57 567 | 95 556 | 67 537 | 82 525 | 91 474 |

Page 2 of 2

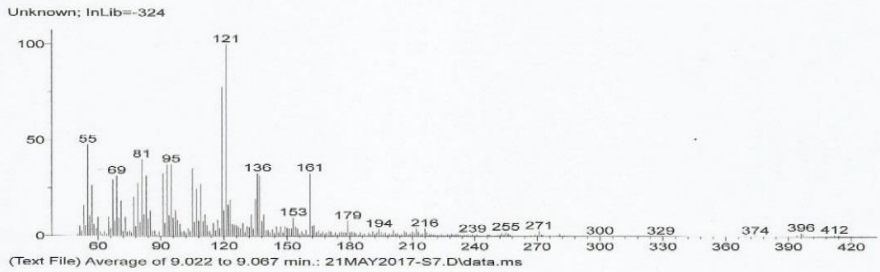

Name: Average of 9.022 to 9.067 min.: 21MAY2017-S7.D\data.ms
MW: N/A ID#: 1655 DB: Text File
Comment: NDH
10 largest peaks:
121 999 | 119 775 | 55 476 | 81 398 | 95 373 | 93 370 | 105 350 | 161 328 | 136 326 | 91 324 |

Page 1 of 2

Appendix 27 Ppropiollic acid

Hit 1 : Ppropiolic acid, 3-(1-hydroxy-2-isopropyl-5-methylcyclohexyl)-
C13H20O3; MF: 703; RMF: 728; Prob 13.1%; Lib: mainlib; ID: 2587.

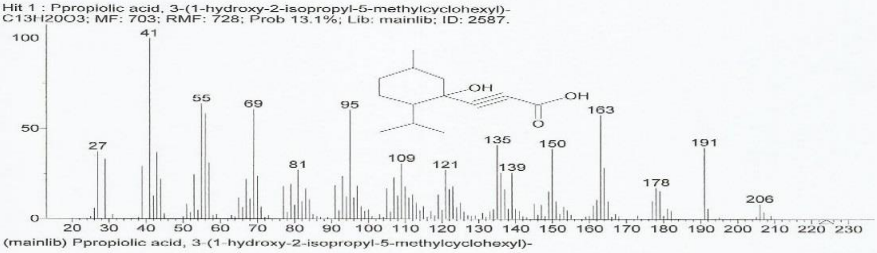

(mainlib) Ppropiolic acid, 3-(1-hydroxy-2-isopropyl-5-methylcyclohexyl)-

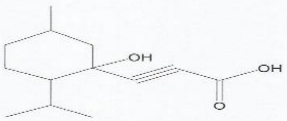

Name: Ppropiolic acid, 3-(1-hydroxy-2-isopropyl-5-methylcyclohexyl)-
Formula: $C_{13}H_{20}O_3$
MW: 224 NIST#: 158619 ID#: 2587 DB: mainlib
Contributor: Chemical Concepts
10 largest peaks:
41 999 | 55 638 | 69 608 | 95 604 | 56 583 | 163 578 | 135 411 | 191 399 | 150 390 | 27 373 |

Page 2 of 2

Unknown; InLib=-897

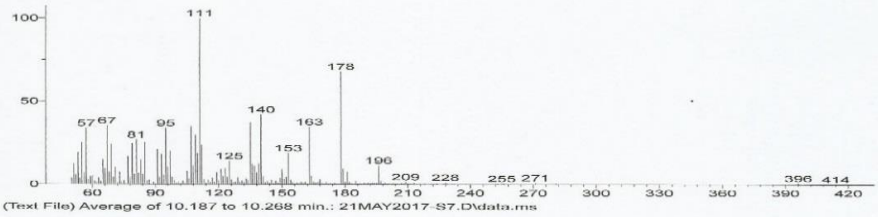

(Text File) Average of 10.187 to 10.268 min.: 21MAY2017-S7.D\data.ms

Name: Average of 10.187 to 10.268 min.: 21MAY2017-S7.D\data.ms
MW: N/A ID#: 1656 DB: Text File
Comment: NDH
10 largest peaks:
111 999 | 178 679 | 140 419 | 135 371 | 67 353 | 107 347 | 163 345 | 95 338 | 57 337 | 109 296 |

Page 1 of 2

Appendix 28 Caffeine

Hit 1 : Caffeine
$C_8H_{10}N_4O_2$; MF: 937; RMF: 937; Prob 96.8%; CAS: 58-08-2; Lib: mainlib; ID: 142426.

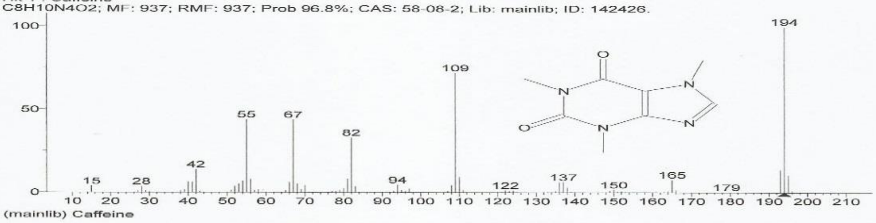

(mainlib) Caffeine

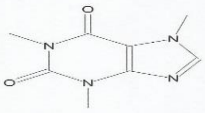

Name: Caffeine
Formula: $C_8H_{10}N_4O_2$
MW: 194 CAS#: 58-08-2 NIST#: 290714 ID#: 142426 DB: mainlib
Other DBs: Fine, TSCA, RTECS, EPA, USP, HODOC, NIH, EINECS, IRDB
Contributor: NIST Mass Spectrometry Data Center, 1998.
10 largest peaks:
194 999 | 109 721 | 55 439 | 67 438 | 82 328 | 42 138 | 193 135 | 195 103 | 110 92 | 81 81 |

Unknown; InLib=490

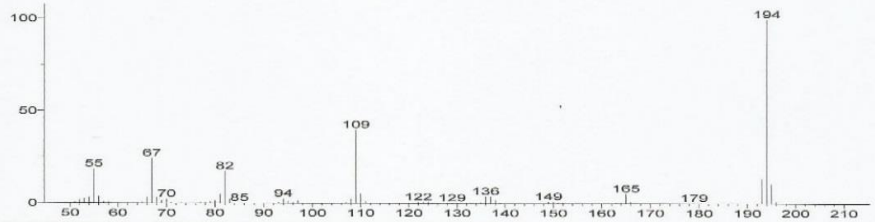

(Text File) Average of 11.083 to 11.281 min.: 21MAY2017-S7.D\data.ms

Name: Average of 11.083 to 11.281 min.: 21MAY2017-S7.D\data.ms
MW: N/A ID#: 1657 DB: Text File
Comment: NDH
10 largest peaks:
194 999 | 109 397 | 67 243 | 55 185 | 82 172 | 193 136 | 195 105 | 110 52 | 165 52 | 81 48 |

Appendix 29 Phthalic acid

Hit 1 : Phthalic acid, butyl tetradecyl ester
$C_{26}H_{42}O_4$; MF: 788; RMF: 886; Prob 11.9%; Lib: mainlib; ID: 109609.

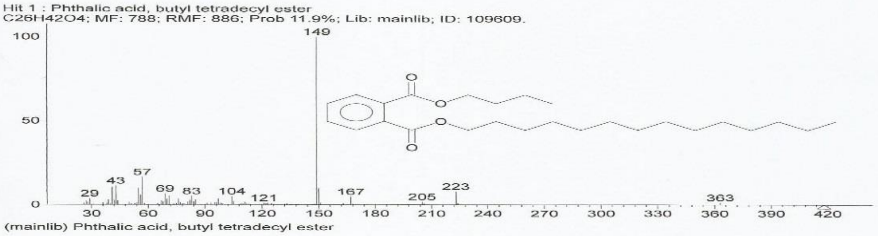

(mainlib) Phthalic acid, butyl tetradecyl ester

Name: Phthalic acid, butyl tetradecyl ester
Formula: $C_{26}H_{42}O_4$
MW: 418 NIST#: 308913 ID#: 109609 DB: mainlib
Contributor: Zaikin V.G., Institute of Petrochemical Synthesis RAS
10 largest peaks:
149 999 | 57 165 | 43 113 | 41 105 | 55 98 | 150 97 | 223 79 | 69 66 | 56 57 | 71 52 |

Unknown; InLib=-520

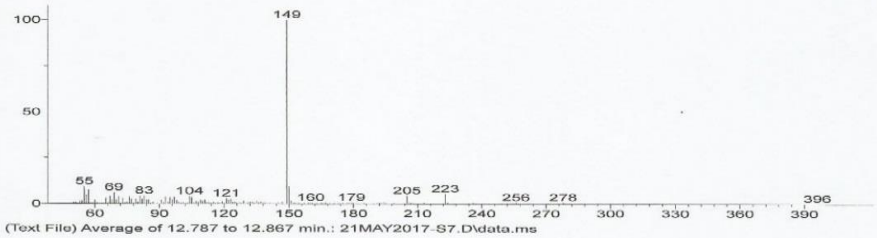

(Text File) Average of 12.787 to 12.867 min.: 21MAY2017-S7.D\data.ms

Name: Average of 12.787 to 12.867 min.: 21MAY2017-S7.D\data.ms
MW: N/A ID#: 1658 DB: Text File
Comment: NDH
10 largest peaks:
149 999 | 55 94 | 150 94 | 57 74 | 69 62 | 223 55 | 56 47 | 83 44 | 205 44 | 104 42 |

Appendix 30 Phytol

Hit 1 : Phytol
C20H40O; MF: 904; RMF: 940; Prob 73.1%; CAS: 150-86-7; Lib: replib; ID: 8051.

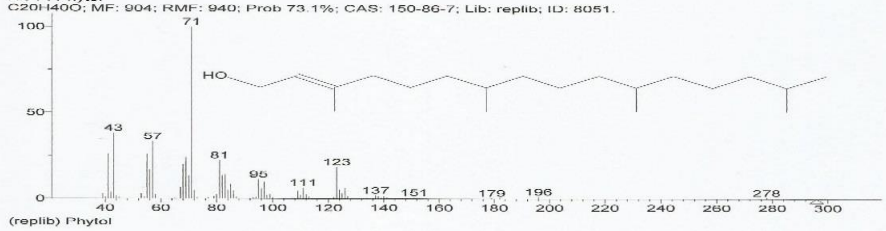

(replib) Phytol

Name: Phytol
Formula: $C_{20}H_{40}O$
MW: 296 CAS#: 150-86-7 NIST#: 108727 ID#: 8051 DB: replib
Other DBs: Fine, TSCA, RTECS, HODOC, EINECS
Contributor: Philip Morris R&D
10 largest peaks:
71 999 | 43 381 | 57 334 | 41 260 | 55 259 | 69 239 | 81 223 | 68 199 | 123 184 | 56 169 |

Unknown; InLib=165

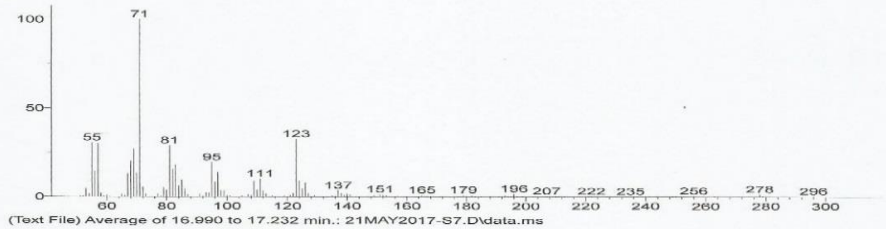

(Text File) Average of 16.990 to 17.232 min.: 21MAY2017-S7.D\data.ms

Name: Average of 16.990 to 17.232 min.: 21MAY2017-S7.D\data.ms
MW: N/A ID#: 1660 DB: Text File
Comment: NDH
10 largest peaks:
71 999 | 123 325 | 55 305 | 57 300 | 81 289 | 69 269 | 68 202 | 95 194 | 83 179 | 82 155 |

Appendix 31 9, 12, 15-octadecatrienoic acid

Hit 1 : 9,12,15-Octadecatrienoic acid, (Z,Z,Z)-
C18H30O2; MF: 874; RMF: 885; Prob 35.9%; CAS: 463-40-1; Lib: replib; ID: 1193.

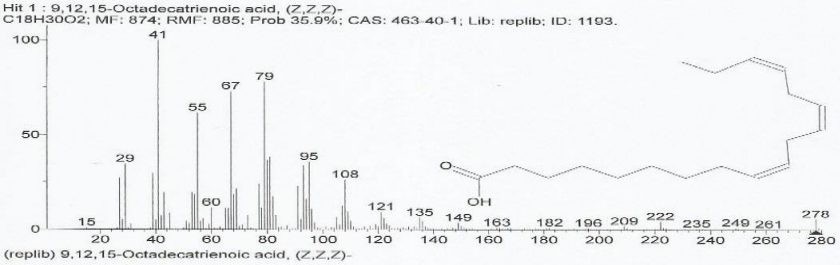

(replib) 9,12,15-Octadecatrienoic acid, (Z,Z,Z)-

Name: 9,12,15-Octadecatrienoic acid, (Z,Z,Z)-
Formula: $C_{18}H_{30}O_2$
MW: 278 CAS#: 463-40-1 NIST#: 230588 ID#: 1193 DB: replib
Other DBs: Fine, TSCA, HODOC, NIH, EINECS
Contributor: Japan AIST/NIMC Database- Spectrum MS-NW-5578
10 largest peaks:
41 999 | 79 780 | 67 730 | 55 616 | 81 383 | 80 365 | 95 358 | 29 345 | 93 338 | 39 297 |

Page 2 of 2

Unknown; InLib=-138

(Text File) Average of 18.317 to 18.998 min.: 21MAY2017-S7.D\data.ms

Name: Average of 18.317 to 18.998 min.: 21MAY2017-S7.D\data.ms
MW: N/A ID#: 1661 DB: Text File
Comment: NDH
10 largest peaks:
67 999 | 79 987 | 81 740 | 55 734 | 95 688 | 93 449 | 80 441 | 82 384 | 69 381 | 68 353 |

Page 1 of 2

Appendix 32 Octadecanoic acid

Hit 1 : Octadecanoic acid
C18H36O2; MF: 814; RMF: 837; Prob 54.9%; CAS: 57-11-4; Lib: mainlib; ID: 8481.

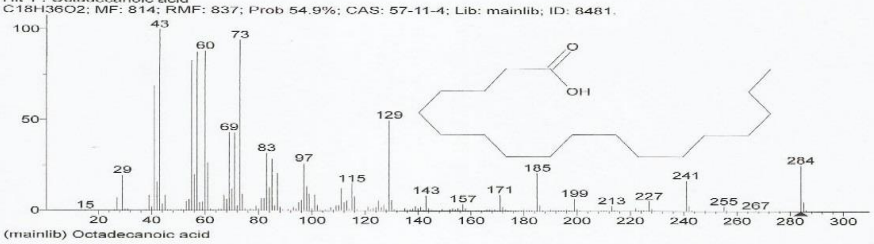

(mainlib) Octadecanoic acid

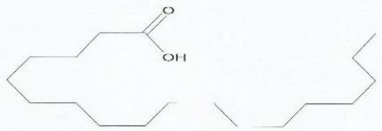

Name: Octadecanoic acid
Formula: $C_{18}H_{36}O_2$
MW: 284 CAS#: 57-11-4 NIST#: 290961 ID#: 8481 DB: mainlib
Other DBs: Fine, TSCA, RTECS, EPA, HODOC, NIH, EINECS, IRDB
Contributor: NIST Mass Spectrometry Data Center, 1998.
10 largest peaks:
43 999 | 73 942 | 60 881 | 57 875 | 55 827 | 41 688 | 129 500 | 69 432 | 71 429 | 83 317 |

Page 2 of 2

Unknown; InLib=-223

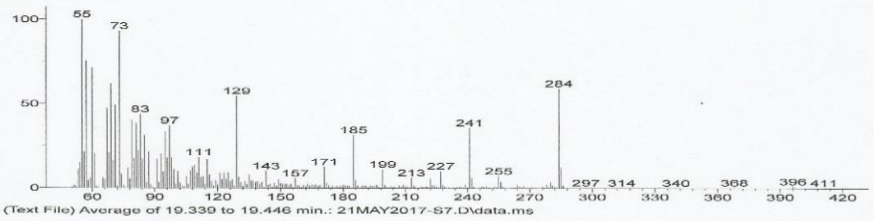

(Text File) Average of 19.339 to 19.446 min.: 21MAY2017-S7.D\data.ms

Name: Average of 19.339 to 19.446 min.: 21MAY2017-S7.D\data.ms
MW: N/A ID#: 1662 DB: Text File
Comment: NDH
10 largest peaks:
55 999 | 73 931 | 57 756 | 60 714 | 69 620 | 284 593 | 129 546 | 71 492 | 67 473 | 83 439 |

Page 1 of 2

Appendix 33 α-Amyrin

Hit 1 : α-Amyrin
C30H50O; MF: 851; RMF: 869; Prob 65.0%; CAS: 638-95-9; Lib: replib; ID: 25159.

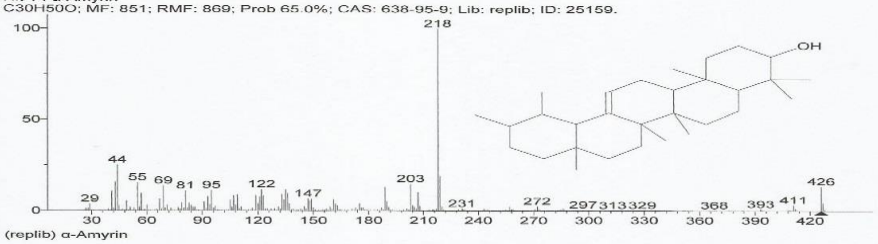

(replib) α-Amyrin

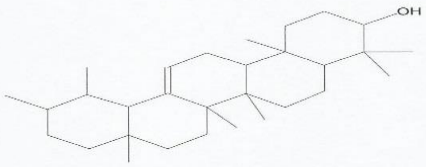

Name: α-Amyrin
Formula: $C_{30}H_{50}O$
MW: 426 CAS#: 638-95-9 NIST#: 197289 ID#: 25159 DB: replib
Other DBs: HODOC, NIH, EINECS
Contributor: Chemical Concepts
10 largest peaks:
218 999 | 44 251 | 219 190 | 43 157 | 55 154 | 203 148 | 69 137 | 426 135 | 189 130 | 122 118 |

Page 2 of 2

Unknown; InLib=-219

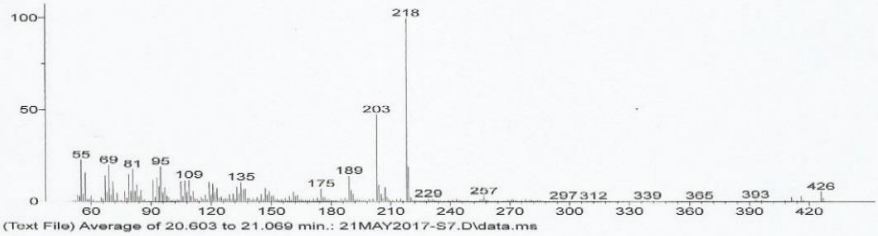

(Text File) Average of 20.603 to 21.069 min.: 21MAY2017-S7.D\data.ms

Name: Average of 20.603 to 21.069 min.: 21MAY2017-S7.D\data.ms
MW: N/A ID#: 1663 DB: Text File
Comment: NDH
10 largest peaks:
218 999 | 203 473 | 55 226 | 69 197 | 95 189 | 219 187 | 81 175 | 57 155 | 79 146 | 67 139 |

Page 1 of 2

Appendix 34 ϒ-Tocopherol

Hit 1 : γ-Tocopherol
$C_{28}H_{48}O_2$; MF: 738; RMF: 802; Prob 59.6%; CAS: 7616-22-0; Lib: replib; ID: 20323.

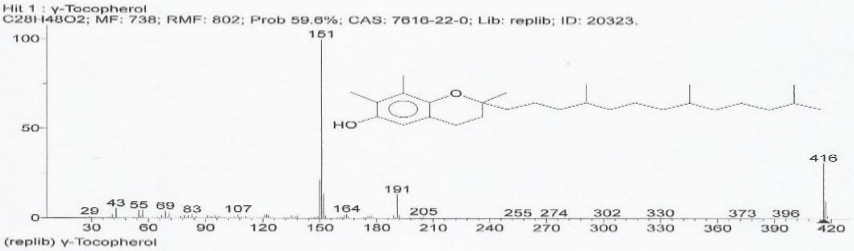

(replib) γ-Tocopherol

Name: γ-Tocopherol
Formula: $C_{28}H_{48}O_2$
MW: 416 CAS#: 7616-22-0 NIST#: 151381 ID#: 20323 DB: replib
Other DBs: TSCA, HODOC, EINECS
Contributor: Chemical Concepts
10 largest peaks:
151 999 | 416 312 | 150 216 | 152 137 | 191 132 | 417 98 | 43 55 | 55 44 | 57 44 | 69 40 |

Page 2 of 2

Unknown; InLib=-521

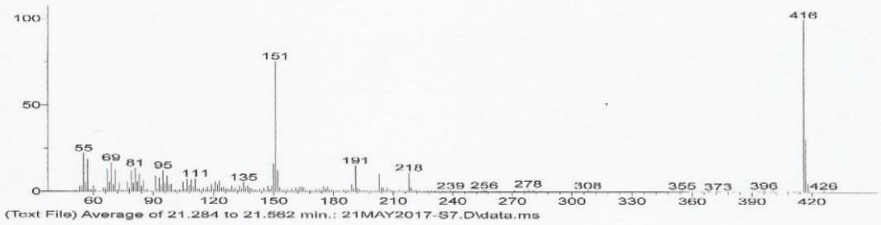

(Text File) Average of 21.284 to 21.562 min.: 21MAY2017-S7.D\data.ms

Name: Average of 21.284 to 21.562 min.: 21MAY2017-S7.D\data.ms
MW: N/A ID#: 1664 DB: Text File
Comment: NDH
10 largest peaks:
416 999 | 151 754 | 417 308 | 55 223 | 57 186 | 69 168 | 150 161 | 191 152 | 81 137 | 67 130 |

Page 1 of 2

Appendix 35 1, 2-Benzenedicarboxylic acid

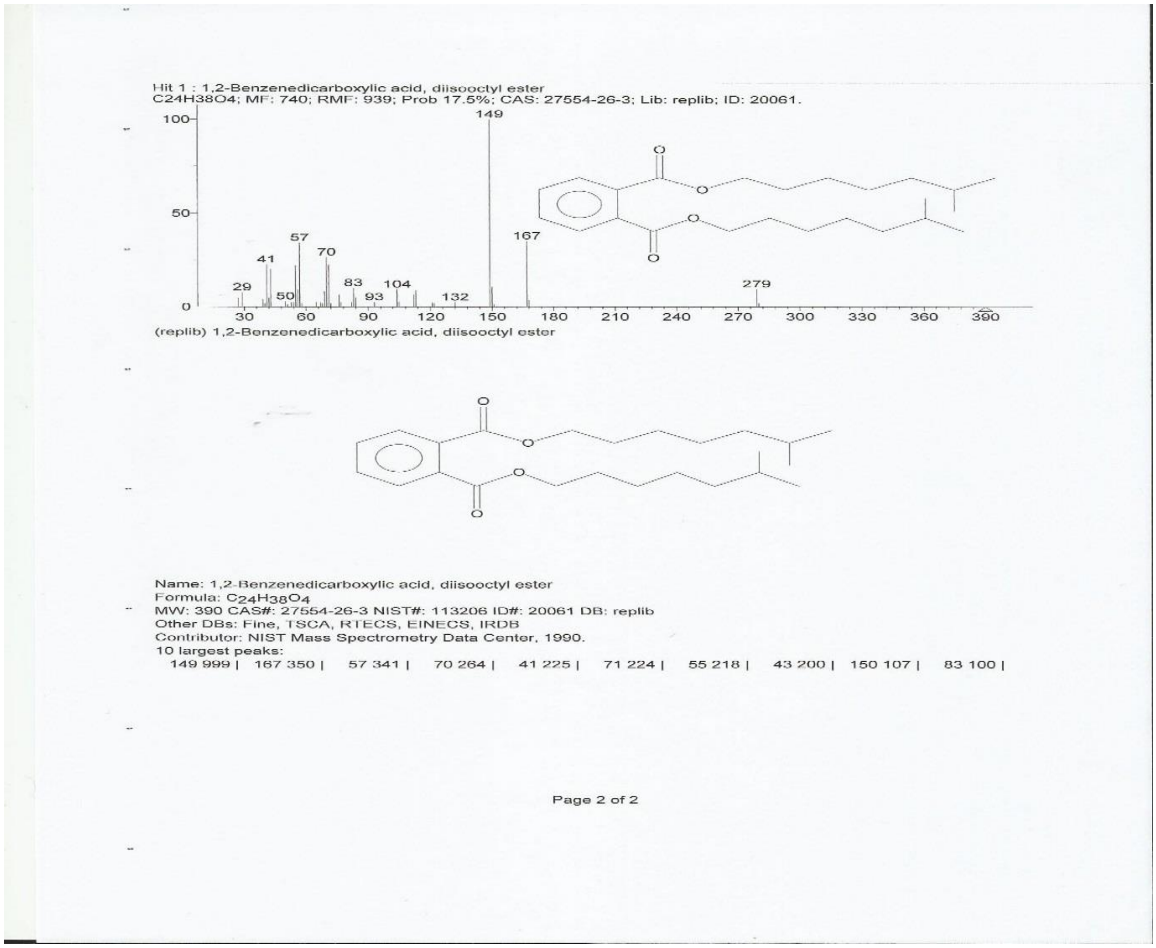

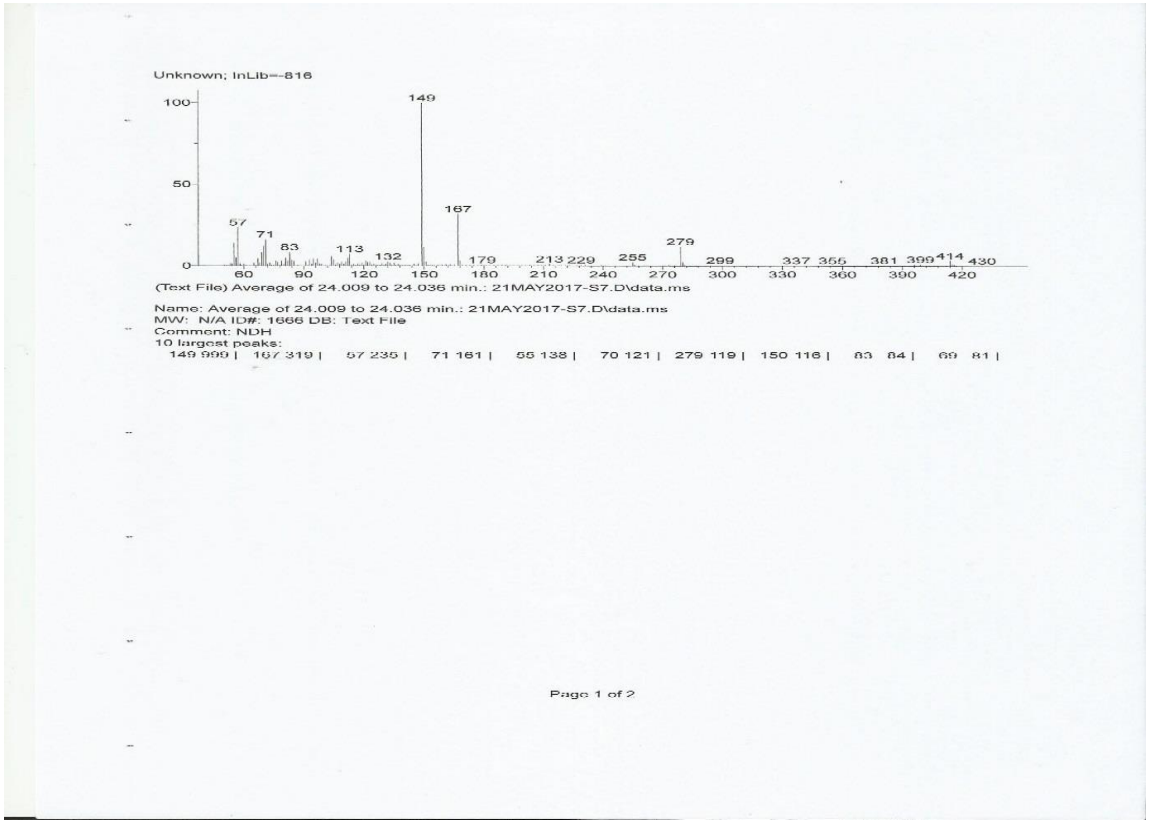

Appendix 36 Vitamin E

Hit 1 : Vitamin E
C29H50O2; MF: 874; RMF: 886; Prob 40.8%; CAS: 59-02-9; Lib: replib; ID: 21723.

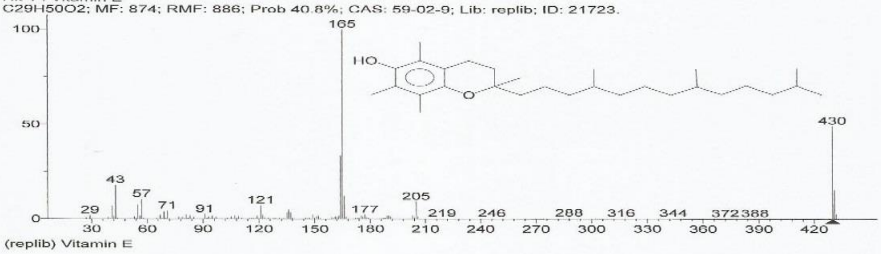

(replib) Vitamin E

Name: Vitamin E
Formula: $C_{29}H_{50}O_2$
MW: 430 CAS#: 59-02-9 NIST#: 290780 ID#: 21723 DB: replib
Other DBs: TSCA, RTECS, HODOC, NIH, EINECS
Contributor: NIST Mass Spectrometry Data Center, 1998.
10 largest peaks:
165 999 | 430 494 | 164 332 | 43 178 | 431 155 | 166 122 | 57 104 | 205 91 | 55 75 | 121 71 |

Page 2 of 2

Unknown; InLib=163

(Text File) Average of 25.694 to 26.080 min.: 21MAY2017-S7.D\data.ms

Name: Average of 25.694 to 26.080 min.: 21MAY2017-S7.D\data.ms
MW: N/A ID#: 1667 DB: Text File
Comment: NDH
10 largest peaks:
430 999 | 165 738 | 431 321 | 164 231 | 57 122 | 55 97 | 166 91 | 205 82 | 69 76 | 71 68 |

Page 1 of 2

Appendix 37 2, 2, 4-Trimethyl-heptadeca-3, 7, 11, 15-tetraenyl)-cyclohexanol

Hit 1 : 2,2,4-Trimethyl-3-(3,8,12,16-tetramethyl-heptadeca-3,7,11,15-tetraenyl)-cyclohexanol
C30H52O; MF: 799; RMF: 833; Prob 24.4%; Lib: mainlib; ID: 30936.

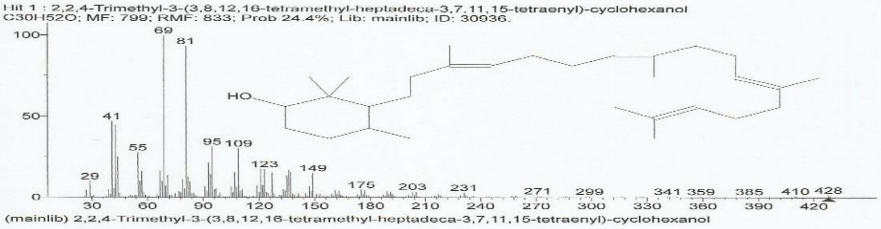

(mainlib) 2,2,4-Trimethyl-3-(3,8,12,16-tetramethyl-heptadeca-3,7,11,15-tetraenyl)-cyclohexanol

Name: 2,2,4-Trimethyl-3-(3,8,12,16-tetramethyl-heptadeca-3,7,11,15-tetraenyl)-cyclohexanol
Formula: $C_{30}H_{52}O$
MW: 428 NIST#: 194014 ID#: 30936 DB: mainlib
Contributor: Chemical Concepts
10 largest peaks:
69 999 | 81 933 | 41 470 | 43 447 | 95 313 | 109 302 | 55 277 | 44 251 | 93 213 | 123 174 |

Unknown; InLib=-285

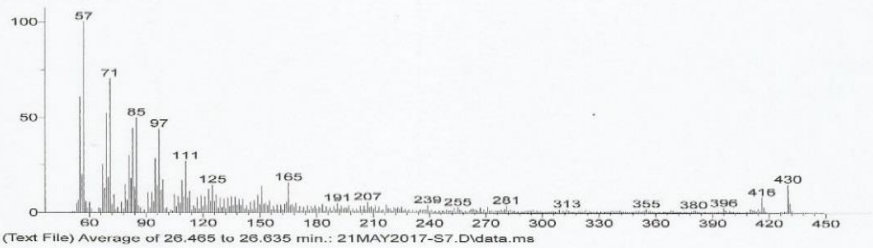

(Text File) Average of 26.465 to 26.635 min.: 21MAY2017-S7.D\data.ms

Name: Average of 26.465 to 26.635 min.: 21MAY2017-S7.D\data.ms
MW: N/A ID#: 1668 DB: Text File
Comment: NDH
10 largest peaks:
57 999 | 71 705 | 55 608 | 69 522 | 85 500 | 83 444 | 97 442 | 81 302 | 95 286 | 111 272 |

APPENDIX IV

LIBS Spectra (TiO_2)

Appendix 38 TiO_2 -pulse energy (70MJ)

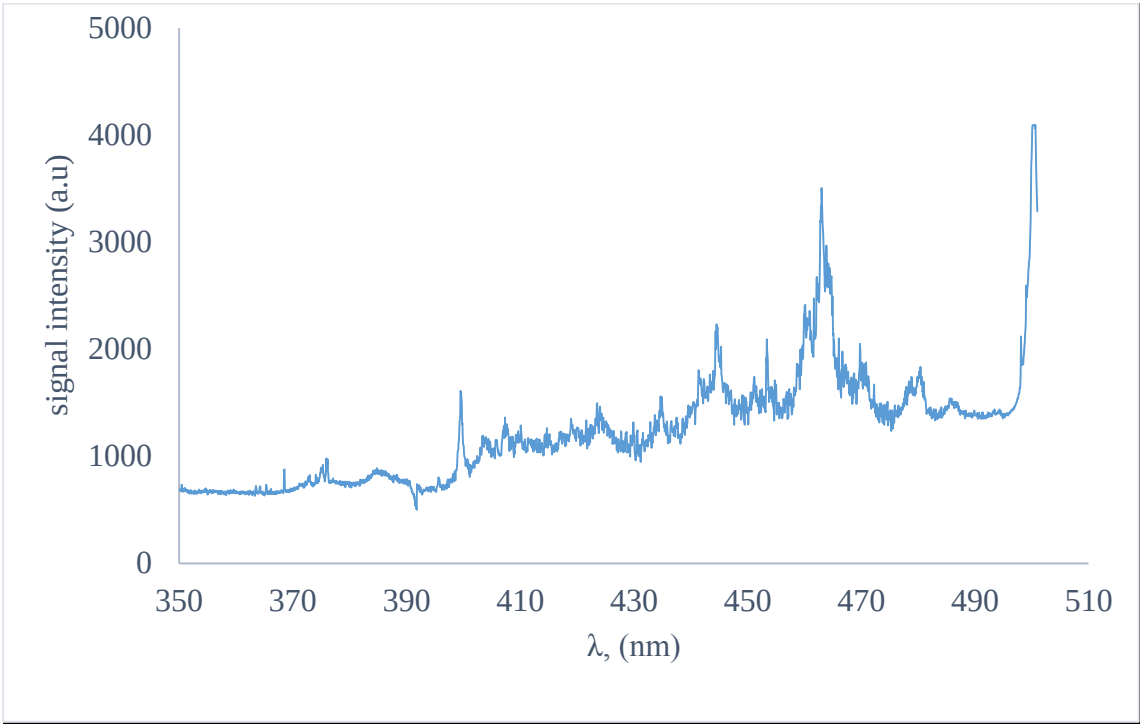

Appendix 39 TiO_2-pulse energy (90MJ)

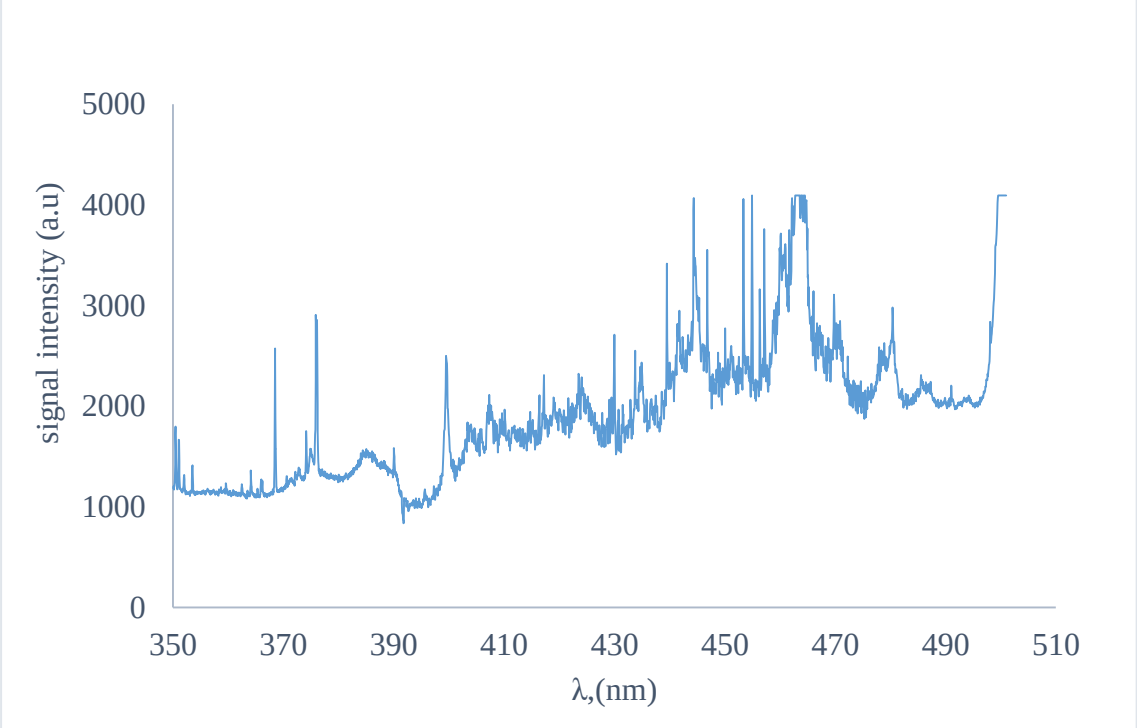

Appendix 40 TiO_2-pulse energy (80MJ)

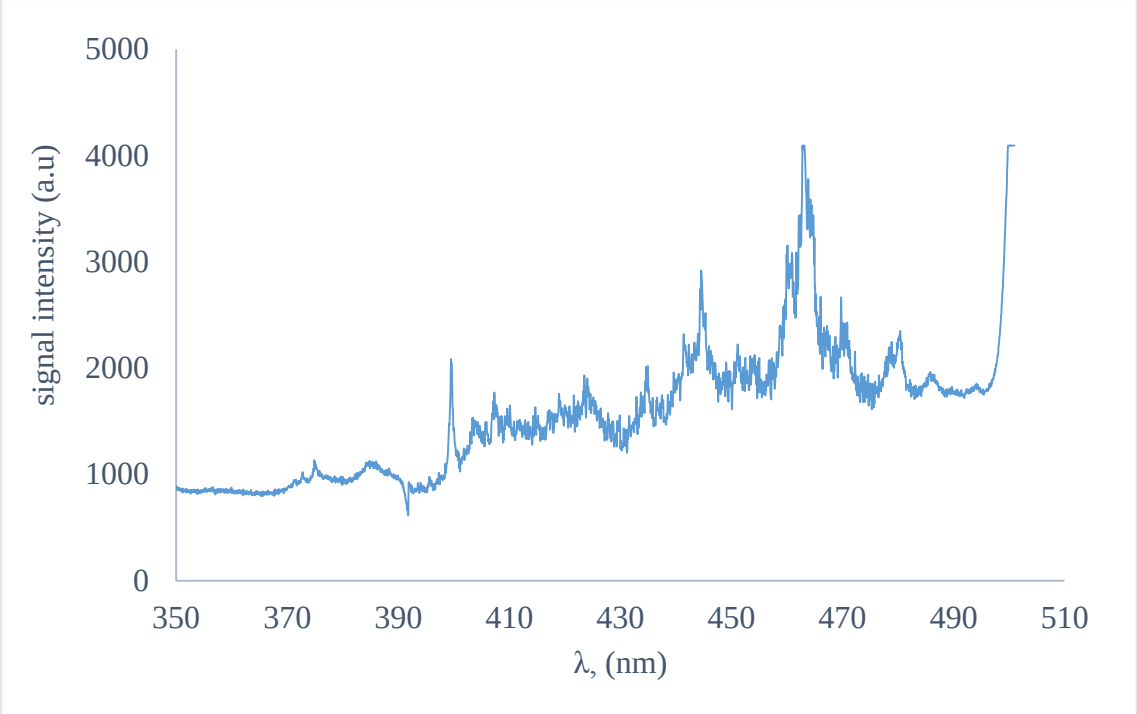

APPENDIX V

LIBS Spectra – (ZnO)

Appendix 41 ZnO-pulse energy (70MJ)

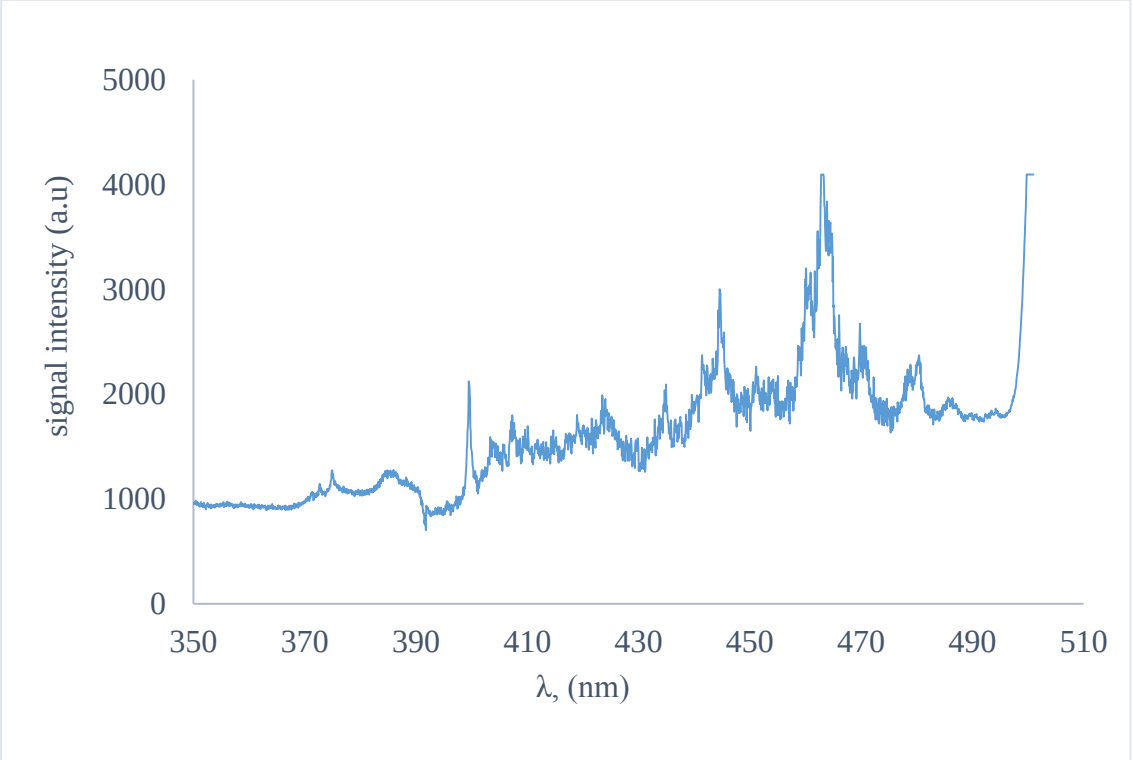

Appendix 42 ZnO-pulse energy (90 MJ)

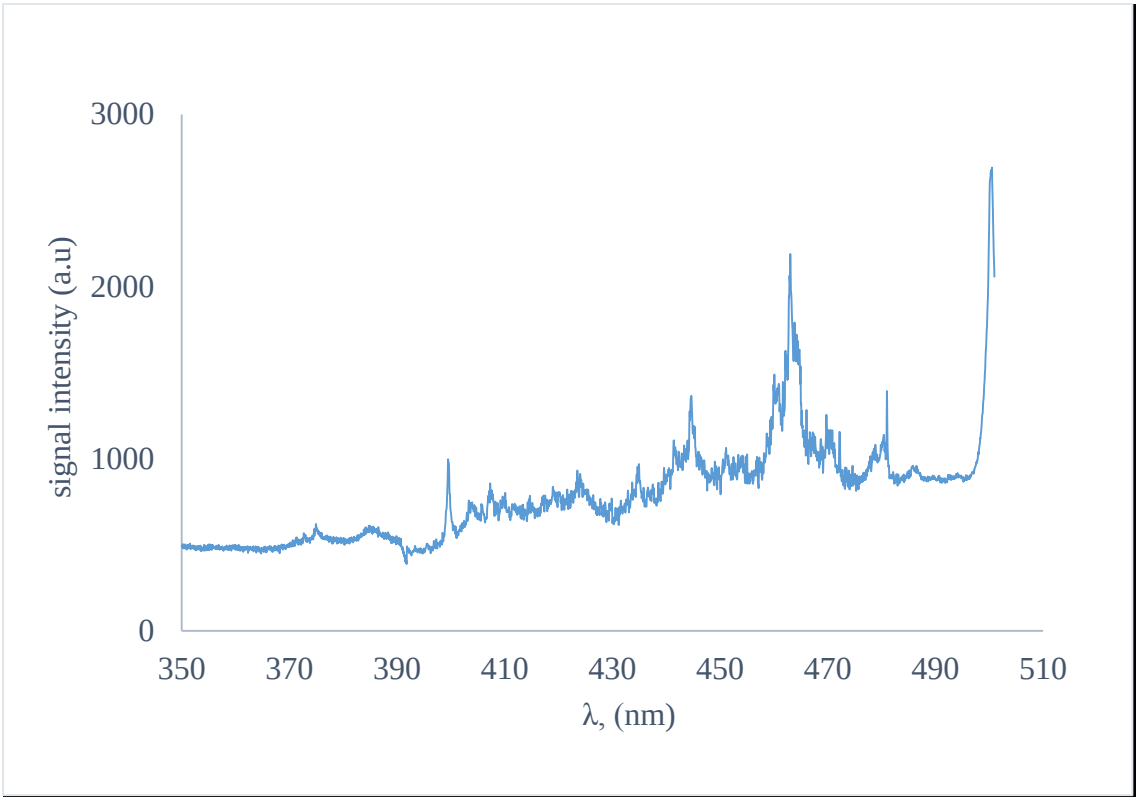

Appendix 43 ZnO-pulse energy (80 MJ))